Novel cell models to study breast tumour microenvironment and disease progression

Marta Maria Vieira Matutino Falcão Estrada

Dissertation presented to obtain the Ph.D degree in Engineering and Technology Sciences – Biomedical Engineering

Instituto de Tecnologia Química e Biológica António Xavier | Universidade Nova de Lisboa

Oeiras, November, 2018

Novel cell models to study breast tumour microenvironment and disease progression

Marta Maria Vieira Matutino Falcão Estrada

The work developed in this thesis was supervised by:

- **Doctor Catarina Brito**, Instituto de Biologia Experimental e Technólogica (iBET) e Instituto de Tecnologia Química e Biológica António Xavier, Universidade Nova de Lisboa (ITQB-NOVA)
- **Doctor Paula Alves**, Instituto de Biologia Experimental e Technólogica (iBET) e Instituto de Tecnologia Química e Biológica António Xavier, Universidade Nova de Lisboa (ITQB-NOVA)

Financial support from:

Fundação para a Ciência e Tecnologia (FCT)

Ph.D grant SFRH/BD/52208/2013

iNOVA4Health (UID/Multi/04462/2013), financially supported by FCT/MEC, through national funds and co-funded by FEDER under the PT2020 Partnership Agreement

IMI Joint Undertaking (grant agreement no. 115188)

Novel cell models to study breast tumour microenvironment and disease progression.

Instituto de Tecnologia Química e Biológica António Xavier, Universidade Nova de Lisboa
Instituto de Biologia Experimental e Tecnológica

À minha família

Acknowledgements

I would like to express my gratitude to all the people who have contributed directly or indirectly to this thesis.

To my supervisor, Dr Catarina Brito, for sharing this journey with me and for the constant support, guidance and mentoring throughout these years. Thank you for trusting me with the great opportunity of integrating the PREDECT European project and for starting a new area of research in the lab with you. Thank you for all the hours of scientific discussions, and for all the mentoring time invested in me. It made me grow in so many different aspects of life in general and in the work environment, such as managing partners, performing multiple tasks, writing emails, projects and papers, amongst many others. Thank you for the freedom to embrace new projects and to conquer impossible dreams. I started as a young wannabe scientist and leave as a mature and confident junior scientist, thanks to you. You made me grow in every possible way and I am eternally grateful for everything you did for me.

To my co-supervisor, Prof Paula Alves, for the opportunity to work in an inspiring and excellent scientific environment at the Animal Cell Technology Unit. Thank you for all the support, knowledge, confidence and also for all the opportunities and challenges that contributed to my development as a scientist.

To Prof Manuel Carrondo for his leadership and inspiring example of excellence, rigor and hard work.

To all the members from the PREDECT consortium, specially to Dr Georgios Sflomos, Dr John Hickman, Dr Ralph Graser, Dr Emma Davies, Dr Elizabeth Anderson, and Elsa Marques, for all the fruitful discussions, mentoring, knowledge and support throughout the years.

To Prof Cathrin Brisken and to Dr Juha Klefström for such a warm welcoming in your laboratories at the Swiss Institute for Experimental Cancer Research at École Polytechnique Fédérale de Lausanne & at the *Cancer Cell Circuitry Laboratory*, at University of Helsinki and for the mentoring, enthusiasm and knowledge shared during my stay and after.

To Dr Joana Paredes and Dr Marta Teixeira Pinto, from IPATIMUP, for all the scientific discussions, support throughout this project and for all the help in the angiogenesis assays.

To Dr Emílio Gualda and Hugo Pereira for all the effort in collaborating to develop new microscopy tools for accurate characterization of the models developed in this work.

To Dr Saudade André and Ruben Roque who believed in the crazy idea of growing human breast cancer explants ex vivo, for all the discussions, teaching and enthusiasm.

To Dr Patricia Alves, Dr Cristina Peixoto and Sara Rosa, for all the indefinite discussions about Mass spectrometry and downstream processing, and for never stop believing that we could enrich complex samples for low abundant proteins.

To the MolBioS PhD program and all my Professors for the intensive learning experience.

To my colleagues at the Animal Cell Technology Unit for creating such a great working environment, where I continuously grow from all the different fields.

To Dr Sofia Rebelo and Dr Catarina Pinto for the great discussions in the cancer field and for always guiding me through the innumerous difficulties throughout the years. Thank you for always believing in me and for pushing me to be a better person.

To the 3D team (and friends) Dr Ana Paula Terrasso, Dr Daniel Simão, Francisca Arez, Dr Marta Silva, João Sá, Rita Costa, Dr Vitor Espirito-Santo, Ana Luisa Cartaxo, Dr Dusica Rados, Sofia Abreu, Teresa Mendes, Dr Maria João Sebastião, Dr Bernardo Abecassis, Rui Portela, Miguel Fuzeta, Ana Raposo and Marcos Sousa, for all the help, discussions, ideas and suggestions shared throughout the years.

Ao meu querido marido, António, o meu pilar, agradeço o seu apoio e amor incondicional que me motivaram nos momentos mais difíceis, me alegraram na partilha das conquistas e que sempre me estimularam a seguir os novos

sonhos e a conquistar horizontes impossíveis. Obrigada pela companhia, pela espera, pela paciência, pela partilha, pela compreensão, pelo enorme reforço positivo e pela força para nunca desistir.

À minha família, especialmente aos meus pais e à minha irmã Mafalda, que sempre me apoiaram em todos os momentos. Obrigada pelos valores de integridade e partilha que são a base de tudo. Obrigada por me terem educado a nunca desistir e por me terem ensinado que se trabalharmos para ser os melhores, chegaremos mais longe do que alguma vez sonhamos.

Aos meus amigos, especialmente, à Pipa, Pintas e à Pipas, que sempre me apoiaram e me deram espaço, força e alegria para seguir os meus sonhos.

Abstract

Breast cancer is the most prevalent and deadly in woman. ER^+ breast cancer represents around two-thirds of all cases and has a favourable prognosis due to good response to endocrine therapy. However, these tumours present 25% of disease relapse due to drug resistance and metastatic behaviour. Tumour progression and acquired drug resistance are modulated by the interactions between tumour cells and the surrounding microenvironment. Most models employed to address these mechanisms fail to reflect the complex tumour microenvironment and do not allow long-term monitoring of tumour progression.

The work presented in this thesis focused on the development of in vitro and ex vivo culture strategies that would overcome these limitations and better mimic the tumour architecture, its microenvironment and recapitulate features of tumour progression.

In chapter 2, stirred-tank culture strategies for large scale production of multicellular spheroid-based tumour models have been developed. Here, cell inoculum and stirring conditions were optimized for efficient aggregation of nine cell lines from three different pathologies (breast, prostate and lung cancer). The presence of oxygen gradients was assessed for three cell lines, which presented different aggregate size and cell compactness. Co-culture of tumour cells with human fibroblasts, heterotypic multicellular spheroids, resulted in different patterns of fibroblast distribution and lack of epithelial cell organization. Tumor cell spheroids and fibroblasts were encapsulated in micro-beads of alginate, a biocompatible and inert hydrogel, in order to provide physical support and confinement to both cell types and to allow the accumulation of secreted factors

In **chapter 3**, the microencapsulation in alginate hydrogel of heterotypic cultures of MCF7 cells (ER^+ breast cancer cell line) and human fibroblasts was implemented and characterized. Epithelial cells organized into tissue-like structures, with apical localization of markers such as ZO-1 and f-actin, and formation of small lumens within spheroids, in contrast with MCF7 spheroids

generated in scaffold-free conditions that lacked epithelial polarization. Moreover, this culture strategy allowed the creation of distinct epithelial and stromal compartments, in contrast to what was observed in the scaffold-free conditions. The close proximity between the two cell types resulted in heterotypic cell crosstalk. This crosstalk, resulted in a pro-inflammatory and pro-angiogenic environment, and led to phenotypical alterations of tumour cell phenotype towards features typical of more aggressive stages of the disease.

In **chapter 4**, a comparative study between different *in vitro* heterotypic tumour cell models was performed. Comparisons were done across several partners of the IMI-funded project PREDECT (www.predect.eu). The MCF-7-based model developed in chapter 3 was compared with 2D and static 3D cultures of the same cell line, in scaffold-free conditions or embedded in different bioactive scaffolds (matrigel and collagen). After harmonization of the culture conditions and analytical methods, the results highlighted that MCF7 cells exhibited distinct phenotypes depending on the scaffold used. Of notice, culture within matrigel masked the stimulatory effect of fibroblasts on MCF7 growth. Treatment with standard of care drugs suggested a protective effect of fibroblasts on tumour cells.

In **chapter 5**, a new methodology for *ex vivo* culture of human-derived ER^+ breast cancer explants was developed, based on the strategy implemented in chapters 2 and 3. Samples from 21 patients were partially digested and encapsulated into alginate hydrogels. In 70% of the cases this methodology allowed the long-term maintenance of the original tumour architecture and phenotype. Epithelial, stromal and immune cells were detected after one moth in culture. Importantly, ER expression and functionality was detected *ex vivo* until at least 30 days of culture. Evaluation of the culture metabolic activity, namely, detection of lactate in the culture supernatant, allowed the distinction of encapsulated explants with a good cellularity from those where cellularity was lost.

Discovery of new molecular players involved in tumour-stroma crosstalk has been hindered not only by the scarcity of adequate cell models but also by

the lack of analytical tools for untargeted discovery of cytokines and chemokines, key mediators of tumour-stromal crosstalk. Therefore, in **chapter 6** we focused on the development of methodologies for identification of low abundant low molecular weight proteins within complex secretome samples. Successful enrichment in low molecular weight proteins was achieved by subjecting cell culture medium samples to a combination of two pre-fractionation methodologies: 1D SDS PAGE in-gel digestion and protein precipitation with ammonium sulphate followed by in solution digestion. This enrichment resulted in the identification by MS of a subset of 450 low abundant proteins, that were not detected in unprocessed samples.

The work developed in this thesis provides novel strategies for 3D cell modelling of ER^+ human breast carcinomas, both *in vitro* and *ex vivo*. These models are reproducible and robust and allow long-term monitoring of disease progression-associated events. The combination of the models developed with the characterization methods implemented along this work represent powerful tools, applicable to study tumour-stroma crosstalk, disease progression and drug resistance mechanisms in preclinical and co-clinical settings.

Key words: 3D cell culture; agitation-based culture systems; alginate microencapsulation; breast cancer; tumour microenvironment; tumour progression.

Resumo

O cancro da mama é o tipo de cancro mais comum e com maior taxa de mortalidade entre as mulheres. O cancro da mama positivo para o receptor de estrogeneos (RE^+) é o mais predominante, representando cerca de dois terços de todos os tipos de cancro da mama. Apesar do bom prognóstico resultante da resposta à terapia endócrina, esta patologia tem uma elevada taxa de recidiva causada pela aquisição de resistência aos fármacos e metastização.

A progressão para estadios mais avançados da doença e aquisição de resistência aos fármacos é provocada , não só por mecanismos intrínsecos das células epiteliais mas também pelas interações que as células cancerígenas estabelecem com o microambiente tumoral. No entanto, a maioria dos estudos realizados recorre a modelos celulares que não têm em conta a complexidade do microambiente tumoral nem permitem a monitorização contínua da progressão tumoral. Assim, esta tese foca-se no desenvolvimento e caracterização de novos modelos celulares de cancro *in vitro* e *ex vivo*, que visam manter ou reconstruir arquitectura do tecido, a comunicação celular, recapitulando aspectos chave do microambiente tumoral para a avaliação da progressão da doença.

No **capítulo 1** foi feita uma revisão bibliográfica da composição e funcionamento do tecido mamário e dos tipos de cancro de mama, com foco especial no subtipo molecular luminal A. Foi também feita uma revisão da dinâmica do microambiente tumoral e de como este promove a progressão do tumor; e ainda dos modelos celulares de cancro rotineiramente utilizados em investigação e de como as suas limitações afectam a compreensão dos mecanismos de resistência a fármacos. No **capítulo 2** foram desenvolvidas estratégias escalonáveis em tanque agitado para cultura *in vitro* de esferóides. A velocidade de agitação e o inóculo celular foram optimizados para promover a agregação de nove linhas celulares de três tipos de cancro diferentes (mama, pulmão e próstata). Os gradientes de oxigénio em esferóides de três linhas celulares que apresentam diferenças de tamanho e de compactação celular foram caracterizados, com base em sondas de hipoxia. Dada a necessidade

de recriar aspectos da arquitectura tumoral observada em estádios iniciais de carcinomas da mama RE^+, **no capítulo 3**, recorremos à microencapsulação de culturas heterotípicas em alginato. Aqui demonstramos que o uso de um suporte inerte permite a organização das células epiteliais em estruturas semelhantes às da glândula mamária. Estes resultados contrastam com os esferóides não encapsulados onde não foi possível recriar a organização epitelial. O uso do alginato permitiu criar compartimentos epiteliais e estromais distintos, com uma distribuição celular semelhante ao carcinoma da mama *in situ.* Este modelo permitiu também a interação entre os vários tipos celulares e com a matriz extracelular secretada. Após 15 dias de co-cultura, a presença dos fibroblastos contribuiu para um ambiente pro-inflamatório e pró-angiogénico, concomitante com o aparecimento de caraterísticas típicas de tumores da mama de estadios mais avançados, tais como o aumento de migração celular e a redução do RE.

Uma vez que as metodologias usadas, como o tipo de matriz e sistema de cultura podem ter impacto no fenótipo celular, **no capítulo 4**, realizámos um estudo comparativo entre vários tipos de modelos heterotípicos. Este estudo foi feito entre vários parceiros pertencentes ao projecto europeu PREDECT. Neste estudo, o modelo *in vitro* desenvolvido no capítulo 3 foi comparado com culturas 2D e 3D estáticas, com ou sem recurso a matrizes. Após harmonização das condições de cultura e métodos analíticos, os resultados demonstraram que a matriz utilizada pode mascarar o efeito estimulador dos fibroblastos no crescimento das células tumorais.

No **capítulo 5** foi desenvolvido um novo método de cultura *ex vivo* de explantes de doentes com cancro de mama RE^+. Também neste modelo o alginato forneceu um suporte físico e permitiu a manutenção da matriz extracelular. Com esta metodologia foi possível estender o tempo de cultura para 30 dias com manutenção da arquitectura e fenótipo originais do tumor. Além da manutenção da expressão do RE, foi também possível detectar células epiteliais, células do estroma e células imunitárias no final da cultura. A análise da actividade metabólica permitiu distinguir os explantes com boa

celularidade e manutenção da expressão RE daqueles cuja celularidade e expressão do RE estavam perdidos.

A descoberta de marcadores moleculares envolvidos na comunicação entre o tumor e o estroma tem sido impossibilitada não só pela escassez de modelos celulares mas também pela falta de ferramentas analíticas para a descoberta não direcionada mediadores chave da comunicação entre o tumor e os estroma. Por este motivo, **capítulo 6** foca-se na implementação de ferramentas de descomplexação de meio condicionado pela cultura com fibroblastos, na presença soro bovino para análise por espectrometria de massa. Mais concretamente, pretendíamos enriquecer o meio de cultura em proteínas de baixo peso molecular, cuja detecção por métodos de espectrometria de massa era impossibilitada pela presença de proteínas abundantes, como a albumina. Através da combinação de SDS-PAGE e de precipitação proteica por *salting-out* com sulfato de amónia, conseguimos o enriquecimento em proteínas de baixo peso molecular, tipicamente pouco abundantes.

O trabalho desenvolvido nesta tese fornece novas estratégias para cultura 3D, *in vitro* e *ex vivo*, de carcinomas humanos da mama RE^+, com aplicação em ensaios pré-clínicos e co-clínicos. A combinação de ambas as estratégias de cultura com os métodos de caracterização implementados, representa uma ferramenta robusta para a investigação em cancro, mais concretamente no estudo da comunicação tumor-estroma, na compreensão de mecanismos de progressão da doença e aquisição de resistência a fármacos.

Palavras chave: cultura celular 3D; sistemas de cultura agitados, microencapsulação em alginato, cancro de mama, microambiente tumoral, progressão tumoral

Thesis publications

Estrada MF, Rosa S, Gomes R, Peixoto C, Alves PM, Gomes-Alves P, Brito C. *Improving MS identification of low molecular weight proteins in complex samples*. Under submission

Estrada MF, Cartaxo A, Domenici G, Pinto C, Roque R, Rados D, Portela R, Fuzeta M, Alves PM, André S and Brito C. *Ex vivo model to study hormone response in human breast cancer.* In preparation

Stock K*, **Estrada MF***, Vidic S*, Gjerde K*, Rudisch A*, Santo VE*, Barbier M, Blom S, (...) Brito S, Weerden W, Rotter V, Boghaert E, Oren M, Sommergruber W, Chong Y, Hoogt R, Graeser R. *Capturing tumor complexity in vitro- Comparative analysis of 2D and 3D tumor models for drug discovery*. Scientific Reports. 2016.

Estrada MF, Rebelo SP, Davies EJ, Pinto MT, Pereira H, Santo VE, Smalley MJ, Barry ST, Gualda EJ, Alves PM, Anderson E, Brito C. *Modelling the tumour microenvironment in long-term microencapsulated 3D co-cultures recapitulates phenotypic features of disease progression.* Biomaterials, 2016.

Estrada MF*, Santo VE*, Rebelo SP, Abreu S, Silva I, Pinto C, Veloso SC, Serra AT, Boghaert E, Alves PM, Brito C. *Adaptable stirred-tank culture strategies for large scale production of multicellular spheroid-based tumor cell models*. J Biotechnol, 2016.

* These authors equally contributed to this work

Other publications

Vidic S*, **Estrada MF***, Gjerde K*,Santo VE*, Osswald A*, Barbier M*, Chong Y, Sommergruber W, de Hoogt R, Brito C, Graeser R. *PREDECT 2D/3D culture protocols*. Systems Chemical Biology. Under final revisions.

Rebelo SP*, Pinto C*, Martins TR, Harrer N, **Estrada MF**, Cabeçadas J, Alves PM, Gualda EJ, Sommergruber W, Brito C. *3D-3-culture: a tool to unveil macrophage plasticity in the tumour microenvironment*. Biomaterials, 2018.

Silva I, **Estrada MF**, Pereira C, Silva AB, Bronze MR, Alves PM, Duarte CMM, Brito C*, Serra AT*. *Polymethoxylated Flavones from Orange Peels Inhibit Cell Proliferation in a 3D Cell Model of Human Colorectal Cancer*. Nutrition and Cancer: An International Journal, 2018.

de Hoogt R*, **Estrada MF***, Vidic S*, Davies EJ*, Osswald A*, Barbier M*, Santo VE*, Gjerde K*, (…), Verschuren EW**, Hickman J** & Graeser R** *Data Descriptor: Protocols and characterization data for 2D, 3D, and slice-based tumor models from the PREDECT project.* Scientific Data, 2017.

Santo VE, Rebelo SP, **Estrada MF**, Alves PM, Boghaert E, Brito C. *Drug screening in 3D in vitro tumor models: overcoming current pitfalls of efficacy read-outs*. Biotechnology Journal. 2016.

Gualda EJ, Pereira H, Vale T, **Estrada MF**, Brito C, Moreno N. *SPIM-fluid: open source light-sheet based platform for high-throughput imaging*. Biomed Opt Express. 2015

* These authors equally contributed to this work

Table of Contents

Chapter I. Introduction ……..1

Chapter II. Adaptable stirred-tank culture strategies for large scale production of multicellular spheroid-based tumour cell models ……41

Chapter III. Modelling the tumour microenvironment in long-term microencapsulated 3D co-cultures recapitulates phenotypic features of disease progression ……..81

Chapter IV. Capturing tumour complexity in vitro- Comparative analysis of 2D and 3D tumour models for drug discovery ……117

Chapter V. ex vivo model to study hormone response in human breast cancer ……155

Chapter VI. Improving MS identification of low molecular weight proteins in complex samples ……185

Chapter VII. Discussion and perspectives ……209

List of Figures

Figure 1.1: Schematic representation of mammary gland architecture and breast cancer progression ……5
Figure 1.2: TGFβ in the normal mammary gland ……...6
Figure 1.3: Histological and molecular subtypes of breast cancer ……8
Figure 1.4: Fibroblast activation states ……16
Figure 1.5: CAF secretome ……19
Figure 1.6: *in vitro* and *ex vivo* models used in cancer research ……...23
Figure 2.1: Optimization for tumor cell spheroid formation in stirred-tank culture systems ……..55
Figure 2.2: Generation of tumor cell spheroids in stirred-tank culture systems across different pathologies ……57
Figure 2.3: Characterization of H1650, BT474 and HT29 spheroid cultures in stirred-tank culture systems ……62
Figure 2.4: Characterization of heterotypic tumor co-cultures in stirred-tank culture systems ……64
Figure 2.5: Characterization of microencapsulated tumor co-cultures in stirred-tank culture systems ……67
Figure S2.1: Phase contrast microscopy of H157 cultures during aggregation phase ……...78
Figure S2.2: Culture of NSCLC cell spheroids in stirred-tank culture systems: spheroid diameter profile and cell concentration of H460, A549 and H1650 cells ……..79
Figure S2.3: Characterization of microencapsulated and non-encapsulated H1650 mono-cultures generated in stirred-tank culture systems ……..80
Figure 3.1: Schematic illustration of the experimental approach – *in vitro* reconstruction of tumour microenvironment in stirred-tank culture systems …94
Figure 3.2: Phenotypic characterization of microencapsulated mono and co-cultures ……..96
Figure 3.3: Collagen accumulation within the stromal compartment ……..97

Figure 3.4: Phenotypic characterization of long-term (up to 15 days) mono and co-cultures ……..99
Figure 3.5: Molecular characterization of ER and E-cadherin in long-term (day 15) mono and co-cultures ……..101
Figure 3.6: Characterization of the inflammatory environment and angiogenic potential of tumour aggregates in co-cultures ……..102
Figure S3.1: Phenotypic characterization of microencapsulated and non-microencapsulated mono-cultures, at day 5 ……113
Figure S3.2: Phenotypic characterization of microencapsulated and non-microencapsulated mono-cultures, at day 15 ……113
Figure S3.3: Characterization of the inflammatory environment in microencapsulated mono-cultures of fibroblasts ……...114
Figure S3.4: Characterization of the CAM ……115
Figure 4.1: The PREDECT 2D/3D model workflow ……..128
Figure 4.2: MCF7 breast cancer model characterization using fluorescence-based growth curves ……..130
Figure 4.3: Fluorescence-based growth curves of MCF7 breast cancer models treated with Fulvestrant or Docetaxel ……..132
Figure 4.4: *in situ* image analysis & quantification of 3D models ……135
Figure 4.5: IHC analysis of breast samples ……...138
Figure 5.1: Schematic illustration of the experimental approach ……168
Figure 5.2: Characterization of the collected tumour samples ……170
Figure 5.3: Evaluation of encapsulated explants viability and phenotype after 30 days in culture ……172
Figure 5.4: Characterization of encapsulated explants after 30 days in culture ……173
Figure 5.5: Characterization of encapsulated explants after Fulvestrant treatment ……...175
Figure S5.1: Phenotypic characterization of alginate encapsulated human breast explant cultures ……..183

Figure 6.1: Secretome analysis of 10% FBS-containing culture medium conditioned by human dermal fibroblast ……195
Figure 6.2: Proteins identified in fibroblast conditioned medium after sample decomplexation by fractionation methods ……..197
Figure 6.3: IPA analysis of the low molecular weight proteins identified ……199
Figure S6.1: SDS-PAGE of the conditions tested for optimization of bovine serum albumin (BSA) removal ……..206
Figure S6.2: Albumin peptides identified by MS-based techniques, after sample decomplexation by 4 different strategies ……...207

List of Tables

Table S3.1: Antibodies used for Immunodetection ……...116
Table 4.1: Cell lines, type, origin, label ……147
Table 4.2: Experimental cell culture conditions ……147
Table 4.3: Overview of platforms with strengths/weaknesses & suggested applications ……148
Table 5.1: Conditions used for immunohistochemistry analysis ……162
Table 5.2: Clinico-pathological parameters of the human breast cancer samples received ……...167

List of abbreviations

2D	Two dimensional
3D	Three dimensional
AF1 domain	Ligand-independent activation function domain 1
AF2 domain	Ligand-independent activation function domain 2
AREG	Amphiregulin
BC	Breast cancer
BM	Basement membrane
BSA	Bovine serum Albumin
CAM	Chicken embryo chorioallantoic membrane
cCK18	Caspase cleaved cytokeratin 18
CK18	Cytokeratin 18
CTGF	Connective tissue growth factor
DBD	DNA-binding domain
DCIS	Ductal carcinoma *in situ*
DCX	Cell line- derived mouse xenografts
E2	17 b-estradiol
ECM	Extracellular matrix
ECP	Extracellular proteins
EGF	Epidermal growth factor
ELISA	Enzyme-linked immunosorbent assays
EMT	Epithelial-to-mesenchymal transition
ER	Oestrogen receptor
FAFs	Fibrosis-associated fibroblasts
FDA	Fluorescein diacetate
FGF2	Fibroblast growth factor 2
GAGs	Glycosaminoglycans
GEMMs	Genetically engineered mouse models
GF	Growth factor
GLUR1	Metabotropic glutamate receptor 1
H/MTS	High/medium throughput screening

H&E	Hematoxylin & Eosin
HAP	Highly abundant proteins
HDFs	Human dermal fibroblasts
HGF	Hepatocyte growth factor
HTS	High throughput screening
ICAM1	Intercellular adhesion molecule 1
IGF	Insulin-like growth factor
IGF-1	Insulin Growth Factor -1
IHC	Immunohistochemistry
IL	Interleukin
IL-6	Interleukin 6
ISC	Intestinal stem cells
LBD	COOH-terminal ligand-binding domain
LCIS	Lobular carcinoma in situ
LMW	Low molecular weight
LOX	Lysyl-oxidase
LSF	Light-sheet fluorescence microscopy
MMPs	Matrix metalloproteases
MS	Mass spectrometry
NAF	Normal-activated fibroblasts
NSCLC	Non-Small Cell Lung Carcinoma
NTD	NH2-terminal domain
PCA	Principal Component Analysis
PCL	Polycaprolactone
PDGF	Platelet-derived growth factor
PDGF α	Platelet-derived growth factor-α
PDX	Patient- derived mouse xenografts
PEG	Poly(ethylene glycol)
pH3	Phospho-Histone H3
PLGA	Poly(lactic-glycolic acid)
PR	Progesterone receptor

RANKL	Receptor activator of nuclear factor κB ligand
RPM	Rotations per minute
RSV	Rous sarcoma virus
RT	Room temperature
SDS-PAGE	Sodium dodecyl sulphate polyacrylamide gel electrophoresis
SERDs	Selective oestrogen receptor degraders
SERMs	Selective oestrogen receptor modulators
SOC	Standard of care
TDLU	Terminal duct-lobular units
TGFβ	Transforming Growth Factor β
TIMP	Tissue inhibitors metalloproteinases
TMAs	Tissue microarrays
TNBC	Triple negative breast cancers
VEGFA	Vascular endothelial growth factor A
WB	Western Blot
YAP	Yes-protein
ZO-1	Zonula Occludens 1
α -SMA	α - smooth muscle actin

Chapter I

Introduction

Table of contents

1 Normal breast development and anatomy 3
2 Breast cancer 5
3 Histological subtypes of Breast cancer 6
4 Molecular subtypes of Breast cancer 8
4.1 Oestrogen receptor function and expression 10
4.2 Targeted therapeutic strategies for ER+ breast cancer 12
5 The tumour microenvironment 14
5.1 Fibroblasts 15
5.2 Extracellular matrix remodelling and tumour cell migration 20
6 Tumour models 22
6.1 in vivo models 22
6.2 ex vivo models 25
6.3 in vitro models 27
7 Aims and Scope of the thesis 31
8 References 33

1 Normal breast development and anatomy

The female human breast is in constant remodelling throughout life. It starts to develop before birth with the invasion of the fat pad by rudimentary ductal structures. Post-Nataly, the gland continues developing in 2 phases: ductal growth and early alveolar development, which occur mainly during the oestrous cycles in puberty. Breast development achieves full maturity and function during pregnancy and lactation. At this stage, the mammary gland goes through cycles of proliferation and differentiation, where the terminal duct-lobular units (TDLU) invade the fat pad and then undergo differentiation and polarization with formation of the secretory alveoli [7]. After the lactation period, the involution process starts with regression of the ducts formed during pregnancy and lactation. Epithelial cells die by apoptosis and are cleared by macrophages and by surviving mammary epithelial cells. Along both processes, the extracellular matrix (ECM) is highly remodelled. During the proliferative phase, ECM is degraded to create space for the growing epithelial structures; whilst in the involution phase, ECM is synthesized and accumulated in the space left by the dying ducts [8,9].

The terminal ducts are formed by a monolayer of secretory luminal cells, polarized on top of a monolayer of myoepithelial cells, that lie on a basement membrane (BM) (Figure 1.1). This membrane physically separates epithelial and stromal compartments and mediates paracrine communication through soluble factors [10-12]. The stromal compartment is mostly composed of adipocytes, fibroblasts, immune cells and a network of blood and lymph vessels [13]. All these cells are embedded in the ECM which is mostly composed of glycosaminoglycans, collagen, fibronectin, elastin and laminin [10]. The BM is secreted by myoepithelial cells and is mostly composed of collagen IV, laminins -111, -332, and -521, and proteoglycans [10,14]. The myoepithelial cells are contractile cells that form a non-contiguous mesh on top of the BM and are responsible for the milk flow from the lobules towards the nipple. Myoepithelial cells are positive for Cytokeratins (CKs) 5 and 14, p63 and α-smooth muscle actin [15]. In contrast with the myoepithelial layer, the luminal layer is formed

by a mono-layer of polarized contiguous luminal cells with strong cell-cell adhesions, mainly through E-cadherin. Apico-basal polarity is established by interactions between β1-integrin from luminal cells and the laminin in the BM [16]. These cells can be distinguished by the expression CKs 8, 18 and 19, [15]. Around 10% of luminal cells are also positive for the nuclear hormone receptors: Oestrogen and Progesterone (ER and PR, respectively). Communication between hormone receptor positive and negative luminal cells is essential for the breast morphogenesis [17]. In healthy tissues, when ER is activated, ER^+ cells initiate the paracrine signalling cascade to trigger proliferation of ER^- cells [17,18]. This signal is often blocked by TGFβ, whose function is to differentially restrict luminal cells from responding to the hormonal proliferative stimulus [19,20] (Figure 1.2). With this restriction, it is possible to observe proliferative and non-proliferative adjacent regions during breast proliferation periods. Additionally, TGFβ also regulates breast morphogenesis through induction of apoptosis and ECM remodelling [21].

The tight regulation of the frequent breast remodelling and hormone stimulation is a major determinant to avoid the appearance of breast lesions that potentially degenerate into many types of breast cancer.

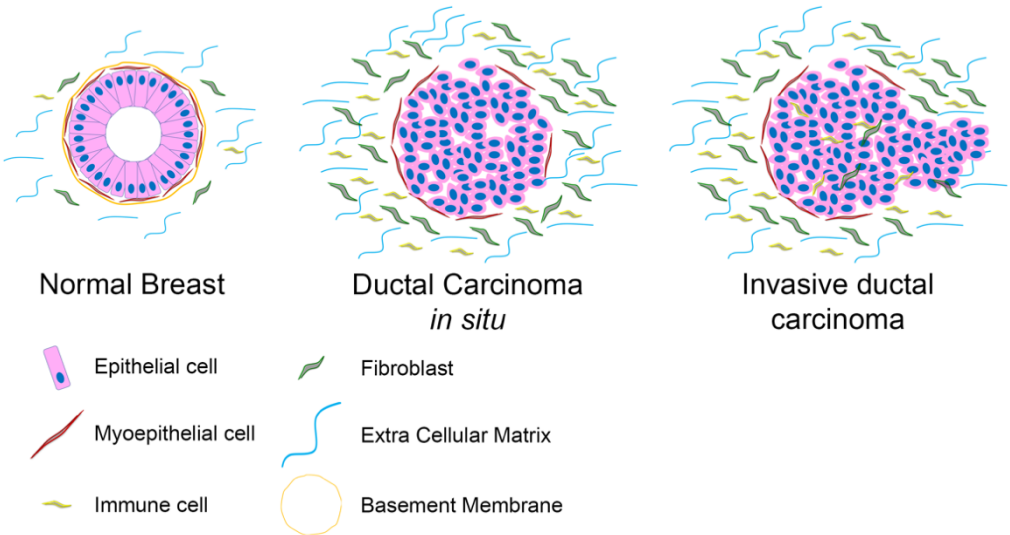

Figure 1.1: Schematic representation of mammary gland architecture and breast cancer progression. Normal breast epithelium is composed by a contiguous monolayer of luminal cells that lay on top of a non-contiguous mesh of myoepithelial cells. The basement membrane (BM) physically separates epithelial and stromal compartments and mediates paracrine communication through soluble factors. The stromal compartment is composed by a network of fibroblasts, immune cells, adipocytes and extracellular matrix (ECM) components. Ductal carcinoma *in situ* is characterized by increased cell proliferation, resulting in filling of the ductal cavity. In invasive ductal carcinoma, the BM is disrupted and tumour cells invade the stromal space, establishing direct contacts with stromal cells and with the surrounding ECM. Adapted from [6].

2 Breast cancer

Cancer is one of the leading causes of morbidity and death worldwide. According to WHO, in 2015, cancer was responsible for 8.8 million deaths and the number of new cases is expected to increase 70% in the next two decades. Amongst all cancers, breast cancer is the most prevalent and deadly in women [1]. In an attempt to cure cancer, many advances have been made in the diagnostic tools and on the development of new targeted drug treatments.

Many of these advances were possible due to the discovery of molecular pathways in tumour cells and on their interaction with the microenvironment [2]. This resulted in earlier diagnosis with a better prognosis and more efficient targeted therapies with reduced side effects [3]. Nonetheless, there is still a very high rate of disease relapse, metastatic behaviour and drug resistance, that together contribute for the high morbidity and mortality indexes of this disease [4,5].

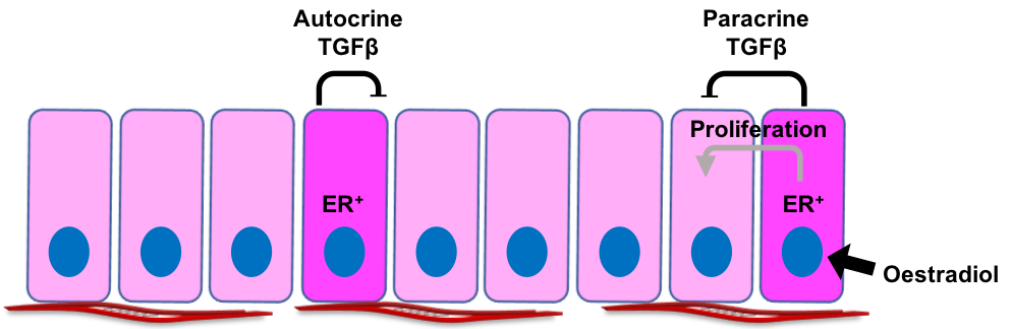

Figure 1.2: TGFβ in the normal mammary gland. TGFβ is an autocrine and paracrine regulator of human mammary epithelial cell proliferation, triggered by ER activation. Adapted from [21].

3 Histological subtypes of Breast cancer

Breast cancer is a heterogeneous disease with many types of biological features and clinical behaviours. Most breast cancers originate from the TDLU, despite their histological subtype [22]. Histological subtypes are defined based on the growth pattern of tumours. Based on the histologic type, breast cancers can be classified as breast carcinomas *in situ* or invasive carcinomas. Breast carcinomas *in situ*, refers to tumours with cell growth restricted to the acinar structures. These include ductal carcinoma *in situ* (DCIS) and lobular carcinoma *in situ* (LCIS). The main difference between these two types is the growth architecture of the tumour, as DCIS are typically well differentiated tumours with cohesive cell-cell adhesions; whilst LCIS present a different morphology with loose epithelial cell-cell adhesions and lack of E-cadherin expression [23]. Based on architectural features, DCIS can be further divided

into comedo, cribiform, micropapillary, papillary and solid [3]. Invasive carcinomas are characterized by tumour cell outgrowth from the ducts with invasion of the surrounding stroma. These include invasive lobular, ductal lobular, tubular, medullary, papillary, mucinous or colloid, and infiltrating ductal [3]. The latter represents around 80% of all invasive lesions and can be further classified according with the differentiation level and mitotic index into grade 1, 2 or 3, being 3 the less differentiated and more aggressive [3,22]. Breast carcinomas with specific histological subtypes only account for 25% of all breast carcinomas. The remaining majority are invasive ductal carcinomas of no special type or not otherwise specified [22,24]. Due to the low incidence of the special types and the lack of robust diagnostic tools, this information is often not determinant for therapy decisions [22]. Instead, the identification of the molecular markers ER, PR, Human Epithermal Growth Factor Receptor 2 (Her2) and the proliferation marker KI67, are determinant for therapy decisions. According to these markers, breast cancers can be divided into molecular subtypes. Although some histological subtypes are exclusive to a molecular subtype, others belong to several molecular subtypes, as illustrated in Figure 1.3 [22].

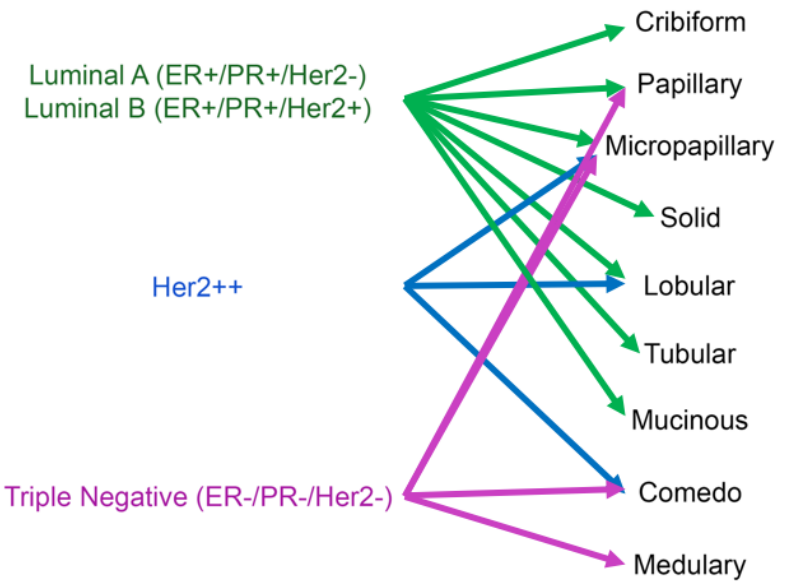

Figure 1.3: Histological and molecular subtypes of breast cancer. The histological subtypes of breast cancer can be exclusive of a molecular subtype, or present characteristics typical of several molecular subtypes. Cribiform, Papillary, Micropapillary, Solid, Lobular, Tubular and Mucinous belong to the luminal subtype; Micropapillary, Lobular and Comedo can present characteristics of Her2++ subtype; Papillary, Micropapillary, Comedo and Medulary also belong to the triple negative subtype. Adapted from [22,23].

4 Molecular subtypes of Breast cancer

The 5 molecular profiles were established by gene expression analysis of a cohort of breast carcinomas, before and after chemotherapy [25,26]. In these studies, 550 genes were identified as reflecting the phenotype of individual tumours. Hierarchical clustering divided tumours in normal-like, as gene expression was very similar to normal breast tissue samples, and two other main clusters: the ER^+ and the ER^-. The ER^- cluster was divided into 2 subgroups: the Her2 enriched and the triple negative breast cancers. Her2 enriched carcinomas account for 10-15% of all breast carcinomas and show increased expression of the receptor tyrosine kinase – Her2 – mostly due to

increased copy number of the Her2 gene [24]. Triple negative breast cancers (TNBC) are negative for the three molecular markers ER, PR and Her2. These tumours are also known as basal-like breast cancers, as cells typically express CKs that are usually detected in myoepithelial or basal epithelial cells, such as CK5 and 14. Basal-like and $Her2^+$ carcinomas, present high proliferation rates and account for 30% of all BC [23]. Patients with this type of carcinomas have the worse prognosis, since there are no targeted therapies available [27] and there is a 40% chance of relapse 5 years after diagnosis [24]. This group is the one presenting the higher intrinsic diversity between patients. Several authors have further segmented TNBC into 4 subgroups: two basal-like with distinct immune responses; 1 mesenchymal; and 1 luminal androgen receptor subtype [28-32].

Of all breast carcinomas, ER^+ are the most prevalent, accounting for two thirds of all breast carcinomas [33]. Cells from ER^+ breast cancers present characteristics typical of luminal cells, such as CK8, 18 and 19, which led to their nomenclature as luminal tumours. These tumours are further divided into luminal A and luminal B. The last presents higher expression of the genes involved in cell proliferation and mitosis [24], which results in higher proliferative indexes (KI67 > 14%). Luminal B can be positive or negative for Her2, are high grade and have a worse prognosis than Luminal A tumours. Luminal A are the most prevalent breast cancers, have low proliferative index (KI67 < 14%), are low grade and have a good prognosis [23]. Most patients with Luminal A tumours have a good response to endocrine therapies, mainly targeting ER. However, many patients develop resistance to these drugs and relapse with incurable metastatic disease [4,5]. Typically, luminal A tumours metastasize to the bone at a very early stage but remain dormant for 5 to 10 years after diagnosis. The mechanisms behind metastization, dormancy and awakening are still under debate, although it is described that immunosurveillance, stromal interactions and angiogenic initiation are triggers to metastatic growth [34].

Further stratification can be performed by Integrative Clustering. This analysis led to the identification of 10 different clusters, based on the

combination of the genomic copy number drivers, gene expression and DNA copy number alterations [24]. However, due to the costs associated with this deep clustering analysis, routine histopathological analysis is performed by immunohistochemistry (IHC) staining against ER, PR, Her2 and KI67 [24]. This technique allows the visual evaluation of the sample and semi-quantification of the number and intensity of the stained cells. However, inter-observer variation is still high. KI67 is assessed mostly because ER^+ patients with higher mitotic index can be treated with adjuvant chemotherapy, in combination with the endocrine therapies [24].

4.1 Oestrogen receptor function and expression

Most of ER^+ breast cancers are treated with endocrine therapies that target either ER or 17 b-estradiol (E2) synthesis. In pre-menopausal woman, E2 is synthesized mainly in the ovaries. On the contrary, in post-menopausal woman, E2 is produced through the conversion of testosterone and androtenedione by aromatase enzymes in extragonadal sites, such as the breast, brain and adipose tissue [35]. E2 is disseminated through the body, activating the ER via paracrine signalling.

The effects of oestrogen can be mediated by two ER subtypes, ERα and ERβ, with different transcriptional activities in different tissues. ERα is expressed in the breast, uterus, prostate stroma, ovarian stroma, Leydig cells in the testes, endometrium, liver and bone; whilst ERβ is expressed in the prostate epithelium, testes, ovarian granulosa cells, bone marrow, brain and bone [36,37]. Typically, the two isoforms present antagonizing effects [35,38].

ER has 3 functional domains: the NH2-terminal domain (NTD), the DNA-binding domain (DBD) and the COOH-terminal ligand-binding domain (LBD). The NTD has 16% similarity between α and β and is a ligand-independent activation function domain 1 (AF1) that functions as a transcriptional activator of target genes. The DBD is highly conserved between α and β (97% homology) and mediates sequence specific binding of ERs to DNA sequences in target genes, the oestrogen responsive elements. Finally, the LBD has only 59% of

sequence similarity between α and β, and contains the ligand-dependent activation domain 2 (AF2) [17,35].

In the breast epithelium, ERα action can either be genomic or non-genomic if localized at the cytoplasm or at the cell membrane, respectively [17]. Membrane bound ERα are monomers that form homodimers in response to estrogenic compounds. ER homodimers rapidly associate with and activate Gα and Gβɣ proteins, to further activate their downstream effectors: proximal kinases (Src and PI3K) and distal kinases (ERK and AKT) [39-41]. This cascade leads to phosphorylation of many proteins that are involved in cell migration, survival and proliferation, and also modulate gene transcription [40]. The activation of membrane ER can also lead to trans-activation of growth factor receptors, such as Her2, Epidermal Growth Factor Receptor (EGFR) and Insulin-like Growth Factor 1 Receptor (IGF – 1R) [42].

The genomic action of ERα is activated when oestrogen diffuses through the cell membrane, binds cytoplasmic ERα and causes the release of heat shock proteins from the ER, allowing it do dimerize and to be translocated into the nuclei [43]. When in the nuclei, ER leads to the up regulation of several target genes, such as PR, gene regulated by oestrogen in breast cancer 1 (GREB1), BCL2, Cyclin D1 (CCND1) and amphiregulin (AREG) [17,39,42,44-48]. These genes are involved in the regulation of many complex physiological processes, such as modulation of reproductive organ development, bone modelling, cardiovascular system function, metabolism and behaviour [37].

In cancerous states, most of ER control mechanisms are dysregulated. For instance, TGFβ control is often bypassed and not only ER^+ cells become resistant to TGFβ, but also, TGFβ becomes a promoter of ER^+ cell proliferation [21]. This was demonstrated by the increased co-localization of ER and KI67, which was not observed in healthy breast tissue [42]. The overexpression of TGFβ, mostly by stromal cells, also promotes matrix remodelling, Epithelial-to-mesenchymal transition (EMT), induction of angiogenesis and an immune-suppressive environment, through recruitment of myeloid immune suppressor cells, which contribute to tumour progression and metastasis [21]. Moreover,

not only the control mechanisms of ER signalling are dysregulated, but also ER protein levels are altered. These alterations can be related to reduced degradation of ERα protein, caused by alterations in ubiquitination and proteasomal pathways; or by upregulation of ER gene expression, due to increased promoter activity of the ERα gene (ESR1) or amplification of ESR1 [42]. In addition, the factors involved in mediating ER transcriptional activity, such as GATA-3 and FOXA1, are also upregulated [42].

As ER is the crucial mediator of all the described dysregulated mechanisms observed in ER^+ breast cancers, it became obvious that the most effective strategy to treat this type of cancer should be through blockage of ER activation and function. This was accomplished with targeted endocrine therapies.

4.2 Targeted therapeutic strategies for ER+ breast cancer

In an attempt to modulate ER activity, several endocrine therapies have been developed, such as aromatase inhibitors, selective oestrogen receptor modulators (SERMs) and selective oestrogen receptor degraders (SERDs) [35,49].

Aromatase inhibitors are the front-line treatment for post-menopausal women due to the successful decrease of E2 levels in these women [50,51]. These include anastrozole, letrozole and exemestane [35]. When compared to tamoxifen, these inhibitors reduced the relapse rates by 30%, which makes them a good complementary therapy to SERMs [50,52] .

SERMs include tamoxifen, raloxifen and toremifene. Tamoxifen blocks ER activity by binding to the AF2 domain. It is the most effective and widely used anti-hormonal therapy but only 70% of the patients respond to therapy, among which 30-40% relapse and become resistant. In addition, tamoxifen has a dual function, as it acts as ER antagonist in the breast but also as an ER agonist in other tissues, like the bone, endometrium and cardiovascular system, thus having severe side effects [35]. For instance, patients under long-term

treatment with Tamoxifen present higher risk of developing endometrial cancer [43,53].

In contrast, Fulvestrant, is considered a SERD and is a pure ER antagonist. Fulvestrant binds to both AF1 and AF2, with a very high affinity (89% compared E2) when compared to tamoxifen (2.5% compared to E2) [54]. When bound to ER, Fulvestrant blocks ER transcriptional activity by blocking nuclear translocation; and induces receptor conformational alterations that impair receptor dimerization and trigger proteasomal degradation, resulting in the reduction of ER protein levels [46,55]. Nonetheless, Fulvestrant formulation is very hard to administer (500 mg/month by a 5 mL intramuscular injection) [52,53] and presents several side effects, such as bone pain (13.9%), nausea (10.9%), arthralgia (9.9%), constipation (9.9%), vomiting (8.9%) and dyspnea (8.9%) [56]. In addition, the prolonged blockage of ER leads to bone loss due to increased bone degradation. Oestrogen is described to promote bone formation and inhibit bone resorption [53]. More specifically, oestrogen stimulates proliferation of the bone producer cells – osteoblasts, inhibits their apoptosis through upregulation of Bcl-2, and represses pro-osteoclastic cytokine production, by T-cells and osteoblasts [36]. Moreover, it also stimulates the production of osteoprotegrin by osteoblasts, in order to block receptor activator of nuclear factor κB ligand (RANKL) action on bone resorption by osteoclasts [36,53]. The imbalance of bone turnover creates an environment favourable for metastasis. This means that prolonged ER blockage by Fulvestrant, might significantly increase the risk for bone metastasis and cancer progression [57].

Many factors involved in cancer progression, *de novo* resistance and metastasis are promoted by the surrounding tumour microenvironment. Along tumour development, tumour and stromal cells reciprocally interact through autocrine and paracrine mechanisms, towards tumour progression [58].

5 The tumour microenvironment

The breast microenvironment is composed of various cell types, including fibroblasts, adipocytes, endothelial and immune cells and a network of blood and lymph vessels all embedded in the interstitial ECM (Figure 1.1).

During tumour initiation and progression, the microenvironment suffers numerous alterations. The presence of tumour cells induces injury on the healthy tissue, which leads to the recruitment of cells needed for the wound healing process, such as fibroblasts and immune cells. Together, these cells try to re-equilibrate tissue homeostasis and architecture, by restraining and destroying tumour cells [2]. This was firstly demonstrated in the 80s, by David Dolberg and Mina Bissel, when injecting Rous sarcoma virus (RSV) in an embryo chicken wing. This virus was already known to induce oncogenic transformation on chicken wings but the chicken embryo microenvironment was able to suppress tumour initiation. However, tumour suppression only lasted a limited time, after which the stroma itself started to accumulate damage [59]. Alterations in the stroma included recruitment of fibroblasts and immune cells, from both innate and adaptive immune system, matrix remodelling and vasculature formation. A typical correlation on how stromal damage promotes tumour initiation is the fibrotic stroma and liver cancer [60]. The same can be observed in breast tumours, which have increased stromal density [2]. Stromal alterations lead to loss of tissue homeostasis and epithelial architecture, including loss of apico-basal cell polarity, alterations in cell shape (atypia) and increased cell proliferation, resulting in filling of the ductal cavity [2] (Figure 1.1). At this stage, DCIS is established in the mammary gland, and the surrounding microenvironment is permissive to tumour progression: stromal cells are continuously recruited, blood and lymph vessels are forming and ECM is remodelled. Next, the BM membrane is disrupted and epithelial tumour cells establish direct contacts with stromal cells and the surrounding ECM, mainly through type I collagen and fibronectin [2]. These interactions together with the increased secretion of growth factors and inflammatory molecules, such as TGFβ, IL8 or IL6; the release of ECM bound growth factors and cytokines, like

TGFβ; the increase in matrix stiffness and fibre alignment, altogether, promote invasion and metastasis [61]. These processes can occur through epithelial-to-mesenchymal transition (EMT) (single cell invasion) or collective migration (invasion in cell clusters) [58].

In the breast cancer microenvironment, fibroblasts are the most prominent cell type and a major determinant for tumour progression [58].

5.1 Fibroblasts

Fibroblasts are the main component of connective tissues and play a critical role in maintaining tissue homeostasis [10,62,63]. These cells have a mesenchymal origin and are responsible for the production and maintenance of the ECM [61,64]. Fibroblasts can undergo 3 different activation states (Figure 1.4), that can either be reversible or irreversible. In healthy tissues, fibroblasts are in a resting or quiescent state where they present a spindle-like shape. In response to tissue injury, fibroblasts are reversibly activated into normal-activated fibroblasts (NAF) and acquire a stellate shape, start expressing α -smooth muscle actin (α -SMA) and vimentin, and gain contractile properties. Upon chronic injury, such as cancer, fibroblasts become hyper-activated into an irreversible state where they are typically called cancer-associated fibroblasts (CAF) [61].

In normal tissues, injury can be caused by mechanical trauma, radiation or extreme temperatures, toxins, pathogens or metabolic deregulations. When injury response is unleashed, a wound healing response is induced leading to inflammation, and consequent recruitment of immune cells and fibroblasts, that promote angiogenesis and ECM remodelling [65]. The remodelling of ECM includes production of collagen I, III, IV and V, laminins and fibronectin together with matrix- metalloproteinases (MMPs) to ensure ECM turnover. At this stage, fibroblasts present a secretory phenotype towards a pro-inflammatory state. When the healing process is completed, the number of activated fibroblasts decreases, by apoptosis, and the remaining fibroblasts are reprogrammed into the initial resting phenotype [61].

Chronic wound healing occurs with wounds that never complete the healing process, such as, chronic physical, toxic, metabolic injuries, autoimmune diseases and cancer. The continuous repair activation causes epigenetic alterations in fibroblasts, leading to hyper-activated fibroblasts with increased proliferation indexes and anti-apoptotic activity. This state results in a pathologic ECM remodelling and tissue fibrosis, that can stimulate cancer initiation [2,66].

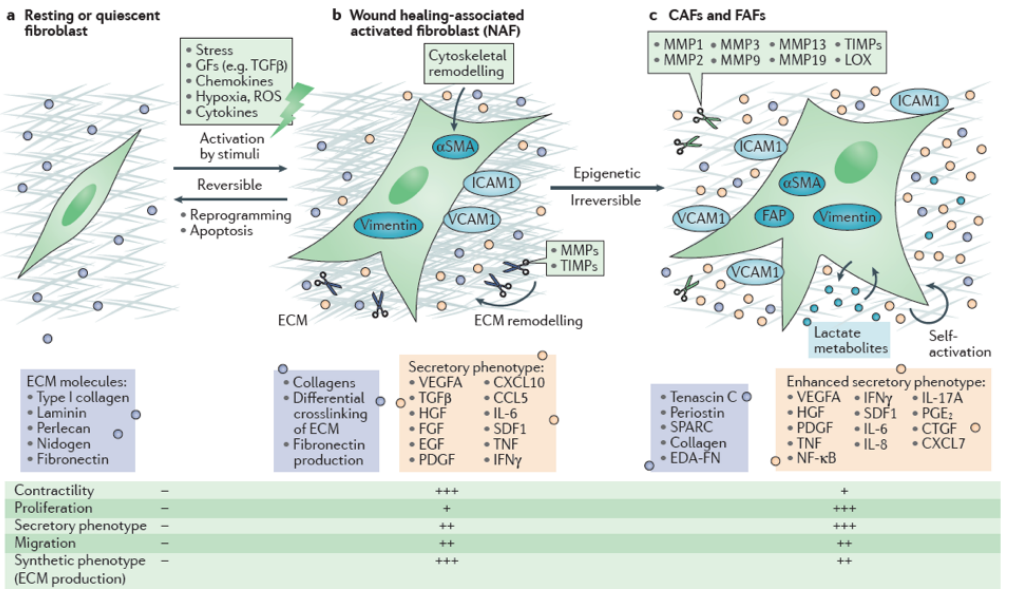

Figure 1.4: Fibroblast activation states. A) Resting or quiescent fibroblasts are embedded in the extracellular matrix (ECM) molecules, spindle-shaped in an inert state. B) When injury response is unleashed, a wound healing response is induced leading to fibroblast activation resulting in inflammation, and consequent recruitment of immune cells and additional fibroblasts, that promote angiogenesis and ECM remodelling. The remodelling of ECM includes production of collagen I, III, IV and V, laminins and fibronectin together with matrix- metalloproteinases (MMPs) to ensure ECM turnover. Fibroblasts present a secretory phenotype towards a pro-inflammatory state. When the healing process is completed, the number of activated fibroblasts decreases, by apoptosis, and the remaining fibroblasts are reprogrammed into the initial quiescent phenotype. C) Chronic wound healing leads to continuous repair activation causing epigenetic alterations in fibroblasts, leading to hyper-activated fibroblasts – fibrosis-associated fibroblasts (FAFs) or cancer-associated fibroblasts

(CAFs) that present increased proliferation indexes, anti-apoptotic activity and immunomodulatory signalling. This state results in a pathologic ECM remodelling and tissue fibrosis, that can stimulate cancer initiation. CCL5, C-C motif chemokine ligand 5 (also known as RANTES); CTGF, connective tissue growth factor; CXCL, CXC motif chemokine ligand; EDA-FN, extradomain A-fibronectin; EGF, epidermal growth factor; FAP, fibroblast activation protein; FGF, fibroblast growth factor; GFs, growth factors; HGF, hepatocyte growth factor; ICAM1, intercellular adhesion molecule 1; IFNγ, interferon γ; IL, interleukin; LOX, lysyl oxidase; MMP, matrix metalloproteinase; NF κB, nuclear factor κB; PDGF, platelet-derived growth factor; PGE2, prostaglandin E2; ROS, reactive oxygen species; SDF1, stromal cell-derived factor 1; TGFβ, transforming growth factor-β; TIMPs, tissue inhibitors of metalloproteinases; TNF, tumour necrosis factor; VEGFA, vascular endothelial growth factor A; VCAM1, vascular adhesion molecule 1. From [61].

Tumour initiation and progression causes extreme damage on healthy tissue, generating a permanent healing process [67]. Fibroblasts are recruited by the growth factors released by tumour cells and by infiltrated immune cells, such as TGFβ. Although the origin of CAFs is still under debate, it is now accepted that these might originate from mesenchymal stem cells, from tumour epithelial cells that underwent EMT, or from resident fibroblasts, that became hyper-activated [68]. In this last scenario, fibroblast activation can be mediated by soluble factors, such as TGFβ, Platelet-derived growth factor (PDGF) and fibroblast growth factor 2 (FGF2) [61,66] . Interestingly, TGFβ effect varies greatly with the context. For instance, during healthy breast remodelling, this molecule contributes to the regulation of tissue homeostasis, through tight control of cell proliferation and apoptosis [17]. However, during tumour progression, TGFβ concentration is much higher than on healthy tissues, as it is produced by tumour cells, CAFs, macrophages and released from the ECM by MMP cleavage [2,69]. As a result, in cancerous states, TGFβ becomes one of the major contributors for tumour cell proliferation, CAF activation and immunomodulation [2,68,70].

Once activated, CAFs are able to induce tumour growth and progression in many ways (Figure 1.5). One example is the contribution of CAFs to endocrine therapy resistance. It is known that CAFs are not only able to secrete oestradiol, that stimulates ER^+ breast cancer cell growth, but also modulate tamoxifen resistance through activation of the PI3K/Akt and MAPK/ERK 1/2 signalling pathways [68]. This was demonstrated by culturing an ER^+ breast cancer cell line with conditioned media obtained from CAFs. In this study, the soluble factors secreted by CAFs activated EGFR which led to the activation of the PI3K/AKT signalling pathways. In addition, the increased production of fibronectin by CAFs, also activated PI3K/AKT and MAPK/ERK 1/2 signalling pathways, through binding to β1-integrin in tumour cells [71]. Activation of these pathways leads to ERα activation through phosphorylation of serine-118 [72] located in the AF-1 domain of the receptor [73], which ultimately contributes to endocrine resistance.

In addition, CAFs also promote angiogenesis and control matrix remodelling through secretion of ECM proteins, such as type I collagen and fibronectin, and production of ECM degrading proteases, such as MMPs (Figure 1.5). These facilitate cell motility [66], and cause the release of ECM-bound growth factors and cytokines, promoting invasion and metastasis [61,64,66].

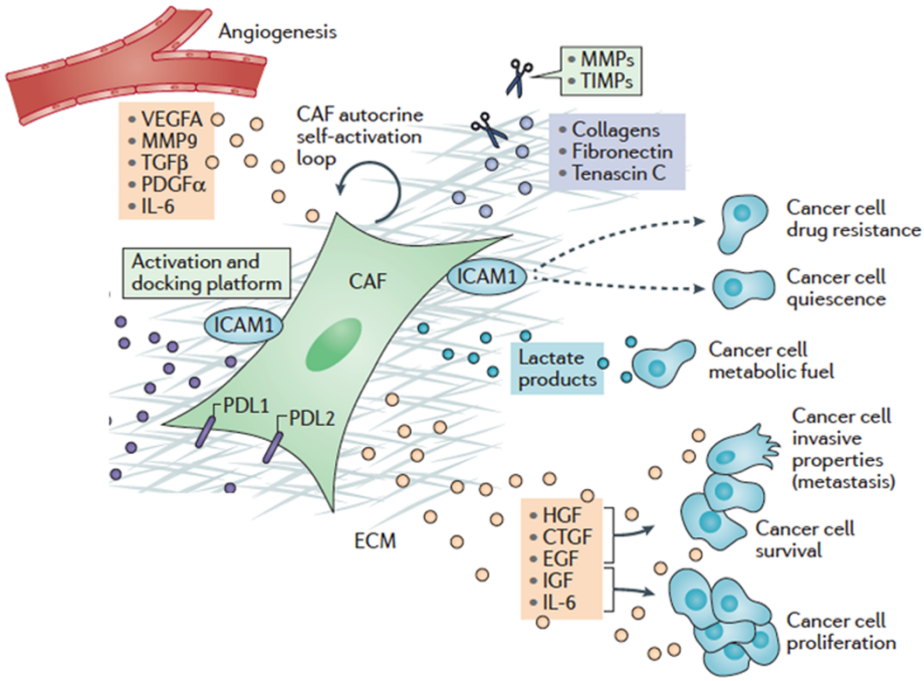

Figure 1.5: CAF secretome. CAF secretome modulates cancer cell phenotype (right) at many levels: metabolism, drug resistance, quiescence, invasive properties, survival and proliferation. Although the molecules responsible for this modulation are not fully elucidated, some were already described: Intercellular adhesion molecule 1 (ICAM1), hepatocyte growth factor (HGF), connective tissue growth factor (CTGF), epidermal growth factor (EGF), insulin-like growth factor (IGF), Interleukin 6 (IL-6), lactate, amongst others. CAFs secretome also leads to dysregulation of the ECM composition, structure and stiffness through secretion of extracellular matrix (ECM) molecules (collagens, fibronectin, tenastin, laminins) and matrix degrader enzymes - matrix metalloproteases (MMPs), adamalysins, meprins and tissue inhibitors metalloproteinases (TIMP). Angiogenesis is also induced by CAFs (top), through the secretion of vascular endothelial growth factor A (VEGFA), MMP9, Transforming Growth Factor β (TGFβ), platelet-derived growth factor-α (PDGF α) and IL6. Adapted from [61].

5.2 Extracellular matrix remodelling and tumour cell migration

The ECM is present in most connective tissues. Its main functions are to provide structural support to tissues and to control tissue homeostasis, by providing signals that maintain the tissue architecture and control cell polarity, proliferation, migration, differentiation and apoptosis [74].

As mentioned above, fibroblasts are the main producers of ECM macromolecules, which can be divided in two main classes: glycosaminoglycans (GAGs) and fibrous proteins. GAGs are glycoproteins (hyaluronan and proteoglycans), negatively charged and covalently linked [10,75] . The fibrous proteins include collagen, elastin, fibronectin and laminins, which have structural and adhesive functions. The ECM surrounds cells providing structural scaffolding and protection from compressive forces. The mechanical strength is mainly provided through fibrous collagen type I, the most abundant component of the ECM in most tissues (approximately 90%), and fibronectin [75]. Cells interact with ECM molecules through different integrins: α2β1 integrin interacts with fibrillar collagen; αVβ3, αVβ1 and α5β1 bind to fibronectin; and α3β1 and α6β1 with laminin [58]. In addition, the extracellular matrix is a natural reservoir of cytokines and soluble factors, that are released upon matrix degradation [74,75].

During tumour progression, the reciprocal interactions between tumour cells and CAFs lead to secretome alterations of both cell types. For instance, CAFs increase collagen production leading to augmented collagen density. This increase causes alterations of the ECM physico-chemical characteristics, such as, stiffness, pore size, fibre organization, adhesive ligand density, binding side presentation, and accumulation and release of autocrine and paracrine signalling molecules that are retained in the ECM. Together, the alteration of these parameters, influences gene expression, cancer motility and differentiation [76]. Although this is well established, there is no consensus onto which parameter causes a specific tumour cell alteration [77]. Most authors claim that increased collagen stiffness promotes secretion of MMPs that together with the collagen cross-linking enzymes, such as lysyl-oxidase (LOX),

degrade and reorganize fibre alignment to facilitate cell motility [75]. It is also described that BC cells seeded in a dense collagen environment, are first trapped but after 1 division cycle, gained highly invasive characteristics and moved in a MMP-dependent manner. In contrast, in a less dense collagen matrix, migration was kept constant before and after cell division, and was MMP-independent [76,77]. Moreover, it was recently demonstrated that increased collagen density but not collagen stiffness promoted transdifferentiation of breast cancer cells towards a cancer phenotype known as Vasculogenic mimicry, which was mediated by β1-integrin [76]. Nonetheless, another study proved that increasing the matrix stiffness but not the amount of ligand accessibility nor pore size, promoted a malignant phenotype in pre-malignant breast epithelial cells [78]. Due to the contradictory results, it is hard to draw conclusions since each study is performed with different cell sources and matrix compositions: the first uses pure collagen while the second uses a matrigel-alginate mix. Nevertheless, all these studies demonstrate that the combination of oncogenic transformation with an altered stromal space - cell and ECM composition, promote tumour progression and cell dissemination.

Early cell dissemination can also occur independently of stromal transformation, as it was described for Her2+ breast cancers. One of these studies claims that Her2+ activation promotes EMT without complete loss of the epithelial phenotype, which led to early cell dissemination [79]. Another study, corroborated the need for HER2 activation but also showed that cells from early stage, low density regions presented a stem phenotype, migrated more and created more metastasis, compared to cells from high density matrix regions. Moreover, this process was accompanied by downregulation of the progesterone receptor [80].

It is the concerted action of all these factors that makes cancer an extremely complex and unpredictable group of diseases. It is urgent that future studies take into account the complexity of oncogenic transformation and the reciprocal interactions that it has with the surrounding tumour

microenvironment. To accomplish that, several *in vivo*, *ex vivo* and *in vitro* models should reflect the complexity observed in human tumours and be used as complementary tools.

6 Tumour models

The existing models have greatly contributed to the understanding of many molecular mechanisms underlying tumour onset and progression, which led to the development of new drugs that everyday save millions of lives. Still, most of these models do not recapitulate the heterogeneity and the complex interactions observed in human tumours nor allow long-term monitoring of disease progression events. Since each model answers specific biological questions, a step forward could be the use of multi-model systems as complementary tools, being aware of the strengths and limitations of each one.

The models used in cancer research can be divided in three categories: *in vivo*, *ex vivo* and *in vitro* model systems (Figure 1.6).

6.1 *in vivo models*

In vivo models rely mostly on mice. These can either be genetically engineered mouse models (GEMMs) or xenografts [33,81].

GEMMs are developed in immune-competent mice and are suitable models employed to study the different phases of tumour development: initiation, maintenance, progression, regression and metastatic spread of the disease [33,82]. However, there are only two available models of ER^+ breast cancers, the $Stat1^{-/-}$ and the Pik3ca-H1047R [83]. STAT-1 are transcription factors that play a major role in suppressing breast tumorigenesis. $STAT1^{-/-}$ mice develop spontaneous ER^+ tumours that recapitulate hormone responsiveness observed in human tumours. However, only a subset of ER^+ BC presents low or undetectable levels of STAT1, which means that the use of these models would allow a suitable study of this subset only [84]. Moreover, GEMMs are typically generated by inducing a specific genetic mutation that will lead to tumour onset. As a result, these tumours do not recapitulate the

heterogeneity observed in human tumours [85]. Although new GEMM models need to be developed, this has proven a very challenging task, as most GEMMs can only develop ER$^-$ breast tumours [86].

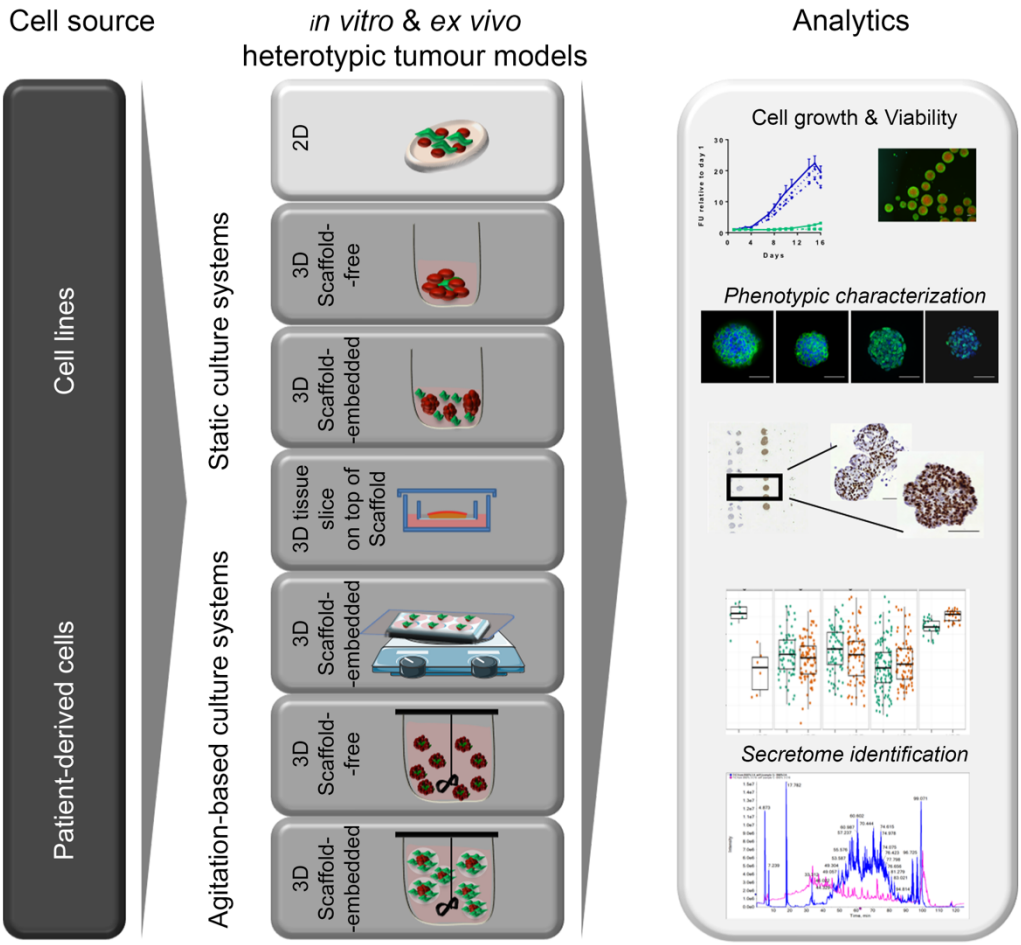

Figure 1.6: in vitro and ex vivo models used in cancer research. Tumour models are generated from cell lines and/or from patient-derived cells. Cells can be cultured in two or three dimensions (2D and 3D), in scaffold-free conditions or embedded into scaffolds, under static or stirred conditions. Assessment of cell growth and viability are methods routinely used for culture progression evaluation. Phenotypic characterization is typically performed by immunostaining methodologies and quantified by mathematical algorithms specific for image analysis. Proteome and metabolome identification by 1H-NMR are often used for an in-depth analysis of the molecular status of the culture.

Mouse xenografts can mimic the disease more accurately than GEMMs, since tumours are generated from a heterogeneous tumour cell population, and not by a single genetic mutation induced on epithelial mouse breast cells. In mouse xenografts, cells can be injected subcutaneously or orthotopically and can be derived from cell lines (CDX) or from patients (PDX). Subcutaneous xenografts have the advantage of allowing easy monitoring of the tumour growth but the engraftment occurs in a microenvironment that is completely unrelated with the organ of origin of the tumour [87]. In contrast, orthotopic xenografts of ER^+ breast cancer, are typically injected in the mammary fat pad. To do so, the fat pad of the mouse mammary gland is cleared before injection and the tumour single-cell suspension is injected in the mouse fat pad, embedded in a matrigel mixture [88]. In this system, tumour cells interact with and invade the surrounding breast stroma. However, the interaction of human BC cells with the mouse stroma does not fully recapitulate the human situation since some cytokines and growth factors produced by the mouse stroma do not interact with the human tumour cell receptors [88]. Another issue is the effect that the injection site has on tumour cell phenotype. It was demonstrated that when luminal tumour cells were injected in the mammary fat pad, the luminal characteristics were lost and cells acquired a basal-like phenotype [33]. Finally, the engraftment rate is very low (2.5%) and ER^+ tumour cells need exogenous E2 to grow. E2 dependency is a limitation of this system due to the non-physiological levels needed: serum levels are equivalent to pre-menopausal woman (100-400 pg/mL) whilst most ER^+ breast cancers develop in post-menopausal woman (E2 less than 18 pg/mL) [33]. Alternatively, tumour cells can be injected in the milk ducts: intraductal mouse model (MIND) [89] Recently, [33] characterized the MIND method to tackle some of the abovementioned limitations. In this model, tumour cells engraft in the ducts, surrounded by the luminal environment and can, at a more advanced stage, breakdown the BM and invade the stromal space into the fat pat. In this setting, engraftment rates raised to 30-100% and cells grew without E2

supplementation. Moreover, engrafted cells maintained the luminal-epithelial phenotype, typical of the ER^+ tumours, in contrast with the fat pad injections where cells gained basal-like phenotypes [33]. Nonetheless, the long time needed for engraftment and expansion of tumour cells in PDX models (at least one month), the lack of an immune system; and the exclusive presence of murine cells in the stromal compartment are major drawbacks of these models [87].

To overcome the long engraftment times in mice, zebrafish xenografts can be used as an alternative method [90]. In this model, cells engraft and grow within 4 days, in zebra-fish larvae. The zebrafish model integrates innate immunity, although not humanized, and can be used for fast short-term pre-clinical assays [91]; or to study breast cancer bone metastasis [92] or alterations in the choline metabolism of ER^+ BC [93].

6.2 *ex vivo models*

Ex vivo cultures of freshly isolated tumour samples aim to preserve the original tissue architecture and heterogeneity, and the surrounding microenvironment. There are numerous types of *ex vivo* cultures, being the most described the tissue slices and the explant cultures. In both culture settings, cells are able to maintain, for a short time (48-72h), the cell-cell communication, the hormone receptor expression and the interactions with the microenvironment [94]. However, most of these models only last for a short-time, not allowing long-term monitoring of disease progression nor interrogation of the long-term effects of drug treatments.

Typical tissue slice cultures have 200 μm thick and can be patient or PDX-derived. Tissue slices can be cultured immersed in the media or in an air-liquid interface, on top of a scaffold [94,95]. Previous studies have demonstrated that tissue slices can be cultured for at least 4 days, with good cellularity and maintenance of the original tissue architecture [94]. These authors demonstrated that culturing slices in a stirred system (approx. 150 rpm) prevents oxygen zonation, which was a limitation observed in previous studies.

Another study tried to improve the maintenance of cell viability and original tissue architecture by culturing tissue slices on an air-liquid interface, on top of a filter [95]. The physical support provided by this scaffold reduced apoptotic cell death and vacuolation. However, the static culture system used by these authors led to oxygen zonation and differential hormone receptor expression within the slice. Cells in contact with the filter were hypoxic and, consequently, became positive for HIF1α and negative for ER expression. In contrast, the normoxic region presented ER^+ cells and mouse macrophages [95]. To solve this issue, slices were cultured with intermittent immersion in the culture media. The use of this dynamic system promoted an increase of oxygen distribution homogeneity [95].

Explant cultures have been successfully implemented for both healthy and cancerous tissues. In order to maintain the cell-matrix and the cell-cell interactions between the various cell types, the isolation and culture methods had to be optimized for each tumour type. [96] demonstrated that breast explants obtained from reduction mammoplasties could be successfully cultured for 7 days in low adhesion plates [96]. In this system, cells maintained viability, the original tissue architecture, the cell-to-cell communication and hormone responsiveness. More specifically, luminal epithelial cells maintained apico-basal polarity and were surrounded by a thin layer of myoepithelial cells. Although the expression of the nuclear hormone receptors, ER and PR, decreased along the 7 days of culture, epithelial cell proliferation was detected in response to E2 stimulation. With this system, RANKL was identified as a paracrine mediator of PR in inducing cell proliferation. The maintenance of the breast architecture was key to maintain the paracrine signalling, as these mechanisms were not observed for breast cancer cell lines nor for dissociated breast tissue. This work reinforces the need to maintain the original tissue architecture to address hormone action in the breast [96]. Recently, [97] demonstrated that by culturing breast cancer explants in a perfusion-based bioreactor, prolonged the culture time to 15 days. This system allowed the maintenance of tissue integrity and cell viability, although cellularity was

decreased along the time. Moreover, hormone responsiveness was evaluated by quantification of cellularity, by H&E staining, upon prolonged Fulvestrant treatment, and no genetic alterations on ER downstream effectors were taken into account.

Up until now, there is no human-derived *ex vivo* breast cancer model system that can be used as a co-clinical tool to help predicting drug-response in a specific patient. Nonetheless, these methods have already been developed for other types of cancer. [98] developed a matrix-specific scaffold for colorectal and head and neck cancer patients, which was adapted for each tumour type and grade. The authors were able to culture the explants for 72h, with maintenance of the initial tumour phenotype. Tumour explants were cultured with the specific patient serum, to guarantee the supply of the original cytokines and growth factors. Moreover, by combining this model system with a machine learning algorithm, it was possible to predict the clinic response to specific drug treatments.

Although *ex vivo* cultures are mostly short-term, these are very useful tools for pre-clinical and co-clinical evaluation of drug response, in an environment where the tissue architecture and the tumour microenvironment are able to influence drug responses. Nonetheless, the primary material is very difficult to obtain and the result interpretation is very complex, due the inter- and intra-patient tumour heterogeneity [99]. Moreover, improvement of these methods towards extension of culture time would allow evaluation the long-term effects of drug treatments and the mechanisms of drug resistance.

6.3 *in vitro models*

In vitro model systems are developed using cell lines or dissociated primary cells that can be cultured either in two-dimensional (2D) or in three-dimensional (3D) culture systems. 2D cultures are very simple to implement, are a cheap and robust method, amenable for high throughput screening (HTS) [100]. Many ground-breaking discoveries have been made on 2D cultures such as the responsiveness of ER^+ breast cancer cells to anti-oestrogen therapies

[101]. Although cell lines in 2D culture recapitulate many molecular pathways and genetic events described *in vivo*, they also present many drawbacks. These cell models do not mimic the cell growth rates nor the cell-cell and cell-ECM interactions observed *in vivo* [94]. In contrast, 3D cultures have the potential to recapitulate the cell-cell and cell-ECM interactions and the diffusion gradients (oxygen, nutrients, metabolites, soluble factors and drugs) described in human tumours, and are also amenable for HTS [99,100].

3D cultures can be generated by many different methods, such as, magnetic levitation, bioprinting or single-cell aggregation into spheroids, by either static or agitation based systems [102,103]. The static systems include hanging drop or free-floating aggregation in ultra-low attachment plates. Agitation-based systems comprise orbital shaking, stirred-tank and rotating wall systems [104,105]. After the aggregation phase, spheroids, can be cultured as mono or co-cultures in scaffold-free conditions or embedded in scaffolds [103]. The disadvantage of not using scaffolds is the difficulty of reconstructing the tumour architecture. When breast cancer cells were co-cultured with fibroblasts in a 3D rotary bioreactor, fibroblasts formed a core which was surrounded by epithelial tumour cells [106]. Although this model was used to investigate how tumour cells invaded the inner stromal compartment, it does not resemble the *in vivo* tumour-stromal organization of early stage breast carcinomas [107]. Alternatively, scaffolds provide physical support to cells and aim to reflect the ECM. These can either be natural derived scaffolds or synthetic polymers. The synthetic polymers include polycaprolactone (PCL), poly(lactic-glycolic acid) (PLGA) or poly(ethylene glycol) (PEG). The naturally derived scaffolds can be non-inert: decellularized ECM, matrigel, collagen, gelatin; or inert: alginate, chitosan or silk fibroin [102]. Amongst the naturally derived scaffolds the most used is collagen, which is the most abundant protein in the human connective tissue and highly produced in cancerous states [102].

Heterotypic cultures are developed mostly in scaffold embedded conditions. By using these systems it is possible to recapitulate some aspects of the tumour-stromal architecture and mimic the heterotypic cell-cell crosstalk

through autocrine and paracrine signalling mechanisms and direct cell-cell interactions [108]. Most heterotypic culture systems use only two cell types due to the complexity of identifying the interactions between different cell types or the origin of the secreted factors [100]. Typically, these cultures combine tumour cells with cells present in the tumour microenvironment, such as, fibroblasts, adipocytes, macrophages, or endothelial cells [100]. One example, is the *in vitro* modulation of colon carcinoma spheroids with fibroblasts, in collagen I gels [108]. In this co-culture system, stromal cells migrated towards the tumour spheroids and, through the concerted action of paracrine signalling and direct cell-cell interactions, modulated tumour progression. Fibroblasts induced tumour cell invasive spreading, both collective and as single cells, and led to the activation of several signalling pathways, such as Ras and NFkB signalling, which are associated with more aggressive stages of the disease. However, cell behaviour is highly influenced by the type of matrix, which poses a main challenge in the choice of the correct scaffold. For instance, when mammary carcinomas were cultured in parallel either in collagen I or in matrigel, cell dissemination occurred in the collagen I gels only. Healthy mammary epithelial fragments showed similar migratory behaviour but cell migration was transient and blocked by integrin binding to newly synthesized laminin-111. In contrast, no cell dissemination was observed when the same carcinomas were cultured in matrigel [109].

Alternatively, some of the synthetic polymers also allow the interrogation of complex molecular cues. One example was the co-culture of prostate epithelial tumour cells and fibroblasts to address the effect of paracrine signalling on tumour progression. In this model, tumour and stromal cells were subjected to a dual step microencapsulation in alginate hydrogel. Tumour cells were confined in the inner compartment whilst stromal cells were in the outer compartment. Although direct epithelial-stromal interactions were not allowed, both cell types communicated through paracrine signalling, which resulted in dysregulated levels of E-cadherin in co-cultures but not in mono-cultures [110]. Another example was the triple co-culture of hepatocarcinoma spheroids with

fibroblasts and endothelial cells to investigate induction of angiogenesis. [111] conjugated a starPEG-heparin hydrogel with adhesion ligands (fibronectin and laminin), growth factors and MMP-sensitive sequences. This system supported vessel formation observed by the growth and polarization of endothelial cells into blood vessels.

Recently, organoid cultures have been proposed as an alternative method for expansion of primary human stem cells in 3D *in vitro* culture systems, followed by differentiation in the several cell lineages present in the adult tissue [85]. These stem cells can be derived from heathy or diseased patients. With this method, it became possible to modulate both organogenesis and disease, and to unravel new cellular and molecular mechanisms that have applications both in basic biology and in translational medicine [85]. The most recent organoid model was developed for primary human mammary carcinomas. The authors were able to grow organoids comprising the different BC subtypes, whilst maintaining the nuclear hormone receptors (ER and PR) and the Human Epithermal Growth Factor Receptor 2 (Her2). Although hormone responsiveness was not demonstrated nor ER expression quantified, Her2+ tumours remained sensitive to Herceptin (anti-Her2) treatments. Analysis of mutational signature, driver gene and copy number alterations, revealed that organoid cultures were comparable to the original tumour [112]. However, these cultures completely lack stromal and immune cells, which results in an incomplete maintenance of the original tissue architecture and thus, loss of the heterotypic cross-talk whose impact on tumour progression and drug response mechanisms is decisive. Another drawback of organoid cultures is the use of undefined animal-derived matrices. To tackle this issue [113] developed a method for culturing mature mammary tissues as human breast organoids by using a defined matrix . Hydrogels were composed of collagen I, hyaluronan, laminin and fibronectin, which mimic the breast ECM [113].

Another example of a fully defined matrix was designed by [114] to support the growth of intestinal organoids. This matrix was based on PEG hydrogels functionalized with adhesion molecules (fibronectin, laminin, type IV collagen,

hyaluronic acid and perclan) and substrate peptides. The binding to fibronectin motifs was enough to promote survival and proliferation of intestinal stem cells (ISC), which was further enhanced by higher matrix stiffness (1.3 kPa) in a Yes-protein (YAP)-dependent mechanism. Matrix softening (300 Pa) and enrichment with laminin-based adhesion molecules was needed to induce ISC differentiation and organoid formation. This method is a well-defined alternative for animal-derived matrices. Nonetheless, these models still lack the tumour microenvironment components.

Although many 3D models have been developed in the past decade, these are typically generated in non-scalable culture systems with poor robustness, no control of the physicochemical parameters and allowing only for end-point analysis [100,115,116]. Thus, there is an urgent need to develop scalable and highly reproducible long-term 3D human breast cancer model systems in which tumour microenvironment can be recapitulated during disease progression.

7 Aims and Scope of the thesis

The development of cell models depicting the tumour microenvironment is expected to increase the clinical translational success rates of novel therapies and help to predict the acquisition of resistance mechanisms to specific drug treatments. The main goal of this thesis was to develop and characterize new model systems for establishment and maintenance of cell-cell and cell-ECM interactions, to mimic the tumour architecture of ER^+ breast carcinomas. The focus was on cell lines and patient-derived tumour material, for generation of *in vitro* and *ex vivo* models, applicable in pre-clinical and co-clinical assays.

In this context, the first aim of this thesis was to optimize the aggregation of a panel of human carcinoma cell lines, in stirred-tank vessels to obtain cancer spheroids, by modulation of the cell inoculum, stirring rate and aggregation time. Aggregation of nine cell lines from three different pathologies: breast, lung and colon cancer, was addressed. Spheroid phenotype was evaluated in terms of spheroid size distribution, compactness, cellular organization and oxygen gradients (**Chapter 2**). The second aim was to implement a model system for

in vitro recapitulation of tumour-stromal interactions. This was pursued by combining agitation-based culture systems and cell microencapsulation in alginate hydrogel (**Chapter 2**).

The third objective was to generate an *in vitro* cell model of ER^+ breast cancer for recapitulation of the epithelial-stromal architecture described for early stage ER^+ breast carcinomas. For this, in **chapter 3**, the culture system developed was applied for co-culture of MCF-7 spheroids, an ER^+ breast cancer cell line, with primary human fibroblasts as single cells. Long-term culture periods were performed for evaluation of the reconstruction of the stromal compartment and to study its impact on tumour progression. The impact of co-culture on tumour progression and drug response was assessed, taking advantage of the non-destructive sampling offered by the stirred culture system. In **chapter 4**, the MCF7-based *in vitro* model developed in chapter 3 was compared with other MCF7-based 3D cell models generated in commonly used culture platforms. The cross-comparison was done across several partners of the IMI-funded project PREDECT (www.predect.eu). The models compared included 2D and static 3D (scaffold-free cultures or embedded into bioactive scaffolds, such as matrigel, collagen or a mix of matrigel-collagen). After harmonization of the culture conditions and analytical methods, cell models were evaluated in terms of cell growth, response to drug treatments and phenotypic alterations along the culture time. For comparison across all models, several methodologies were optimized, such as tissue microarrays and automated image analysis.

As a fourth aim of this thesis, *ex vivo* cultures of patient-derived ER^+ breast carcinomas were implemented and characterized, employing the same strategy developed for the *in vitro* culture system (**chapter 5**) Samples were partially digested into explants, encapsulated in alginate and cultured under orbital shaking for 30 days. Tissue processing and culture conditions were optimized towards the maintenance of the original tissue architecture, epithelial/stroma cell ratio and hormone receptor expression along 30 days of

culture. Culture exometabolome was analysed as a complementary tool for tissue vitality evaluation.

As a final aim of this thesis, new tools to address the influence of the tumour microenvironment dynamics on disease progression were implemented. In **chapter 6**, the identification of the fibroblast secretome analysis by MS-based tools after implementation of sample decomplexation methods. More specifically, the comparison of affinity-based albumin removal kits with fractionation techniques was performed for identification of low molecular weight proteins present in the secretome of fibroblasts. In parallel, a wide range of characterization methods were implemented and/or improved.

The results obtained in this thesis were further discussed and contextualized in **chapter 7**.

8 References

[1] R.L. Siegel, K.D. Miller, A. Jemal, Cancer statistics, 2016, CA Cancer J Clin. 66 (2016) 7–30. doi:10.3322/caac.21332.

[2] M.J. Bissell, W.C. Hines, Why don't we get more cancer? A proposed role of the microenvironment in restraining cancer progression, Nat. Med. 17 (2011) 320–329. doi:10.1038/nm.2328.

[3] G.K. Malhotra, X. Zhao, H. Band, V. Band, Histological, molecular and functional subtypes of breast cancers, Cancer Biol. Ther. 10 (2010) 955–960. doi:10.4161/cbt.10.10.13879.

[4] N. Yoshida, Y. Omoto, A. Inoue, H. Eguchi, Y. Kobayashi, M. Kurosumi, et al., Prediction of prognosis of estrogen receptor-positive breast cancer with combination of selected estrogen-regulated genes, Cancer Sci. 95 (2004) 496–502.

[5] M.P.V. Shekhar, S. Santner, K.A. Carolin, L. Tait, Direct involvement of breast tumor fibroblasts in the modulation of tamoxifen sensitivity, Am. J. Pathol. 170 (2007) 1546–1560. doi:10.2353/ajpath.2007.061004.

[6] Z.I. Khamis, Z.J. Sahab, Q.-X.A. Sang, Active roles of tumor stroma in breast cancer metastasis, Int J Breast Cancer. 2012 (2012) 574025–10. doi:10.1155/2012/574025.

[7] I.S. Paine, M.T. Lewis, The Terminal End Bud: the Little Engine that Could, J Mammary Gland Biol Neoplasia. 22 (2017) 93–108. doi:10.1007/s10911-017-9372-0.

[8] M.M. Richert, K.L. Schwertfeger, J.W. Ryder, S.M. Anderson, An atlas of mouse mammary gland development, J Mammary Gland Biol Neoplasia. 5 (2000) 227–241.

[9] F.A. Tavassoli, Pathology of the Breast, McGraw Hill Professional, 1999.

[10] B. Alberts, A. Johnson, J. Lewis, D. Morgan, M. Raff, K. Roberts, et al., Molecular Biology of the Cell, Sixth Edition, Garland Science, 2014.

[11] J. Muschler, C.H. Streuli, Cell-matrix interactions in mammary gland development and breast cancer, Cold Spring Harb Perspect Biol. 2 (2010) a003202–a003202. doi:10.1101/cshperspect.a003202.

[12] H. Tanjore, R. Kalluri, The role of type IV collagen and basement membranes in cancer progression and metastasis, Am. J. Pathol. 168 (2006) 715–717. doi:10.2353/ajpath.2006.051321.

[13] B. Weigelt, M.J. Bissell, Unraveling the microenvironmental influences on the normal mammary gland and breast cancer, Semin. Cancer Biol. 18 (2008) 311–321. doi:10.1016/j.semcancer.2008.03.013.

[14] J.E. Fata, Z. Werb, M.J. Bissell, Regulation of mammary gland branching morphogenesis by the extracellular matrix and its remodeling enzymes, Breast Cancer Res. 6 (2004) 1–11. doi:10.1186/bcr634.

[15] C. Angelucci, G. Maulucci, G. Lama, G. Proietti, A. Colabianchi, M. Papi, et al., Epithelial-stromal interactions in human breast cancer: effects on adhesion, plasma membrane fluidity and migration speed and directness, PLoS ONE. 7 (2012) e50804. doi:10.1371/journal.pone.0050804.

[16] S.M. Myllymäki, T.P. Teräväinen, A. Manninen, Two distinct integrin-mediated mechanisms contribute to apical lumen formation in epithelial cells, PLoS ONE. 6 (2011) e19453. doi:10.1371/journal.pone.0019453.

[17] T. Tanos, L. Rojo, P. Echeverria, C. Brisken, ER and PR signaling nodes during mammary gland development, Breast Cancer Res. 14 (2012) 210. doi:10.1186/bcr3166.

[18] E. Anderson, R.B. Clarke, A. Howell, Estrogen responsiveness and control of normal human breast proliferation, J Mammary Gland Biol Neoplasia. 3 (1998) 23–35.

[19] K.B. Ewan, G. Shyamala, S.A. Ravani, Y. Tang, R. Akhurst, L. Wakefield, et al., Latent transforming growth factor-beta activation in mammary gland: regulation by ovarian hormones affects ductal and alveolar proliferation, Am. J. Pathol. 160 (2002) 2081–2093.

[20] T.A. Petrel, R.W. Brueggemeier, Increased proteasome-dependent degradation of estrogen receptor-alpha by TGF-beta1 in breast cancer cell lines, J. Cell. Biochem. 88 (2003) 181–190. doi:10.1002/jcb.10353.

[21] H. Moses, M.H. Barcellos-Hoff, TGF-beta biology in mammary development and breast cancer, Cold Spring Harb Perspect Biol. 3 (2011) a003277–a003277. doi:10.1101/cshperspect.a003277.

[22] B. Weigelt, F.C. Geyer, J.S. Reis-Filho, Histological types of breast cancer: how special are they? Mol Oncol. 4 (2010) 192–208. doi:10.1016/j.molonc.2010.04.004.

[23] J. Makki, Diversity of Breast Carcinoma: Histological Subtypes and Clinical Relevance, Clin Med Insights Pathol. 8 (2015) 23–31. doi:10.4137/CPath.S31563.

[24] H.G. Russnes, O.C. Lingjærde, A.-L. Børresen-Dale, C. Caldas, Breast Cancer Molecular Stratification: From Intrinsic Subtypes to Integrative Clusters, Am. J. Pathol. 187 (2017) 2152–2162. doi:10.1016/j.ajpath.2017.04.022.

[25] T. Sørlie, C.M. Perou, R. Tibshirani, T. Aas, S. Geisler, H. Johnsen, et al., Gene expression patterns of breast carcinomas distinguish tumor subclasses with clinical implications, Proc. Natl. Acad. Sci. U.S.a. 98 (2001) 10869–10874. doi:10.1073/pnas.191367098.

[26] C.M. Perou, T. Sørlie, M.B. Eisen, M. van de Rijn, S.S. Jeffrey, C.A. Rees, et al., Molecular portraits of human breast tumours, Nature. 406 (2000) 747–752. doi:10.1038/35021093.

[27] D.J. Toft, V.L. Cryns, Minireview: Basal-like breast cancer: from molecular profiles to targeted therapies, Mol. Endocrinol. 25 (2011) 199–211. doi:10.1210/me.2010-0164.

[28] J.I. Herschkowitz, K. Simin, V.J. Weigman, I. Mikaelian, J. Usary, Z. Hu, et al., Identification of conserved gene expression features between murine mammary carcinoma models and human breast tumors, Genome Biology. 8 (2007) R76. doi:10.1186/gb-2007-8-5-r76.

[29] B.D. Lehmann, B. Jovanović, X. Chen, M.V. Estrada, K.N. Johnson, Y. Shyr, et al., Refinement of Triple-Negative Breast Cancer Molecular Subtypes: Implications for Neoadjuvant Chemotherapy Selection, PLoS ONE. 11 (2016) e0157368. doi:10.1371/journal.pone.0157368.

[30] M.D. Burstein, A. Tsimelzon, G.M. Poage, K.R. Covington, A. Contreras, S.A.W. Fuqua, et al., Comprehensive genomic analysis identifies novel subtypes and targets of triple-negative breast cancer, Clin. Cancer Res. 21 (2015) 1688–1698. doi:10.1158/1078-0432.CCR-14-0432.

[31] A.E. Teschendorff, A. Miremadi, S.E. Pinder, I.O. Ellis, C. Caldas, An immune response gene expression module identifies a good prognosis subtype in estrogen receptor negative breast cancer, Genome Biology. 8 (2007) R157. doi:10.1186/gb-2007-8-8-r157.

[32] A.E. Teschendorff, C. Caldas, A robust classifier of high predictive value to identify good prognosis patients in ER-negative breast cancer, Breast Cancer Res. 10 (2008) R73. doi:10.1186/bcr2138.

[33] G. Sflomos, V. Dormoy, T. Metsalu, R. Jeitziner, L. Battista, V. Scabia, et al., A Preclinical Model for ERα-Positive Breast Cancer Points to the Epithelial Microenvironment as Determinant of Luminal Phenotype and Hormone Response, Cancer Cell. 29 (2016) 407–422. doi:10.1016/j.ccell.2016.02.002.

[34] X.H.-F. Zhang, M. Giuliano, M.V. Trivedi, R. Schiff, C.K. Osborne, Metastasis dormancy in estrogen receptor-positive breast cancer, Clin. Cancer Res. 19 (2013) 6389–6397. doi:10.1158/1078-0432.CCR-13-0838.

[35] M. Jia, K. Dahlman-Wright, J.-Å. Gustafsson, Estrogen receptor alpha and beta in health and disease, Best Practice & Research Clinical Endocrinology & Metabolism. 29 (2015) 557–568. doi:10.1016/j.beem.2015.04.008.

[36] A.B. Khalid, S.A. Krum, Estrogen receptors alpha and beta in bone, Bone. 87 (2016) 130–135. doi:10.1016/j.bone.2016.03.016.

[37] H.-R. Lee, T.-H. Kim, K.-C. Choi, Functions and physiological roles of two types of estrogen receptors, ERα and ERβ, identified by estrogen receptor knockout mouse, Laboratory Animal Research. 28 (2012) 71–76. doi:10.5625/lar.2012.28.2.71.

[38] C. Williams, K. Edvardsson, S.A. Lewandowski, A. Ström, J.Å. Gustafsson, A genome-wide study of the repressive effects of estrogen receptor beta on estrogen receptor alpha signaling in breast cancer cells, Oncogene. 27 (2008) 1019–1032. doi:10.1038/sj.onc.1210712.

[39] A.M. Band, M. Laiho, Crosstalk of TGF-β and estrogen receptor signaling in breast cancer, J Mammary Gland Biol Neoplasia. 16 (2011) 109–115. doi:10.1007/s10911-011-9203-7.

[40] E.R. Levin, Plasma membrane estrogen receptors, Trends Endocrinol. Metab. 20 (2009) 477–482. doi:10.1016/j.tem.2009.06.009.

[41] M.S. Mehta, S.C. Dolfi, R. Bronfenbrener, E. Bilal, C. Chen, D. Moore, et al., Metabotropic glutamate receptor 1 expression and its polymorphic variants associate with breast cancer phenotypes, PLoS ONE. 8 (2013) e69851. doi:10.1371/journal.pone.0069851.

[42] Y. Miyoshi, K. Murase, M. Saito, M. Imamura, K. Oh, Mechanisms of estrogen receptor-α upregulation in breast cancers, Med Mol Morphol. 43 (2010) 193–196. doi:10.1007/s00795-010-0514-3.

[43] C.K. Osborne, A. Wakeling, R.I. Nicholson, Fulvestrant: an oestrogen receptor antagonist with a novel mechanism of action, British Journal of Cancer. 90 (2004) S2–S6. doi:10.1038/sj.bjc.6601629.

[44] J.M. Rae, M.D. Johnson, J.O. Scheys, K.E. Cordero, J.M. Larios, M.E. Lippman, GREB 1 is a critical regulator of hormone dependent breast cancer growth, Breast Cancer Res. Treat. 92 (2005) 141–149. doi:10.1007/s10549-005-1483-4.

[45] M. Giuliano, H. Hu, Y.-C. Wang, X. Fu, A. Nardone, S. Herrera, et al., Upregulation of ER Signaling as an Adaptive Mechanism of Cell Survival in HER2-Positive Breast Tumors Treated with Anti-HER2 Therapy, Clin. Cancer Res. 21 (2015) 3995–4003. doi:10.1158/1078-0432.CCR-14-2728.

[46] C.-Y. Lin, A. Ström, V.B. Vega, S.L. Kong, A.L. Yeo, J.S. Thomsen, et al., Discovery of estrogen receptor alpha target genes and response elements in breast tumor cells, Genome Biology. 5 (2004) R66. doi:10.1186/gb-2004-5-9-r66.

[47] C. Yang, L. Chen, C. Li, M.C. Lynch, C. Brisken, E.V. Schmidt, Cyclin D1 enhances the response to estrogen and progesterone by regulating progesterone receptor expression, Mol. Cell. Biol. 30 (2010) 3111–3125. doi:10.1128/MCB.01398-09.

[48] A. Agrawal, J.F.R. Robertson, K.L. Cheung, E. Gutteridge, I.O. Ellis, R.I. Nicholson, et al., Biological effects of fulvestrant on estrogen receptor positive human breast cancer: short, medium and long-term effects based on sequential biopsies, Int. J. Cancer. 138 (2016) 146–159. doi:10.1002/ijc.29682.

[49] W.-L. Yeh, K. Shioda, K.R. Coser, D. Rivizzigno, K.R. McSweeney, T. Shioda, Fulvestrant-Induced Cell Death and Proteasomal Degradation of Estrogen Receptor α Protein in MCF-7 Cells Require the CSK c-Src Tyrosine Kinase, PLoS ONE. 8 (2013) e60889. doi:10.1371/journal.pone.0060889.

[50] Aromatase inhibitors versus tamoxifen in early breast cancer: patient-level meta-analysis of the randomised trials, The Lancet. 386 (2015) 1341–1352. doi:10.1016/S0140-6736(15)61074-1.

[51] M.J. Brier, D.L. Chambless, R. Gross, J. Chen, J.J. Mao, Perceived barriers to treatment predict adherence to aromatase inhibitors among breast cancer survivors, Cancer. 123 (2017) 169–176. doi:10.1002/cncr.30318.

[52] C.K. Osborne, Aromatase inhibitors in relation to other forms of endocrine therapy for breast cancer, Endocr. Relat. Cancer. 6 (1999) 271–276.

[53] B. Ramaswamy, C.L. Shapiro, Osteopenia and osteoporosis in women with breast cancer, Semin. Oncol. 30 (2003) 763–775.

[54] A.E. Wakeling, J. Bowler, Steroidal pure antioestrogens, J. Endocrinol. 112 (1987) R7–10.

[55] K. Boér, Fulvestrant in advanced breast cancer: evidence to date and place in therapy, Ther Adv Med Oncol. 9 (2017) 465–479. doi:10.1177/1758834017711097.

[56] E. Ciruelos, T. Pascual, M.L. Arroyo Vozmediano, M. Blanco, L. Manso, L. Parrilla, et al., The therapeutic role of fulvestrant in the management of patients with hormone receptor-positive breast cancer, Breast. 23 (2014) 201–208. doi:10.1016/j.breast.2014.01.016.

[57] I. Bado, Z. Gugala, S.A.W. Fuqua, X.H.-F. Zhang, Estrogen receptors in breast and bone: from virtue of remodeling to vileness of metastasis, Oncogene. 36 (2017) 4527–4537. doi:10.1038/onc.2017.94.

[58] P. Friedl, S. Alexander, Cancer invasion and the microenvironment: plasticity and reciprocity, Cell. 147 (2011) 992–1009. doi:10.1016/j.cell.2011.11.016.

[59] D.S. Dolberg, M.J. Bissell, Inability of Rous sarcoma virus to cause sarcomas in the avian embryo, Nature. 309 (1984) 552–556.

[60] J.J. Maher, D.M. Bissell, Cell-matrix interactions in liver, Semin. Cell Biol. 4 (1993) 189–201.

[61] R. Kalluri, The biology and function of fibroblasts in cancer, Nature Reviews Cancer. 16 (2016) 582–598. doi:10.1038/nrc.2016.73.

[62] Y. Mao, E.T. Keller, D.H. Garfield, K. Shen, J. Wang, Stromal cells in tumor microenvironment and breast cancer, Cancer Metastasis Rev. 32 (2013) 303–315. doi:10.1007/s10555-012-9415-3.

[63] S. Busch, D. Andersson, E. Bom, C. Walsh, A. Ståhlberg, G. Landberg, Cellular organization and molecular differentiation model of breast cancer-associated fibroblasts, Mol. Cancer. 16 (2017) 73. doi:10.1186/s12943-017-0642-7.

[64] R. Kalluri, M. Zeisberg, Fibroblasts in cancer, Nature Reviews Cancer. 6 (2006) 392–401. doi:10.1038/nrc1877.

[65] M. Lech, H.-J. Anders, Macrophages and fibrosis: How resident and infiltrating mononuclear phagocytes orchestrate all phases of tissue injury and repair, Biochimica Et Biophysica Acta (BBA) - Molecular Basis of Disease. 1832 (2013) 989–997. doi:10.1016/j.bbadis.2012.12.001.

[66] A. Qiao, F. Gu, X. Guo, X. Zhang, L. Fu, Breast cancer-associated fibroblasts: their roles in tumor initiation, progression and clinical applications, Front Med. 10 (2016) 33–40. doi:10.1007/s11684-016-0431-5.

[67] H.F. Dvorak, Tumors: wounds that do not heal. Similarities between tumor stroma generation and wound healing, N. Engl. J. Med. 315 (1986) 1650–1659. doi:10.1056/NEJM198612253152606.

[68] R.J. Buchsbaum, S.Y. Oh, Breast Cancer-Associated Fibroblasts: Where We Are and Where We Need to Go, Cancers (Basel). 8 (2016) 19. doi:10.3390/cancers8020019.

[69] S. Herold, K. Mayer, J. Lohmeyer, Acute lung injury: how macrophages orchestrate resolution of inflammation and tissue repair, Front Immunol. 2 (2011) 65. doi:10.3389/fimmu.2011.00065.

[70] C. Neuzillet, A. Tijeras-Raballand, R. Cohen, J. Cros, S. Faivre, E. Raymond, et al., Targeting the TGFβ pathway for cancer therapy, Pharmacol. Ther. 147 (2015) 22–31. doi:10.1016/j.pharmthera.2014.11.001.

[71] O. Pontiggia, R. Sampayo, D. Raffo, A. Motter, R. Xu, M.J. Bissell, et al., The tumor microenvironment modulates tamoxifen resistance in breast cancer: a role for soluble stromal factors and fibronectin through β1 integrin, Breast Cancer Res. Treat. 133 (2012) 459–471. doi:10.1007/s10549-011-1766-x.

[72] R. de Leeuw, J. Neefjes, R. Michalides, A role for estrogen receptor phosphorylation in the resistance to tamoxifen, Int J Breast Cancer. 2011 (2011) 232435–10. doi:10.4061/2011/232435.

[73] D. Chen, T. Riedl, E. Washbrook, P.E. Pace, R.C. Coombes, J.M. Egly, et al., Activation of estrogen receptor alpha by S118 phosphorylation involves a ligand-dependent interaction with TFIIH and participation of CDK7, Mol. Cell. 6 (2000) 127–137.

[74] C. Bonnans, J. Chou, Z. Werb, Remodelling the extracellular matrix in development and disease, Nat. Rev. Mol. Cell Biol. 15 (2014) 786–801. doi:10.1038/nrm3904.

[75] T.R. Cox, J.T. Erler, Remodeling and homeostasis of the extracellular matrix: implications for fibrotic diseases and cancer, Dis Model Mech. 4 (2011) 165–178. doi:10.1242/dmm.004077.

[76] D.O. Velez, B. Tsui, T. Goshia, C.L. Chute, A. Han, H. Carter, et al., 3D collagen architecture induces a conserved migratory and transcriptional response linked to vasculogenic mimicry, Nat Commun. 8 (2017) 1651. doi:10.1038/s41467-017-01556-7.

[77] B. Gligorijevic, A. Bergman, J. Condeelis, Multiparametric classification links tumor microenvironments with tumor cell phenotype, PLoS Biol. 12 (2014) e1001995. doi:10.1371/journal.pbio.1001995.

[78] O. Chaudhuri, S.T. Koshy, C. Branco da Cunha, J.-W. Shin, C.S. Verbeke, K.H. Allison, et al., Extracellular matrix stiffness and composition jointly regulate the induction of malignant phenotypes in mammary epithelium, Nat Mater. 13 (2014) 970–978. doi:10.1038/nmat4009.

[79] K.L. Harper, M.S. Sosa, D. Entenberg, H. Hosseini, J.F. Cheung, R. Nobre, et al., Mechanism of early dissemination and metastasis in Her2+ mammary cancer, Nature. 540 (2016) 588–592. doi:10.1038/nature20609.

[80] H. Hosseini, M.M.S. Obradović, M. Hoffmann, K.L. Harper, M.S. Sosa, M. Werner-Klein, et al., Early dissemination seeds metastasis in breast cancer, Nature. 540 (2016) 552–558. doi:10.1038/nature20785.

[81] T. Vargo-Gogola, J.M. Rosen, Modelling breast cancer: one size does not fit all, Nature Reviews Cancer. 7 (2007) 659–672. doi:10.1038/nrc2193.

[82] J. Heyer, L.N. Kwong, S.W. Lowe, L. Chin, Non-germline genetically engineered mouse models for translational cancer research, Nature Reviews Cancer. 10 (2010) 470–480. doi:10.1038/nrc2877.

[83] A.D. Pfefferle, J.I. Herschkowitz, J. Usary, J. Harrell, B.T. Spike, J.R. Adams, et al., Transcriptomic classification of genetically engineered mouse models of breast cancer identifies human subtype counterparts, Genome Biology. 14 (2013) R125. doi:10.1186/gb-2013-14-11-r125.

[84] S.R. Chan, W. Vermi, J. Luo, L. Lucini, C. Rickert, A.M. Fowler, et al., STAT1-deficient mice spontaneously develop estrogen receptor α-positive luminal mammary carcinomas, Breast Cancer Res. 14 (2012) R16. doi:10.1186/bcr3100.

[85] D. Dutta, I. Heo, H. Clevers, Disease Modeling in Stem Cell-Derived 3D Organoid Systems, Trends in Molecular Medicine. 23 (2017) 393–410.

[86] S. Mohibi, S. Mirza, H. Band, V. Band, Mouse models of estrogen receptor-positive breast cancer, J Carcinog. 10 (2011) 35. doi:10.4103/1477-3163.91116.

[87] A.F. Gazdar, F.R. Hirsch, J.D. Minna, From Mice to Men and Back: An Assessment of Preclinical Model Systems for the Study of Lung Cancers, Journal of Thoracic Oncology. 11 (2016) 287–299.

[88] J.R. Whittle, M.T. Lewis, G.J. Lindeman, J.E. Visvader, Patient-derived xenograft models of breast cancer and their predictive power, Breast Cancer Res. 17 (2015) 17. doi:10.1186/s13058-015-0523-1.

[89] F. Behbod, F.S. Kittrell, H. LaMarca, D. Edwards, S. Kerbawy, J.C. Heestand, et al., An intraductal human-in-mouse transplantation model mimics the subtypes of ductal carcinoma in situ, Breast Cancer Res. 11 (2009) R66. doi:10.1186/bcr2358.

[90] R. White, K. Rose, L. Zon, Zebrafish cancer: the state of the art and the path forward, Nature Reviews Cancer. 13 (2013) 624–636. doi:10.1038/nrc3589.

[91] R. Fior, V. Póvoa, R.V. Mendes, T. Carvalho, A. Gomes, N. Figueiredo, et al., Single-cell functional and chemosensitive profiling of combinatorial colorectal therapy in zebrafish xenografts, Proc. Natl. Acad. Sci. U.S.a. 34 (2017) 201618389. doi:10.1073/pnas.1618389114.

[92] L. Mercatali, F. La Manna, A. Groenewoud, R. Casadei, F. Recine, G. Miserocchi, et al., Development of a Patient-Derived Xenograft (PDX) of Breast Cancer

Bone Metastasis in a Zebrafish Model, Int J Mol Sci. 17 (2016) 1375. doi:10.3390/ijms17081375.

[93] M. Jia, T. Andreassen, L. Jensen, T.F. Bathen, I. Sinha, H. Gao, et al., Estrogen Receptor α Promotes Breast Cancer by Reprogramming Choline Metabolism, Cancer Res. 76 (2016) 5634–5646. doi:10.1158/0008-5472.CAN-15-2910.

[94] H. van der Kuip, T.E. Mürdter, M. Sonnenberg, M. McClellan, S. Gutzeit, A. Gerteis, et al., Short term culture of breast cancer tissues to study the activity of the anticancer drug taxol in an intact tumor environment, BMC Cancer. 6 (2006) 86. doi:10.1186/1471-2407-6-86.

[95] E.J. Davies, M. Dong, M. Gutekunst, K. Närhi, H.J.A.A. van Zoggel, S. Blom, et al., Capturing complex tumour biology in vitro: histological and molecular characterisation of precision cut slices, Sci Rep. 5 (2015) 17187. doi:10.1038/srep17187.

[96] T. Tanos, G. Sflomos, P.C. Echeverria, A. Ayyanan, M. Gutierrez, J.-F. Delaloye, et al., Progesterone/RANKL is a major regulatory axis in the human breast, Sci Transl Med. 5 (2013) 182ra55–182ra55. doi:10.1126/scitranslmed.3005654.

[97] M.G. Muraro, S. Muenst, V. Mele, L. Quagliata, G. Iezzi, A. Tzankov, et al., Ex-vivo assessment of drug response on breast cancer primary tissue with preserved microenvironments, Oncoimmunology. 6 (2017) e1331798. doi:10.1080/2162402X.2017.1331798.

[98] B. Majumder, U. Baraneedharan, S. Thiyagarajan, P. Radhakrishnan, H. Narasimhan, M. Dhandapani, et al., Predicting clinical response to anticancer drugs using an ex vivo platform that captures tumour heterogeneity, Nat Commun. 6 (2015) 6169. doi:10.1038/ncomms7169.

[99] S. Nath, G.R. Devi, Three-dimensional culture systems in cancer research: Focus on tumor spheroid model, Pharmacol. Ther. 163 (2016) 94–108. doi:10.1016/j.pharmthera.2016.03.013.

[100]B. Weigelt, C.M. Ghajar, M.J. Bissell, The need for complex 3D culture models to unravel novel pathways and identify accurate biomarkers in breast cancer, Adv. Drug Deliv. Rev. 69-70 (2014) 42–51. doi:10.1016/j.addr.2014.01.001.

[101]C. Unger, N. Kramer, A. Walzl, M. Scherzer, M. Hengstschläger, H. Dolznig, Modeling human carcinomas: physiologically relevant 3D models to improve anti-cancer drug development, Adv. Drug Deliv. Rev. 79-80 (2014) 50–67. doi:10.1016/j.addr.2014.10.015.

[102]G. Rijal, W. Li, 3D scaffolds in breast cancer research, Biomaterials. 81 (2016) 135–156.

[103]W. Asghar, R. El Assal, H. Shafiee, S. Pitteri, R. Paulmurugan, U. Demirci, Engineering cancer microenvironments for in vitro 3-D tumor models, Materials Today. 18 (2015) 539–553.

[104]J.A. Hickman, R. Graeser, R. de Hoogt, S. Vidic, C. Brito, M. Gutekunst, et al., Three-dimensional models of cancer for pharmacology and cancer cell biology: Capturing tumor complexity in vitro/ex vivo, Biotechnology Journal. 9 (2014) 1115–1128. doi:10.1002/biot.201300492.

[105]S. Breslin, L. O'Driscoll, Three-dimensional cell culture: the missing link in drug discovery, Drug Discovery Today. 18 (2013) 240–249.

[106]P. Kaur, B. Ward, B. Saha, L. Young, S. Groshen, G. Techy, et al., Human breast cancer histoid: an in vitro 3-dimensional co-culture model that mimics breast cancer tissue, J. Histochem. Cytochem. 59 (2011) 1087–1100. doi:10.1369/0022155411423680.

[107]A. Sadlonova, Z. Novak, M.R. Johnson, D.B. Bowe, S.R. Gault, G.P. Page, et al., Breast fibroblasts modulate epithelial cell proliferation in three-dimensional in vitro co-culture, Breast Cancer Res. 7 (2005) R46–59. doi:10.1186/bcr949.

[108]H. Dolznig, C. Rupp, C. Puri, C. Haslinger, N. Schweifer, E. Wieser, et al., Modeling colon adenocarcinomas in vitro a 3D co-culture system induces cancer-relevant pathways upon tumor cell and stromal fibroblast interaction, Am. J. Pathol. 179 (2011) 487–501. doi:10.1016/j.ajpath.2011.03.015.

[109]K.-V. Nguyen-Ngoc, K.J. Cheung, A. Brenot, E.R. Shamir, R.S. Gray, W.C. Hines, et al., ECM microenvironment regulates collective migration and local dissemination in normal and malignant mammary epithelium, Proc. Natl. Acad. Sci. U.S.a. 109 (2012) E2595–604. doi:10.1073/pnas.1212834109.

[110]X. Fang, S. Sittadjody, K. Gyabaah, E.C. Opara, K.C. Balaji, Novel 3D co-culture model for epithelial-stromal cells interaction in prostate cancer, PLoS ONE. 8 (2013) e75187. doi:10.1371/journal.pone.0075187.

[111]K. Chwalek, M.V. Tsurkan, U. Freudenberg, C. Werner, Glycosaminoglycan-based hydrogels to modulate heterocellular communication in in vitro angiogenesis models, Sci Rep. 4 (2014) 4414. doi:10.1038/srep04414.

[112]N. Sachs, J. de Ligt, O. Kopper, E. Gogola, G. Bounova, F. Weeber, et al., A Living Biobank of Breast Cancer Organoids Captures Disease Heterogeneity, Cell. (2017). doi:10.1016/j.cell.2017.11.010.

[113]E.S. Sokol, D.H. Miller, A. Breggia, K.C. Spencer, L.M. Arendt, P.B. Gupta, Growth of human breast tissues from patient cells in 3D hydrogel scaffolds, Breast Cancer Res. 18 (2016) 19. doi:10.1186/s13058-016-0677-5.

[114]N. Gjorevski, N. Sachs, A. Manfrin, S. Giger, M.E. Bragina, P. Ordóñez-Morán, et al., Designer matrices for intestinal stem cell and organoid culture, Nature. 539 (2016) 560–564. doi:10.1038/nature20168.

[115]L.C. Kimlin, G. Casagrande, V.M. Virador, In vitro three-dimensional (3D) models in cancer research: an update, Mol. Carcinog. 52 (2013) 167–182. doi:10.1002/mc.21844.

[116]J.W. Haycock, 3D cell culture: a review of current approaches and techniques, Methods Mol. Biol. 695 (2011) 1–15. doi:10.1007/978-1-60761-984-0_1.

Chapter II

Adaptable stirred-tank culture strategies for large scale production of multicellular spheroid-based tumour cell models

This Chapter was adapted from:

Santo VE*, **Estrada MF*** Rebelo SP, Abreu S, Silva I, Pinto C, Veloso SC, Serra AT, Boghaert E, Alves PM, Brito C. *Adaptable stirred-tank culture strategies for large scale production of multicellular spheroid-based tumor cell models*. J Biotechnol, 2016.

* These authors equally contributed to this work

Table of contents

1 Abstract 43
1 Introduction 44
2 Materials and methods 47
2.1 Cell lines and 2D cell culture 47
2.2 Generation of tumour cell spheroids in stirred-tank culture systems 48
2.3 Generation of heterotypic spheroids in stirred-tank culture systems 48
2.4 Cell microencapsulation and culture in stirred-tank culture systems 49
2.5 Cell culture characterization 50
2.5.1 Total cell concentration 50
2.5.2 Cell viability 50
2.6 Spheroid size determination 51
2.7 Phenotypic characterization of the 3D tumour cell models 51
2.7.1 Hypoxia Detection 51
2.7.2 Apoptotic activity 52
2.7.3 Immunofluorescence microscopy and image analysis 52
2.7.4 Drug perturbation 53
2.8 Statistical analysis 53
3 Results 53
3.1 Generation of tumour cell spheroids in stirred-tank culture systems 53
3.2 Tumour spheroid culture in stirred-tank culture systems 60
3.3 Generation of heterotypic 3D tumour cell models in absence/presence of physical support 63
4 Discussion 68
5 Acknowledgments 74
6 References 74
7 Supplementary Figures 78

Abstract

Currently there is an effort towards the development of *in vitro* cancer models more predictive of clinical efficacy. The onset of advanced analytical tools and imaging technologies has increased the utilization of spheroids in the implementation of high throughput approaches in drug discovery. Agitation-based culture systems are commonly proposed as an alternative method for the production of tumour spheroids, despite the scarce experimental evidence found in the literature. In this study, we demonstrate the robustness and reliability of agitation-based culture conditions for the scalable generation of 3D cancer models. We developed standardized protocols for a panel of tumour cell lines from different cancer types and attained efficient tumour cell aggregation by tuning the hydrodynamic parameters. Large numbers of spheroids were obtained (typically 1000-1500 spheroids/mL) presenting features of native tumours, namely morphology, proliferation and hypoxia gradients, in a cell line-dependent mode. Heterotypic 3D cancer models, based on co-cultures of tumour cells and fibroblasts, were also established in the absence or presence of additional physical support from an alginate matrix, with maintenance of high cell viability. Altogether, we demonstrate that stirred-tank culture systems are a robust and versatile approach to generate 3D tumour cell spheroids, providing reproducible tools for drug screening and target verification in pre-clinical oncology research.

Keywords: *in vitro* cancer models; tumour spheroids; stirred-tank culture systems; drug discovery; 3D cell culture

1 Introduction

The high attrition rates observed in cancer drug discovery (up to 95% of drugs tested in phase I clinical trials) have raised the awareness of the scientific and industrial communities towards the need for more advanced pre-clinical models. These models should be more reflective of the disease and consequently help to eliminate drug candidates that lack efficacy or safety at pre-clinical stages [1, 2].

In this context, three dimensional (3D) *in vitro* cancer models can provide a cell organization with higher physiological relevance when compared to typical two dimensional (2D) monolayers. Gene expression profiles, as well as phenotypic and functional characteristics, of cells cultured in 3D are different from monolayer cultures and more closely resemble the features of the tissues of origin than their 2D counterparts [3-8]. 2D cell cultures are easily established, monitored and characterized. Nonetheless, the spatial environment, cell morphology, polarity, receptor expression, oncogene expression and overall structural architecture are less reflective of the tumour environment than the 3D systems. 3D cell models enable tumour cells to establish and maintain cell-cell and cell-extracellular matrix (ECM) interactions, which are crucial mediators of cell signalling and modulators of response to therapeutic agents [9, 10]. These interactions are essential for tumour cell differentiation, proliferation and survival *in vivo* [11]. Moreover, increased drug sensitivity due to higher cell surface exposure is expected in 2D cultures when compared to the *in vivo* conditions [12, 13]. A 3D tumour model mimics the architecture of cancer cells in a tumour to a greater extent than 2D cell models and can therefore represent a more predictable model of drug sensitivity.

Multicellular spheroids were first established to investigate aspects of gastrulation movements in amphibian embryos [14]. Later, they attracted attention of the cancer research community after demonstration of similarity between the zonal morphological and functional distribution in aggregates of Chinese hamster V79 lung cells and histopathological structure of carcinomas from several patients [15, 16]. The growth pattern of spheroids resembles the

initial and avascular phase of solid tumours *in vivo*, not-yet-vascularized micrometastasis or intercapillary tumour microsites [17]. These functional properties make spheroids a powerful model to investigate intercellular relationships and nutrient and oxygen diffusion in solid tumours [18, 19]. Despite the initial enthusiasm surrounding spheroids as cancer cell models, technical challenges have hindered their implementation in the drug development cascade [20]. To make this translation efficient, high levels of standardization are required, namely reproducible spheroid sizes and cell numbers. Additionally, the cell culture techniques must be amenable for scale up as high numbers of spheroids are required [21]. Quantitative read-outs for 3D cultures were still limited which contributed for the choice of 2D cultures as predominant tool [20]. Nevertheless, new analytical tools such as imaging technologies have been increasingly implemented into rapid and high throughput approaches for spheroid analysis [22-24].

Static and dynamic methods to produce spheroids have been developed over the years and currently there is no agreement on a single standard 3D model which could be used across the field. Force floating methods (low attachment plates or agarose underlayer) [25, 26], hanging-drop method [18, 27, 28] or embedding in 3D matrices [29] are some examples of current strategies implemented to produce spheroids. Besides the static methodologies, dynamic approaches can also be used [18, 30]. Agitation-based approaches to culture cells as spheroids include gyratory rotation techniques, such as gyratory shakers, rotary culture systems and stirred suspension culture systems [20, 31]. In these dynamic approaches, hydrodynamic forces generated by the agitation are adjusted during cell culture to promote cell interactions and consequently cell aggregation [32]. Increased shear introduced by hydrodynamic culture environments can regulate spheroid formation and control their size and shape through alterations in cell-cell collisions and adhesion binding kinetics at the cellular and molecular level, respectively [33]. In addition, the agitation-based cultures provide an efficient mass transport of nutrients and cell waste products to and from the spheroids,

respectively [31]. Large-scale stirred-tank culture systems present several features for the generation of an adequate culture environment for production of spheroids, namely reproducibility, scalability, adaptability and feeding for high throughput formats amenable to automation and drug screening [20]. Nevertheless, stirring rates must be tightly controlled to prevent physiological damage of the spheroids induced by the shear force [31].

For all these reasons, stirred-tank culture systems have been used for establishing 3D cultures due to its simplicity, low cost and efficient production of aggregates [1, 31, 34]. Nonetheless, despite the recognized potential for the production of tumour spheroids, these culture systems have not been used for the generation of a wide array of 3D tumour cell models for drug screening and target verification in oncology.

In this report we provide experimental evidence on the robustness, reliability and versatility of agitation-based culture systems for the large scale generation of 3D tumour cell models for a wide array of tumour cell lines. The robust character of stirred-tank culture methodologies herein described was demonstrated by the successful production of reproducibly sized spheroids from a panel of 9 different tumour cell lines from various pathologies, using the same cell inoculum. More than 10 independent biological replicates were performed for several of the tumour cell lines (MCF7, H1650, H157, HT29) with reproducible outcomes in spheroid concentration and size, highlighting the reliability of the proposed strategy. Moreover, the versatility of the stirred-tank culture methodologies was demonstrated by the application of different strategies for the establishment of mono- and co-culture 3D tumour models in the presence or absence of a hydrogel. Altogether, we demonstrate that stirred-tank culture systems represent a fast and reproducible method, which may be used as 3D model source to feed high throughput screenings of new drug candidates.

2 Materials and methods

2.1 Cell lines and 2D cell culture

Human tumour cell lines derived from various cancer types (indicated in table S1) were tested for their ability to grow as multicellular spheroids in stirred-tank culture systems.

Two ER^+ (MCF7 and BT474) and two ER^- (HCC1954 and HCC1806) breast cancer cell lines of human origin were selected. MCF7 and BT474 are amongst the most frequently used luminal-like cell lines and HCC1954 and HCC1806 are comprised within the subset of basal-like breast cancer cells. A549, H460, H1650 and H157 Non-Small Cell Lung Carcinoma (NSCLC) cell lines were selected for the development of lung cancer spheroids because they represent the major NSCLC subtypes: adenocarcinoma (A549, H1650), squamous (H157) and large-cell lung carcinomas (H460). HT29 was selected as colorectal carcinoma cell line.

H1650, H157, BT474, HCC1806, HCC1954 and HT29 cells were obtained from ATCC. Human Dermal Fibroblasts (hDFs) were obtained from Innoprot. MCF7 cells, transduced with the lentiviral vectors PGK-RFP and pCDH-CMV-MCS-EF1-Puro, were kindly provided by C. Brisken's laboratory. A549 and H460, modified to stably express TurboGFP using a lentiviral system (Sigma-Aldrich, SHC003V), were kindly supplied by W. Sommergruber, Boehringer Ingelheim. All abovementioned transformed cells were generated and provided under the scope of the Innovative Medicines Initiative Joint undertaking project, PREDECT (www.predect.eu).

2D static cultures (in t-flasks) were maintained at 37 °C in an incubator with humidified atmosphere containing 5% CO_2 and 21% of O_2. Tumour cells were sub-cultured twice a week at $1.5x10^4$ cell/cm^2; hDFs were split once a week at a seeding density of 0.5×10^4 cell/cm^2. For each sub-culture, cells were trypsinized using 0.05% trypsin-Ethylenediaminetetraacetic acid (trypsin-EDTA; Invitrogen), for 3-5 min. Viable cells were counted using trypan blue exclusion method. All cell lines were routinely cultured in adherent and static

conditions until establishment of the 3D cultures, using the culture media described in Table S1.

2.2 Generation of tumour cell spheroids in stirred-tank culture systems

Tumour cells were inoculated as single cell suspension into 125 mL or 500 mL wall-baffled spinner-flasks with straight blade paddle impeller (Corning® Life Sciences), placed on a magnetic stirrer in an incubator at 37ºC, with humidified atmosphere containing 5% CO_2 and 21% of O_2. Optimization of cell inoculum was performed by testing initial cell concentrations of $0.2x10^6$ cell/mL and $0.5x10^6$ cell/mL. To prevent cell attachment to the spinner vessel walls, these were pre-coated with 2-3 ml of dimethyldichlorosilane (Merck 8.03452, Germany), as described previously [35]. Initial stirring rates were set as indicated in Figure 2.2B, according to the cell line characteristics and previous reports from our group [36, 37] in order to promote cell interactions. For each cell line, cell aggregation and spheroid size were determined and controlled through manipulation of stirring rate (Figure 2.2B). This rate was adjusted along culture time to promote initial aggregate formation and spheroid compaction while limiting spheroid fusion.

Spheroid shape was classified according to the image analysis “Shape Parameters” function from ImageJ software. “Solidity” function represents an indicator of the roughness of the spheroid surface and provided information on the regularity of the aggregate. A spheroid was considered regular for solidity values higher than 0.90 (in a scale from 0 to 1).

Cultures were pursued up to 17 days, with 50% medium exchange every 3-4 days.

2.3 Generation of heterotypic spheroids in stirred-tank culture systems

For breast co-cultures, MCF7 cells and hDFs were inoculated simultaneously as single cell suspensions, at a concentration of $2x10^5$ cell/mL

and $4x10^4$ cell/mL for MCF7 and hDFs, respectively (MCF7:hDFs 5:1 cell ratio), into spinner-flasks and cultured as described in section 2.2. Lung heterotypic cultures were performed as indicated above by simultaneous inoculation of H1650 and hDFs at 5:1 cell ratio. The stirring profile optimized for MCF7 and H1650 mono-cultures was selected to generate the MCF7-hDFs and H1650-hDFs heterotypic cultures.

2.4 Cell microencapsulation and culture in stirred-tank culture systems

Tumour cell spheroids were microencapsulated after tumour cells formed compact and spherical aggregates (*e.g.* 1 and 3 days for MCF7 and H1650 cells, respectively). For mono-cultures, spheroids were collected from culture, washed twice with PBS and dispersed in 1.1% (w/v) of Ultrapure Ca^{2+} MVG alginate (UP MVG NovaMatrix, Pronova Biomedical, Oslo, Norway), dissolved in NaCl 0.9% (w/v) solution, as previously described [38].

For the establishment of co-cultures of tumour cells with fibroblasts, a single cell suspension of hDFs was mixed with a suspension of tumour spheroids (MCF7 and H1650 cells) to generate a 1:1 cell ratio for co-cultures. Cell counting on tumour spheroids was performed after spheroid dissociation with trypsin of a representative sample of the culture. Prior to microencapsulation and co-culture with H1650 cells, hDFs were labeled with PKH dye (PKH26 Red Fluorescent Cell Linker Kit, Sigma-Aldrich) according with manufacturers' instructions for cell monitoring by fluorescence microscopy.

Microencapsulation was performed using an electrostatic bead generator (Nisco Encapsulator) with an air flow rate of 10 mL/h, at 5.3 volts with air pressure of 1 bar. Alginate droplets were cross-linked either in a 100 mM $CaCl_2$ solution with 10mM Hepes (pH 7.4) or a 20 mM $BaCl_2$, adjusted to 290-300 mOsm, using NaCl, buffered at pH 7.4 with 5 mM histidine bath for 10 min. The resulting cell-loaded microcapsules were further washed three times in a 0.9% (w/v) NaCl solution [39]. Alginate microcapsules with a diameter of approximately 500 µm were generated.

Cancer cell spheroids (mono-culture) and cancer cell spheroids mixed with fibroblasts (co-culture) were enmeshed in the alginate hydrogels. The resulting microcapsules were transferred to spinner vessels, at a concentration of tumour cells of $2x10^5$ cell/mL, and cultured at 80 rpm for additional 5 days. At the third day of culture, agitation was briefly stopped (to let the aggregates deposit) and 50% of the culture medium was replaced with fresh culture medium [37]. Samples were collected throughout the culture period for further characterization.

2.5 Cell culture characterization

2.5.1 Total cell concentration

To access cell concentration the total number of viable cells was determined by counting the colourless cells in a Fuchs-Rosenthal hemocytometer chamber after incubation with a solution of 0.1% (v/v) of Trypan Blue dye (Gibco, Invitrogen Corporation, Paisley, UK) in PBS. Alternatively, total cell nuclei was assessed by the crystal violet method. Briefly, cells were centrifuged at 300x *g*, for 5 min and then lysed using lysis solution (1% Triton X-100 in 0.1 M citric acid), overnight at 37ºC. For microencapsulated spheroids, alginate microcapsules were first dissolved with a solution of 50 mM EDTA in mQ water. Aggregate suspension was centrifuged at 50x *g* for 5 min and, when in co-culture, the aggregate pellet was washed twice with PBS and centrifuged at 50x *g,* to remove the remaining fibroblasts and dissolved alginate. The aggregate pellets were then lysed, overnight at 37ºC. Total cell number was determined after incubation with 0.1% (v/v) crystal violet in lysis solution. Nuclei density was assessed using a Fuchs-Rosental hemocytometer and a microscope with phase contrast (DM IRB, Leica, Germany).

2.5.2 Cell viability

Cell viability was evaluated using the enzyme substrate fluorescein diacetate (FDA; Sigma-Aldrich, Steinheim, Germany) at 10 µg/mL in PBS to label live cells, and TO-PRO-3 iodide (Invitrogen) at 1 µM in PBS to identify

dead cells. Cultures were incubated for 5 min at RT with the fluorescent labels and then analyzed using a fluorescence microscope (DMI6000 Leica Microsystems GmBH, Wetzlar, Germany). To assess cell apoptosis NucView 488 Apoptosis Kit was used according to the manufacturer's instructions (Biotium, Hayward, CA, USA). Briefly, the cultures were exposed to NucView ^{TM} 488 diluted 1:200 in culture medium for 2h. NucView TM 488 is a caspase-3 substrate that detects caspase-3 in live cells without interfering with the enzyme activity. Cultures were then analysed using a fluorescence microscope (DMI 6000 Leica Microsystems GmBH, Wetzlar, Germany).

2.6 Spheroid size determination

Aggregates were imaged in a fluorescence microscope (DMI6000, Leica Microsystems GmbH, Wetzlar, Germany) and aggregate area and Ferret diameter was measured by adjusting the threshold until the border of each aggregate, which was then quantified using the area measurement algorithm from ImageJ open source software (Rasband, WS, ImageJ, U. S. National Institutes of Health, Bethesda, MD, USA, http://imagej.nih.gov/ij/, 1997–2012). Aggregates with less than 20 µm diameter were not included since they represent less than 5% of total number of aggregates in culture.

2.7 Phenotypic characterization of the 3D tumour cell models

2.7.1 Hypoxia Detection

HT29, H1650 and BT474 spheroids were placed in a 24 well-plate at 100 spheroids/well, the medium was removed and the spheroids were incubated for 2 hours with Hypoxyprobe^{TM}-1 (Hypoxyprobe, Burlington, MA) solution at 0.2 mM. The plate was centrifuged (SIGMA 3K15, Sigma Laborzentrifugen, Germany) for 5 min at 200x *g*, the spheroids were washed twice with PBS and directly frozen in liquid nitrogen until cryosectioned into 10 µm sections in a cryostat (Leica, Germany). After defrosting, sections were fixed in cold acetone (4^{o}C) for 10 min, washed twice with PBS and blocked with 0.2% Fish Skin Gelatin (FSG; Sigma-Aldrich) solution for 30 min at RT. Mouse monoclonal anti-

pimonidazole antibody (clone 4.3.11.3)(MAb1) was diluted 1:50 in PBS containing 0.1% BSA and 0.1% Tween 20 and incubated overnight at 4°C. After 2 washes with PBS, cells were incubated for 1 hour with Anti-mouse Alexa Fluor 594 (Invitrogen, Grand Island, NY) 1:500 in 0.2% FSG solution. Finally, the cryosectioned spheroids were mounted in ProLong Gold Antifade Mountant with DAPI (Invitrogen, Grand Island, NY, USA) and the staining distribution was assessed using a fluorescence microscope (Leica DM6000, Germany).

2.7.2 Apoptotic activity

HT29 spheroids were placed in a 24-well plate at 100 spheroids/well prior to the incubation with NucViewTM 488 (Biotium, Hayward, CA). Cells were incubated with fluorescent dye diluted 1:200 in culture medium for 2h. Spheroids were centrifuged for 5 min at 200x g and washed twice with PBS and immediately fixed in 4% (w/v) paraformaldehyde (PFA) and 4% (w/v) sucrose solution in PBS for 30 min at RT. After 2 washes with PBS, spheroids were dehydrated in 30% (w/v) sucrose solution in PBS. For the cryosectioning, spheroids were frozen at -80 ºC in Tissue Teck OCTtm (Sakura Finetek Europe B.V., Zoeterwoude, The Netherlands) and were sectioned in cryostat in sections of 10 µm. Cryosections were washed twice with PBS, mounted in ProLong Gold Antifade Mountant with DAPI (Invitrogen, Grand Island, NY) and NucViewTM 488 staining was assessed using a fluorescence microscope (Leica DM6000, Germany).

2.7.3 Immunofluorescence microscopy and image analysis

Non-microencapsulated MCF7/hDFs and H1650/hDFs co-culture samples were collected at day 5 and 7 of culture, respectively, and fixed in 4% PFA / 4% Sucrose for 20 min. Samples were dehydrated and cryosectioned as described in the “Apoptotic Activity” subsection. Cells were permeabilized for 10 min with 0.1% TX-100 and blocked in 0.2% FSG. Anti-vimentin (ab16700, Abcam) was diluted in 0.2% FSG and incubated for 2h at room temperature (RT) and secondary antibody Anti-mouse Alexa 488 (A11001, Life Technologies) was

diluted in 0.125% FSG and incubated for 1h at RT. Samples were mounted in ProLong Gold Antifade Mountant with DAPI (Life Technologies) and visualized using a fluorescence microscope (Leica DM6000, Germany).

2.7.4 Drug perturbation

Non-microencapsulated and microencapsulated mono-cultures of H1650 cells were collected from the stirred-tank culture system during exponential growth phase (day 6) and plated in 96-well plates, with approximately 10 microcapsules per well, under orbital agitation. The cultures were then treated with a range of Docetaxel (A-872960, Sagent) concentrations for 4 days and cell viability was determined with CellTiter-Glo® 3D Cell Viability Assay (Promega). For total cell lysis, aggregates were incubated with the CellTiter-Glo® reagent for 40 min under strong agitation, pipetted up and down quickly 10 times each well, and placed under strong agitation for another 40 min. DMSO was used as vehicle control. IC50 was determined using GraphPad Prism 5 software. Every condition was run at least in triplicate.

2.8 Statistical analysis

Statistical analysis was carried out using GraphPad Prism 5 software. D'Agostino & Pearson normality tests were performed on the analyzed samples to determine if the datasets followed a normal distribution. The non-parametric Kruskal-Wallis test was used to compare spheroid area and diameter between cell aggregation conditions and different days of culture. Levene's test was used to assess the equality of variances between spheroid populations. Data are shown as mean ± standard deviation of the mean.

3 Results

3.1 Generation of tumour cell spheroids in stirred-tank culture systems

Generation of tumour cell spheroids in stirred-tank culture systems was evaluated for a heterogeneous panel of tumour cell lines to evaluate the

applicability of the strategy proposed. Cells were inoculated as single cell suspensions in stirred-tank culture systems. Optimal conditions for spheroid formation were established by variation of cell concentration at inoculation [31] and stirring rate [32], which have been previously described to have an impact on dynamic cell aggregation. Aggregation time was defined as the number of days necessary to establish compact spheroids, which was qualitatively measured by microscopic analysis of the spheroids and based on the observation of higher cell packing densities within the cellular aggregates. Spheroids were classified either as compact or loose aggregates based on how tightly packed tumour cells were within the spheroid volume. The shape of the spheroid was classified as spherical-shaped (when the aggregates had a round morphology with no surface edges) and irregular (comprising all the non-spherical shapes). An image J software tool ("Solidity") was used to classify the spheroids and 0.90 was considered the threshold to classify the aggregate as spherical and regular. Average spheroid diameter, spheroid diameter dispersion and spheroid morphology were monitored as indicators of culture performance. Figure 2.1 reports the optimization steps for the successful aggregation of tumour cells and comprises the experimental basis proposed in this work for the generation of tumour spheroids in agitation-based culture systems.

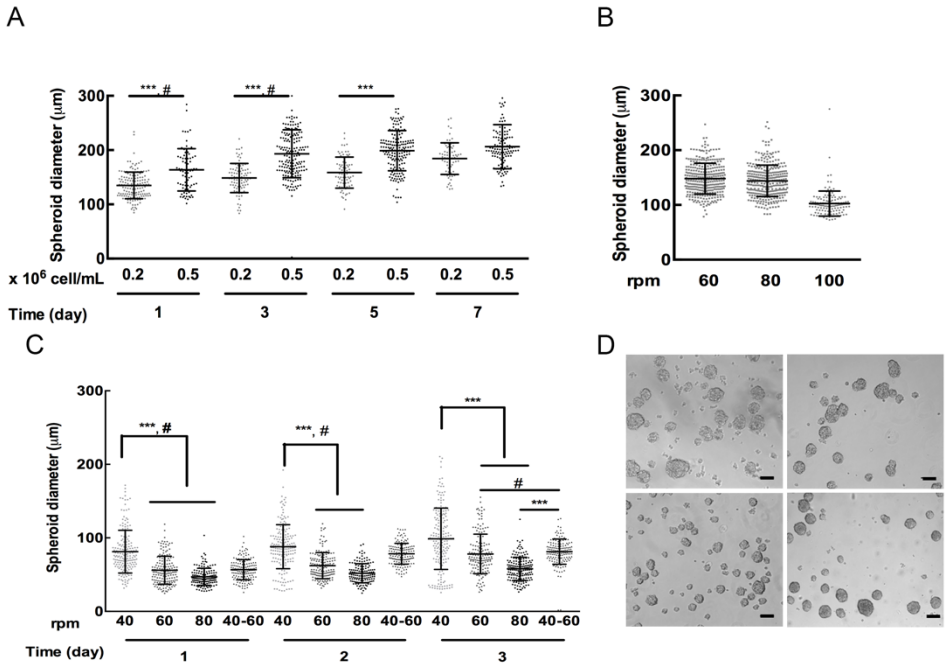

Figure 2.1: Optimization for tumor cell spheroid formation in stirred-tank culture systems. (A) Assessment of the effect of cell inoculum on the diameter of MCF7 spheroids with a starting stirring rate of 60 rpm over culture time. (B) Assessment of the effect of stirring rate on the diameter of MCF7 spheroids at 24 h of culture with an inoculum of 0.2 × 10^6 cell/mL. (C) Assessment of the effect of stirring rate on the diameter of H460 spheroids at day 1, 2 and 3 of culture with an inoculum of 0.2 × 10^6cell/mL. (D) Phase contrast microscopy imaging of H460 spheroids at day 3, aggregated with starting stirring rates of 40, 60, 80 rpm and 40–60 rpm. In (A) and (B), the data represented are from3 independent experiments (mean ± _SD) and statistical analyses were performed by non-parametric Kurskal–Wallis test for comparison of aggregate diameter (***p < 0.001) between the different inocula, at each time point (A) or stirring rate (B) and Levene's test for comparison of spheroid diameter dispersion (#p < 0.00001) with the different inocula, at each time point (A). Scale bars represent 100 µm.

Three-dimensional monocultures of MCF7 cells were obtained by day 1 of culture, for all tested conditions: two different cell inocula and three sets of starting stirring rates (Figure 2.1A and 2.1B). The cell inoculum of 0.2x10^6

cell/mL resulted in spheroids with an average diameter of 148±28.1 μm at day 1 of culture, which is significantly lower than the one obtained with an inoculum of $0.5x10^6$ cell/mL (160.6±34.6 μm) by the same culture time (Figure 2.1A). This tendency was maintained until day 5 of culture. Moreover, the lower cell inoculum also resulted in significantly lower variance ($p<0.00001$) of the aggregate diameter at days 1 and 3 (Figure 2.1A). Nonetheless, by the 7^{th} day of culture, no significant differences in both average spheroid diameter and its variance were detected between both culture conditions (184.3±29.1 and 204.2±33.5 μm, for 0.2 and $0.5x10^6$ cell/mL, respectively). Based on these results, the lower cell inoculum concentration ($0.2x10^6$ cell/mL) was used for the following experiments with MCF7 cells.

Three starting stirring rates were tested for the generation of MCF7 spheroids: 60, 80 and 100 rpm (Figure 2.1B). These are within the ranges reported to induce cell aggregation in the culture vessels used in this study, without significant impact on cell viability [40]. All the selected agitations led to the formation of spherical and compact MCF7 spheroids. Spheroids obtained with starting stirring rates of 60 and 80 rpm had similar average spheroid diameter (148±28.2 and 143.9±28.7 μm, respectively, Figure 2.1B). A stirring rate of 100 rpm led to the formation of spheroids with a mean diameter of 101.2±17.3 μm at day 1, significantly ($p<0.001$) lower than for the other conditions assessed.

When a starting stirring rate of 60 rpm was applied, spheroid diameter increased to 120 μm within the first hours of aggregation (data not shown), most probably due to aggregate fusion [37]. Stirring rate was then adjusted to 80 rpm at 5h of culture, which led to a stabilization of spheroid size (average diameter of 148 μm) at day 1 (Figure 2.1B). Since no major differences were observed at day 1, between initial stirring rates of 60 and 80 rpm, the optimal conditions of MCF7 aggregation were defined by a constant stirring rate of 80 rpm and a cell inoculum of $0.2x10^6$ cell/mL.

A

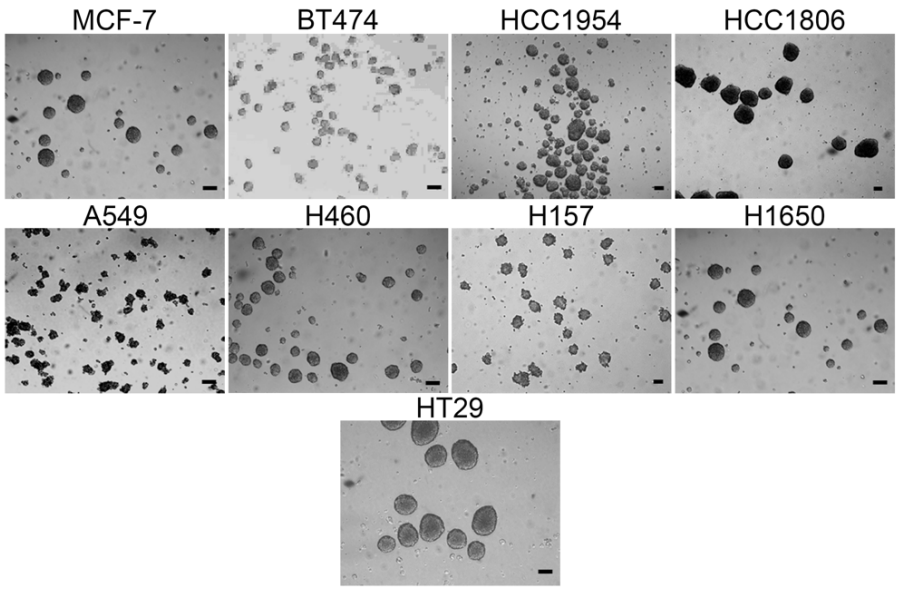

B

Pathology (Carcinoma)	Aggregation time (day)	Spheroid shape	Average diameter (µm)
ER^+ PR^+ $HER2^-$ Breast	1	Spherical	144 ± 29
ER^+ PR^+ $HER2^+$ Breast	1	Spherical	107 ± 29
ER^- PR^- $HER2^-$ Breast	4	Spherical	149 ± 32
ER^- PR^- $HER2^-$ Breast	4	Irregular	238 ± 41
NSCLC	3	Irregular	125± 28
NSCLC	3	Spherical	81.± 17
NSCLC	3	Irregular	141 ± 21
NSCLC	3	Spherical	100± 22
Colon	3,00	Spherical	298 ± 92

Pathology (Carcinoma)	Cell line	Source/Tumor histology	Agitation rate range (rpm)
ER^+ PR^+ $HER2^-$ Breast	MCF7	Mammary gland breast adenocarcinoma derived from metastatic site (pleural effusion)	80
ER^+ PR^+ $HER2^+$ Breast	BT474	Mammary gland breast ductal carcinoma	80
ER^- PR^- $HER2^-$ Breast	HCC1954	Mammary gland/Breast ductal carcinoma	80-100
ER^- PR^- $HER2^-$ Breast	HCC1806	Mammary gland breast squamous carcinoma	80-100
NSCLC	A549	Alveolar adenocarcinoma	40-60
NSCLC	H460	Lung large cell carcinoma (pleural effusion)	40-60
NSCLC	H157	Oral squamous carcinoma	80-100
NSCLC	H1650	Lung adenocarcinoma derived from metastatic site (pleural effusion)	40-60
Colon	HT29	Colorectal adenocarcinoma	40-60

Figure 2.2: Generation of tumor cell spheroids in stirred-tank culture systems across different pathologies. (A) Phase contrast imaging of representative

samples of tumor spheroids at the end of the aggregation phase. Scale bar represents 100 µm. (B) Description of aggregation conditions for the selected cell lines in stirred-tank culture systems. Abbreviations: ER: Estrogen Receptor; PR: Progesterone Receptor; HER2: Human Epidermal Growth Factor Receptor 2; NSCLC: Non-Small Cell Lung Carcinoma.

In the case of H460 cells, 3 days of culture with constant stirring rate of 40, 60 and 80 rpm and an inoculum of $0.2x10^6$ cell/mL resulted in the successful aggregation of the tumour cells with a mean diameter of 98.8±41.7, 78.1±26.9 and 57.9±15.8 µm, respectively (Figure 2.1C). By changing the stirring rate from an initial value of 40 rpm to 60 rpm at the end of aggregation phase, H460 spheroids were formed at day 3 with 81.2±17.1 µm of diameter (Figure 2.1C), with a compact and spherical shape (Figure 2.1D).

Our results on the aggregation of H460 cells with different stirring profiles (low, medium and high) demonstrated that spheroid diameter and size dispersion can be tailored by adjusting hydrodynamic conditions. Spheroid diameter increased with lower stirring rates but that also led to higher size dispersion and fusion of the aggregates. The optimal condition for the aggregation of H460 cells was then chosen to be 40-60 rpm, as it formed spheroids with the best combination of mean diameter and size dispersion. Moreover, spheroid number and spheroid size were correlated in an inversely proportional manner.

For H157 cells, a starting stirring rate of 80 rpm resulted in irregular spheroids at day 1 of culture (Figure S2.1); an increase to 100 rpm in stirring rate by that time resulted in the gradual compaction of spheroids, until day 3 of culture. This example also highlights the rationale for the increase in stirring rate during the aggregation phase of some of these tumour cell lines in stirred-tank culture systems.

In this study, spheroid formation in stirred-tank culture systems was achieved for nine distinct tumour cell lines (Figure 2.2), under the conditions described in Figure 2.2B.

All tumour cell lines were inoculated at a cell density of $0.2x10^6$ cell/mL. This was based on the cell aggregation results obtained for MCF7 (Figure 2.1A), which were also in accordance with data from our group for other non-tumour cell sources [37]. The aggregation period was optimized to occur up to a maximum of 4 days of culture from single cell inoculation.

MCF7 spheroids were tightly-packed with a well-defined border. Across NSCLC pathology, H460 and H1650 cells formed spherical and compact aggregates whereas A549 and H157 aggregates presented a less uniform shape, with typical cell spreading and branching at the edges of the spheroids (Figure S2.1). On the other hand, HT29 cells formed large and smooth spheroids (Figure 2.2A). BT474 cells aggregated in one day of culture and quickly increased in size (Figure 2.3B).

At the end of aggregation, BT474 and HT29 cells formed the largest spheroids with a maximum diameter of approximately 287 and 298 μm, whereas H460 spheroids were the smallest with approximately 81 μm, all attained at day 3. For each cell line, cell aggregation and spheroid size was controlled by manipulation of stirring rate, which was adjusted throughout the culture period. Typically, cell aggregation was initiated at stirring rates between 60 and 80 rpm (stirring profile of medium intensity) in order to maximize cell collisions and simultaneously avoid cell damage due to high shear stress [40, 41]. Changes of those stirring profiles to higher (*e.g.* H157 cells) or lower stirring rates (HT29, A549 and H1650 cells) were selected based on the aggregative ability of the cell lines. The rationale for tailoring the stirring rate was selected to favour spheroid formation, to promote their compaction, to limit spheroid clumping and fusion and ideally to form spherical and compact spheroids between 100 and 300 μm of diameter, with low levels of variance on spheroid diameter and amenable for characterization and drug screening [42].

The aggregation of these tumour cells in stirred-tank culture systems was proven to be a highly reliable methodology since several tumour cell lines (MCF7, H1650, H157 and HT29) were cultured in more than 10 independent biological replicates with reproducible results in spheroid size and

concentration. Moreover, high concentrations of spheroids were attained for all the tested cell lines, typically in the range of 1000-1500 spheroids/mL. Total volume of culture was adjusted, depending on the needs for the experimental design, but typically ranged from 50 to 500 mL, with generation of up to around 750 thousand spheroids in a single batch.

3.2 Tumour spheroid culture in stirred-tank culture systems

In addition to cell aggregation, agitation-based culture systems are also a powerful tool to maintain long-term 3D cultures. Figure S2.2 reports the characterization of culture progression for spheroids of three different NSCLC cell lines (H460, A549 and H1650) cultured in stirred-tank culture systems.

Aggregation of H460, H1650 and A549 cells in stirred-tank culture systems led to the formation of compact spheroids with different morphologies and average diameters ranging from 80 to 125 μm by day 3 of culture (Figure S2.2B). Aggregation was initiated at low stirring rates (40 rpm), followed by an increase to medium stirring rates (60 rpm) to induce compaction. After aggregation phase, spheroid cultures of the three cell lines were maintained at 60 rpm. By day 10, spheroids of all cell lines showed high cell viability, as indicated by FDA dye (Figure S2.2A).

H460 cells showed a significant ($p<0.001$) and continuous increase in average spheroid diameter (Figure S2.2B), from an early stage of aggregation (56.7±13.8 μm at day 1), to 81.2±17.2 μm at day 3 and up to 115.8±24.2 μm at day 10 of culture. Variance of spheroid diameter size remained constant throughout the culture period. Amongst all the evaluated NSCLC cells, A549 spheroids presented the lowest variation in spheroid diameter during the 10 days of culture. Despite the significant ($p<0.01$) size increase during aggregation (from 107.5±26.2 μm at day 1 to 125±27.7 μm at day 3), A549 spheroid diameter was not higher after 10 days of culture (114.3±41.1 μm, Figure S2.2B). Nevertheless, size dispersion of these aggregates increased significantly with time ($p<0.000001$), especially after the aggregation phase. This result probably reflects the higher degree of irregularity of these spheroids

(Figure S2.2A). The culture of H1650 cells in stirred-tank culture systems was comprised of an initial period of spheroid stabilization that lasted for 3 days and was associated to the aggregation step (Figure S2.2B). During this period, H1650 spheroids did not increase significantly in diameter, starting from 93.1±19.2 μm at day 1 up to 100.3±21.5 μm at day 3 of culture (Figure S2.2B). Nevertheless, at days 7 and 10 of culture, H1650 spheroids presented significantly ($p<0.001$) higher diameters (152.7±33.9 μm at day 10), which led to a significant increase on the variance of spheroid diameter dispersion ($p<0.000001$).

Cell expansion along culture time was observed for the 3 cell lines (Figure S2.2C). The fold increase in cell concentration was of 11.01, at day 7, for H460 cells and of 6.57, at day 8, for H1650, which were both reflected on the observed increase in spheroid diameter during culture (Figure S2.2B). A549 cells presented the lowest cell expansion, with a maximum fold increase in cell concentration of 5.83 (Figure S2.2C), attained only at day 10 of culture. This, together with the high irregularity of A549 spheroids, might justify the observed constant average spheroid diameter along culture time and the significant increase in spheroid diameter variance (Figure S2.2B).

For HT29 colon cancer cells, aggregation and compaction took place in the first 3 days of culture (Figure 2.2B). By that time, the average diameter was of approximately 300 μm (Figure 2B and Figure 3A).

HT29 spheroids presented a significant increase in average diameter along culture time. From day 7 (512.3±76.4 μm) onwards, a clear zonal distinction between the core and the outer layer of the spheroids was observed by fluorescence microscopy of spheroid cryosections (Figure 2.3B). HT29 cells were highly proliferative in 3D culture, achieving a fold increase in cell concentration of 19.6±1.4 at day 12 of culture. By day 7, the spheroid core presented low compactness degree, with empty extracellular spaces. At this time point, cells in the core region of the spheroids accumulated the fluorescent product of a caspase-3 substrate, indicating that apoptosis was occurring in this region (Figure 2.3B).

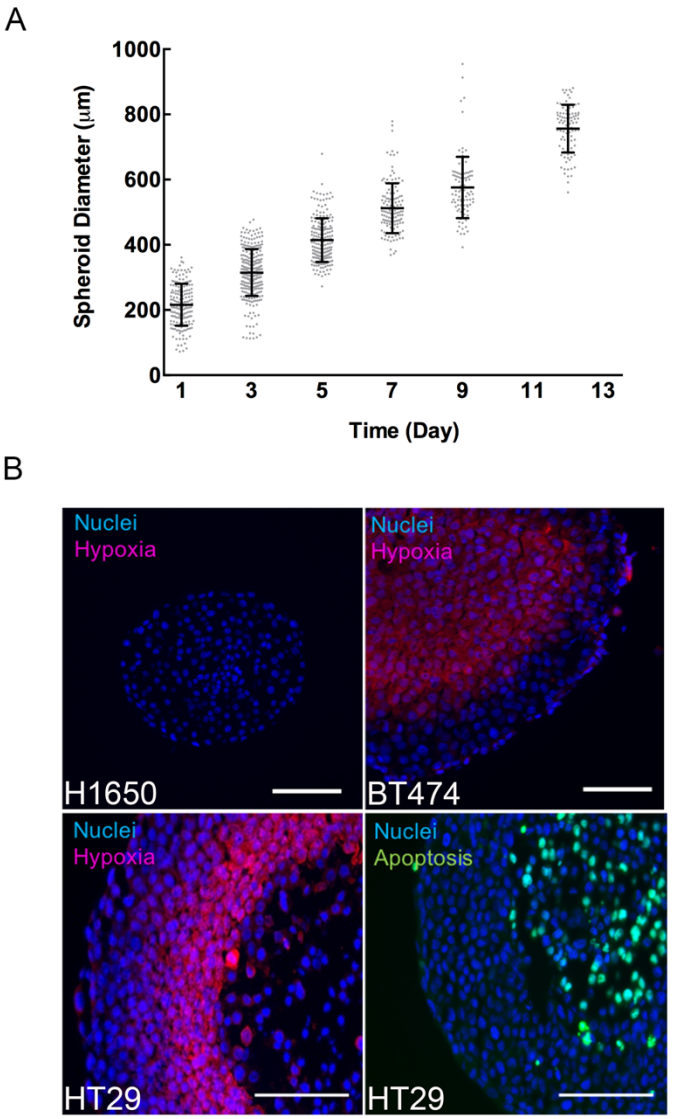

Figure 2.3: Characterization of H1650, BT474 and HT29 spheroid cultures in stirred-tank culture systems. (A) Profile of HT29 spheroid diameter throughout the culture period. (B) Immunofluorescence characterization of H1650, BT474 and HT29 spheroids in 10 μm thick cryosections at day 7, 17 and 7, respectively, for the detection of hypoxia (hypoxyprobe, red) and DAPI (blue). Immunofluorescence characterization of HT29 spheroids in 10 μm thick cryosections at day 7, for the detection of caspase 3 (green) and DAPI (blue). Scale bar represents 100 μm for H1650 and BT474 cells and 200 μm for HT29 cells.

Additionally, hypoxia was detected in spheroids at day 7 of culture by immunofluorescence analysis of protein adducts with pimonidazole (Figure 2.3B, in red), with increased detection towards the inner part of the spheroid. Apoptotic cells and hypoxic regions were not detected in the HT29 spheroids at day 3 of culture (data not shown). These results indicated the presence of apoptotic cores in HT29 spheroids, with diameters of 500 μm, are concomitant with the occurrence of hypoxia. Figure 2.3B also depicts hypoxia stainings for H1650 and BT474 cells. No hypoxic regions were detected in H1650 spheroids throughout the culture period. H1650 spheroids achieved a mean diameter of 150 μm (at day 10 of culture) and no hypoxic regions were detected, therefore confirming the lack of oxygen gradients in these aggregates. On the other hand, BT474 spheroids, with a mean diameter of 304±77 μm, displayed hypoxic regions, more prominent towards the inner region of the spheroid. No apoptotic cores were detected in either H1650 or BT474 spheroids. Altogether, these results suggest that the presence of apoptotic cores is associated with gradients of hypoxia and oxygen diffusion limitations due to increased dimensions of the spheroids, confirming earlier literature [42].

In summary, aggregation of tumour cell lines in stirred-tank culture systems allows for the flexibility to produce spheroids with a variety of cell lines that yield spheroids with different sizes and characteristics, dependent on the cell type used for the establishment of the 3D tumour model.

3.3 Generation of heterotypic 3D tumour cell models in absence/presence of physical support

Co-cultures of tumour cells with fibroblasts are currently highly coveted in cancer research to assess the role of the cross-talk between these two cell types in tumour progression and drug resistance [43]. There is a need for cell models that enable interrogation, identification and contribution of each cell type. In this study, co-cultures were generated by simultaneous inoculation of both cell types in stirred-tank culture systems (Figure 2.4A). In the case of co-cultures of MCF7 cells with fibroblasts, after 5 days of culture heterotypic

aggregates were composed of breast tumour cells and fibroblasts (Figure 2.4B).

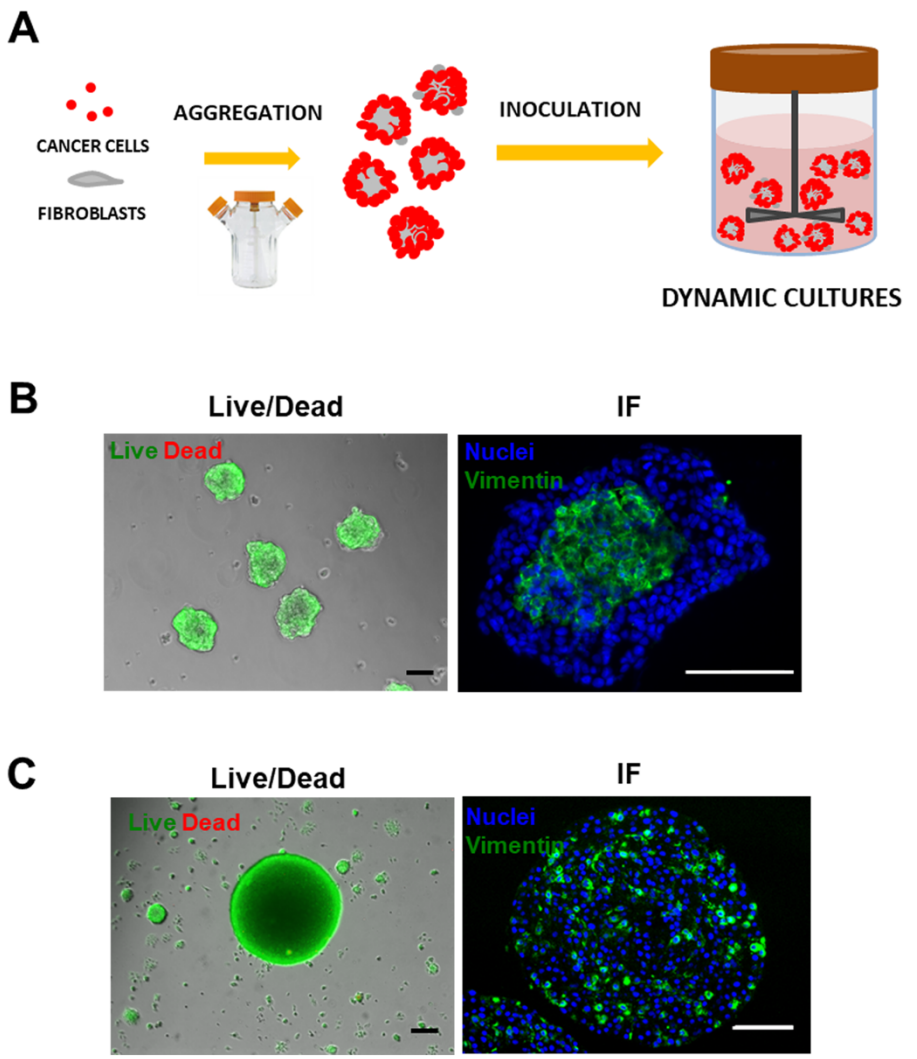

Figure 2.4: Characterization of heterotypic tumor co-cultures in stirred-tank culture systems. (A) Schematic diagram of the strategy followed for the establishment of heterotypic tumor-fibroblasts co-cultures. (B) Characterization of co-cultures of MCF7 spheroids and hDFs at day 5 of culture by live/dead assay (FDA-green, live cells; To-PRO3-red, dead cells; respectively) and by immunofluorescence (IF) with vimentin (fibroblasts, green); Nuclei were stained with DAPI (blue). (C) Characterization of co-cultures of H1650cells and hDFs at day 7 of culture by live/dead assay (FDA-green,

live cells; ToPRO3-red, dead cells; respectively) and by immunofluorescence (IF) with vimentin (fibroblasts, green); Nuclei were stained with DAPI (blue). Scale bar represents 100 µm.

Cells in heterotypic spheroids remained viable and fibroblasts, detected by vimentin immunolabeling (Figure 2.4B, in green), accumulated in the centre of the spheroid. This has been previously reported for MCF7 cells and proposed to be associated with the poorly invasive phenotype of these cells that would therefore infiltrate in a lesser extent to the core of fibroblasts [44, 45]. Heterotypic MCF7 co-cultures are heterogeneous and aggregates display different ratios of tumour cells and fibroblasts per aggregate. This has also been observed for heterotypic aggregates of H1650 cells and fibroblasts (Figure 2.4C). After 7 days of culture, co-cultures of H1650 cells and hDFs in stirred-tank culture systems led to the formation of spheroids with high diameters (higher than 500 µm) and others with approximately 100 µm. Fibroblast distribution within the spheroids was not located in the core but dispersed throughout the aggregate, as indicated by the vimentin staining in Figure 2.4C (in green).

As alternative to heterotypic tumour spheroids, a microencapsulation strategy (Figure 2.5A) was pursued for the establishment of co-cultures of tumour and stromal cells. To provide an artificial scaffold for both cell types, an alginate matrix was used for microencapsulation of tumour spheroids (generated in stirred-tank culture systems, as described above) together with fibroblasts, in a 1:1 cell ratio. Cells entrapped in the alginate microcapsules were further cultured in stirred-tank culture systems.

By day 5 of culture, microencapsulated MCF7 spheroids presented a compact morphology and high cell viability (Figure 2.5B), in both mono- and co-cultures. In co-cultures, MCF7 spheroids were surrounded by fibroblasts, which also remained viable after microencapsulation. The same microencapsulation strategy was pursued for the H1650 cells. Compact H1650 spheroids (day 3 of aggregation, Fig 2B), were microencapsulated in alginate, with and without

hDFs for generation of mono and co-cultures. By day 5 of culture, alginate microcapsules contained up to three H1650 spheroids in both mono-culture and co-culture conditions (Figure 2.5B). In co-culture, hDFs surrounded H1650 spheroids, similarly to what was observed for MCF7 co-cultures. Both in mono- and co-cultures, spheroids were mainly composed of viable cells, with just few non-viable cells detected (Figure 2.5B). Apoptosis characterization of the microencapsulated mono- and co-cultures of H1650 cells also revealed that, at day 5 of culture, the spheroids did not present apoptotic cells, with few apoptotic fibroblasts detected in co-cultures (Figure 2.5B). No apoptotic cores were found, which suggested that the stirring conditions provided an efficient nutrient and oxygen distribution within the vessel and that alginate microcapsules permitted an efficient mass transport.

Several other tumour cell lines were successfully microencapsulated in alginate hydrogels, including H157, H460 and HCC1954 cells. All microencapsulated spheroids maintained high levels of viability throughout the culture period and presented increasing diameters (up to 400 μm) within the microcapsules along culture time (data not shown), indicating that physical support from the artificial alginate scaffold is suitable for generation of heterotypic cancer models. Alginate hydrogels provide a physical support allowing cell growth of embedded tumour spheroids, although at slightly lower rates than the ones observed for the non-microencapsulated spheroids (124 μm vs 153 μm for H1650 cells at day 7, respectively, Figure S2.3A). These differences further support the relevance of providing an artificial matrix support for the embedding of tumour spheroids, as this organization will recapitulate more closely the growth kinetics and the physical constraints found in tumours *in vivo*. Perturbation studies with a standard of care chemotherapeutic agent (Docetaxel) were also performed for determination of dose response curves. Cells were treated for 4 days and a typical dose response curve was generated for the microencapsulated and non-microencapsulated H1650 tumour spheroids (Figure S2.3B). IC50 values of 45.8 and 2.7 nM were determined for non-microencapsulated and microencapsulated tumour cells, indicating that

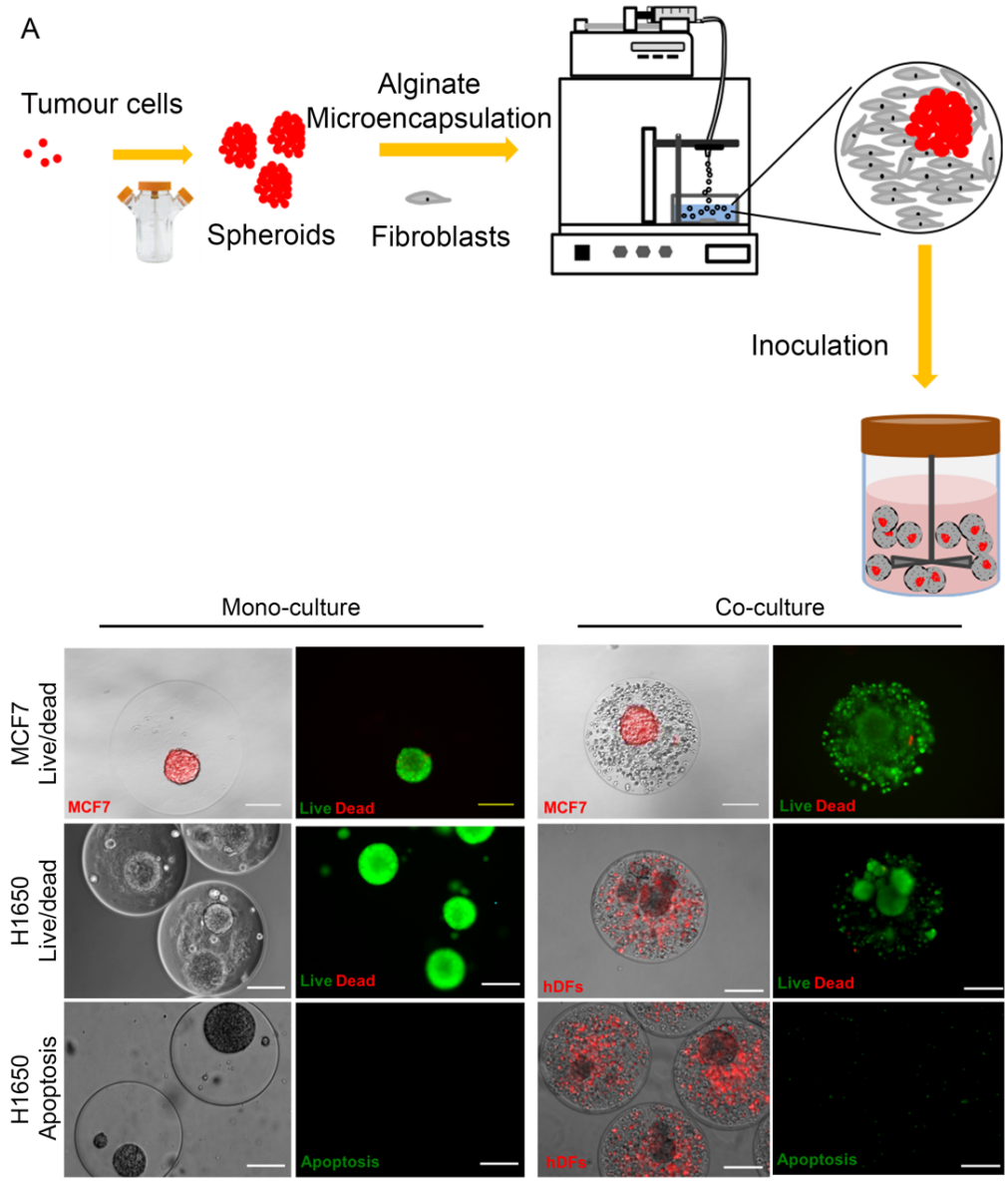

Figure 2.5: Characterization of microencapsulated tumor co-cultures in stirred-tank culture systems. (A) Schematic diagram for the strategy followed for the establishment of encapsulated tumor and fibroblasts co-cultures. (B) Qualitative characterization of encapsulated mono- and co-cultures of MCF7 and H1650 spheroids together with hDFs, at day 5 of culture by live/dead assay (FDA-green, live cells; To-PRO3-red, dead cells; respectively); For the phase contrast imaging and identification of cell populations, MCF7 cells were RFP-labeled (red) and hDFs co-cultured with

H1650 cells were labelled with PKH26 (red). Apoptosis characterization of microencapsulated H1650 mono-and co-cultures was performed with NucView488TMcaspase 3 activity probe (green). Scale bar represents 200 µm.

embedding with alginate hydrogels did not compromise drug efficacy. In summary, we demonstrated that different approaches can be implemented for the generation of 3D heterotypic *in vitro* cancer models, which will allow the evaluation of cell-cell interactions in various physiologically relevant processes, specifically distinct tumour types with different levels of tumour/stroma distribution, cell ratios and heterogeneity.

4 Discussion

In this study, we demonstrate that agitation-based technologies are feasible for the generation of 3D tumour *in vitro* models and amenable for feeding automated platforms and high throughput screenings. We have developed standardized protocols for the efficient generation of compact spheroids for a panel of 9 tumour cell lines, demonstrating the robustness of the strategy proposed herein. This is the first systematic study on application of stirred-culture culture systems for production of tumour cell spheroids. Despite being frequently suggested in the literature as a suitable technology [1], experimental reports using agitation-based technologies are scarce [20, 47].

Tumour spheroids, which to some extent resemble the tumour architecture *in vivo* [48, 49], are usually generated in hanging drop or liquid overlay techniques [25, 27], embedded or on top of scaffolds and hydrogels [50, 51]. The dynamic culture system herein described promotes cell-cell interactions due to hydrodynamic forces [52] that lead to efficient generation of spheroids. Our results show that high numbers of spheroids can be produced using stirred-tank culture systems, which display phenotypic features previously described for spheroids generated in more conventional and widely used culture systems. Our strategy led to the generation of 1000-1500 tumour spheroids/mL; no other culture strategy enabled the production yields we describe for agitation-based

technology [21]. Current demands on cancer drug discovery cascade require the generation of extensive numbers of cell models for assessment of drug efficacy of compound libraries. The ability to scale up the production of spheroids within a large range of culture volumes offered by stirred-tank culture systems represents an important step towards the large numbers required for screening applications [33]. Additionally, automated monitoring and control of physico-chemical parameters can be introduced by using stirred-tank bioreactors. Another important benefit of stirred-tank culture systems is the capacity for continuous monitoring of the cultures with non-destructive sampling, avoiding the introduction of operation artefacts on the read-out measurements [53]. Moreover, the reproducibility of well-defined 3D models enables translation between laboratories [54].

Additional advantages of stirred-tank culture systems for the generation of 3D spheroids in comparison with static conventional culture systems include the ability to customize culture parameters to induce aggregation and to allow spheroid culture for cell lines displaying different properties and phenotypes, as it has been shown in figures 2.1 and 2.2. Size dispersion of the produced spheroids in stirred-tank culture systems can be high, nevertheless adjustments on stirring parameters have an impact on the culture hydrodynamics manifesting via alterations in cell aggregation and phenotype and effectively controlling size and shape of spheroids, avoiding aggregate clumping and enabling an efficient transport of nutrients and oxygen to the spheroids [33]. Differences on impeller geometry, inoculum concentration and stirring rate induce variations on the frequency of cell-cell collisions and hydrodynamic forces created in the culture vessel, thus possibly contributing for different cell aggregation kinetics [41]. Spinner vessels with straight blade paddle impellers and baffles were selected for the aggregation of tumour cells as this configuration improves aeration and agitation of spheroids, promoting efficient mixing with reduced shear stress [39]. In addition to this hydrodynamic parameter, the influence of cellular inoculation density and stirring rate on the dynamics of tumour cell aggregation was studied and the fine tuning of these

parameters enabled the formation of high numbers of homogeneous populations of spheroids. As it was reported in figures 2.1 and 2.2, bioprocess optimization for the aggregation of tumour cell lines led to the development of a robust protocol, in which slight variations in stirring conditions did not significantly impact the aggregation ability of tumour cells. Simultaneously, the proposed methodology also provided the versatility to adjust culture parameters in order to fine tune the aggregation, compaction and long-term culture of each tumour cell line in dynamic conditions, maintaining the inherent biological properties of the cells and forming spheroids with different levels of compactness, geometry and size.

Currently, there is a need to distinguish tumour cell properties in 3D, in order to understand the role of key hallmarks of cancer on drug response [55]. Interestingly, the different stirring profiles used for aggregation of tumour cells may present correlation with the different tumour histotypes (adenocarcinomas; squamous, ductal or large-cell carcinomas), origin (basal or luminal) and whether the cells are derived from the parental tumour or from the metastatic location. In this study, H157 cells aggregated in stirred-tank culture systems formed irregular spheroids with branching on the edges of the spheroids, a feature that has already been reported in *in vitro* matrix-embedded 3D cell models and was suggested to be associated with the high invasive potential of these cells [43]. The versatility of our culture strategy was also particularly evident on the cross-comparison established in figure 2.3 between the selected NSCLC cell lines. H460, A549 and H1650 cells were successfully aggregated and cultured under similar agitation profiles, generating spheroids with high levels of cell viability with distinct shapes, sizes and proliferation levels. For instance, H460 cells, which presented the highest fold increase in cell concentration out of these three selected lung cancer cell lines, was originated from a large cell carcinoma, known for fast spreading as pathological feature [56, 57]. Nevertheless, the establishment of a correlation between spheroid-forming ability and clinico-pathological features of the original tumour is not straightforward. Rather, each cell line and its various subpopulations are

unique, thus presenting an individual ability to generate spheroids [58]. Relationships between molecular phenotype, tumourigenicity and spheroid-forming ability are complex as the stratification of tumour cell lines into specific categories is most of the times not achieved. Nevertheless, previous studies reported that breast cancer cell lines with similar morphologies clustered together by gene expression analysis [6]. Moreover, cancer patient databases have previously demonstrated the correlation between spheroid morphology and clinical outcome of lung cancer [59]. These results reinforce the notion that tumour cell lines retain critical clinical information about the tumours from which they are derived, which is revealed in a microenvironment that models cellular interactions found in solid tumours, such as 3D spheroid cultures. Therefore, tumour cell lines placed in the appropriate context represent potentially powerful tools both for the identification of key processes involved in disease progression [46] and as models for evaluating potential therapeutic strategies [59]. In the future, application of the methodology proposed herein to an even larger panel of tumour cell lines will allow to inquiry on correlations between tumour origin, histotype and cell aggregation, spheroid size and shape at a deeper level.

Stirred-tank culture systems enable efficient mass transport with diffusion of oxygen, nutrients and pro-survival signals between cells within the spheroids and removal of waste metabolites, contributing for high levels of cell viability and lack of hypoxia gradients and apoptotic cores [1], as observed in our study for aggregates below 300 μm diameter (H1650 cells). Nonetheless, for HT29 and BT474 cells that generated large spheroids, distinct zonal properties have been identified within aggregates of at least 500 μm (figure 3), with detection of oxygen gradients and hypoxia. HT29 cells have been described to be highly enriched in $CD44^+$ cancer stem cell-like cells and the relative numbers of dividing cells *in vitro* have been proposed to be proportional to clonogenicity and tumour-formation capacity *in vivo* [60]. The features obtained in this work for large HT29 and BT474 spheroids have been repeatedly described for tumour spheroids obtained in other culture systems [61] and have been

correlated with the characteristics of the native tumour microenvironment, including the aforementioned regions of hypoxia and necrosis [62]. The scarce and heterogeneous distribution of vascularization in primary tumours contributes to poor diffusion of oxygen and nutrients, thus leading to the formation of those gradients [61].

In this work we also focused on the establishment of tumour/stromal (fibroblasts) co-cultures in stirred-tank culture systems. This was achieved by two different approaches: (i) simultaneous inoculation of both cell types in stirred-tank culture systems; (ii) confinement of both cell populations within an artificial hydrogel, through microencapsulation of tumour spheroids and fibroblasts, as indicated in figures 2.4 and 2.5. The two strategies resulted in different organizations of tumour cells and fibroblast populations, with initial cell-cell contact (non-microencapsulated) and no initial contact (microencapsulated). The alginate microencapsulation strategy was performed with different tumour cell lines, such as MCF7 and H1650 (figure 2.5). The physical support from an artificial scaffold can contribute to mimic the cell-ECM interactions, which are a driving force for tumour organization and progression [63]. Different materials are currently used for the establishment of *in vitro* cancer models, such as ECM components (collagen I, Matrigel) and polymers (hyaluronic acid, alginate and polyethylene glycol) [20]. Matrigel is widely used for the establishment of *in vitro* 3D cultures but its biological origin (tumour) and ill-defined composition can lead to uncontrolled morphological and phenotypic changes of tumour cells and generate bias on tumour progression [64]. Inert alginate hydrogels provide an aqueous environment for cell microencapsulation [38]. Alginate microcapsules have high permeability, stability and elasticity, with bi-directional diffusion of nutrients, oxygen and soluble factors, supporting an efficient and long-term culture with high levels of cell viability. Moreover, the dimensions and shape of the hydrogel microcapsules were set for an optimal surface to volume ratio, to ensure a good mass diffusion to the centre of the microcapsule and to accommodate tumour spheroids [39]. Cell proliferation (data not shown) and absence of apoptotic centres (figure 2.5B) observed in

the microencapsulated cultures suggest that oxygen and nutrient diffusion were not compromised in the implemented culture conditions. This outcome shows that the alginate microencapsulation strategy as a valid alternative to ensure the *in vitro* culture of these tumour cells in dynamic culture systems, enabling their growth and avoiding cell death. In particular, the interactions between tumour and stromal cells can be monitored along the culture time. These results demonstrate the flexibility of the proposed approaches, as different co-culture systems can be established in stirred-tank culture systems. These 3D tumour models generated in stirred-tank culture systems were also validated for perturbation studies by incubating non-microencapsulated and microencapsulated H1650 tumour spheroids with Docetaxel. Dose response curves were obtained upon few days of treatment, indicating levels of drug efficacy dependent on the concentration of the compound, as expected. The production of large numbers of 3D tumour models and their consequent feasible use for perturbation studies was therefore demonstrated in this study. Generation of large numbers of spheroids from a single batch bioreactor represents an advantage for testing the libraries of compounds available in the pharmaceutical companies. In order to fully implement this system in current drug screening set-ups, new low volume dynamic culture systems such as ambr® or Sartorius can be used for repeated dose drug testing, as it also provides pH and dissolved oxygen control and it enables running up to 48 parallel experiments. Moreover, microfluidic tools coupled to these stirred-tank culture systems for spheroid distribution and size separation might be promising strategies to integrate these models into the current drug discovery cascade.

Taken together, our results demonstrate the reliability, robustness and versatility of agitation-based technology for the large scale generation of 3D *in vitro* cancer models from an extensive list of tumour cell lines. Additionally, these 3D cell models can be developed with the additional support of an artificial matrix and can be engineered to incorporate stromal cell components. Altogether, 3D cell cancer models produced in stirred-tank culture systems are

an alternative for drug screening and target validation in pre-clinical oncology research.

5 Acknowledgments

We acknowledge support from the Innovative Medicines Initiative Joint Undertaking (IMI grant agreement n° 115188), resources composed of financial contribution from EU - FP7 and EFPIA companies in kind contribution. iNOVA4Health - UID/Multi/04462/2013, a program financially supported by Fundação para a Ciência e Tecnologia / Ministério da Educação e Ciência, through national funds and co-funded by FEDER under the PT2020 Partnership Agreement is also acknowledged. This research has also received support from Fundação para a Ciência e Tecnologia, Portugal – PTDC/BBB-BIO/1240/2012. MFE and CP are the recipients of PhD fellowships from FCT (SFRH/BD/52208/2013 and SFRH/BD/52202/2013, respectively).

6 References

1. Breslin, S. and L. O'Driscoll, *Three-dimensional cell culture: the missing link in drug discovery.* Drug Discov Today, 2013. **18**(5-6): p. 240-9.

2. Ekert, J.E., et al., *Three-dimensional lung tumour microenvironment modulates therapeutic compound responsiveness in vitro--implication for drug development.* PLoS One, 2014. **9**(3): p. e92248.

3. Lee, J.M., et al., *A three-dimensional microenvironment alters protein expression and chemosensitivity of epithelial ovarian cancer cells in vitro.* Lab Invest, 2013. **93**(5): p. 528-42.

4. Guo, W.M., et al., *Development of a magnetic 3D spheroid platform with potential application for high-throughput drug screening.* Mol Pharm, 2014. **11**(7): p. 2182-9.

5. Ghosh, S., et al., *Three-dimensional culture of melanoma cells profoundly affects gene expression profile: a high density oligonucleotide array study.* J Cell Physiol, 2005. **204**(2): p. 522-31.

6. Kenny, P.A., et al., *The morphologies of breast cancer cell lines in three-dimensional assays correlate with their profiles of gene expression.* Mol Oncol, 2007. **1**(1): p. 84-96.

7. Rohwer, N. and T. Cramer, *Hypoxia-mediated drug resistance: novel insights on the functional interaction of HIFs and cell death pathways.* Drug Resist Updat, 2011. **14**(3): p. 191-201.

8. Friedrich, J., R. Ebner, and L.A. Kunz-Schughart, *Experimental anti-tumour therapy in 3-D: spheroids--old hat or new challenge?* Int J Radiat Biol, 2007. **83**(11-12): p. 849-71.

9. Pickup, M.W., J.K. Mouw, and V.M. Weaver, *The extracellular matrix modulates the hallmarks of cancer.* EMBO Rep, 2014. **15**(12): p. 1243-53.

10. Howes, A.L., et al., *The phosphatidylinositol 3-kinase inhibitor, PX-866, is a potent inhibitor of cancer cell motility and growth in three-dimensional cultures.* Mol Cancer Ther, 2007. **6**(9): p. 2505-14.
11. Seguin, L., et al., *Integrins and cancer: regulators of cancer stemness, metastasis, and drug resistance.* Trends Cell Biol, 2015. **25**(4): p. 234-40.
12. Bechyne, I., et al., *Functional heterogeneity of non-small lung adenocarcinoma cell sub-populations.* Cell Biol Int, 2012. **36**(1): p. 99-103.
13. Pampaloni, F., E.G. Reynaud, and E.H. Stelzer, *The third dimension bridges the gap between cell culture and live tissue.* Nat Rev Mol Cell Biol, 2007. **8**(10): p. 839-45.
14. Holtfreter, J., *A study of the mechanics of gastrulation.* Journal of Experimental Zoology, 1944. **95**(2): p. 171-212.
15. Sutherland, R.M., J.A. McCredie, and W.R. Inch, *Growth of multicell spheroids in tissue culture as a model of nodular carcinomas.* J Natl Cancer Inst, 1971. **46**(1): p. 113-20.
16. McCredie, J.A., W.R. Inch, and R.M. Sutherland, *Differences in growth and morphology between the spontaneous C3H mammary carcinoma in the mouse and its syngeneic transplants.* Cancer, 1971. **27**(3): p. 635-42.
17. Knuchel, R., et al., *Interactions between bladder tumour cells as tumour spheroids from the cell line J82 and human endothelial cells in vitro.* J Urol, 1988. **139**(3): p. 640-5.
18. Kelm, J.M., et al., *Method for generation of homogeneous multicellular tumour spheroids applicable to a wide variety of cell types.* Biotechnol Bioeng, 2003. **83**(2): p. 173-80.
19. Kumar, H.R., et al., *Three-dimensional neuroblastoma cell culture: proteomic analysis between monolayer and multicellular tumour spheroids.* Pediatr Surg Int, 2008. **24**(11): p. 1229-34.
20. Hickman, J.A., et al., *Three-dimensional models of cancer for pharmacology and cancer cell biology: capturing tumour complexity in vitro/ex vivo.* Biotechnol J, 2014. **9**(9): p. 1115-28.
21. Hirschhaeuser, F., et al., *Multicellular tumour spheroids: an underestimated tool is catching up again.* J Biotechnol, 2010. **148**(1): p. 3-15.
22. Gualda, E.J., et al., *Imaging of human differentiated 3D neural aggregates using light sheet fluorescence microscopy.* Front Cell Neurosci, 2014. **8**: p. 221.
23. Celli, J.P., et al., *An imaging-based platform for high-content, quantitative evaluation of therapeutic response in 3D tumour models.* Sci. Rep., 2014. **4**.
24. Gualda, E.J., et al., *SPIM-fluid: open source light-sheet based platform for high-throughput imaging.* Biomed Opt Express, 2015. **6**(11): p. 4447-56.
25. Ivascu, A. and M. Kubbies, *Rapid generation of single-tumour spheroids for high-throughput cell function and toxicity analysis.* J Biomol Screen, 2006. **11**(8): p. 922-32.
26. Friedrich, J., et al., *Spheroid-based drug screen: considerations and practical approach.* Nat Protoc, 2009. **4**(3): p. 309-24.
27. Amann, A., et al., *Development of an innovative 3D cell culture system to study tumour--stroma interactions in non-small cell lung cancer cells.* PLoS One, 2014. **9**(3): p. e92511.
28. Fennema, E., et al., *Spheroid culture as a tool for creating 3D complex tissues.* Trends Biotechnol, 2013. **31**(2): p. 108-15.

29. Sodunke, T.R., et al., *Micropatterns of Matrigel for three-dimensional epithelial cultures.* Biomaterials, 2007. **28**(27): p. 4006-16.
30. Lin, R.Z. and H.Y. Chang, *Recent advances in three-dimensional multicellular spheroid culture for biomedical research.* Biotechnol J, 2008. **3**(9-10): p. 1172-84.
31. Serra, M., et al., *Process engineering of human pluripotent stem cells for clinical application.* Trends Biotechnol, 2012. **30**(6): p. 350-9.
32. Alves, P.M., et al., *Two-dimensional versus three-dimensional culture systems: Effects on growth and productivity of BHK cells.* Biotechnol Bioeng, 1996. **52**(3): p. 429-32.
33. Kinney, M.A., C.Y. Sargent, and T.C. McDevitt, *The multiparametric effects of hydrodynamic environments on stem cell culture.* Tissue Eng Part B Rev, 2011. **17**(4): p. 249-62.
34. Benien, P. and A. Swami, *3D tumour models: history, advances and future perspectives.* Future Oncol, 2014. **10**(7): p. 1311-27.
35. Rebelo, S., et al., *Establishing Liver Bioreactors for In Vitro Research*, in *Protocols in In Vitro Hepatocyte Research*, M. Vinken and V. Rogiers, Editors. 2015, Springer New York. p. 189-202.
36. Simao, D., et al., *Modeling human neural functionality in vitro: three-dimensional culture for dopaminergic differentiation.* Tissue Eng Part A, 2015. **21**(3-4): p. 654-68.
37. Serra, M., et al., *Integrating human stem cell expansion and neuronal differentiation in bioreactors.* BMC Biotechnol, 2009. **9**: p. 82.
38. Rebelo, S.P., et al., *HepaRG microencapsulated spheroids in DMSO-free culture: novel culturing approaches for enhanced xenobiotic and biosynthetic metabolism.* Arch Toxicol, 2014.
39. Serra, M., et al., *Microencapsulation technology: a powerful tool for integrating expansion and cryopreservation of human embryonic stem cells.* PLoS One, 2011. **6**(8): p. e23212.
40. Correia, C., et al., *Combining hypoxia and bioreactor hydrodynamics boosts induced pluripotent stem cell differentiation towards cardiomyocytes.* Stem Cell Rev, 2014. **10**(6): p. 786-801.
41. Olmer, R., et al., *Suspension culture of human pluripotent stem cells in controlled, stirred bioreactors.* Tissue Eng Part C Methods, 2012. **18**(10): p. 772-84.
42. Mehta, G., et al., *Opportunities and challenges for use of tumour spheroids as models to test drug delivery and efficacy.* J Control Release, 2012. **164**(2): p. 192-204.
43. Rudisch, A., et al., *High EMT Signature Score of Invasive Non-Small Cell Lung Cancer (NSCLC) Cells Correlates with NFkappaB Driven Colony-Stimulating Factor 2 (CSF2/GM-CSF) Secretion by Neighboring Stromal Fibroblasts.* PLoS One, 2015. **10**(4): p. e0124283.
44. Angelucci, C., et al., *Epithelial-stromal interactions in human breast cancer: effects on adhesion, plasma membrane fluidity and migration speed and directness.* PLoS One, 2012. **7**(12): p. e50804.
45. Kaur, P., et al., *Human breast cancer histoid: an in vitro 3-dimensional co-culture model that mimics breast cancer tissue.* J Histochem Cytochem, 2011. **59**(12): p. 1087-100.
46. Estrada, M.F., et al., *Modelling the tumour microenvironment in long-term microencapsulated 3D co-cultures recapitulates phenotypic features of disease progression.* Biomaterials, 2016. **78**: p. 50-61.

47. Goodwin, T.J., J.M. Jessup, and D.A. Wolf, *Morphological-Differentiation of Colon-Carcinoma Cell-Lines Ht-29 and Ht-29km in Rotating-Wall Vessels.* In Vitro Cellular & Developmental Biology-Animal, 1992. **28a**(1): p. 47-60.

48. Longati, P., et al., *3D pancreatic carcinoma spheroids induce a matrix-rich, chemoresistant phenotype offering a better model for drug testing.* BMC Cancer, 2013. **13**: p. 95.

49. LaBarbera, D.V., B.G. Reid, and B.H. Yoo, *The multicellular tumour spheroid model for high-throughput cancer drug discovery.* Expert Opin Drug Discov, 2012. **7**(9): p. 819-30.

50. Godugu, C., et al., *AlgiMatrix based 3D cell culture system as an in-vitro tumour model for anticancer studies.* PLoS One, 2013. **8**(1): p. e53708.

51. Zhang, M., et al., *The use of porous scaffold as a tumour model.* Int J Biomater, 2013. **2013**: p. 396056.

52. Moreira, J.L., et al., *Hydrodynamic effects on BHK cells grown as suspended natural aggregates.* Biotechnol Bioeng, 1995. **46**(4): p. 351-60.

53. Kinney, M.A., et al., *Engineering three-dimensional stem cell morphogenesis for the development of tissue models and scalable regenerative therapeutics.* Ann Biomed Eng, 2014. **42**(2): p. 352-67.

54. Nsiah, B.A., et al., *Fluid shear stress pre-conditioning promotes endothelial morphogenesis of embryonic stem cells within embryoid bodies.* Tissue Eng Part A, 2014. **20**(5-6): p. 954-65.

55. Härmä, V., et al., *A Comprehensive Panel of Three-Dimensional Models for Studies of Prostate Cancer Growth, Invasion and Drug Responses.* PLoS One, 2010. **5**(5): p. e10431.

56. Popper, H., et al., *[Histology-based algorithm in the molecular diagnosis of mutations of the Epidermal Growth Factor Receptor (EGFR) in non-small cell lung cancer].* Wien Klin Wochenschr, 2011. **123**(9-10): p. 316-21.

57. Freitas, D.P., et al., *Therapy-induced enrichment of putative lung cancer stem-like cells.* International Journal of Cancer, 2014. **134**(6): p. 1270-1278.

58. Smart, C.E., et al., *In vitro analysis of breast cancer cell line tumourspheres and primary human breast epithelia mammospheres demonstrates inter- and intrasphere heterogeneity.* PLoS One, 2013. **8**(6): p. e64388.

59. Cichon, M.A., et al., *Growth of lung cancer cells in three-dimensional microenvironments reveals key features of tumour malignancy.* Integr Biol (Camb), 2012. **4**(4): p. 440-8.

60. Yeung, T.M., et al., *Cancer stem cells from colorectal cancer-derived cell lines.* Proc Natl Acad Sci U S A, 2010. **107**(8): p. 3722-7.

61. Thurber, G.M., M.M. Schmidt, and K.D. Wittrup, *Antibody tumour penetration: Transport opposed by systemic and antigen-mediated clearance.* Advanced drug delivery reviews, 2008. **60**(12): p. 1421.

62. Mikhail, A.S., S. Eetezadi, and C. Allen, *Multicellular tumour spheroids for evaluation of cytotoxicity and tumour growth inhibitory effects of nanomedicines in vitro: a comparison of docetaxel-loaded block copolymer micelles and Taxotere(R).* PLoS One, 2013. **8**(4): p. e62630.

63. Erler, J.T. and V.M. Weaver, *Three-dimensional context regulation of metastasis.* Clinical & Experimental Metastasis, 2009. **26**(1): p. 35-49.

64. Chambers, K.F., et al., *3D cultures of prostate cancer cells cultured in a novel high-throughput culture platform are more resistant to chemotherapeutics compared to cells cultured in monolayer.* PLoS One, 2014. **9**(11): p. e111029.

7 Supplementary Figures

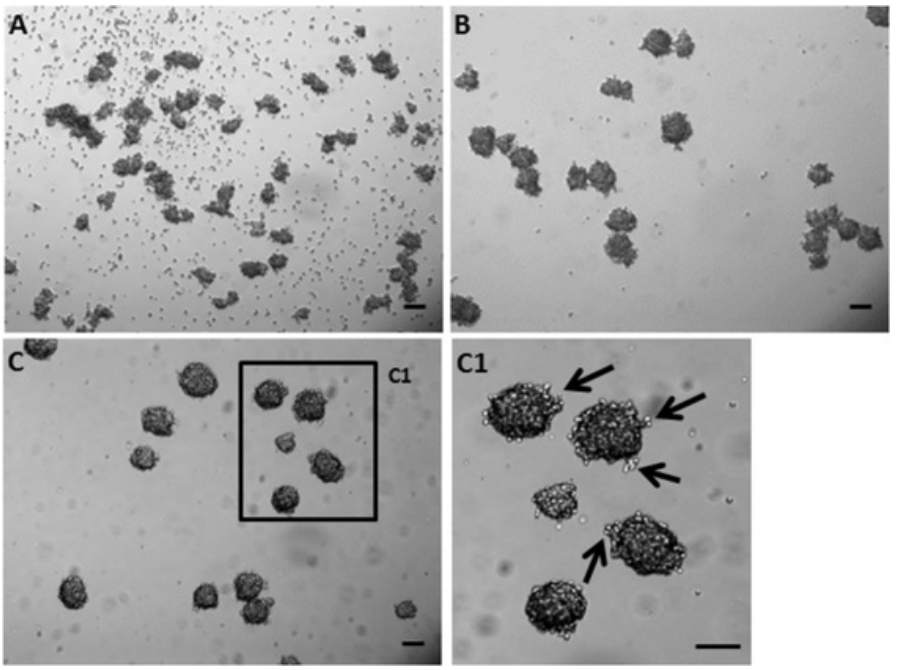

Figure S2.1: Phase contrast microscopy of H157 cultures during aggregation phase. A) day 1. B) day 2. C) day 3. C1) High magnification inset representing the region indicated in the black square. The black arrows indicate the edges on the surface of H157 spheroids. Scale bar represents 100 µm.

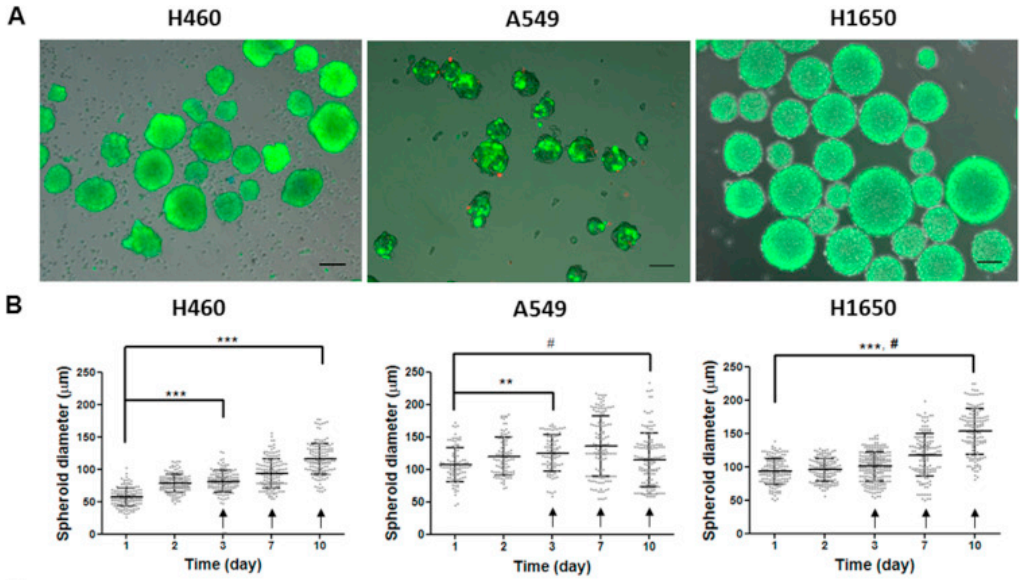

C

Cell Line	Maximum fold increase in cell concentration	Maximum in cell concentration (day)
H460	11.0 ± 0.7	7
A549	5.8 ± 0.4	10
H1650	6.6 ± 0.3	8

Figure S2.2: Culture of NSCLC cell spheroids in stirred-tank culture systems: spheroid diameter profile and cell concentration of H460, A549 and H1650 cells. A) Spheroids of the selected NSCLC cell lines, collected at day 10 of culture, incubated with fluorescein diacetate (FDA, green) for indication of live cells and TO-PRO iodide (TOPRO, red) for identification of dead cells. Scale bars represent 100 µm. B) Average diameter of spheroids was determined by calculation of Feret's diameter using the open source ImageJ software. Statistical differences (***, $p < 0.001$; **, $p < 0.01$) were determined using non-parametric Kurskal–Wallis test for comparison of spheroid diameter throughout the culture period. Levene's test was performed for comparison of spheroid diameter dispersion (#, $p < 0.00001$) at different culture times. Arrows indicate 50% culture medium exchange. C) Maximum fold increase in cell concentration was determined by crystal violet method.

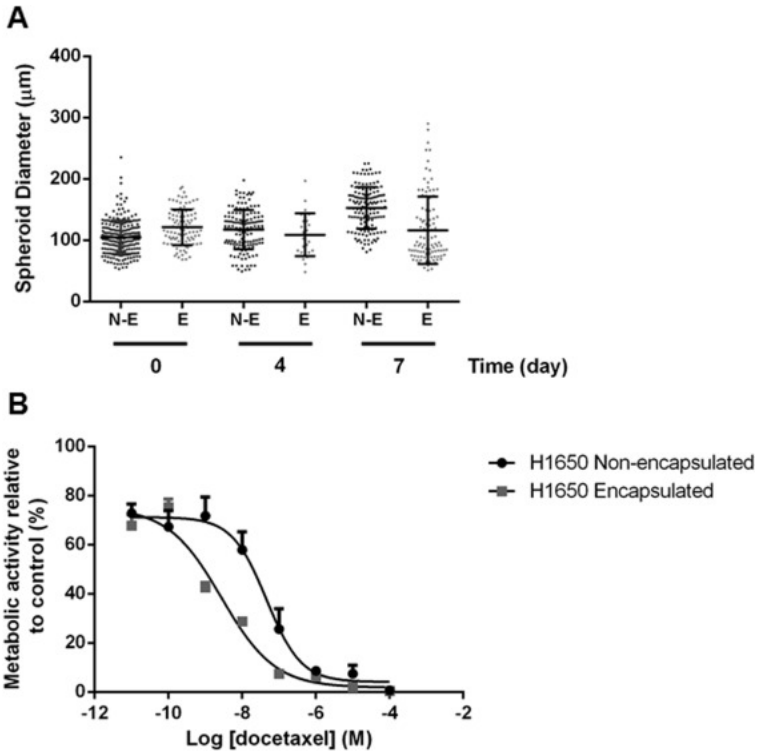

Figure S2.3: Characterization of microencapsulated and non-encapsulated H1650 mono-cultures generated in stirred-tank culture systems. A) Assessment of the effect of microencapsulation of H1650 spheroid growth. N-E: Non-microencapsulated H1650 cultures; E: Microencapsulated H1650 cultures. B) Dose response curves of microencapsulated and non-encapsulated H1650 tumour spheroids for docetaxel treatment. Cell viability was used as read-out for drug response determination.

Chapter III

Modelling the tumour microenvironment in long-term microencapsulated 3D co-cultures recapitulates phenotypic features of disease progression.

This Chapter was adapted from:

Estrada MF, Rebelo SP, Davies EJ, Pinto MT, Pereira H, Santo VE, Smalley MJ, Barry ST, Gualda EJ, Alves PM, Anderson E, Brito C. *Modelling the tumour microenvironment in long-term microencapsulated 3D co-cultures recapitulates phenotypic features of disease progression.* Biomaterials, 2016.

Table of contents

Abstract 83
1 Introduction 84
2 Materials and Methods 86
2.1 2D cell culture 86
2.2 3D cell culture 86
2.3 Cell Viability 87
2.4 Aggregate size 87
2.5 Total Cell concentration 88
2.6 Immunofluorescence microscopy and image analysis 88
2.7 Image acquisition and analysis in SPIM-FLUID 89
2.8 Immunohistochemistry and Image analysis 90
2.9 Western Blot 91
2.10 Collagen quantification 91
2.11 Cytokine arrays 92
2.12 Chicken embryo chorioallantoic membrane angiogenesis assay 93
3 Results 94
3.1 Alginate microencapsulation combined with stirred-tank culture for long term 3D heterotypic cell culture 94
3.2 MCF-7 cell proliferation and partial polarisation in microencapsulated cultures 95
3.3 Cell organization and collagen accumulation in alginate microcapsules resemble structures observed in human tumours 97
3.4 The effect of stroma on disease progression events can be monitored and further investigated in long-term stirred-tank cultures 98
3.5 Tumour-stroma crosstalk within alginate microcapsules results in a pro-inflammatory environment and increased angiogenic response to MCF7 cells 102
4 Discussion 103
5 Acknowledgments 108
6 References 109
7 Supplementary Figure 113
8 Supplementary Table 116

Abstract

3D cell tumour models are generated mainly in non-scalable culture systems, using bioactive scaffolds. Many of these models fail to reflect the complex tumour microenvironment and do not allow long-term monitoring of tumour progression. To overcome these limitations, we have combined alginate microencapsulation with agitation-based culture systems, to recapitulate and monitor key aspects of the tumour microenvironment and disease progression. Aggregates of MCF-7 breast cancer cells were microencapsulated in alginate, either alone or in combination with human fibroblasts, then cultured for 15 days. In co-cultures, the fibroblasts arranged themselves around the tumour aggregates creating distinct, appropriately oriented, epithelial and stromal compartments. The presence of fibroblasts resulted in secretion of pro-inflammatory cytokines and deposition of collagen in the stromal compartment. Tumour cells established cell-cell contacts and polarised around small lumina in the interior of the aggregates. Over the culture period, there was a reduction in oestrogen receptor and membranous E-cadherin alongside loss of cell polarity, increased collective cell migration and enhanced angiogenic potential in co-cultures. These phenotypic alterations, typical of advanced stages of cancer, were not observed in the mono-cultures of MCF-7 cells. The proposed model system constitutes a new tool to study tumour-stroma crosstalk, disease progression and drug resistance mechanisms.

Key words: 3D, co-culture, alginate microencapsulation, stirred-tank bioreactors, tumour microenvironment, tumour progression.

1 Introduction

The tumour microenvironment is composed of cancer cells, fibroblasts, endothelial cells, immune cells and extracellular matrix (ECM), whose interactions are critical for tumour initiation and progression [1]. Tumour cells can induce a phenotypic change in healthy fibroblasts to become cancer associated fibroblasts (CAFs) with cancer-promoting properties such as secretion of matrix components (collagen and fibronectin), growth and inflammation factors [1]. Abnormal deposition of collagen has been associated with cancerous states due to increased matrix stiffness which is known to contribute to tumour cell dissemination [2]. Additionally, the activated stromal cells promote tumour progression by stimulating cancer cell proliferation and migration, and ultimately tumour metastasis [3]. Infiltrating stromal cells in the tumour are the main providers of matrix metalloproteinases (MMPs) that, through remodelling of ECM, release chemotactic agents and loosen the matrix contributing to tumour cell dissemination [4]. These changes are responsible for the recruitment of immune cells and for increasing chronic inflammation, which also contributes to tumour aggressiveness [5].

In an attempt to mimic the complexity of the tumour microenvironment, many *in vitro* models have been developed in the recent years [6]. In most of these models however, tumour cells are grown as monotypic cultures in two-dimensions (2D). In 2D, cells are not able to organize into tissue-like structures since they lack the tridimensionality (3D) bestowed by the surrounding microenvironment [7]. In contrast, heterotypic tumour aggregate 3D cultures enable tumour cells to establish cell-cell and cell-ECM interactions, which are important elements in tumour signalling and which modulate tumour responses to therapeutic agents [8]. However, tumour aggregates are mostly cultured in low-adherence conditions [9] or embedded in bioactive scaffolds such as collagen I or matrigel [6]. These scaffolds also have limitations, including batch-to-batch variation and an incomplete understanding of their impact on cell behaviour [10,11]. In contrast, hydrogels such as alginate present many advantages over bioactive scaffolds due to their inert properties, biocompatible

gelation and ease of cell recovery. Hydrogels also provide the possibility of conjugation with defined adhesion ligands or delivery of specific biomolecules (growth factors, pro-angiogenic factors, amongst others) [12,13].

Alginates are polysaccharide hydrogels composed of β-D-mannuronic acid (M) and α-L-guluronic acid (G) obtained from particular brown algae species [13]. Alginate comprises 99% water, but still retains high plasticity and mechanical strength. Gelling occurs almost instantaneously by cross-linking with divalent ions, like Ca^{2+}, allowing for cell entrapment under physiological conditions and rapid cell recovery by gel dissolution [14]. Most cell lines are able to grow in non-functionalized alginates, despite the absence of cell adhesion sites [13]. Alginate microencapsulation has been used to investigate the effect of biomechanical forces exerted on tumour aggregates [15]. More recently, alginate microencapsulation and microfluidic devices have been used to study the interaction between different cell types [11,16]. However, these models have been generated in non-scalable culture systems, with no control of the physicochemical parameters and which allow end-point analysis only [17,18]. As a result, studies on the molecular mechanisms behind disease progression and drug resistance as well as high-throughput drug screening are performed in models that lack the complexity of human tumours and which do not allow continuous monitoring of the culture progression.

Herein, we describe a novel *in vitro* culture model system that allows for long-term co-culture of tumour and stromal cells, based on the combination of alginate microencapsulation with suspension cultures in agitation-based culture systems. This model aims to recapitulate tumour-stroma crosstalk and monitoring of disease progression *in vitro*. We used alginate as a scaffold for cell entrapment not only due to its properties outlined above, but also to provide physical support and cell confinement, in a manner compatible with stirred-tank systems. This strategy provides a means of long-term culture of tumour cell aggregates either alone or in combination with fibroblasts, continuously monitored without invasive sampling.

In summary, we have developed a scalable and robust model system for long-term *in vitro* recapitulation of tumour-stroma cross talk and monitoring of disease progression. The developed model system can be transferred across several pathologies and will provide a new tool for characterization of disease progression and drug resistance mechanisms *in vitro*. In addition, it is easily transferable to industry for feeding high-throughput systems or miniaturized bioreactors used in drug development and in target validation.

2 Materials and Methods

2.1 2D cell culture

MCF-7 cells, transduced with the lentiviral vectors PGK-GFP and pCDH-CMV-MCS-EF1-Puro, were kindly provided by Professor Cathrin Brisken (EPFL, Switzerland) within the scope of the PREDECT consortium. Cell expansion was performed in Dulbecco's Modified Eagle Medium (DMEM) with 25 mM Glucose, supplemented with 1% (v/v) penicillin-streptomycin, 4 mM Glutamax, 1 mM sodium pyruvate and 10% (v/v) fetal bovine serum (FBS). Cells were passaged twice weekly at a inoculum concentration of 1.5 x 10^4 cell/cm^2. Human Dermal Fibroblasts (HDF), from Innoprot, were passaged once weekly for up to 10 to 12 passages at a seeding density of 0.5 x 10^4 cell/cm^2, in Iscove's Modified Dulbecco's Medium (IMDM) supplemented with 1% (v/v) penicillin-streptomycin and 10% (v/v) FBS (all from Life Technologies). Both the MCF-7 cells and the HDFs were cultured in static culture systems, in an incubator at 37ºC with humidified atmosphere containing 5% CO_2 in air.

2.2 3D cell culture

MCF-7 cells, transduced with the lentiviral vectors described above, were inoculated as single cell suspensions (0.2 x 10^6 cell/mL) into 125 mL stirred-tank vessels with flat centred cap and angled side arms (Corning - http://catalog2.corning.com/LifeSciences/en-US/Shopping/ProductDetails.aspx?categoryname=&productid=4500-125%28Lifesciences%29) and cultured at 80 rpm, to induce aggregation. For

alginate microencapsulation, tumour cell aggregates were collected from the stirred-tank vessels after 24 h of culture. Aggregates corresponding to approximately 25 x 10^6 tumour cells were dispersed in 3 mL of 1.1% (w/v) of Ultrapure Ca^{2+} MVG alginate (UP MVG NovaMatrix, Pronova Biomedical, Oslo, Norway) dissolved in NaCl 0.9% (w/v) solution either alone (mono-cultures) or together with HDFs, in a 1:1 ratio for approximately 50 x 10^6 total cells (co-cultures). Microencapsulation was performed using an electrostatic bead generator (Nisco VarV1, Zurich, Switzerland), to produce beads of approximately 500 µm in diameter [19]. The alginate droplets were cross-linked in a 100 mM $CaCl_2$ / 10mM HEPES (pH 7.4) solution for 10 min, further washed three times in a 0.9% (w/v) NaCl solution and finally equilibrated in culture medium before being transferred to stirred-tank vessels. The microencapsulated mono and co-cultures were kept in 125 mL stirred-tank vessels at 80 rpm, in a humidified incubator, with 5% CO_2 in air, for 15 days with 50% medium exchange every 3-4 days.

2.3 Cell Viability

Cell viability was assessed using fluorescein diacetate (FDA; Sigma-Aldrich, Steingeim, Germany) at 10 µg/mL to label live cells, and To-PRO-3 iodite (LifeTechnologies) at 1 µM, for dead cells. Microencapsulated tumour aggregates and fibroblasts were incubated for 5 min at RT with the labels then visualized using a fluorescence microscope (DMI6000, Leica Microsystems GmbH, Wetzlar, Germany) or a spinning disk microscope (Andor Revolution Å~ D, Andor Technology PLC, Belfast, Northern Ireland).

2.4 Aggregate size

To measure aggregate size, alginate microcapsules were dissolved in a chelating solution (Sodium citrate 50 mM / Sodium chloride 100 mM), for 5 min at room temperature (RT), and washed twice with Phosphate-Buffered Saline (PBS; Life Technologies). Aggregates were imaged using a fluorescence microscope (DMI6000, Leica Microsystems GmbH, Wetzlar, Germany).

Aggregate surface area was quantified using FIJI open source software (Rasband, WS, ImageJ, U. S. National Institutes of Health, Bethesda, MD, USA, http://imagej.nih.gov/ij/, 1997–2012.), by applying automated threshold adjustment followed by the area measurement algorithm.

Statistical analysis was carried out using GraphPad Prism 5 software. Data is presented as mean ± SD from three independent experiments. The non-parametric Kruskal-Wallis test was used to compare aggregate surface area differences between mono and co-cultures, at days 2, 5, 10 and 15.

2.5 Total Cell concentration

To assess cell concentration, alginate microcapsules were firstly dissolved, as described in the previous section. After dissolution of alginate, aggregates were pelleted by centrifugation at 50x *g* for 5 min at RT. Cells were lysed with 0.1 M of citric acid / 1% (w/v) Triton - X100 in water. After cell lysis, nuclei were stained with 0.1% (v/v) Crystal Violet and counted in a Fuchs-Rosenthal haemacytometer chamber, using a phase contrast microscope (DMIRB, Leica, Germany).

Statistical analysis was carried out using GraphPad Prism 5 software. Data is presented as mean ± SD from four independent experiments. A two way ANOVA test of significance was used to compare tumour cell growth in mono and co-cultures over time.

2.6 Immunofluorescence microscopy and image analysis

Microencapsulated aggregate culture samples were collected at days 5 and 15 of culture and fixed in 4% (v/v) paraformaldehyde (PFA) / 4% (v/v) Sucrose for 20 min. For cryosectioning samples were dehydrated with 30% (w/v) sucrose overnight, frozen at −80 °C in Tissue-Tek O.C.T. (Sakura, Alphen aan den Rijn, Netherlands) and sectioned at a thickness of 10 µm using a cryomicrotome (Cryostat I, Leica, Wetslar, Germany).

Immunofluorescence was performed according to previously published methods [19,20]. In brief, cells were permeabilized with 0.1% Triton X-100 (w/v)

(10 min for cryosections; 2 hours for whole aggregates) and blocked in 0.2% (w/v) Fish Skin Gelatin (FSG; Sigma-Aldrich). Primary antibodies were diluted in 0.2% (w/v) FSG and incubated for 2h at RT and secondary antibodies diluted in 0.125% (w/v) FSG and incubated for 1h at RT (Supplementary Table 1) Samples were mounted in ProLong containing DAPI (Life Technologies) and visualized using either a fluorescence microscope (DMI6000, Leica Microsystems GmbH, Wetzlar, Germany, a 2-photon microscope (Prairie TPE) or a Light Sheet Microscope (SPIM-FLUID).

2.7 Image acquisition and analysis in SPIM-FLUID

In order to facilitate automated sample loading, critical for high-throughput screening, we used a system based on light-sheet fluorescence microscopy (LSFM), SPIM-Fluid [21]. Across a water filled chamber, at 45 degrees, a FEP tube positioned at the intersection of the illumination and detection focal plane transports the samples, which can be aspired and pushed back and forward with an Arduino controlled stepper motor attached to a syringe (Eppendorf CellTram). Images are acquired sequentially, as the samples cross the light-sheet plane. The illumination block consists of a home-made laser combiner including two laser lines: 473 nm (DPSSL MBL-III-473-50) and 561 nm (Coherent OBIS 561-50 LS), selected using an Arduino controlled filter wheel with two filters (Semrock 473/10, 561/10). Laser scanning is carried out in the vertical axis using an Arduino controlled galvanometric mirror (6210H Cambridge Technologies) in which the optical plane is conjugated with the back focal aperture of an objective lens (Plan Fluor 4× 0.13 WD17.4 mm) using a 3.5× telescope system. For detection, an air objective (Nikon 10x 0.3NA WD 16.7 mm), placed perpendicularly to the excitation plane, is used to collect fluorescence emission. Excitation light is rejected using emission filters placed in infinity space before the camera. Finally a 200 mm tube lens creates the image on the chip of the sCMOS cameras (Hamamatsu Orca-Flash4).

A controller for sample positioning and scanning allows micro-steps up to 0.225º, which translate into sample steps of 2 microns (FEP tube of 1 mm inner

diameter). To automatise the acquisition process, we have designed a photometer using a photodiode to detect sample passage. The system also permits control of a secondary camera, allowing fast two colour imaging. We have also created a dedicated java Plugin for Micromanager acquisition software [22], which enables easy control of sample positioning and data acquisition from a single window, creating a modular open source platform for high throughput screening on 3D cell cultures.

After image acquisition, images were processed using a kit of tools from FIJI image processing software [23]. In first place, data were sorted by image intensities in order to separate individual capsules. Subsequently, images having 2 capsules were processed with a different set of FIJI's tools to separate correctly the capsules and different aggregates per capsule in order to accurately estimate aggregate volume. Finally we used Image J plugins, such "3D Objects Counter", "Analyze Particles" and "3D Manager", to measure aggregate volume, fibroblast numbers and circularity.

2.8 Immunohistochemistry and Image analysis

Samples were collected and fixed as described above. Aggregates were pelleted and then embedded in 1% (w/v) high melting temperature agarose (Lonza), dehydrated in graded alcohols and then embedded in paraffin wax. Paraffin blocks were sectioned (3 μm) for Hematoxylin & Eosin and immunohistochemical staining. Immunohistochemistry was carried out using standard protocols [24]. Briefly, antigen retrieval was performed using histoprocessing modules (Milestone Medical) at 110 ºC under pressure, for 2 min, using pH6 antigen retrieval solution (Dako). Staining was performed using a Labvision Autostainer 720 (Thermo Scientific). Stained slides were scanned using a ScanScope AT Turbo slide scanner (Aperio) and images were analysed using Aperio image analysis software (Aperio). Aperio image analysis software is able to recognise either nuclear or membrane specific staining, and was trained to discern between negative, weak, medium and strong staining intensities.

Statistical analysis was carried out using GraphPad Prism 5 software. Data is presented as mean ± SD from more than 70 aggregates. Two-way ANOVA statistics test was used to compare the intensity of membranous E-cadherin and ER staining, in both mono and co-cultures, at days 5 and 15 of culture.

2.9 Western Blot

Encapsulated aggregates were sampled and alginate capsules dissolved, as described above. Following 2 steps of aggregate washing, cell pellets were snap frozen and stored at -80ºC. For Western Blot analysis aggregates were lysed in Tx-100 lysis buffer (50 mM Tris, 5 mM EDTA, 150 mM NaCl, 1% (w/v) Triton X-100 and 1x (w/v) complete protease and phosphatase inhibitor cocktail (Roche)). Protein quantification was performed using the Micro-BCA Protein Assay Kit (Thermo Scientific). Proteins were denatured, loaded in an electrophoresis gel (NuPAGE 4-12% Bis–Tris Gel) under reducing conditions for 40 min (200 V, 400 mA) and then electrophoretically transferred to a polyvinylidene difluoride (PVDF) membrane (Millipore). Membranes were blocked for 1h in PBS with 0.1% (w/v) Tween 20 / 5% (w/v) non-fat dried milk powder and further incubated with the primary and secondary antibodies. Anti-tubulin was used as a loading control. Membranes were developed using Amersham ECL Prime Western Blot Detection Reagent (GE Healthcare) and visualized using a ChemiDocTM XRS + System (BioRad). Chemifluorescence was quantified using Quantity One (Bio-rad).

Statistical analysis was carried out using GraphPad Prism 5 software. Data is presented as mean ± SD from three independent experiments. Two-way ANOVA statistics test was used to compare the average average protein levels of ER, in both mono and co-cultures, at days 5 and 15 of culture.

2.10 Collagen quantification

Collagen was quantified in both alginate microcapsules and culture supernatants, using the Sircol Collagen Colorimetric assay kit (Biocolor Ltd., U.K.), according to the manufacturer's instructions.

Statistical analysis was carried out using GraphPad Prism 5 software. Data is presented as mean ± SD from three independent experiments. The non-parametric Kruskal-Wallis test was used to compare collagen concentration between mono and co-cultures, at days 5 and 15.

2.11 Cytokine arrays

Culture samples were collected and alginate microcapsules were pelleted by centrifugation at 50x *g*. Alginate microcapsules were dissolved as described above and the microcapsule soluble fraction (MSF) separated from the cell fraction by centrifugation. Cells and cell debris were removed from both culture supernatant and the MSF by additional centrifugation at 300x *g* followed by 1000x *g* for 5 min at 4ºC.

After concentration and buffer exchange of MSF to 1 mL, using centrifugal filter units with a 3 kDa membrane cut off (Amicon, Millipore), cytokine array analysis was performed using the Human Cytokine Array, Panel A (R&D Systems; ARY005), according to the manufacturer's instructions. Membranes were exposed to X-Ray films for 1, 5 and 10 min. The developed films were digitalized at 600 dpi using LabScan 5 Software (Amersham Biosciences, Switzerland). Spot analysis was performed using the Progenesis SameSpots software, version 4.5 (NonLinear Dynamics, UK). All films were quality checked, aligned and spots were quantified based on the volume and area of each spot. Relative secretion of each cytokine was calculated according with the following formula [25]:

$$Relative\ secretion\ (\%) = \frac{Cytokine\ expression - negative\ control}{positive\ control - negative\ control}\ X\ 100\%$$

Statistical analysis was carried out using GraphPad Prism 5 software. Data is presented as mean ± SD from two independent experiments. The non-parametric Man-Whitney U Test (two-tailed p-value) was used to compare the cytokines present in culture supernatant vs MSF and the differences between

mono and co-cultures; all comparisons were performed at days 5 and 15. Microencapsulated mono-cultures of fibroblasts were used as controls.

2.12 Chicken embryo chorioallantoic membrane angiogenesis assay

The chicken embryo chorioallantoic membrane (CAM) assay was used to evaluate the angiogenic response to tumour aggregates from mono and co-cultures collected at day 15 of culture. Fertilized chicken (*gallus gallus*) eggs, obtained from commercial sources, were incubated horizontally at 37.8 °C in a humidified atmosphere. On embryonic day (E) 3 a square window was opened in the shell after removal of 2-2.5 mL of albumen, to allow detachment of the developing CAM. The window was sealed with adhesive tape and the eggs returned to the incubator. To remove the fibroblasts, ECM and soluble factors, alginate microcapsules were dissolved, as described above, and tumour aggregates were washed twice with PBS (Ca^{2+}/Mg^{2+}). Tumour aggregates were re-suspended in 10 µl of medium and placed in a 3 mm silicone ring on the E10 growing CAM ($1x10^6$ cell per embryo) under sterile conditions. The eggs were re-sealed and returned to the incubator for 3 days. After removing the ring, the CAM was excised from the embryos, photographed ex-ovo under a stereoscope, at 20x magnification (Olympus, SZX16 coupled with a DP71 camera).

The number of new vessels (less than 15 µm in diameter) growing radially towards the ring area, in which the cells had been applied to the CAM, were counted blinded. Statistical analysis was carried out using GraphPad Prism 5 software. Data is presented as mean ± SD from 18 eggs. A t- Test (two-tailed p-value) was used to test significance.

3 Results

3.1 Alginate microencapsulation combined with stirred-tank culture for long term 3D heterotypic cell culture

To establish microencapsulated cultures, a dual step strategy in a stirred-tank culture system was adopted (Figure 3.1).

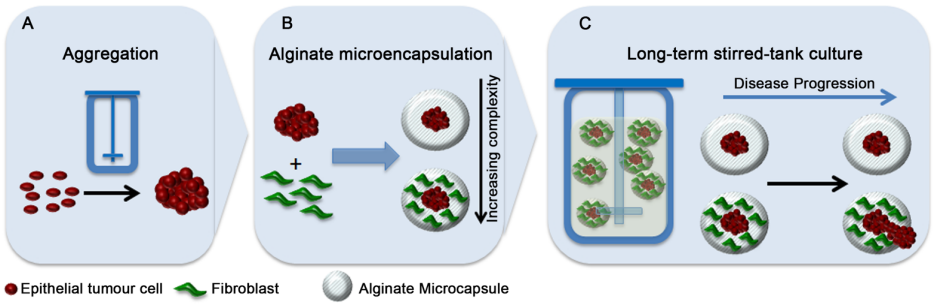

Figure 3.1: Schematic illustration of the experimental approach – *in vitro* reconstruction of tumour microenvironment in stirred-tank culture systems. (A) MCF-7 cells were allowed to aggregate in stirred-tank vessels for 24h and then harvested and pelleted for further microencapsulation. (B) Tumour aggregates were microencapsulated in alginate alone (tumour mono-cultures) or together with fibroblasts, inoculated as single cells (tumour – stromal co-cultures). (C) Microencapsulated cells were cultured in stirred-tank vessels for up to 15 days during which culture characterization was carried out at the indicated intervals.

In the first stage, tumour cells were inoculated as single cell suspensions and cultured for 24h to induce cell aggregation. Tumour aggregates were then collected (see materials and methods for details) and microencapsulated in alginate either alone (mono-culture) or together with human fibroblasts (tumour-stromal co-cultures), and further cultured in stirred-tank vessels for up to 15 days (Figure 3.1). This strategy has been applied to both breast and lung cancer cell lines, as described by us in [26]. The ability to sample in a non-invasive manner, offered by this system, allowed us to continuously monitor the culture progression and to take samples throughout the culture period without sacrificing the whole culture vessel. All cell types maintained viability throughout the duration of culture nonetheless cell growth kinetics and

aggregate morphology varied from cell line to cell line. More specifically, whereas the MCF-7 breast cancer cell line only presented a significant increase in cell concentration during the first 6 days of culture, cell concentration of the lung cancer cell line NCI-H157 continued to increase throughout the 15 days of culture (data not shown). ER^+ breast cancers are described to present high frequency of disease relapse associated with metastasis and drug resistance, despite the initial response to endocrine therapy [27,28]. MCF-7 cells, one of the most widely used ER^+/PR^+ cell lines [29] were chosen as the focus of Work Package 1 of the PREDECT consortium (www.predect.eu) and therefore were used herein for characterization of our model system.

3.2 MCF-7 cell proliferation and partial polarisation in microencapsulated cultures

Live/dead assays show MCF-7 aggregates with circular morphology, defined edges, high cell viability and the absence of necrotic centres in both mono and co-cultures (Figure 3.2A). After an initial growth phase, up to day 6, MCF-7 cell number reached a plateau that remained constant until day 15 of culture (Figure 3.2B). A slight increase in tumour cell concentration was observed in co-cultures by day 15, but this was not statistically significant. Aggregates from both culture types (mono and co-cultures) contained small lumina surrounded by polarised cells, as shown by apical accumulation of f-actin and ZO-1 (Figure 3.2C1 and 3.2C2), together with pyknotic nuclei within the lumens (Figure 3.2C3). Partial cell polarisation was seen at the outer rim of the aggregates as indicated by ZO-1 apical accumulation. Tumour cells were also cytokeratin 18 (CK18) positive, with localisation of E-cadherin (Figure S3.1) and β-catenin (Figure 3.2) at the cell membranes. In contrast, in non-microencapsulated cultures, tumour cells did not polarise, although cell-cell adhesions through E-cadherin were formed and CK18 expression was maintained (Figure S3.1). Additionally, proliferation (Ki67) and apoptosis (as indicated by caspase cleaved CK18 or M30) markers showed that proliferating cells were distributed homogeneously through the aggregates and that the

number of apoptotic cells was very low. No apoptotic cell centres were detected in the aggregates. Overall, no phenotypic differences were observed between microencapsulated mono and co-cultures, until day 5 of culture.

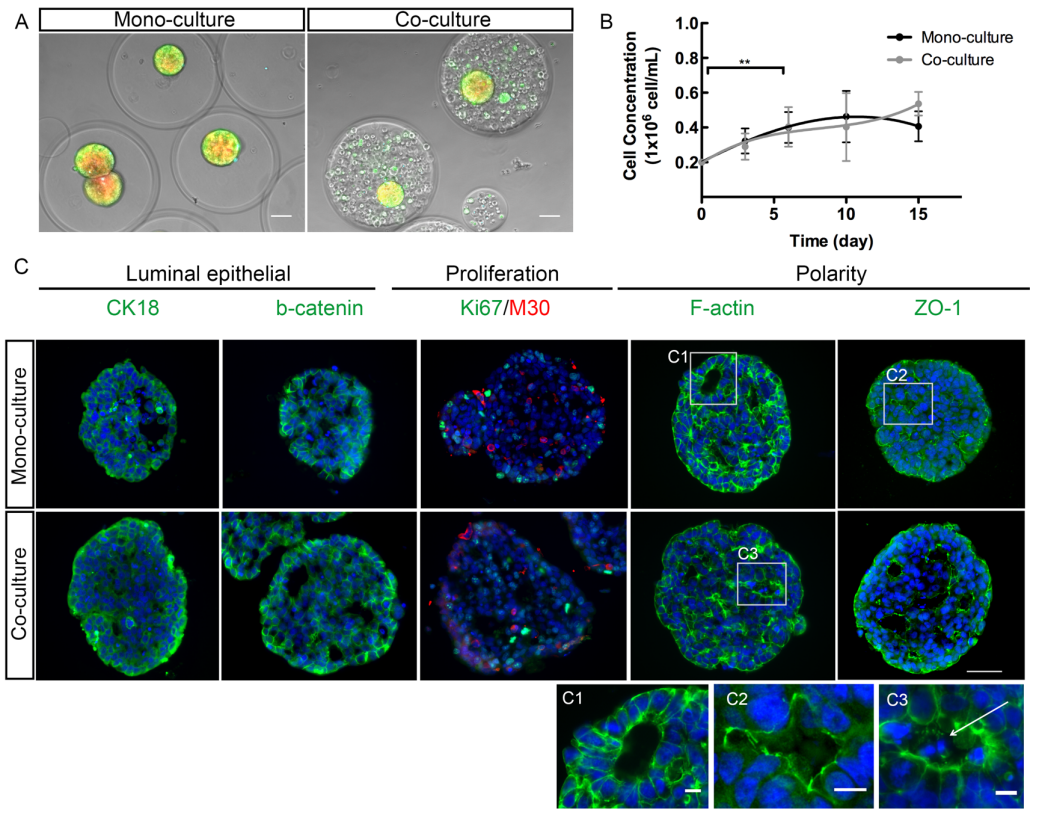

Figure 3.2: Phenotypic characterization of microencapsulated mono and co-cultures. (A) Live/dead assay (FDA – green; ToPro3 – blue, respectively) of MCF-7 (red) tumour aggregates in mono and in co-culture, at day 5. (B) cell concentration profile of mono and co-cultures along 15 days of culture; data are mean ± SD from four independent experiments; ** indicate significant difference with $p < 0.003$ by two way ANOVA. (C) Immunofluorescence microscopy of alginate microcapsules in 10 µm thick cryosections , at day 5, show mono-culture and co-culture aggregates in the upper and lower panels, respectively. From the left: Cytokeratin 18 (green), KI67 (green) and cleaved cytokeratin 18 (M30 cytodeath, red), f-actin (phalloidin; green), Zonula Occludens 1 (ZO-1, green) and DAPI (blue). (C1), (C2) and (C3) High magnification inset represents the region indicated by the white square. The white arrowhead indicates the pyknotic nuclei. Scale bars: 50 µm, 10 µm for high-magnification inset.

3.3 Cell organization and collagen accumulation in alginate microcapsules resemble structures observed in human tumours

Immunofluorescence analysis by Light Sheet Microscopy of alginate microcapsules from co-cultures showed that fibroblasts were distributed around tumour aggregates (Figure 3.3A), creating a "stromal compartment," correctly oriented to the tumour cells.

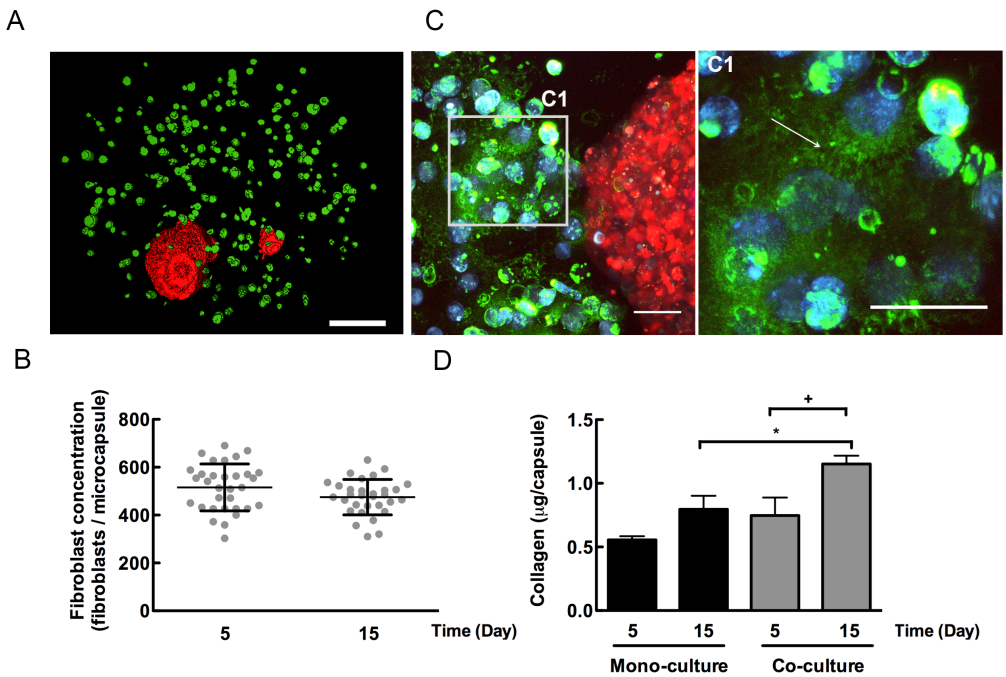

Figure 3.3: Collagen accumulation within the stromal compartment. (A) Immunofluorescence microscopy of whole mount co-cultures of MCF-7 aggregates (red) and fibroblasts (anti-vimentin - green), at day 5 - 3D volume rendering was done with a light sheet microscope (SPIM). (B) Number of fibroblasts *per* microcapsule, in co-cultures, at days 5 and 15 – images acquired by light sheet microscopy (SPIM); quantification method described in [21]. (C) Immunofluorescence microscopy of collagen I (anti-collagen I - green) of whole mount MCF-7 aggregates (red) and fibroblasts (blue), at day 5 – maximum intensity z-projection of 125 optical sections with 2 µm z-step in a 2-photon microscope. (C1) High magnification inset represents the region indicated by the white square. The white arrowhead indicates the collagen I

fibres. (D) Total collagen quantification of mono and co-cultures, at days 5 and 15; data are mean ± SD from three independent experiments; * or + indicate significant difference with $p < 0.01$ by non-parametric Kruskal-Wallis test.

In non-microencapsulated cultures, fibroblasts accumulated in the centre of the aggregate [26]. Quantification of the number of fibroblasts *per* microcapsule, demonstrated that the number of fibroblasts was similar across microcapsules, that fibroblast concentration remained constant throughout the culture time (Figure 3.3B) and that vimentin and collagen (Type I and IV) expression was kept throughout the culture time (data not shown).

A 1.5-fold increase in collagen concentration was found in co-cultures at day 15 as compared to day 5. Furthermore, comparison of both types of culture revealed that the co-cultures had accumulated significantly higher levels of collagen than mono-cultures by day 15 (Figure 3.3D). Using whole mount immunofluorescence of the co-cultures, we observed that collagen I accumulated in the stromal compartment (Figure 3.3C) and assembled into fibres (Figure 3.3C1), as typically observed in tissues [30].

3.4 The effect of stroma on disease progression events can be monitored and further investigated in long-term stirred-tank cultures

At day 15, aggregates in co-cultures presented with an altered phenotype in that there was loss of aggregate circularity (Figure 3.4A) and unidirectional aggregate migration from the microcapsules (Figure 3.4B). Whilst in mono-cultures, 90% of the aggregates maintained the circularity observed at day 5 (95% in both cultures), in the co-cultures, the aggregate population became very heterogeneous, with 40% of the aggregates presenting an altered shape (Figure 3.4A). These alterations were reflected in a significant increase in aggregate size between days 10 and 15 (Figure 3.4C). Additionally, the co-culture aggregates were less compact, cell-cell contacts were decreased and cell polarity was lost in the surfaces of the lumens, as indicated by ZO-1

translocation to the cytoplasm (Figure 3.4D). In contrast, the mono-cultures kept their initial phenotype throughout the culture period.

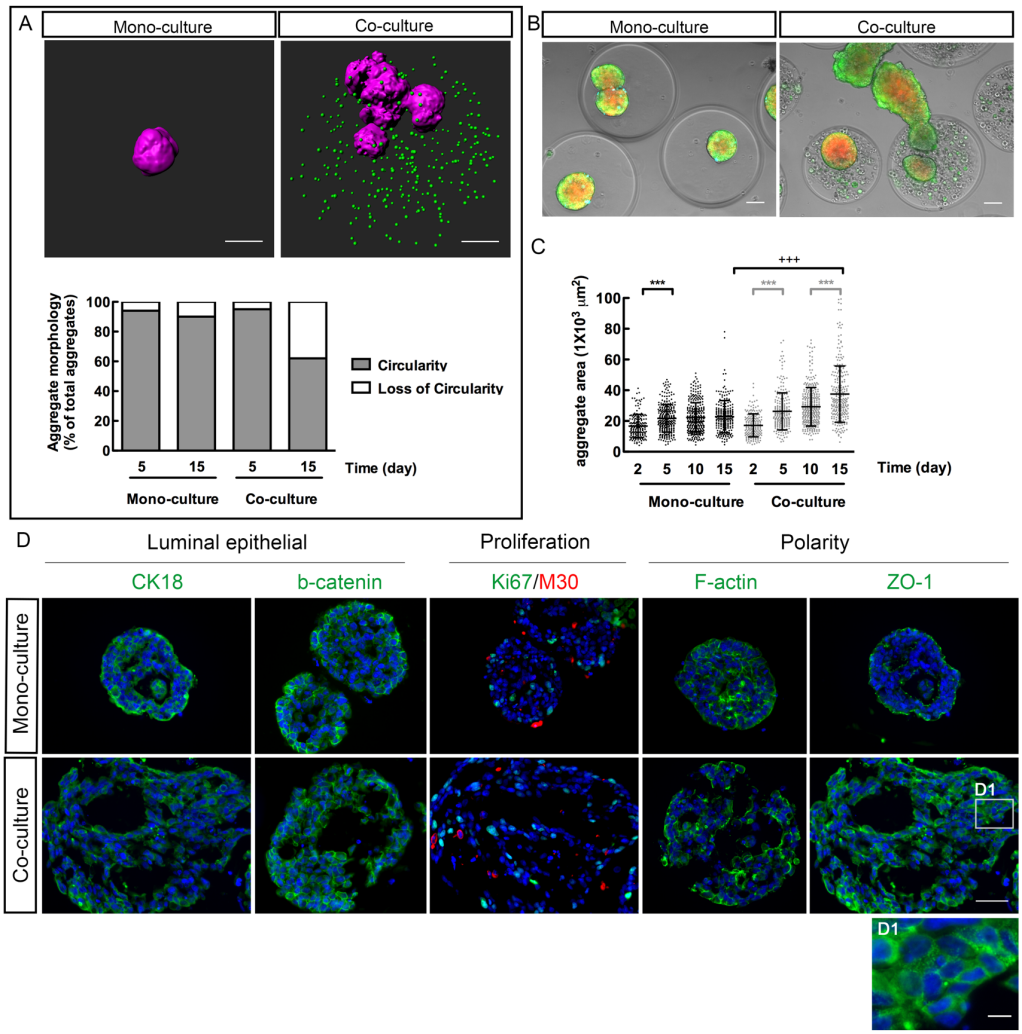

Figure 3.4: Phenotypic characterization of long-term (up to 15 days) mono and co-cultures. (A) Immunofluorescence microscopy of whole mount MCF-7 aggregates (red) with or without fibroblasts (anti-vimentin - green), at day 15 - 3D volume rendering was carried out with a light sheet microscope (SPIM); Morphologic analysis of approximately 100 aggregates from mono and co-cultures – images acquired using a light sheet microscope (SPIM). (B) Live/dead assay (FDA – green; ToPro3 – blue, respectively) of MCF-7 (red) tumour aggregates in mono and in co-culture, at day 15. (C) Size distribution plot: aggregate surface area from mono and co-

cultures, at days 2, 5, 10 and 15; data are mean ± SD from three independent experiments; *** and $^{+++}$ indicate significant difference with $p < 0.0001$ by the non-parametric Kruskal-Wallis test. (D) Immunofluorescence microscopy of alginate microcapsules 10µm thick cryosections, at day 15, show mono-culture and co-culture aggregates in the in the upper and lower panel, respectively. From the left: Cytokeratin 18 (green), KI67 (green) and cleaved cytokeratin 18 (M30 cytodeath, red), f-actin (phalloidin; green), Zonula Occludens 1 (ZO-1, green) and DAPI (blue). (D1) High magnification inset represents the region indicated by the white square. Scale bars: 50 µm, 10 µm for high-magnification inset.

Oestrogen Receptor (ER) and E-cadherin protein expression and localisation in the aggregates were assessed by IHC and by WB (Figure 3.5). At day 5, the proportion of cells showing strong nuclear ER staining was significantly lower in the co-cultures compared to the mono-cultures but did not reduce further over the culture period (Figure 3.5A). The proportion of tumour cells in the mono-cultures showing strong ER staining intensity was reduced only after 15 days in culture. This reduction in strong ER staining was accompanied by a significant increase in cells showing moderate staining intensity. The reduction in strong ER staining was also reflected in a reduction of total ER protein, detectable by WB (Figure 3.5A). E-cadherin was present at the membrane in the majority of the cells in both mono and co-cultures. To determine whether the level of membranous E-cadherin expression altered throughout the culture period, an image analysis algorithm was trained to recognise staining at four threshold levels: weak, medium, strong and negative (Figure 3.5B). Quantification of membranous E-cadherin staining, revealed that at day 5, the level of membranous E-cadherin was similar in both mono- and co-cultures. In the mono-cultures however, E-cadherin localisation at the membrane increased over time as indicated by a significant increase in strong membranous staining, and a concomitant decrease in moderate membranous staining (Figure 3.5B). In contrast, in the co-cultures, membranous E-cadherin was reduced at day 15, which is consistent with the observed changes in polarity in the co-cultures over time (Figure 3.4D). It is of note that the inter-

aggregate heterogeneity of E-cadherin staining by IHC was higher than that observed for the ER.

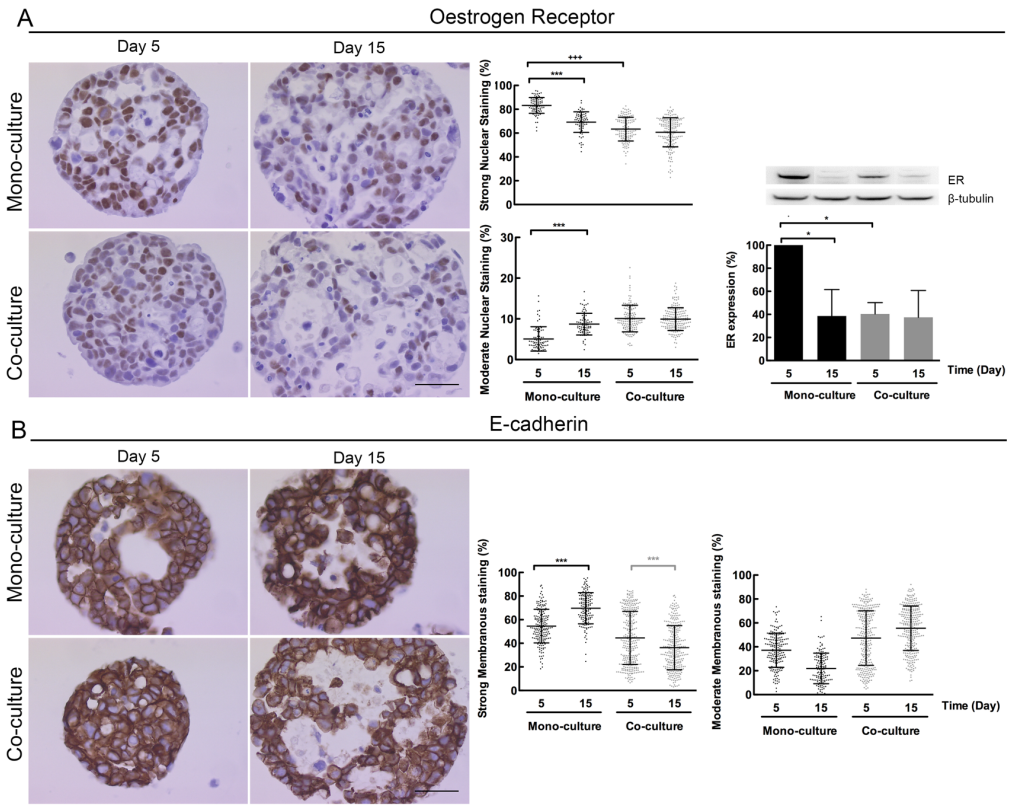

Figure 3.5: Molecular characterization of ER and E-cadherin in long-term (day 15) mono and co-cultures. (A) Immunohistochemistry staining of 3 µm thick paraffin sections of alginate microcapsules taken at days 5 and 15, show mono-culture and co-culture aggregates stained with (A) Oestrogen Receptor (ER); and (B) E-cadherin, and respective quantification of nuclear ER and membranous E-cadherin. (B1) and (B2) High magnification inset represents the region indicated by the white square. ER quantification by Western Blot from total protein extracts. Data are mean ± SD from two independent experiments; * indicate significant difference with $p < 0.01$* and ***or $^{+++}$ indicate significant difference with $p < 0.0001$, both by a two way ANOVA statistics test. Scale bar: 50 µm.

3.5 Tumour-stroma crosstalk within alginate microcapsules results in a pro-inflammatory environment and increased angiogenic response to MCF-7 cells

We next evaluated the production of cytokines in the microencapsulated monocultures of tumour cells and of fibroblasts, as well as in co-cultures over time (Figure 3.6A and Supplementary Figure S3.3). Supernatants from the extracellular fractions of the culture supernatant (CS) and the microcapsule soluble fraction (MSF) were assayed for a panel of 36 cytokines.

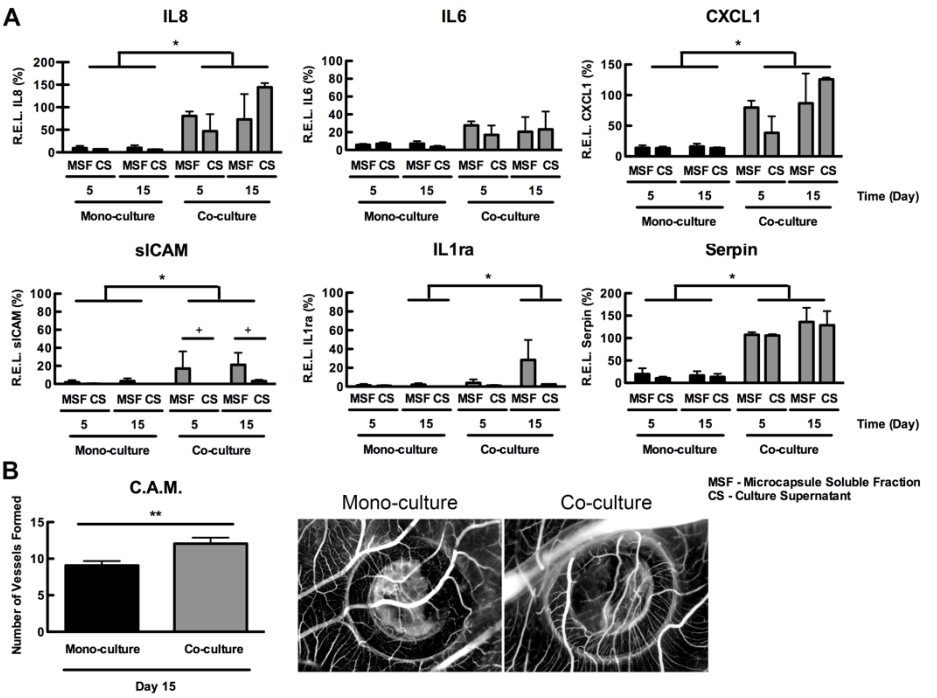

Figure 3.6: Characterization of the inflammatory environment and angiogenic potential of tumour aggregates in co-cultures. (A) Cytokine arrays of mono and co-cultures from days 5 and 15, were performed for both culture and capsule supernatant. Data are mean ± SD from two independent experiments. * or $^{+}$ indicate significant difference with $p < 0.01$ by a non-parametric Man-Whitney U Test (two-tailed p-value). Microencapsulated mono-cultures of fibroblasts were used as controls. (B) Quantification and representative images of Chick Chorioallantoic Membrane (CAM) Assays of tumour aggregates from both mono and co-cultures, at day 15. Vessels with less than 20 μm of diameter, growing in a wheel shape manner towards the inoculation

area, were quantified as newly formed vessels. Data are mean ± SD from 18 eggs. ** indicate significant difference with $p < 0.001$ by a t- Test (two-tailed p-value).

Six cytokines were significantly higher in the co-cultures compared to the mono-cultures. These were Serpin-E1, CXCL1, IL8, IL6, IL1ra and sICAM-1 (Figure 3.6A). Of these, the latter 2 appeared to be specifically retained inside the alginate microcapsules (Figure 3.6A). No statistically significant differences were observed between co-cultures and fibroblast controls (Figure S3.3).

Since CXCL1, IL8 and sICAM-1 are known to promote angiogenesis [31-34], we analysed the impact of the co-culture system on the angiogenic potential of tumour cells at day 15 using a standard Chick Chorioallantoic Membrane (CAM) assay. After removal of stromal cells, ECM and soluble factors, tumour cell aggregates from both types of culture, were inoculated on the top of the CAM and incubated for 3 days. The results obtained show that the number of new blood vessels induced by the aggregates derived from co-cultures was higher than that induced by mono-cultures (Figure 3.6B).

4 Discussion

Multiple attempts have been made in the last decade towards the improvement of *in vitro* preclinical models for cancer research [6]. Despite these efforts, most of the available models still fail to mimic several important aspects of the tumour microenvironment, and do not reflect the complexity of human tumours [6,7]. In addition, most *in vitro* experiments can only be carried out over short culture periods which, clearly, does not allow examination of longer term effects of the microenvironment or drug treatments on disease progression [35].

In this work we have developed a new strategy for *in vitro* reconstruction of tumour microenvironment complexity, using a robust culture system that allows long-term culture with continuous monitoring. This system uses alginate microencapsulation of epithelial tumour cell aggregates either alone or together with human fibroblasts. Tumour-stroma crosstalk was achieved by keeping cells in close proximity and by allowing the accumulation of ECM components

and soluble factors in the alginate microcapsules. Culture progression over time could be evaluated due to the non-invasive sampling offered by this culture system.

Our results demonstrate that in microencapsulated aggregates, MCF-7 cells self-organized into tissue-like structures by establishing cell-cell contacts presumably via E-cadherin, by partial polarisation at the surface of multiple small lumina and inverse polarisation at the outer rim of the aggregate. Pyknotic nuclei were also detected within the lumina, suggestive of lumen formation via cell death and subsequent cavitation [36]. These features together with the relatively limited proliferative capacity are reminiscent of well differentiated human breast tumours of the luminal subtype or, indeed, the normal human breast epithelium [37,38]. The absence of myoepithelial cells with a resulting lack of basement membrane [39] may have contributed to the observed inverse polarity seen at the rims of the aggregates [40]. However, inverse polarity has also been described to occur *in vivo,* during tumorigenesis [41]. Therefore, we could recapitulate certain features of epithelial carcinomas such as breast by combining 3D aggregates with alginate microencapsulation. Other groups have shown that MCF-7 cells can polarise and maintain the luminal epithelial phenotype but only when cultured in Matrigel for 7 days [9] or in very long culture times in scaffold-free conditions (155 days) [42]. Similarly, we have also demonstrated that MCF-7 cells are unable to polarise when cultured over 5 days without scaffolds (i.e. non-microencapsulated), in our stirred-tank culture system although the luminal-epithelial phenotype was maintained (Figure S3.1). Overall our results demonstrate that aggregate microencapsulation in alginate, an inert scaffold, allows cell movement required for lumen formation and cell polarisation [37], by day 5 of culture.

We hypothesised that alginate entrapment of tumour cell aggregates together with human fibroblasts would further help reconstruction of the different aspects of the tumour microenvironment. Our results show the differential distribution of tumour and stromal cells. Epithelial tumour aggregates appear surrounded by fibroblasts, creating appropriately oriented

"epithelial tumour" and "stromal" compartments within the alginate microcapsules. In contrast, when cultured without a scaffold, fibroblasts accumulated in the centre of the aggregates forming a core, as shown by us [26] and by others [43,44]. In cultures without scaffolds, the fibroblasts remained viable and maintained collagen expression, however the cellular organization did not resemble the human tumours where epithelial and stromal cells are organized into distinct compartments [3].

Imaging and quantification of collagen within the microcapsules demonstrated a significant increase of collagen deposition over the time in the co-cultures, suggesting that fibroblasts were playing their biologic role by actively producing collagen [45]. Furthermore, collagen type I appeared to be assembled into fibers within the stromal compartment, as typically observed in breast tissues [46,47]. Collagen is the major component of human breast stroma [48] and it is though that mammary epithelial cells migrate along type I collagen fibres during branching morphogenesis and tumour cell dissemination [49,50]. Additionally, other studies have shown that stiffer collagen matrices may promote mammary tumour cell dissemination [49,51]. Accordingly, many 3D tumour models have been developed using collagen type I matrices in order to determine the impact on tumour behaviour [2,6]. However, cell growth and migration is dependent on collagen physical properties, which, in turn, are greatly dependent on the type of cross-linking used [52]. For this reason, the *de novo* synthesis of collagen by stromal cells and its accumulation within the stromal compartment is a major advantage of the alginate microencapsulated culture system.

To further understand the role played by fibroblasts in our culture system, analysis of the profile of cytokines produced at early and late time points was carried out using cytokine arrays. Overall the results indicate increased secretion of pro-inflammatory cytokines, such as, IL6, IL8 and CXCL1 in the co-cultures. These pro-inflammatory cytokines have been linked with increased tumour aggressiveness, cell dissemination and angiogenesis [32]. Paradoxically, an anti-inflammatory cytokine (IL1ra) was also increased in the

co-cultures. The reason for this is unclear but may be an intrinsic feedback mechanism that limits the effects of pro-inflammatory cytokines. Nevertheless, the overall balance of cytokines suggests a pro-inflammatory environment in the co-cultures. Furthermore, sICAM, a cytokine associated with tumour cell growth and angiogenesis [34] was higher in the co-cultures and specifically accumulated in the alginate microcapsule. It is well known that a shift in the cytokine balance from an anti- to a pro-inflammatory environment may lead to chronic inflammation that consequently promotes tumour progression [53,54]. Our results recapitulate this inflammatory shift, which strengthens our model as a good alternative in which to study tumour-stroma crosstalk mechanisms.

The non-invasive sampling allowed us to continuously monitor the effect of the reconstructed microenvironment on culture progression throughout the culture time. By the day 15, tumour aggregates in co-cultures had an altered phenotype that was not observed in mono-cultures. Analysis of aggregate morphology by SPIM-FLUID microscopy [21] demonstrated that approximately 40% of the aggregates in co-culture had become irregular in shape and had lost their circularity. In contrast 90% of the aggregates in the mono-cultures retained their circularity. This change in shape in the co-cultures resulted in increased aggregate surface area and was accompanied by aggregate cell migration out of the microcapsules. The directionality of aggregate migration accompanied by the stabilization of tumour cell concentration, is suggestive of an event of collective cell migration rather than the cell movement associated with expansive cell growth [50]. Ductal elongation, such as that occurring during breast morphogenesis, is described as a directional collective migration process [37], which might explain the observed directionality in aggregate migration from the microcapsules. The accumulation of collagen exclusively in the stromal compartment, of co-cultures might be enough to stimulate collective tumour cell migration. Furthermore, collective cell migration typically occurs in carcinomas and has been described as an crucial step in the disease progression towards metastatic cancer [55].

The altered aggregate morphology and loss of cell polarity observed at day 15 in co-cultures appears to be heralded by reduced nuclear expression of ER which could be seen as early as day 5 of co-culture compared to the aggregates in mono-culture. The reasons underlying this early reduction in ER expression are not, as yet, known but we speculate that reduction of signalling through this receptor may be necessary before other phenotypic changes can occur. Nuclear ER expression also declined in the mono-cultures but at a much slower rate and was only apparent after 15 days of culture. It is possible that the aggregates in the mono-cultures would also have undergone a change in behaviour and phenotype similar to that seen in the co-cultures if they had been maintained in culture for long enough. This difference between mono and co-culture suggests that fibroblasts are accelerating ER depletion, as previously demonstrated by others [56]. ER^+ breast cancers are described to present high frequency of disease relapse associated with metastasis and drug resistance, despite an initial response to endocrine therapy [27,28]. Loss of hormone dependency accompanied by altered sub-cellular localization of E-cadherin and altered cell polarity have been described as common features of more aggressive and invasive breast cancers [57-59]. Quantification of membranous E-cadherin revealed a very high percentage of aggregate heterogeneity in co-cultures compared to mono-cultures, which was similar to the heterogeneity in aggregate circularity, although the correlation between these two parameters has not been addressed. The reduction in E-cadherin membrane staining could contribute to the observed loss of aggregate circularity. Furthermore, the intra-culture heterogeneity observed in co-cultures is critical, since it may recapitulate the intra-tumour heterogeneity observed in human tumours [50].

The angiogenic potential of both mono and co-cultures was analysed by Chick Chorioallantoic Membrane (CAM) assay. Our results demonstrate that, by day 15, tumour aggregates from co-cultures have a higher capacity to induce angiogenesis, which was indicated by the significant increase in the number of new radial blood vessels formed towards the aggregates from co-cultures, when compared to those from mono-cultures. This increase might be related to

the increased expression of pro-angiogenic cytokines in co-cultures, such as CXCL1 and IL8 in the co-cultures [31-33]. Overall, our results show that tumour cells were indeed educated by the stroma, since the new blood vessels formed in the CAM assay were induced only by those tumour cells that had been cultured for 15 days within the reconstructed tumour microenvironment in this culture system.

In conclusion, we have developed a robust and versatile model system for long-term *in vitro* recapitulation of tumour-stroma crosstalk, *via* reconstruction of key aspects of the tumour microenvironment such as *de novo* synthesis and accumulation of ECM and cytokines, and allowing continuous monitoring of tumour progression events *in vitro*. Entrapment of tumour cells and fibroblasts in an inert scaffold allowed *de novo* synthesis and deposition of extracellular matrix (ECM) by the cells, and the accumulation of soluble factors, promoting tumour-stroma crosstalk. This model system is transferrable to other types of tumour cells and provides a new tool for further understanding tumour progression and drug resistance mechanisms using either cell lines or patient-derived primary cultures. In addition, it is easily transferable to industry for feeding high-throughput systems or miniaturised bioreactors used for drug development and target validation.

5 Acknowledgments

We gratefully acknowledge Dr Cathrin Brisken for the supply of the MCF-7-rfp cell line within the scope of the IMI-funded project PREDECT and for valuable advice. We are grateful to the PREDECT consortium partners, especially to Dr John Hickman, Dr Juha Klefström and Dr Georgios A. Sflomos for fruitful discussions. We also thank Dr Joana Paredes for critical advice. We acknowledge support from the Innovative Medicines Initiative Joint Undertaking (IMI grant agreement n° 115188), resources composed of financial contribution from EU - FP7 and EFPIA companies in kind contribution. We also acknowledge support from Fundação para a Ciência e Tecnologia (FCT), Portugal (EXPL/BBB-IMG/0363/2013); MFE is the recipient of a PhD fellowship

from FCT (SFRH/BD/52208/2013).

6 References

[1] Bissell MJ, Hines WC. Why don't we get more cancer? A proposed role of the microenvironment in restraining cancer progression. Nat Med 2011;17:320–9.

[2] Nguyen-Ngoc K-V, Cheung KJ, Brenot A, Shamir ER, Gray RS, Hines WC, et al. ECM microenvironment regulates collective migration and local dissemination in normal and malignant mammary epithelium. Proc Natl Acad Sci USa 2012;109:E2595–604.

[3] Khamis ZI, Sahab ZJ, Sang Q-XA. Active roles of tumor stroma in breast cancer metastasis. Int J Breast Cancer 2012;2012:574025–10.

[4] Kessenbrock K, Plaks V, Werb Z. Matrix metalloproteinases: regulators of the tumor microenvironment. Cell 2010;141:52–67.

[5] “Cancer associated fibroblasts--”more than meets the eye. 2013;19:447–53.

[6] Weigelt B, Ghajar CM, Bissell MJ. The need for complex 3D culture models to unravel novel pathways and identify accurate biomarkers in breast cancer. Adv Drug Deliv Rev 2014;69-70:42–51.

[7] Hirt C, Papadimitropoulos A, Muraro MG, Mele V, Panopoulos E, Cremonesi E, et al. Bioreactor-engineered cancer tissue-like structures mimic phenotypes, gene expression profiles and drug resistance patterns observed "in vivo". Biomaterials 2015;62:138–46.

[8] Ekert JE, Johnson K, Strake B, Pardinas J, Jarantow S, Perkinson R, et al. Three-dimensional lung tumor microenvironment modulates therapeutic compound responsiveness in vitro--implication for drug development. PLoS ONE 2014;9:e92248.

[9] Smart CE, Morrison BJ, Saunus JM, Vargas AC, Keith P, Reid L, et al. In vitro analysis of breast cancer cell line tumourspheres and primary human breast epithelia mammospheres demonstrates inter- and intrasphere heterogeneity. PLoS ONE 2013;8:e64388.

[10] Mafi P, Hindocha S, Mafi R, Khan WS. Evaluation of biological protein-based collagen scaffolds in cartilage and musculoskeletal tissue engineering--a systematic review of the literature. Curr Stem Cell Res Ther 2012;7:302–9.

[11] Sung KE, Beebe DJ. Microfluidic 3D models of cancer. Adv Drug Deliv Rev 2014;79-80:68–78.

[12] Chwalek K, Tsurkan MV, Freudenberg U, Werner C. Glycosaminoglycan-based hydrogels to modulate heterocellular communication in in vitro angiogenesis models. Sci Rep 2014;4:4414.

[13] Andersen T, Auk-Emblem P, Dornish M. 3D Cell Culture in Alginate Hydrogels. Microarrays 2015, Vol 4, Pages 133-161 2015;4:133–61.

[14] Sun J, Tan H. Alginate-Based Biomaterials for Regenerative Medicine Applications. Materials 2013;6:1285–309.

[15] Alessandri K, Sarangi BR, Gurchenkov VV, Sinha B, Kießling TR, Fetler L, et al. Cellular capsules as a tool for multicellular spheroid production and for investigating the mechanics of tumor progression in vitro. Proc Natl Acad Sci USa 2013;110:14843–8.

[16] Lan S-F, Starly B. Alginate based 3D hydrogels as an in vitro co-culture model platform for the toxicity screening of new chemical entities. Toxicol Appl Pharmacol 2011;256:62–72.

[17] Kimlin LC, Casagrande G, Virador VM. In vitro three-dimensional (3D) models in cancer research: an update. Mol Carcinog 2013;52:167–82.

[18] Haycock JW. 3D cell culture: a review of current approaches and techniques. Methods Mol Biol 2011;695:1–15.

[19] Rebelo SP, Costa R, Estrada M, Shevchenko V, Brito C, Alves PM. HepaRG microencapsulated spheroids in DMSO-free culture: novel culturing approaches for enhanced xenobiotic and biosynthetic metabolism. Arch Toxicol 2014:1–12.

[20] Simão D, Pinto C, Piersanti S, Weston A, Peddie CJ, Bastos AEP, et al. Modeling human neural functionality in vitro: three-dimensional culture for dopaminergic differentiation. Tissue Eng Part A 2015;21:654–68.

[21] Gualda EJ, Pereira H, Vale T, Estrada MF, Brito C, Moreno N. SPIM-fluid: open source light-sheet based platform for high-throughput imaging. Biomedical Optics Express 2015;6:4447–56.

[22] Gualda EJ, Vale T, Almada P, Feijó JA, Martins GG, Moreno N. OpenSpinMicroscopy: an open-source integrated microscopy platform. Nat Methods 2013;10:599–600.

[23] Schindelin J, Arganda-Carreras I, Frise E, Kaynig V, Longair M, Pietzsch T, et al. Fiji: an open-source platform for biological-image analysis. Nat Methods 2012;9:676–82.

[24] Davies EJ, Marsh Durban V, Meniel V, Williams GT, Clarke AR. PTEN loss and KRAS activation leads to the formation of serrated adenomas and metastatic carcinoma in the mouse intestine. J Pathol 2014;233:27–38.

[25] Sakai A, Ohshima M, Sugano N, Otsuka K, Ito K. Profiling the cytokines in gingival crevicular fluid using a cytokine antibody array. J Periodontol 2006;77:856–64.

[26] Santo VE, Estrada MF, Silva I, Rebelo SP, Pinto AC, Veloso SC, et al. Novel versatile *in vitro* 3D models generated in agitation-based culture systems with the ability to capture key tumor features for pre-clinical research. Journal of Biotechnology n.d.

[27] Yoshida N, Omoto Y, Inoue A, Eguchi H, Kobayashi Y, Kurosumi M, et al. Prediction of prognosis of estrogen receptor-positive breast cancer with combination of selected estrogen-regulated genes. Cancer Sci 2004;95:496–502.

[28] Shekhar MPV, Santner S, Carolin KA, Tait L. Direct involvement of breast tumor fibroblasts in the modulation of tamoxifen sensitivity. Am J Pathol 2007;170:1546–60.

[29] Holliday DL, Speirs V. Choosing the right cell line for breast cancer research. Breast Cancer Res 2011;13:215.

[30] Kakkad SM, Solaiyappan M, Argani P, Sukumar S, Jacobs LK, Leibfritz D, et al. Collagen I fiber density increases in lymph node positive breast cancers: pilot study. J Biomed Opt 2012;17:116017–7.

[31] Singh JK, Simões BM, Howell SJ, Farnie G, Clarke RB. Recent advances reveal IL-8 signaling as a potential key to targeting breast cancer stem cells. Breast Cancer Res 2013;15:210.

[32] DelNero P, Lane M, Verbridge SS, Kwee B, Kermani P, Hempstead B, et al. 3D culture broadly regulates tumor cell hypoxia response and angiogenesis via pro-inflammatory pathways. Biomaterials 2015;55:110–8.

[33] Acharyya S, Oskarsson T, Vanharanta S, Malladi S, Kim J, Morris PG, et al. A CXCL1 paracrine network links cancer chemoresistance and metastasis. Cell 2012;150:165–78.

[34] Chen C, Duckworth CA, Fu B, Pritchard DM, Rhodes JM, Yu L-G. Circulating galectins -2, -4 and -8 in cancer patients make important contributions to the increased circulation of several cytokines and chemokines that promote

angiogenesis and metastasis. British Journal of Cancer 2014;110:741–52.

[35] Unger C, Kramer N, Walzl A, Scherzer M, Hengstschläger M, Dolznig H. Modeling human carcinomas: physiologically relevant 3D models to improve anti-cancer drug development. Adv Drug Deliv Rev 2014;79-80:50–67.

[36] Bryant DM, Mostov KE. From cells to organs: building polarized tissue. Nat Rev Mol Cell Biol 2008;9:887–901.

[37] Ewald AJ, Brenot A, Duong M, Chan BS, Werb Z. Collective epithelial migration and cell rearrangements drive mammary branching morphogenesis. Dev Cell 2008;14:570–81.

[38] Piccart-Gebhart MJ. New developments in hormone receptor-positive disease. Oncologist 2011;16 Suppl 1:40–50.

[39] Gudjonsson T, Rønnov-Jessen L, Villadsen R, Rank F, Bissell MJ, Petersen OW. Normal and tumor-derived myoepithelial cells differ in their ability to interact with luminal breast epithelial cells for polarity and basement membrane deposition. J Cell Sci 2002;115:39–50.

[40] Akhtar N, Streuli CH. An integrin-ILK-microtubule network orients cell polarity and lumen formation in glandular epithelium. Nat Cell Biol 2013;15:17–27.

[41] Adams SA, Smith MEF, Cowley GP, Carr LA. Reversal of glandular polarity in the lymphovascular compartment of breast cancer. J Clin Pathol 2004;57:1114–7.

[42] do Amaral JB, Urabayashi MS, Machado-Santelli GM. Cell death and lumen formation in spheroids of MCF-7 cells. Cell Biol Int 2010;34:267–74.

[43] Kaur P, Ward B, Saha B, Young L, Groshen S, Techy G, et al. Human breast cancer histoid: an in vitro 3-dimensional co-culture model that mimics breast cancer tissue. J Histochem Cytochem 2011;59:1087–100.

[44] Angelucci C, Maulucci G, Lama G, Proietti G, Colabianchi A, Papi M, et al. Epithelial-stromal interactions in human breast cancer: effects on adhesion, plasma membrane fluidity and migration speed and directness. PLoS ONE 2012;7:e50804.

[45] Weigelt B, Bissell MJ. Unraveling the microenvironmental influences on the normal mammary gland and breast cancer. Semin Cancer Biol 2008;18:311–21.

[46] Alberts B, Johnson A, Lewis J, Morgan D, Raff M, Roberts K, et al. Molecular Biology of the Cell, Sixth Edition. Garland Science; 2014.

[47] Kakkad SM, Solaiyappan M, O'Rourke B, Stasinopoulos I, Ackerstaff E, Raman V, et al. Hypoxic tumor microenvironments reduce collagen I fiber density. Neoplasia 2010;12:608–17.

[48] Conklin MW, Keely PJ. Why the stroma matters in breast cancer: insights into breast cancer patient outcomes through the examination of stromal biomarkers. Cell Adh Migr 2012;6:249–60.

[49] Cox TR, Erler JT. Remodeling and homeostasis of the extracellular matrix: implications for fibrotic diseases and cancer. Dis Model Mech 2011;4:165–78.

[50] Friedl P, Alexander S. Cancer invasion and the microenvironment: plasticity and reciprocity. Cell 2011;147:992–1009.

[51] Bonnans C, Chou J, Werb Z. Remodelling the extracellular matrix in development and disease. Nat Rev Mol Cell Biol 2014;15:786–801.

[52] Vaissiere G, Chevallay B, Herbage D, Damour O. Comparative analysis of different collagen-based biomaterials as scaffolds for long-term culture of human fibroblasts. Med Biol Eng Comput 2000;38:205–10.

[53] Yuzhalin A, Kutikhin A. Interleukins in Cancer Biology. Academic Press; 2014.

[54] Zellmer VR, Zhang S. Evolving concepts of tumor heterogeneity. Cell

& Bioscience 2014;4:69.

[55] Cheung KJ, Gabrielson E, Werb Z, Ewald AJ. Collective invasion in breast cancer requires a conserved basal epithelial program. Cell 2013;155:1639–51.

[56] Holton SE, Bergamaschi A, Katzenellenbogen BS, Bhargava R. Integration of molecular profiling and chemical imaging to elucidate fibroblast-microenvironment impact on cancer cell phenotype and endocrine resistance in breast cancer. PLoS ONE 2014;9:e96878.

[57] Robinson JLL, Holmes KA, Carroll JS. FOXA1 mutations in hormone-dependent cancers. Front Oncol 2013;3:20.

[58] Scherbakov AM, Andreeva OE, Shatskaya VA, Krasil'nikov MA. The relationships between snail1 and estrogen receptor signaling in breast cancer cells. J Cell Biochem 2012;113:2147–55.

[59] Suh YJ, Chang JH, Chun CS. Restoration of Hormone Dependency in Estrogen Receptor-Lipofected MDA-MB-231 Human Breast Cancer Cells. Journal of the Korean Cancer Association 1999.

7 Supplementary Figure

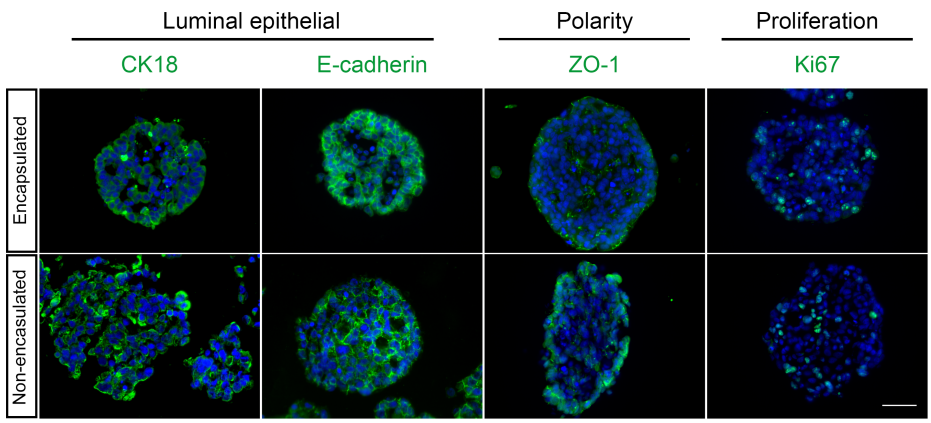

Figure S3.1: Phenotypic characterization of microencapsulated and non-microencapsulated mono-cultures, at day 5. Immunofluorescence microscopy of tumour aggregates in cryosections with 10 µm thick, at day 5, show microencapsulated and non-microencapsulated mono-culture aggregates in the upper and lower panel, respectively. From the left: Cytokeratin 18 (green), E-cadherin (green), Zonula Occludens 1 (ZO-1, green), KI67 (green) and DAPI (blue). Scale bar: 50 µm.

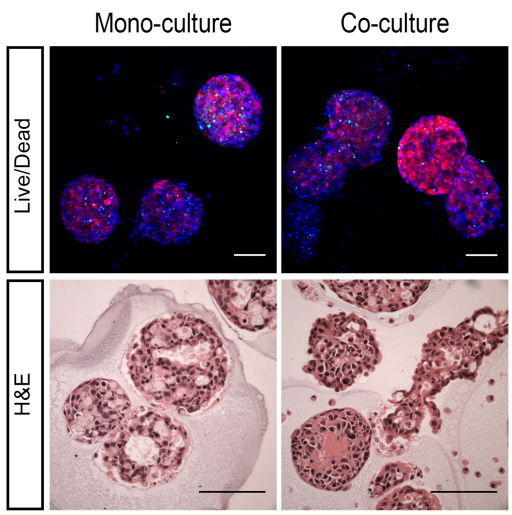

Figure S3.2: Phenotypic characterization of microencapsulated and non-microencapsulated mono-cultures, at day 15. Live/dead assay (ToPro3 – green and

and DAPI - blue) of MCF-7 (red) tumour aggregates in mono and in co-culture, at day 15 (upper panel). Hematoxylin & Eosin (H&E) staining of mono and co-cultures, in paraffin sections with 3 µm thick. Scale bar: 50 µm (lower panel).

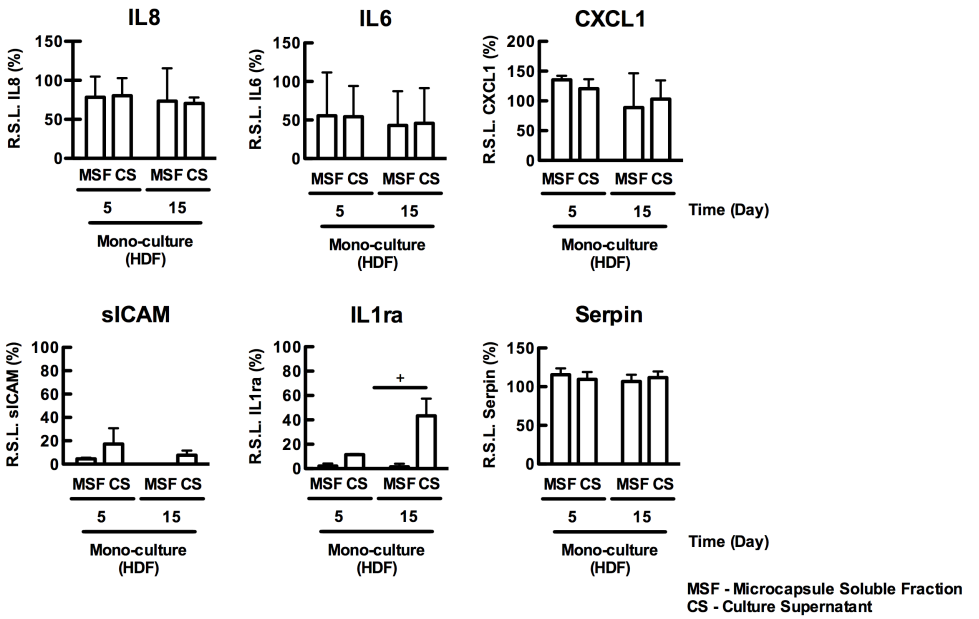

Figure S3.3: Characterization of the inflammatory environment in microencapsulated mono-cultures of fibroblasts. Cytokine arrays of mono-cultures of fibroblasts (HDF), at days 5 and 15 of culture, were performed for both culture supernatant (CS) and capsule soluble fraction (CSF). Data are mean ± SD from two independent experiments. $^{+}$ indicates significant difference with $p < 0.01$ by a non-parametric Man-Whitney U Test (two-tailed p-value).

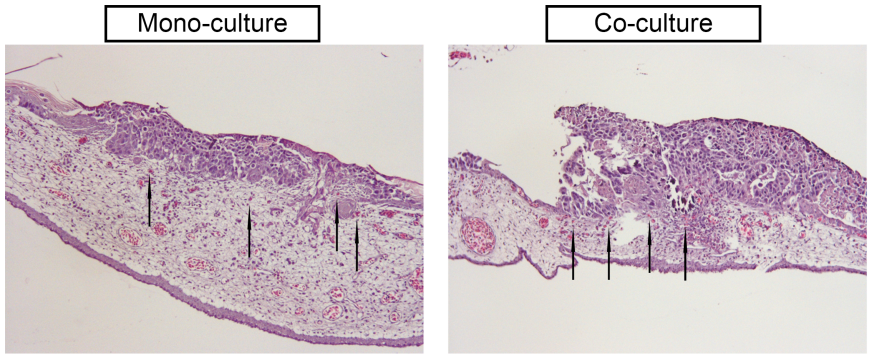

Figure S3.4: Characterization of the CAM. Representative images of Haematoxylin & Eosin staining from Chick Chorioallantoic Membrane (CAM) Assays, 3 days after inoculation of tumour aggregates from both mono and co-cultures, at day 15. Paraffin sections with 3 µm thickness**;** Arrows indicate nucleated erythrocytes in the lumen of *micro*-vessels.

8 Supplementary Table

Table S3.1: Antibodies used for Immunodetection

Antibody description	Clone	Reference	Supplier	Anaytical method
Anti-CK 18 – FITC conjugate	CY-90	F 4772	Sigma	IF
Anti-ER receptor	ID5	M7047	DAKO	IF, IHC, WB
Anti-ki67	SP6	ab27619	Abcam	IF
Anti-vimentin	V9	ab16700	Abcam	IF
Anti-collagen I	Polyclonal	ab292	Abcam	IF
Anti-collagen IV	Polyclonal	ab6586	Abcam	IF
Anti-Phalloidin – 488 conjugate		A12379	Life Technologies	IF
Anti-E-cadherin	36	610181	BD Biosciences	IF
Anti-E-cadherin	24 E 10	#3195	Cell Signalling	IHC
Anti-ZO-1	Polyclonal	40-2200	Life Technologies	IF
Anti-β-catenin	Polyclonal	sc-7199	Santa Cruz	IF
Anti-M30 CytoDEATH	M30	12 140 322 001	Roche	IF
Anti-b tubulin	Polyclonal	sc-9104	Santa Cruz	WB
Anti-rabbit Alexa 647	Polyclonal	A31571	Life Technologies	IF
Anti-mouse Alexa 488	Polyclonal	A11001	Life Technologies	IF

Note: Immunofluorescence (IF); Immunohistochemistry (IHC); Western Blot (WB)

Chapter IV

Capturing tumour complexity *in vitro* - Comparative analysis of 2D and 3D tumour models for drug discovery

This Chapter was adapted from:

Stock K*, **Estrada MF***, Vidic S*, Gjerde K*, Rudisch A*, Santo VE*, Barbier M, Blom S, (...) Brito S, Weerden W, Rotter V, Boghaert E, Oren M, Sommergruber W, Chong Y, Hoogt R, Graeser R. *Capturing tumor complexity in vitro- Comparative analysis of 2D and 3D tumor models for drug discovery*. Scientific Reports. 2016.

Table of contents

Abstract 119
1 Introduction 120
2 Materials and Methods 122
2.1 Cell passaging 122
2.2 2D culture 122
2.3 Floater culture 122
2.4 3D Alginate-embedded stirred-tank Bioreactor cultures (alginate-BR) 123
2.5 3D embedded culture 123
2.6 Standard-of-care treatment 124
2.7 Fluorescence in situ microscopy and analysis 124
2.8 Paraformaldehyde fixation and paraffin-embedding 125
2.9 TMA preparation from FFPE blocks, staining, and analysis 126
2.10 Statistical analysis 127
3 Results 128
3.1 Generation of model platforms 128
3.2 Characterization of model platforms using growth curves 129
3.3 Response of model platforms to standard of care treatment 133
3.4 Image analysis of 3D cultures 136
4 Discussion 140
5 Acknowledgements 145
6 Author contributions 146
7 Tables 147
8 References 150

Abstract

Two-dimensional (2D) cell cultures growing on plastic do not recapitulate the three dimensional (3D) architecture and complexity of human tumours. More representative models are required for drug discovery and validation. Here, 2D culture and 3D mono- and stromal co-culture models of increasing complexity have been established and cross-comparisons made using MCF7 cell line. Fluorescence-based growth curves, 3D image analysis, immunohistochemistry and treatment responses showed that end points differed according to cell type, stromal co-culture and culture format.

The adaptable methodologies described here should guide the choice of appropriate simple and complex *in vitro* models.

1 Introduction

Despite the increase in the survival rates for many cancers over the past four decades, the discovery of novel effective drugs has decreased [1]. Overall, the success rate of novel oncology drugs transitioning in the clinic from phase 2 to phase 3 is low [2]. A lack of efficacy was suggested as a main reason for failure [3]. Since novel drugs are propelled to clinical trial based on evidence of efficacy in preclinical models, clearly these models are questionable.

Despite the wealth of data generated, and strong recommendations to upgrade cell culture from 2D to 3D models [4], few of these more complex model systems have been incorporated into the drug discovery funnel. Reproducibility, cost, time to set up, and limited throughput are some of the issues precluding their routine use. Importantly, a lack of detailed characterization and cross-comparison of complex models to show added value relative to simple 2D models is absent from many published studies. Thus there is still a need for a better understanding of these complex models in order to define their utility and limitations so as to then place them in a more comprehensive drug discovery cascade.

The PREDECT consortium (www.predect.eu) has assumed the task to compare and better characterize *in vitro* models for oncology research, particularly models that attempt to capture the complexity and heterogeneity of human cancers [5]. Models were set up for breast carcinomas. MCF7 cell line was chosen due to their responsiveness to anti-hormone treatment as a standard of care (SOC). Human non-immortalized dermal fibroblasts (HDF) were used as the stromal cell component. Albeit not breast-derived, HDFs are specialized in producing collagen [6], which is a predominant ECM component in breast cancer [7]. In previous publications, we have demonstrated that these fibroblasts contribute to a pro-inflammatory and pro-angiogenic environment [8] [9]. Indeed, fibroblasts may be defined by their functionality rather than by their origin [10], and HDFs may functionally be re-programmed by tumour cells to become CAFs [11]. Thus given their ready availability, greater robustness, and

suggested functional adequacy, we decided to use HDFs as a surrogate for breast-derived CAFs.

Starting from simple 2D monocultures, the complexity was increased stepwise to include stromal cells in 2D and in 3D co-cultures. 3D cultures were set up either as free-floating spheroids ("floaters"), microencapsulated into inert hydrogels (alginate) and grown in bioreactors ("alginate-BR"), or embedded in ECM, all in the presence or absence of stromal cells. ECM embedded cultures were established in, (1), Matrigel, a basal membrane extract that induces polarization of normal epithelial cells [12], and would thus reflect a localized tumour environment, (2), collagen I as an interstitial stroma matrix component, providing an invasive growth environment [13], and, (3), a 1:1 mix of both. The alginate hydrogel microcapsules used in the alginate-BR models show some similarity to the glycosaminoglycan structure present in the stromal compartment, such as the ability to form gels at very low concentrations, to attract a cloud of cations, such as Na^+ or $Ca2^+$ and to incorporate high amounts of water into the matrix [14]. In addition, the inert structure keeps tumour spheroids and stromal cells in close proximity, and may be model-tailored by ECM depositions from the embedded cells. In contrast to the other models, stirred-tank bioreactors allow for control of physicochemical parameters such as pH, O_2 and perfusion rates.

Cell growth was monitored in all models by fluorescence measurements. Also, response to standard of care (SOC) hormonal treatment and chemotherapy was measured and compared between all models. When stationary growth phase was reached, cultures were analyzed in more depth by fluorescence imaging of *in situ* fixed cultures, as well as immunohistochemistry (IHC) on paraffin embedded samples processed into tissue micro-arrays (TMAs). The decision to choose imaging methods that leave the cellular organization of the models intact rather than disruptive technologies like genomic or transcriptional profiling, which may provide higher throughput, was taken considering the increasingly recognized role of tumour cell heterogeneity in drug response and resistance. The robust protocols

established by this collaborative effort in combination with the cross-comparisons performed to characterize the models provide a toolbox that should help to better incorporate complex models in the drug discovery process.

2 Materials and Methods

2.1 Cell passaging

MCF-7 cells, transduced with the lentiviral vectors PGK-GFP and pCDH-CMV-MCS-EF1-Puro, were kindly provided by Professor Cathrin Brisken (EPFL, Switzerland) within the scope of the PREDECT consortium. Cell expansion was performed in Dulbecco's Modified Eagle Medium (DMEM) with 25 mM Glucose, supplemented with 1% (v/v) penicillin-streptomycin, 4 mM Glutamax, 1 mM sodium pyruvate and 10% (v/v) fetal bovine serum (FBS). Cells were passaged twice weekly at a inoculum concentration of 1.5 x 10^4 cell/cm^2. Human Dermal Fibroblasts (HDF), from Innoprot, were passaged once weekly for up to 10 to 12 passages at a seeding density of 0.5 x 10^4 cell/cm^2, in Iscove's Modified Dulbecco's Medium (IMDM) supplemented with 1% (v/v) penicillin-streptomycin and 10% (v/v) FBS (all from Life Technologies). Both the MCF-7 cells and the HDFs were cultured in static culture systems, in an incubator at 37ºC with humidified atmosphere containing 5% CO_2 in air.

2.2 2D culture

Cells were seeded in black 96-well clear-bottom microplates (Greiner Bio-One #655-088). For cell numbers, medium, and FCS concentration see Table 4.2. The plates were incubated in a humidified atmosphere with 5% CO_2 at 37°C.

2.3 Floater culture

Cells were seeded in 40µl of medium into 1.5% (w/v) agarose-coated 384-well plates (Greiner #781090). See Table 4.2 for cell numbers, medium, and

FCS concentration. The plates were incubated in a humidified atmosphere with 5% CO_2 at 37°C.

2.4 3D Alginate-embedded stirred-tank Bioreactor cultures (alginate-BR)

Tumour cells were inoculated as single cell suspensions at a density of $2x10^5$ cell/ml into 125 ml stirred tank bioreactors (spinner vessels with straight blade paddle impeller, Corning® Life Sciences, BR). Cell aggregation and spheroid size were controlled through manipulation of the stirring rate [15]. Once compact and spherical shaped spheroids were attained (24h), tumour spheroids were microencapsulated in alginate with or without fibroblasts as single cells at a 1:1 cell ratio [8]. The resulting microcapsules, with 500 µm of diameter, were transferred to 125 ml stirred-tank bioreactors and cultured at 80 rpm. Cultures were grown in humidified incubators with 5% CO_2 and 21% O_2, with 50% medium exchange every 3-4 days.

2.5 3D embedded culture

3D cultures were embedded in Matrigel (Corning 356231, Lot 3198769, growth factor reduced, phenol red, and LDEV-free), Collagen Type I (BD Bioscience 354236, Lot 07484), or a 1:1 mix between the two. Collagen was neutralized according to Artym and Matsumoto [16]. A pH in the range 7.1-7.4 was crucial for cells to grow in collagen. Matrigel was used at a final concentration of 4 mg/ml, collagen at 1.5 mg/ml, and the mix contained 4 mg/ml Matrigel and 1.5 mg/ml collagen. Cells were suspended in the appropriate matrix (for cell numbers, medium, and FCS concentration see Table 2) and seeded in 60 µl/well into black 96-well plates (Greiner, #655090), pre-coated with the respective matrix (30 µl/well). Matrix without cells served as a background control. The matrix was allowed to set for 30 min at 37°C before adding 90 µl growth medium into each well. Growth medium was carefully removed and replenished every 3 days.

Tumour and stromal cell growth was followed via fluorescence measurements of their respective fluorescent protein markers (see Table 4.1), using a plate reader (see Table S4.1 for details). Readings from each well were normalized to the reading at day 1 and averaged for each condition. Every condition was run at least in triplicate.

2.6 Standard-of-care treatment

Drug treatment started when cells entered the exponential growth phase. In a first experiment, IC_{50} and IC_{80} values were determined for Fulvestrant, an Oestrogen Receptor (ER) antagonist (ICI 182,780), using fluorescence as a read-out for growth (drug concentration ranges are listed in Table S4.2).

For alginate-BR cultures, microencapsulated mono and co-cultures were collected from the stirred-tank and plated in 96-well plates, with approximately 10 aggregates per well, under orbital agitation. Treatments lasted 4 days for Docetaxel and 10 days for Fulvestrant with medium and drug replenishment every 3-4 days. Cell viability was determined with CellTiter-Glo® 3D Cell Viability Assay (Promega). For total cell lysis, aggregates were incubated with the CellTiter-Glo® reagent for 40 min under strong agitation, pipetted up and down quickly 10 times each well, and placed under strong agitation for another 40 min.

In a second experiment, fixed drug concentrations (IC_{80} for Fulvestrant) and IC_{50} for Docetaxel; see Table S4.2) or an equivalent volume of DMSO as vehicle control were selected for growth curves and sample analysis at endpoint.

Tumour and stromal cell growth was followed via fluorescence measurements as above.

2.7 Fluorescence in situ microscopy and analysis

At the endpoint, samples of all 3D models were fixed *in-situ* and imaged via fluorescence microscopy. Alginate-BR and embedded 3D cultures were additionally incubated with 10 μM Click-iT® 5-ethynyl-2'-deoxyuridine (EdU)

Alexa Fluor 647 (Life Technologies #C10356) for 2h and 5 µg/ml Hoechst 33342 (Invitrogen, H3570) for the last 30 min before fixation.

Images were acquired by bright-field and confocal microscopy, depending on the type of analysis. Microscopes, lenses, and settings are summarized in Table S4.1.

For visualization purposes, the z-stacks, with inter-slice z-distances of 10 µm for embedded samples and 1 µm for bioreactor samples, are shown in maximum intensity z-projections, with all channels merged as RGB values. Linear brightness and contrast adjustments of the images were performed using the ImageJ open source software [17].

Analysis of fluorescent cultures was a multi-step procedure, consisting of: (1), image acquisition as 3D image stacks; (2), annotation of culture parameters; (3), image processing & feature acquisition, done by a dedicated (semi-)automated 3D image analysis procedure (described in [18]), which includes the segmentation of the tumour cell spheroids, detection of EdU positive cells within the spheroids, and extraction of features pertaining to the size, shape, number of the cancer spheroids; and, (4), data analysis of the features using dedicated R-scripts.

Exceptions to this procedure were necessary for size and shape analysis of alginate-BR and floater cultures, for which 2D images were analyzed using dedicated CellProfiler pipelines. Also, for the quantification of EdU-positive cells in alginate-BR cultures, 2D spheroid masks were drawn manually using the RoiManager plugin in ImageJ.

2.8 Paraformaldehyde fixation and paraffin-embedding

3D floater, alginate-BR, and collagen or Matrigel/collagen mixed embedded cultures were fixed and paraffin embedded for TMA analysis. For the floater cultures, 100 spheroids were collected into a falcon tube, washed with PBS and fixed in 5 ml 4% (w/v) paraformaldehyde (PFA, Sigma) for 15 min at room temperature (RT). For 3D embedded cultures, the supernatant was carefully removed before filling the wells with 4% (w/v) PFA for 20 min at RT.

After fixation, samples were washed with PBS and stained with Hematoxylin (Mayer's, 1:1 Hematoxylin: PBS) for 10 sec in order to identify the spheroids in the paraffin blocks, and then washed three times in PBS. In order to preserve the 3D complex (co)-culture structure during the dehydration procedure and consecutive embedding in paraffin, a slightly modified protocol from Pinto *et al* [19] was used: Fixed spheroid pellets were suspended in 30 µl warm Histogel (Thermo Scientific HG-4000-012). For Matrigel/collagen and collagen embedded cultures, three 96-well gel plugs were extracted from the wells and sandwiched between two layers of Histogel in 8-well chamber slides (Labtek #155411). Cooled Histogel plugs containing the samples were dehydrated in 1 x 50% isopropanol (20 min), 2 x 70% isopropanol (20 min), 2 x 95% isopropanol (30 min) and 3 x 100% isopropanol (30 min) at 37°C. At this point samples could be stored overnight in 100% isopropanol at 4°C before further processing. For good infiltration of paraffin, samples underwent 3 changes with paraffin wax (each 30 min, at 65 ˚C) before paraffin embedding.

Alginate-BR samples were collected and fixed in 4% PFA (w/v) / 4% sucrose (w/v) for 20 min at RT. As above, microencapsulated mono- and co-cultures were pre-stained with Hematoxylin for 10 sec and then washed three times with PBS. Cultures were pelleted and embedded in 1% (w/v) high melting temperature agarose (Lonza), dehydrated as above, and then embedded in paraffin wax.

2.9 TMA preparation from FFPE blocks, staining, and analysis

FFPE blocks are archived centrally at The Institute for Molecular Medicine Finland (FIMM) as tissue microarrays (TMA). TMAs were constructed by punching a single core with a diameter of 5 mm from the FFPE block using a semi-automatic punching device (MiniCore, Mitogen, UK). For FFPE samples with high cell density, a 1 mm core diameter was used. After arraying, TMAs were cut in 4 µm sections on Superfrost objective glasses (O. Kindler Gmbh, Germany) using Microm 355S microtome (Thermo Scientific, Waltham, MA). Slides were dried and stored at -20°C.

For histopathological examination, paraffin sections (4 µm) of TMAs were stained with hematoxylin and eosin (H&E). IHC was carried out by a standard protocol (details in supplementary methods). Primary antibodies used were as follows: Ki67 (Abcam; EPR3610; #92742; 1:4000), oestrogen receptor (Abcam; SP1; #16660; 1:100), cleaved CK18 (Roche; M30 Cytodeath; #12140322001; 1:200), gamma H2AX (Cell Signaling 2577; 1:200), phospho-Histone H3 (Upstate 06-570; 1:1000), cytokeratin 8 (Abcam 53280; 1:2000), Vimentin (Dako M0725; 1:10000), and E-cadherin (Cell Signaling 3195; 1:1000). Stained TMAs were imaged at 0.33 µm/pixel resolution using a Panoramic P250 Flash whole slide scanner (3DHistech, Hungary) equipped with a Plan-Apochromat 20x (NA 0.8) objective (Zeiss, Germany). Scanned images were uploaded on a Webmicroscope platform, to which all PREDECT members had access (http://predect.webmicroscope.net/).

After downloading the images at a scale of 1:4 from the Webmicroscope using SpotFinder, they were analyzed using the cell counter plugin from imageJ [17].

2.10 Statistical analysis

Data sets were analyzed statistically using GraphPad Prism 6, or R scripts for image analysis, and tested for normality using the Shapiro-Wilks test. Two-tailed significance tests were performed with $p < 0.05$ considered significant. Non-parametric analyses were done with the Mann-Whitney-U-Test, parametric with the t-test. For image analysis data, the extension by Welch for unequal variances was used along with a multivariate ANOVA for the comparison of proliferating cells and spheroid size. Multiple groups were compared using a one-way ANOVA using the Tukey post-hoc test. Significances are depicted as n.s.: not significant, *: $p < 0.05$, **: $p < 0.01$, ***: $p < 0.001$.

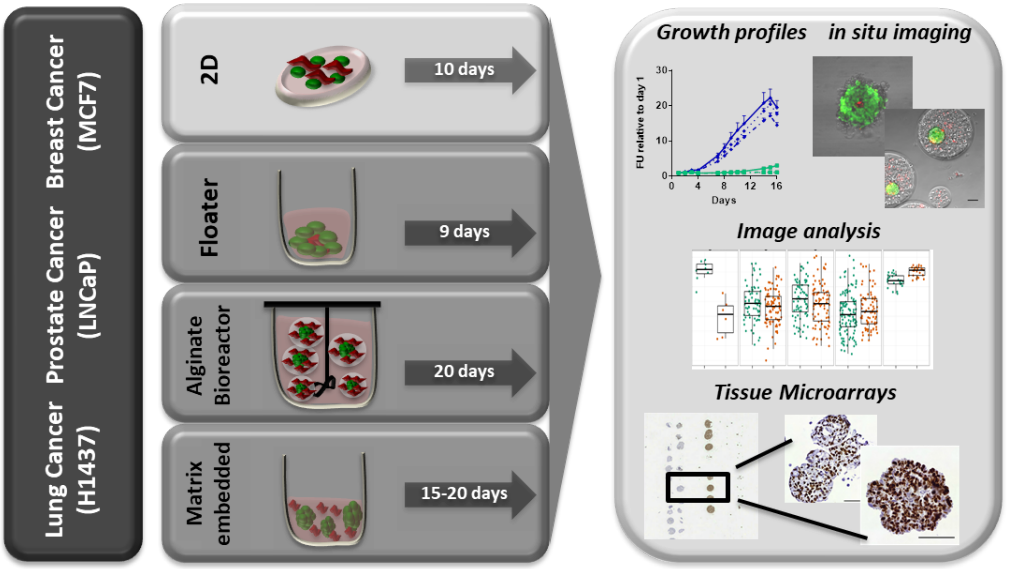

Figure 4.1: The PREDECT 2D/3D model workflow. MCF7, a breast cancer cell line was set up as 2D or 3D models in mono- and co-cultures. Growth was monitored via fluorescence, and the cultures imaged *in situ* by confocal microscopy and analyzed via dedicated 2D/3D imaging software, or fixed, paraffin embedded, and processed into TMAs and then analyzed via immunohistochemistry (IHC).

3 Results

3.1 Generation of model platforms

The goal of the PREDECT consortium is to characterize *in vitro* tumour models for target identification and validation by multi-modal cross-comparisons. Models described here include 2D and floating spheroid cultures ("floaters"), cultures embedded in alginate and grown in stirred-tank bioreactors ("alginate-BR"), as well as extracellular matrix (ECM) embedded cultures, all as mono- and co-cultures with stromal fibroblasts (Figure 4.1). Cell lines and respective fluorescence tags are listed in Table 4.1, culture set up in Table 4.2.

3.2 Characterization of model platforms using growth curves

Growth curves, based on fluorescence measurements, were established for all the models. Growth of MCF7 breast cancer cells in 2D cultures was stimulated by the presence of human dermal fibroblasts (HDFs) from day six on. Both mono- and co-cultures reached the stationary phase around day ten, but the co-cultures attained more than triple the signal of the mono-cultures (Figure 4.2A).

Also, in floaters, the presence of HDFs stimulated growth by about ten-fold (Figure 4.2B). Co-cultures formed inside-out spheroids, with the fibroblasts in the spheroid core (Figure 4.2H).

For the alginate-BR cultures, MCF7 cells were aggregated for 24 hours and then microencapsulated in alginate in the presence or absence of HDFs as a single cell suspension, as described in [9]. This protocol aims to keep the two compartments in close proximity but prevents the formation of inside-out spheroids as observed in the floater cultures (Figure 4.2I)

The presence of HDFs in the alginate microcapsules lead to a growth stimulation of the tumour cells compared to mono-cultures, which reached significance at day 20 (Figure 4.2C). Interestingly, co-cultures presented an altered morphology and behavior: aggregates formed irregular structures that leaked out of the alginate microcapsules (Figure 4.2I). This was rarely observed in MCF7 mono-cultures (Figure 4.2I). HDFs deposit collagen and other ECM components in the alginate capsule, and also secrete pro-inflammatory factors [8] [20]. Increased collagen density [21], but also paracrine factors, *e.g.*, the cytokine IL6 [22], or growth factors like SDF1 and FGF2, amongst others [23], have been shown to drive growth and invasion of mammary tumour cells *in vitro* as well as in mouse models.

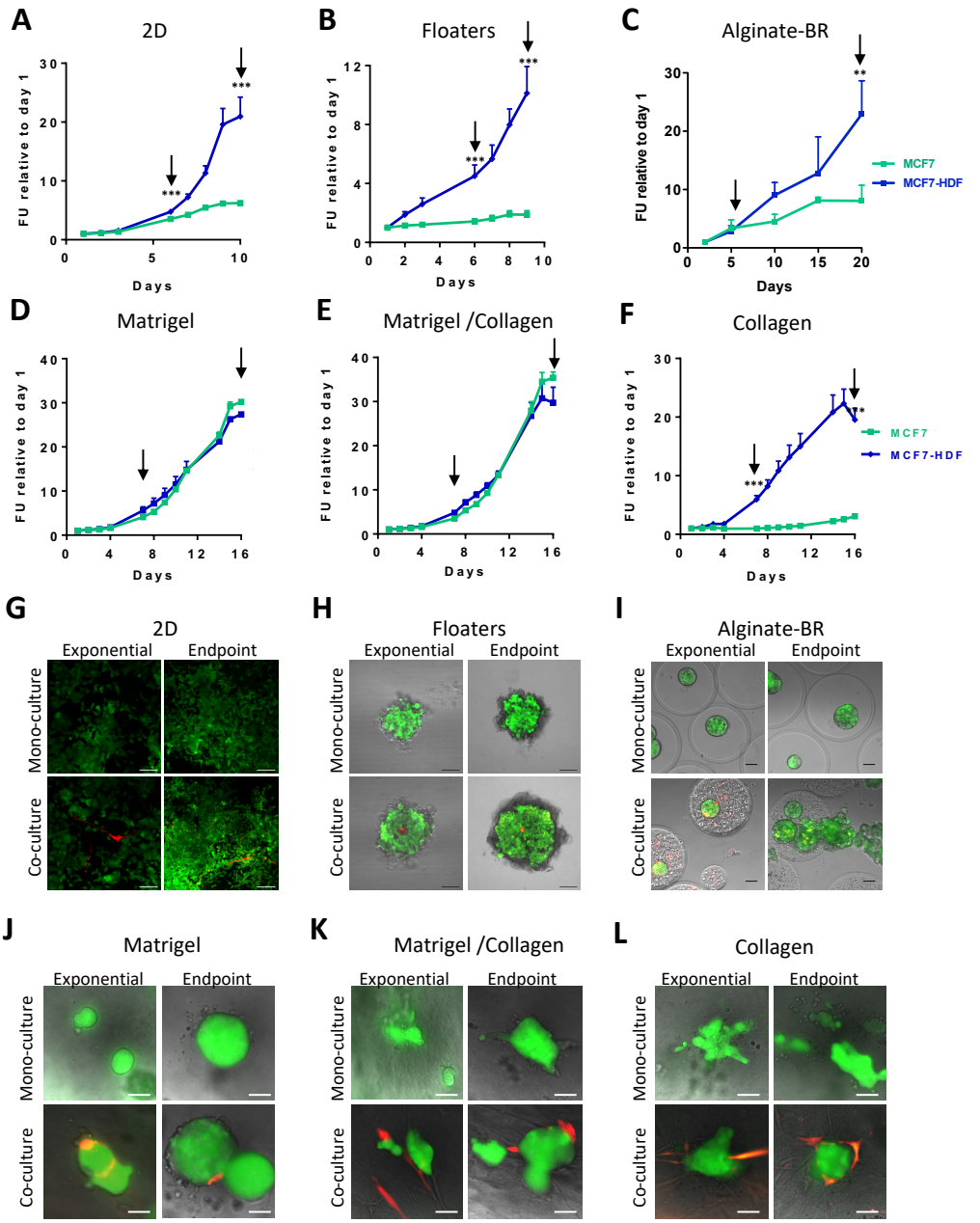

Figure 4.2: MCF7 breast cancer model characterization using fluorescence-based growth curves. Models were set up, and growth of MCF7 tumour cells was measured via GFP fluorescence as described in M&M. Stromal cell growth could not be detected. The graphs in the upper panels show growth curves of the mono- (green) and co-cultures (blue) grown in (A), 2D, (B), floaters, (C), alginate-BR, (D) Matrigel, (E)

Matrigel/collagen, (F) collagen. Arrows indicate time-points when pictures were taken; significant differences between mono- and co-cultures are indicated (**p < 0.01; ***p < 0.001). In G-L, fluorescence images corresponding to A-F are shown. GFP-labeled tumour cells in green, RFP-labeled HDF stromal fibroblasts in red. Scale bars: 2D, floaters: 100 µm; alginate-BR, embedded: 50 µm.

MCF7 growth as embedded mono-cultures was strongly matrix-dependent. Matrigel-containing matrices supported growth well, as shown by an approx. 30-fold fluorescence increase over time (Figure 4.2D-E), whereas the tumour cells alone hardly grew in pure collagen (Figure 4.2F). Admixing HDFs to the collagen-embedded cultures stimulated MCF7 cell growth approximately 6-fold, but fluorescence levels, reached at stationary phase, were still lower than observed in Matrigel-based cultures (Figure 4.2D-F, please note different Y-axes). These results confirmed observations made by Krauss and co-workers who described poor growth of MCF7 mono-cultures in collagen [24]. MCF7 cultures grown in Matrigel-containing matrices did not benefit from the addition of HDFs (Figure 4.2D-E). In all matrices, fibroblasts were observed to closely contact the tumour spheroids (Figure 4.2J-L).

To conclude, HDFs stimulated MCF7 growth in all culture formats, except for Matrigel-containing embedded models. Besides structural basement membrane constituents such as laminin, fibronectin, collagen IV, amongst others, Matrigel (although growth factor depleted) still contains significant amounts of growth factors that may partially obfuscate the effect of the stromal cells [25].

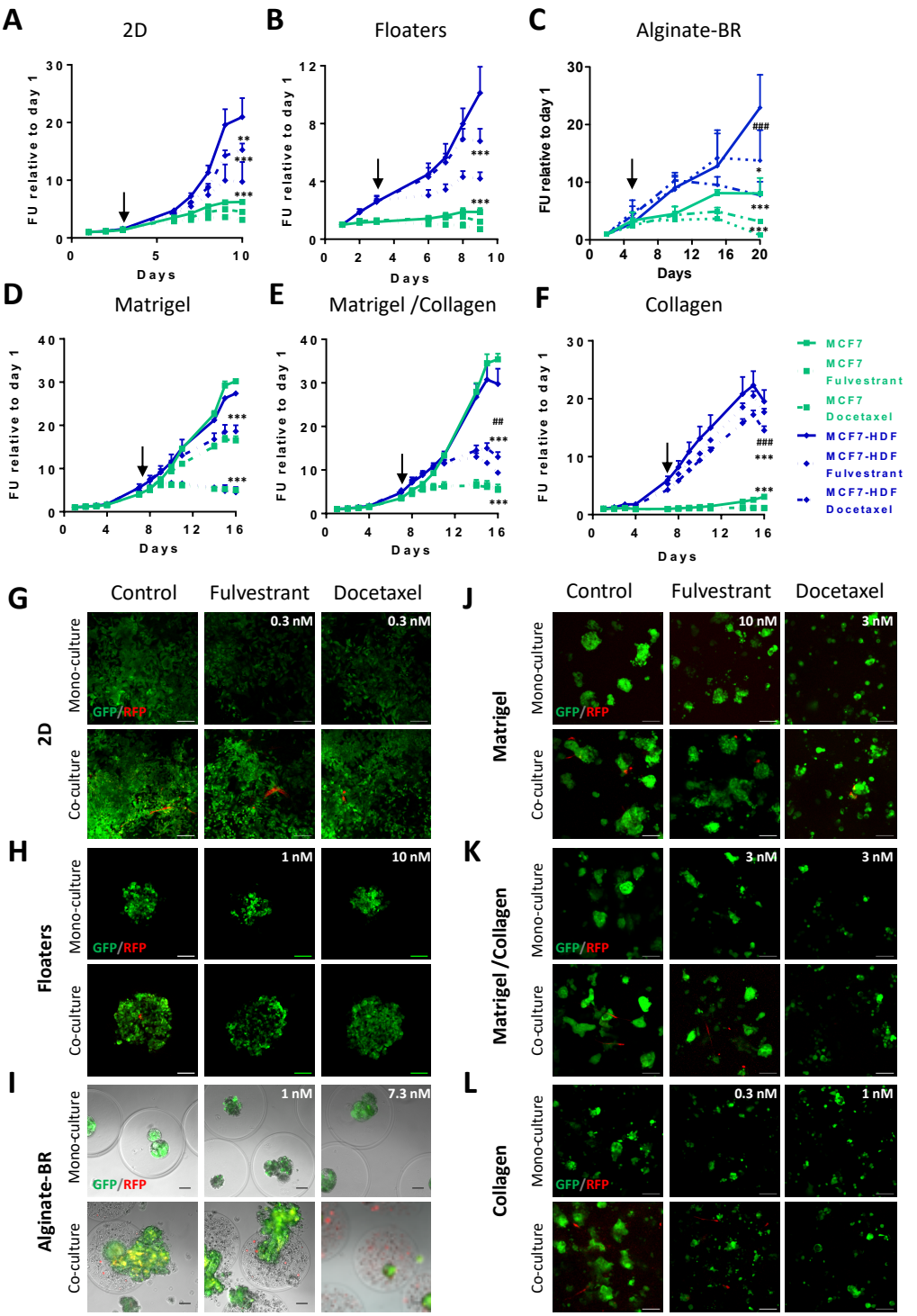

Figure 4.3. Fluorescence-based growth curves of MCF7 breast cancer models treated with Fulvestrant or Docetaxel. Models were set up, and growth of

MCF7 tumour cells was measured via GFP fluorescence as described in M&M. Stromal cell growth could not be detected. Mono- and co-cultures were treated with Fulvestrant or Docetaxel at the concentrations indicated in the fluorescence images (G-L), corresponding to IC_{80} and IC_{50} values on mono-cultures. Untreated DMSO control curves are indicated with a straight, Fulvestrant with a dotted, and Docetaxel with a broken line. Shown are the graphs for mono-cultures (in green) or HDF co-cultures (in blue) grown in (A), 2D, (B), floaters, (C), alginate-BR, (D) Matrigel, (E) Matrigel/collagen, (F) collagen. Arrows indicate start of treatment. Significances are indicated for comparison to DMSO treated controls (*) or monocultures (#) (*$p < 0.05$; **$p < 0.01$; ***$p < 0.001$). In G-L, fluorescence images corresponding to A-F are shown. GFP-labeled tumour cells in green, RFP-labeled HDF stromal fibroblasts in red. Scale bars: 2D and floaters: 100 µm; alginate-BR, embedded cultures: 50 µm.

3.3 Response of model platforms to standard of care treatment

Fulvestrant, a pure oestrogen receptor antagonist [26], was chosen as a targeted compound, and Docetaxel, an anti-mitotic agent, was selected as a chemotherapeutic SOC agent [27].

In a first step, IC_{50} values (IC_{50}s) were established by generating dose-response curves for all models, starting treatment once exponential cell growth was observed (table S4.2). In a second step, growth curves were established for a single drug concentration per model in order to characterize the effect of the stromal cells on the treatments on a cellular level. At the endpoint, when control cultures reached the stationary phase, samples were fixed *in situ* for fluorescence analysis, and formalin-fixed and paraffin embedded for IHC. For Fulvestrant, an IC_{80} concentration was used, whereas Docetaxel, as a cytotoxic agent, was used at an IC_{50} concentration, in order to obtain analyzable samples at the endpoint.

Fulvestrant and Docetaxel affected MCF7 growth in 2D and floater cultures (Figure 4.3A/B). The percent inhibition was comparable between mono and co-cultures, indicating that HDFs did not provide protection against either of the treatments. It should be noted, however, that Docetaxel and Fulvestrant treated

co-cultures had higher GFP signals at the endpoint than untreated mono-cultures (Figure 4.3A/B).

Docetaxel treatment decreased cell growth in alginate-BR mono- and co-cultures. In stark contrast, co-cultures appeared refractory to Fulvestrant treatment until day 16 (Figure 4.3C). The latter cultures were indistinguishable from controls, showing a loss of spheroid roundness, and leakage from the alginate microcapsules (Figure 4.3I). HDFs thus protected MCF7 from Fulvestrant in this culture format.

High-energy metabolites released by stromal fibroblasts may induce tumour cell mitochondria activity to protect from Fulvestrant [28]. Also, IL-6 secretion has been shown to confer oestrogen-independence to MCF7 and other oestrogen-dependent breast cancer cell lines [22]. Corroborating the latter, slightly increased levels of IL6 and IL8 were found in alginate-BR:HDF co-cultures [8].

In the matrix-embedded 3D format, Docetaxel and Fulvestrant reduced MCF7 growth in all three matrices tested (Figure 4.3D-F). Co-cultures provided only a minimal growth benefit in Matrigel, whereas in the Matrigel/collagen mix and collagen alone, the fibroblast co-cultures protected the tumour cells from treatment (Figure 4.3D-F). Thus HDFs provided not only a growth advantage, as described in the previous section, but also a treatment protection to MCF7 cells, mainly in culture formats with lower levels of nutrients and growth factors (i.e. alginate-BR and collagen).

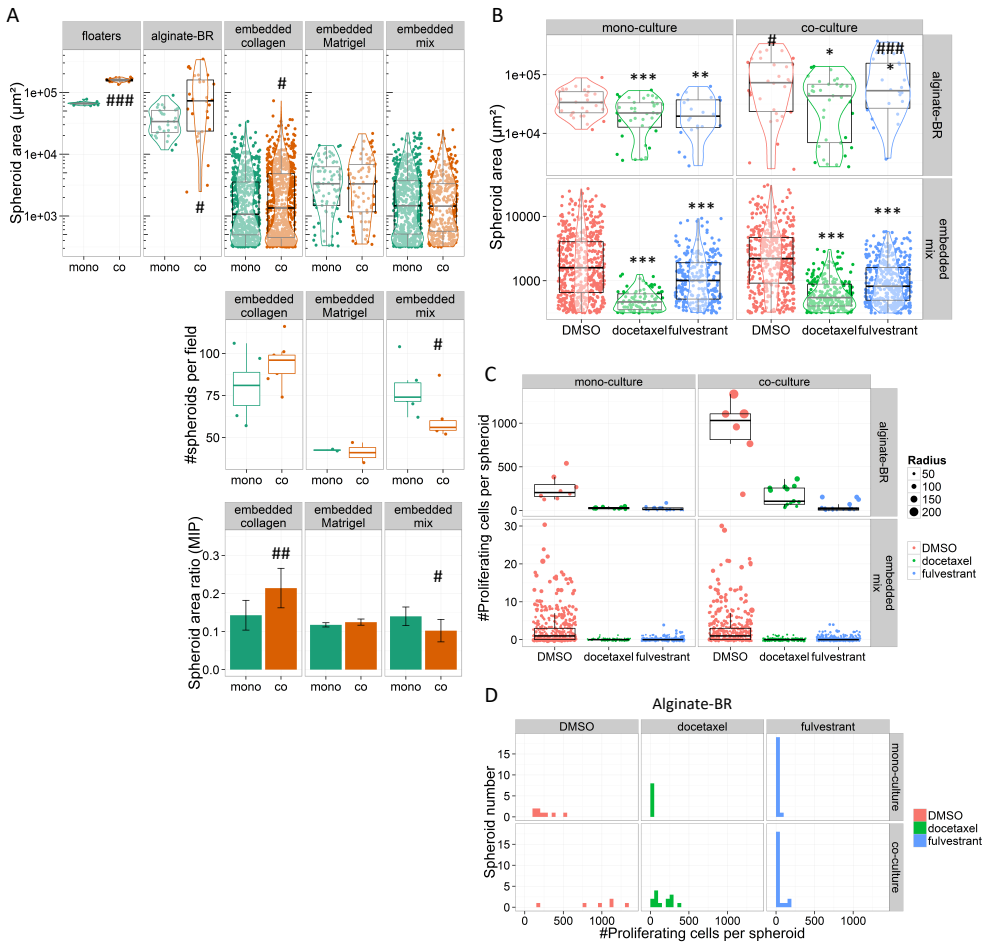

Figure 4.4: *in situ* image analysis & quantification of 3D models. A. Scatter plots comparing MCF7 3D models by spheroid sizes (upper graph) and numbers (lower graph). Mono- (green dots) and HDF co-culture (orange) spheroid areas and numbers derived from maximal intensity projection (MIP) analyses are displayed. The size analysis is shown on a logarithmic scale (upper graph). B. Scatter plots comparing unperturbed (red) and Docetaxel (green) or Fulvestrant (blue) treated MCF7 3D cultures via spheroid areas, displayed on a logarithmic scale. C. Quantification of EdU-positive cells in mixed matrix embedded or alginate-BR MCF7 mono- and HDF co-cultures, treated with Docetaxel (green), Fulvestrant (blue) and DMSO control (red). Scatter plots of EdU-positive cells per spheroid, with the size of the dots corresponding to the radii of the spheroids, are displayed. Negative spheroids are collapsed to the bottom of the plot. D. the alginate-BR data of (C) is shown as a histogram indicating the number of proliferating cells per spheroid. Note the increase of EdU-positive

spheroids in the HDF co-cultures, and the large number of non-proliferating spheroids in Fulvestrant treated cultures. P-values for the comparison between treatment conditions are represented by *-symbols (*p< 0.05; **p<0.01; ***p<0.001), while #-symbols are used for comparison between mono- and co-cultures (#p < 0.05; ##p < 0.01; ###p < 0.001).

3.4 Image analysis of 3D cultures

In order to validate data from the growth curves, and to gain additional information on the characteristics of the models, fluorescence images were taken from cultures *in situ* and subjected to analysis by dedicated image software developed within the consortium [18]. Size, numbers, and proliferation rates of tumour spheroids in 3D cultures were measured, and correlated with the presence or absence of stromal cells, SOC treatment, and culture format. In order to adequately compare treated with untreated cultures, images taken at the end of the culture period were analyzed.

Size analysis revealed a characteristic mean and spread for each of the 3D culture formats. Floater cultures formed the largest spheroids, with a very small size distribution (0.066 ±0.004 mm^2), and a large gain induced by HDF co-cultures (0.16 ±0.01 mm^2). Alginate-BR spheroids were next in size, but showed a wider spread size distribution (0.10 ±0.09 mm^2 for co-, and 0.037 ±0.018 mm^2 for mono-cultures; Figure 4A). Matrix-embedded spheroids were clearly smaller than the previous two models, ranging between 0.001-0.003 mm^2. Amongst the latter, Matrigel supported the largest, and collagen the smallest spheroids, corroborating observations from growth curves (Figure 4.4A and 2D-F). The strong effect of the HDFs on collagen-embedded samples observed in the growth curves (Figure 4.2F) translated into significantly increased average spheroid areas, although the difference was not as striking as observed in the growth curves (Figure 4.4A, upper panel). When counting spheroids per area, we found that HDFs also affected MCF7 spheroid numbers (Figure 4.4A, lower panel). As a result, the total spheroid density is higher, as illustrated by the spheroid foreground area fraction in Figure 4.4A, lower panel.

Docetaxel and Fulvestrant treatment reduced spheroid sizes of alginate-BR and embedded samples, confirming the results from fluorescence-based growth curves (Figure 4.4B).

Analysis of tumour spheroid size and numbers *in situ* represents a relatively simple imaging tool that may be used to validate and complement simple fluorescence growth analysis. The results from the growth curve analyses shown in the previous sections were largely confirmed, validating the approach of using fluorescence as a proxy for cell culture growth.

In order to measure effects of the culture formats or SOC treatment on proliferation, alginate-BR and embedded samples were incubated with EdU before fixation to label cells with ongoing DNA synthesis. EdU-positive cells were counted per spheroid using an algorithm developed to analyze spheroids in 3D [18].

For both alginate-BR, and mixed matrix embedded cultures, a clear treatment-dependent reduction of EdU positive nuclei/spheroid was detected (Figure 4.4C, compare DMSO (red) with Docetaxel (green) and Fulvestrant (blue) treated cultures). The growth-stimulatory effect of admixing HDFs to MCF7 alginate-BR cultures was also evident by the increase of EdU-positive nuclei per spheroid and the concomitant boost of the average spheroid size (Figure 4.4C). In Docetaxel treated samples, the presence of HDFs in MCF7 alginate-BR cultures sustained some EdU-positive nuclei, whereas Fulvestrant imposed a total proliferation block, as suggested by the total lack of EdU-positive cells (Figure 4.4C). The histogram representation of the above results reveals the large number of non-proliferative spheroids in the Fulvestrant treated cultures, which amassed at the baseline in the previous scatter plot (Figure 4.4E). Fulvestrant thus imposed a relatively slow-acting proliferation block, leaving the spheroids mostly intact, whereas Docetaxel killed proliferating cells, resulting in the dissolution of the spheroids. In conclusion, both treatments were ultimately active against alginate-BR cultures, but the timing and the effect on the cells (cytostatic versus cytotoxic) varied, explaining the differential effect on the growth curves in the bioreactor (Figure 4.3C).

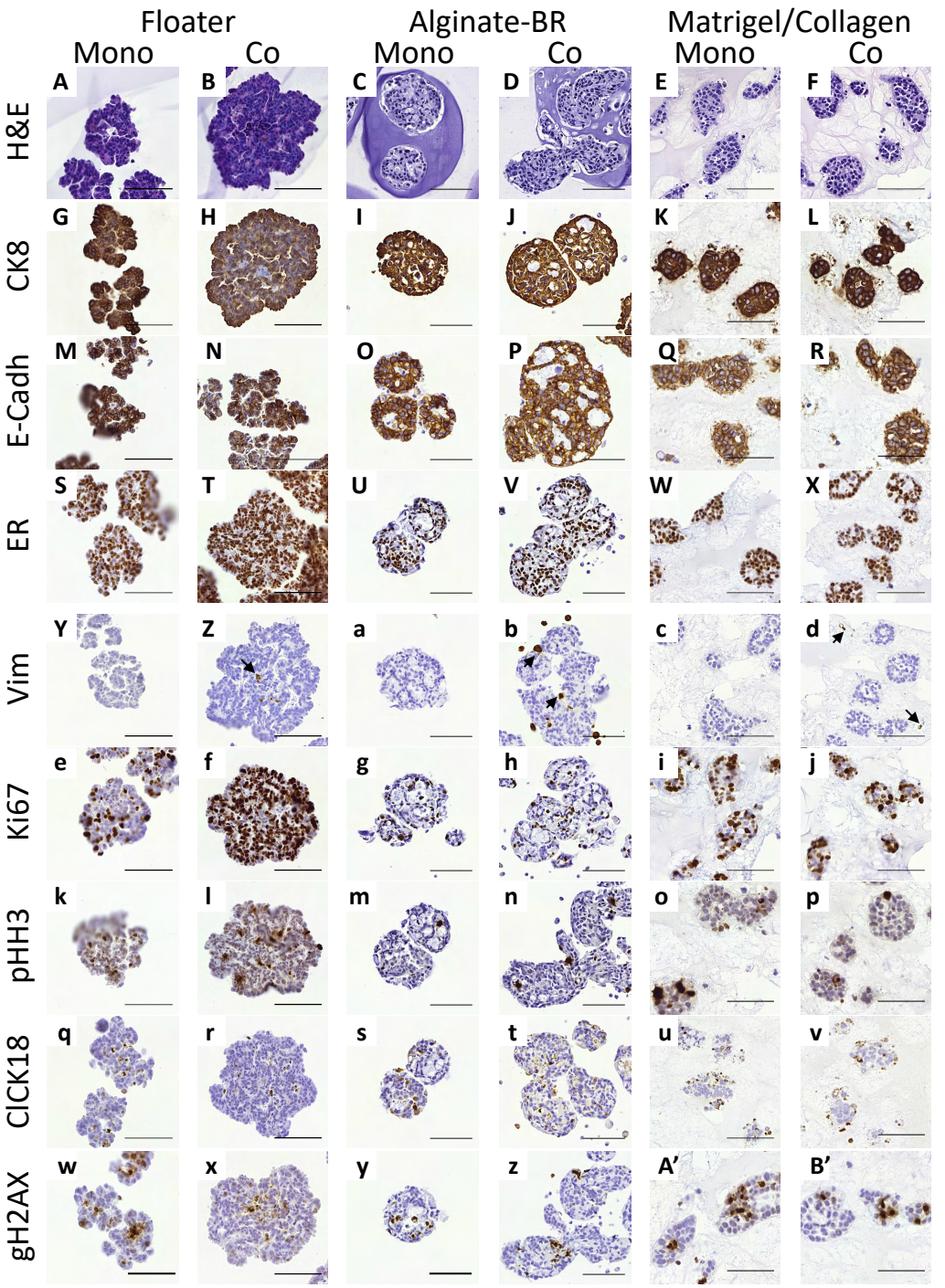

Figure 4.5: IHC analysis of breast samples. Cultures were fixed, paraffin embedded, and arrayed into TMAs as described in Materials and Methods. TMAs were then stained H&E (A-F), as well as for cytokeratin 8 (G-L), E-cadherin (M-R), oestrogen

receptor (S-X), Vimentin (Y-d), Ki67 (e-j), phospho-Histone H3 (k-p), cleaved CK18 (q-v), and gamma H2AX (w-B'), respectively. Antibodies were detected using a chromogenic DAB assay (brown), and samples were counterstained with hematoxylin (blue). Scale bars indicate 100 µm.

In order to enable the PREDECT consortium to perform a side-by-side comparison of models and patient samples, protocols were developed. These allowed for fixing, adequate paraffin embedding and staining of the samples, in order to prepare TMAs. The 3D conformation of all model formats could be preserved through paraffin-embedding, except for Matrigel, which dissolved during fixation. The TMAs were stained for a number of markers in order to characterize cell types and cell cycle status (cytokeratin 8 (CK8), E-cadherin, oestrogen receptor (ER), Vimentin, Ki67, phospho-Histone H3 (pH3), caspase cleaved cytokeratin 18 (cCK18), gamma H2AX, cleaved caspase 3 (cC3)).

H&E staining of the MCF7 models showed the characteristic 3D morphology of the spheroids grown in the various culture formats, and revealed differences in their cellular organization, *e.g.*, while floater spheroids were compact, alginate-BR spheroids displayed small lumens inside (Figure 4.5 A-F). CK8 and E-Cadherin, as epithelial cell markers, were expressed on MCF7 tumour cells in all models (Figure 4.5 G-R). As expected, MCF7 cells expressed ER in the nucleus, although some negative cells were found in the alginate-BR, indicating model-induced heterogeneity (Figure 4.5 S-X). Vimentin-positive fibroblasts were found in all co-culture models (indicated by arrows in Figure 4.5 Z, b, d). As suggested by the fluorescence images, fibroblasts localized to the core of the floater cultures (Figure 4.5 Z). Whereas most of the fibroblasts in the alginate-BR format were found outside of the spheroids, some had invaded the spheroid core (Figure 4.5 b). This was not observed in embedded cultures (Figure 4.5 d). Proliferation was assessed with the general proliferation marker Ki67 and the M-phase-specific marker phospho-Histone H3 (Figure 4.5 e-p). HDF co-cultivation in floater cultures resulted in enhanced proliferation compared to mono-cultures (Ki67: 20.9 ±1.8% vs. 84.8 ±1.7% ***p; pHH3: 1.9

±0.4% vs. 6.2 ±1.4% **p). In alginate-BR mono- and co-cultures, approximately 40% or 10% of MCF7 cells were KI67 and phH3 positive, respectively. No significant differences were observed between mono- and co-cultures. The same was observed for embedded samples.

Unfortunately, despite employing IC_{50} or IC_{80} concentrations rather than maximally efficacious doses for Docetaxel and targeted therapies, respectively, treated samples proved very fragile and unstable, and many were lost during processing, rendering analysis of treatment effects by TMAs very difficult.

In conclusion, protocols have been established for *in vitro* tumour models with increasing complexity. They were validated by growth and response to SOC treatment via fluorescence-based growth curves. These results were corroborated and complemented by *in situ* 3D image analysis, as well as IHC on TMAs from most models. Our results demonstrate that in order to more faithfully evaluate the relative contributions of co-cultured cells or matrix composition on baseline tumour cell growth rates or responses to drug treatments, a multi-pronged approach to the analysis and set-up of complex 3D assays is required.

4 Discussion

The goal of the present study was to establish robust protocols for 2D and 3D culture methods and thoroughly characterize them via side-by-side comparisons in order to better understand their applicability for oncology drug discovery. The outcome showed that even with a relatively small matrix of tumour and stromal cells in a set of different culture formats, the interactions of the individual components result in altered growth characteristics or drug responses of the cultures. Thus none of the models presented here will be able to capture all of the aspects of tumour biology, but they differ in the degree to which they represent such aspects, and should be used accordingly. Below, we will try to disentangle these observations, and come up with some recommendations that should help to set up complex models in a robust and informative manner for drug discovery and validation purposes.

As shown in the Results section, appropriate analysis of the data from complex 3D models is of utmost importance. While fluorescence based growth curves are simple and applicable to relatively high throughput experiments, crucial information may be lost by looking at an average response of a whole culture set-up. In the first section of the Discussion, the approaches to analyze complex 3D models presented in this study will be compared with respect to their cost and benefit.

Since potentially very labor- and time consuming, complex image analyses should strictly focus on key questions. Here, image analysis was used mainly for two questions, (1) is the approach of using fluorescence intensity measurements valid as a proxy for tumour cell growth? and, (2), can we define effects of the culture format and the treatments more precisely by molecular imaging, in this case using EdU as a label for replicating cells?

Requirements on image quality (and hence also equipment) depend on the analyses to be performed. Number, size, and shape analyses are less demanding than molecular imaging. Sample number and related microscope and computing time were the main issues, requiring the availability of an automated imaging system. In the present study, spheroid size analyses generally confirmed the data obtained from fluorescence growth curves, thus fulfilling its pre-defined task. Discrepancies between fluorescence growth curves and size analyses were found when spheroid size was not the main differentiator between treated and untreated cultures (*e.g.* Figure 4.4A, HDF effect on collagen-embedded MCF7 cultures). Shape analysis, which may contribute further relevant information, *e.g.* invasiveness of 3D cultures [29], was also performed, but did not provide much additional insight for this study.

Analysis of the proliferation index of the spheroids by quantifying EdU-stained nuclei proved a much more difficult task, despite the availability of a '2.5D analysis' workflow that reduced the complexity of real 3D analysis to a combination of maximal intensity projection and height mapping [18]. Image quality had to be adequate: lateral and axial resolution as well as inter-slice distance had to be well below cell-radius (estimated 5 µm), and spheroids

needed to be physically separated by at least 10 µm along the axial direction, and non-overlapping in the lateral direction. Moreover, spheroids larger than 100 µm could not be analyzed because of light attenuation. However, despite being resource-intense and demanding on image quality, the analyses performed for the present manuscript provided relevant information. The pro-proliferative effect of the HDFs on MCF7 could be shown on a cellular level, and the anti-proliferative effect of Fulvestrant as opposed to the cell killing mediated by Docetaxel could clearly be distinguished (Figure 4.4 C/D). Thus, if probes are available to monitor the effect of a given treatment by molecular imaging, the investment in molecular image analysis may be worthwhile.

TMA-based analysis was chosen by the PREDECT consortium as the means of choice for the cross-comparison of models, and ultimately patient material, since tissue heterogeneity is preserved, and it represents the gold standard for pathologists.

Processing samples for TMAs proved labor intensive, and was not entirely successful, *e.g.* analysis of treated samples was severely hampered by the loss of treatment-reduced sample material. However, successful analyses addressed several open questions, or independently confirmed previous findings. These included the differences in cellular organization, hormone receptor expression, proliferation indexes, amongst others (Figure 4.5). Thus albeit labor intensive, once samples have been generated and arrayed into TMAs, the depth of analysis possible is only restricted by the number of antibodies that work in FFPE material.

As mentioned above, some observations appeared model/set-up specific, and are therefore likely to translate to additional cell systems or pathologies, whereas others were clearly cell-type-specific, and will need to be established for every model. However, also for the latter, some general guidelines that may help to speed up the set-up time for new models will be discussed.

Spheroid sizes were platform-dependent. Spheroid size matters, since only when a minimal radius of about 200 µm is exceeded, spheroids may form apoptotic cores due to hypoxia and lacking nutrients [30-32]. Hypoxia is

prevalent in human tumours due to lacking, or disorganized vasculature, and numerous approaches have been explored to target hypoxia as a treatment paradigm [33]. Another aspect of spheroid size is drug penetration. Spheroid cultures have been shown to be resistant to cytotoxic agents due to lack of appropriate drug exposure [34,35] [36]. For some drugs, this could be directly correlated with spheroid sizes [37]. Ineffective drug penetration into solid tumours indeed has been suggested to lead to drug resistance [38]. Not surprisingly, also gene transcription is strongly affected by spheroid sizes [39].

Differences between Matrigel and Collagen embedded cultures have been observed. Overall, cultures containing Matrigel tended to grow better, or be less sensitive to growth inhibition, or both. (1), MCF7 cells grew well in Matrigel or mixed matrix, but collagen was a poor substrate; Growth factors present in the Matrigel preparation (even if growth-factor reduced) may provide cues for growth, survival, and invasion of the tumour cells, although the differential composition of the extracellular matrices may also play an important role. Various Matrigel lots may behave differently, which is why performance tests are imperative, and all groups working on this manuscript used the same Matrigel batch. Growth factors and/or cues from basement membrane components within Matrigel also appeared to override aspects of co-cultures. Breast MCF7 cultures responded with a growth boost when incubated with HDFs in all but Matrigel-containing culture formats (Figure 4.2). Also, the protective effect of HDFs was much more pronounced in collagen than in Matrigel-containing culture formats. Thus, this would be consistent with a certain Matrigel-induced override of the communication between co-cultured stromal cells and tumour cells.

How important is the correct source of stromal fibroblasts? CAFs were compared to HDFs in the spheroid model. A comparable growth stimulation was found for both types of fibroblasts (data not shown), suggesting functional adequacy of the HDFs, as also observed by other groups [11]. Thus, although it may have to be confirmed on a case-to-case basis, HDFs appear to represent a viable substitute for tumour-specific CAFs.

No single tumour:stroma ratio could be identified that would be optimal for all models. For MCF7 cultures, a strong growth-promoting effect by HDFs was observed in most culture formats, across ratios of 1:1 to 10:1. However, such an initial tumour:stroma ratio is not expected to remain constant over the course of an experiment. For example, in the MCF7/HDF alginate-BR co-culture model, the original 1:1 ratio shifted in the course of the experiment to approximately 6:1, mainly due to a lack of stromal cell proliferation (data not shown). In the floater cultures, the original 3:1 ratio likely increased even more dramatically over time, since at the end of the experiment only very few stromal cells were left at the center of the tumour (Figure 4.5). In an experiment to check the optimal tumour:stroma ratio for collagen embedded MCF7 cultures, a range of ratios between 1:1 to 20:1 was tested. Only at a ratio of 20:1 dropped the growth rate down to near mono-culture levels (data not shown). Thus, even though human pathology should be used as a rough guideline for a given pathology, a range of tumour:stroma ratios between 1:1 to 10:1 appears to be a good starting point for a co-culture set-up.

In conclusion, there is no one-fits-all model, the choice of the model depends entirely on the question that needs to be answered (see table 3). If the genetic make-up of a tumour cell that responds to a given treatment needs to be found, then a screen of a large number of molecularly characterized cell lines in 2D may be sufficient [40]. However, if a given target relies on cell-cell, or cell-ECM interactions, more complex models will be required. This is also true if not only sensitivity, but also resistance to a given new treatment should be investigated. Thus, for studies, which consider drug penetration issues, or target hypoxia (*e.g.* [41]), floater spheroid cultures appear best suited since appropriate spheroid sizes are reached. Alternatively, pre-grown larger spheroids embedded in ECM, hypoxia chambers, or the alginate-BR system in low O_2 conditions may be applied for such studies. When looking at the effect of the ECM, Matrigel embedded cultures are most widely used. However, results may be confounded by the presence of growth factors and their concentration heterogeneity in different batches. Therefore, collagen or, ,

synthetic matrices in the presence or absence of stromal co-cultures may be a better choice [42,43]. Also alginate-BR cultures, which provide a biologically inert structure appear to be a viable alternative. Tumour:stroma ratios between 1:1 and 10:1 were found to be functional, with lower ratios to be used in systems where fibroblast growth is expected to be minimal, resulting in decreased, more physiologically relevant ratios in 'mature' cultures. This should also be considered when looking at compounds that specifically target the interface between tumour and stromal cells [44]. If looking at compounds that target stroma for resistance mechanisms, a small matrix of tumour and stroma cells should be tested in order to best cover tumour heterogeneity, as has already been performed in 2D [45]. Also, not only stromal cells but also macrophages and other constituents of the immune system, as well as components of the vasculature play important roles in treatment resistance and should be included in *in vitro* assays that may ultimately get closer to model patient tumours [46-48].

5 Acknowledgements

The authors would like to thank Ingrid Verberne for the construction and testing of lentiviral plasmids as well as cell transduction, Katja Välimäki and Antonio Ribeiro for the assistance in TMA construction and IHC. Further, we would want to acknowledge Tauno Metsalu for the generation and constant adaptation of the MBase database for the sample annotations, and Mikael and Johan Lundin for organizing and adapting the webmicroscope, and annotation of images. We acknowledge support from the Innovative Medicines Initiative Joint Undertaking (IMI grant agreement n° 115188), resources composed of financial contribution from EU - FP7 and EFPIA companies in kind contribution. We also acknowledge support from Fundação para a Ciência e Tecnologia (FCT), Portugal (EXPL/BBB-IMG/0363/2013); MFE is the recipient of a PhD fellowship from FCT (SFRH/BD/52208/2013). Finally the authors are very grateful to Emmy Verschuren, Julia Schueler, Liz Anderson, and John Hickman for critically reading the manuscript.

6 Author contributions

KS, ME, SV, KG, AR, VES planned the studies, developed the protocols & performed 2D/3D assays, analysed results, provided samples for image and TMA analysis, and contributed to the manuscript.

MB developed the image analysis software and analysed all 3D images.

SB organized FFPE material processing to TMA, IHC assays, and uploading and annotation of samples for the web-microscpe.

IS performed 2D/3D assays, analysed results, and contributed to the manuscript.

SCA, YS performed 2D assays, analysed results, and contributed to the manuscript.

AO performed 3D assays, analysed results, and contributed to the manuscript.

WvW, EB, CB, VR, MO, YC, SG, RdH, WS contributed to study planning, analysis, and manuscript.

RG planned the study, analysed results, and contributed to the manuscript.

7 Tables

Table 4.1: Cell lines, type, origin, label

Cell line (source)	Type	Origin	Label
MCF7 (ATCC HTB-22)	Epithelial	Breast Adenocarcinoma	eGFP-FLuc2
HDF (Innoprot P10857)	Fibroblast	Skin	tagRFP

Table 4.2: Experimental cell culture conditions

1. Stromal cells were added on top

2D			3D floater		
Tumour cells[1]	**Tumour: stroma**	**FBS (%)**	**Tumour cells[1]**	**Tumour: stroma**	**FBS (%)**
6,000	03:01	10	1,000	03:01	10

3D matrix			3D bioreactor		
Tumour cells[1]	**Tumour: stroma**	**FBS (%)**	**Tumour cells[1]**	**Tumour: stroma**	**FBS (%)**
10,000	10:01	2	20000/ml	01:01	10

Table 4.3: overview of platforms with strengths/weaknesses & suggested applications

Model		Plus	Minus	Applications
2D	mono	- simple, cheap - reproducible - fully automatable - H/MTS amenable	- limited predictivity for drug effects in patients - lack of 3D architecture	- (TD) tumour cell signaling - (TD, R) genetic alterations in tumour cells
	co	- stroma derived growth benefit/drug resistance	- space restriction	- (TD, R) tumour-stroma interactions
floater	mono	- 3D architecture - drug penetration through tumour cell layers - hypoxic core (if large enough) - fully automatable - MTS amenable	- not all tumour cells form spheroids - - complex assay analysis	- (TD, R) 3D architecture - (TD, R) tumour hypoxia - (R) drug penetration
	co		- often form inside-out spheroids - very few stromal cells survive	

Model		Plus	Minus	Applications
BR	mono	- control of physico-chemical parameters - large batches of uniformly encapsulated spheroids - tumour-specific ECM deposition	- re-plating of spheroids for multi-parameter testing - initial investment for set-up	- (TD, R) tumour-specific ECM deposition
	co	- preformation prevents inside-out spheroids - stromal cells provide GF and ECM		- (TD, R) stromal GF, ECM deposition
matrigel	mono	- provides rich basement membrane-like matrix - widely used, well published	- contains variable amounts of GF - considerable batch-to-batch variations - melts upon fixation in formalin	- (TD, R) extracellular matrix - (TD) invasion - (R) matrix-derived GF
	co		- fibroblasts do not differentiate - co-culture effects may be masked by matrix GF	

Model		Plus	Minus	Applications
collagen	mono	- provides interstitial stroma matrix environment - simulates invasive environment	- some epithelial tumour cells may not grow	
	co	- natural environment for fibroblasts - no/low confounding GF present	- activated fibroblasts contract matrix	- (TD, R) stromal GF

Italic: apply for methods below as well (tumour-stroma effects only for co-culture models);

Abbreviations: H/MTS: high/medium throughput screening; GF: growth factor(s); ECM: extracellular matrix; (TD): find targets/test drugs addressing; (R): resistance mechanisms.

8 References

[1] J.W. Scannell, A. Blanckley, H. Boldon, B. Warrington, Diagnosing the decline in pharmaceutical R&D efficiency, Nat Rev Drug Discov. 11 (2012) 191–200. doi:10.1038/nrd3681.

[2] M. Hay, D.W. Thomas, J.L. Craighead, C. Economides, J. Rosenthal, Clinical development success rates for investigational drugs, Nat. Biotechnol. 32 (2014) 40–51. doi:10.1038/nbt.2786.

[3] J. Arrowsmith, Trial watch: phase III and submission failures: 2007-2010, Nat Rev Drug Discov. 10 (2011) 87–87. doi:10.1038/nrd3375.

[4] Goodbye, flat biology? Nature. 424 (2003) 861–861. doi:10.1038/424861b.

[5] J.A. Hickman, R. Graeser, R. de Hoogt, S. Vidic, C. Brito, M. Gutekunst, et al., Three-dimensional models of cancer for pharmacology and cancer cell biology: Capturing tumor complexity in vitro/ex vivo, Biotechnology Journal. 9 (2014) 1115–1128. doi:10.1002/biot.201300492.

[6] C. Prost-Squarcioni, S. Fraitag, M. Heller, N. Boehm, [Functional histology of dermis], Ann Dermatol Venereol. 135 (2008) 1S5–20. doi:10.1016/S0151-9638(08)70206-0.

[7] M.W. Conklin, P.J. Keely, Why the stroma matters in breast cancer: insights into breast cancer patient outcomes through the examination of stromal biomarkers, Cell Adh Migr. 6 (2012) 249–260. doi:10.4161/cam.20567.

[8] M.F. Estrada, S.P. Rebelo, E.J. Davies, M.T. Pinto, H. Pereira, V.E. Santo, et al., Modelling the tumour microenvironment in long-term microencapsulated 3D co-cultures recapitulates phenotypic features of disease progression, Biomaterials. (2015). doi:10.1016/j.biomaterials.2015.11.030.

[9] A. Rudisch, M.R. Dewhurst, L.G. Horga, N. Kramer, N. Harrer, M. Dong, et al., High EMT Signature Score of Invasive Non-Small Cell Lung Cancer (NSCLC) Cells Correlates with NFκB Driven Colony-Stimulating Factor 2 (CSF2/GM-CSF) Secretion by Neighboring Stromal Fibroblasts, PLoS ONE. 10 (2015) e0124283. doi:10.1371/journal.pone.0124283.

[10] J.A. Rudnick, L.M. Arendt, I. Klebba, J.W. Hinds, V. Iyer, P.B. Gupta, et al., Functional heterogeneity of breast fibroblasts is defined by a prostaglandin secretory phenotype that promotes expansion of cancer-stem like cells, PLoS ONE. 6 (2011) e24605. doi:10.1371/journal.pone.0024605.

[11] J. Albrengues, I. Bourget, C. Pons, V. Butet, P. Hofman, S. Tartare-Deckert, et al., LIF mediates proinvasive activation of stromal fibroblasts in cancer, Cell Rep. 7 (2014) 1664–1678. doi:10.1016/j.celrep.2014.04.036.

[12] O.W. Petersen, L. Rønnov-Jessen, A.R. Howlett, M.J. Bissell, Interaction with basement membrane serves to rapidly distinguish growth and differentiation pattern of normal and malignant human breast epithelial cells, Proc. Natl. Acad. Sci. U.S.a. 89 (1992) 9064–9068.

[13] P. Lu, V.M. Weaver, Z. Werb, The extracellular matrix: a dynamic niche in cancer progression, J. Cell Biol. 196 (2012) 395–406. doi:10.1083/jcb.201102147.

[14] S.P.M. Bohari, D.W.L. Hukins, L.M. Grover, Effect of calcium alginate concentration on viability and proliferation of encapsulated fibroblasts, Biomed Mater Eng. 21 (2011) 159–170. doi:10.3233/BME-2011-0665.

[15] V.E. Santo, M.F. Estrada, S.P. Rebelo, S. Abreu, I. Silva, C. Pinto, et al., Adaptable stirred-tank culture strategies for large scale production of multicellular spheroid-based tumor cell models, Journal of Biotechnology. 221 (2016) 118–129.

[16] V.V. Artym, K. Matsumoto, Imaging cells in three-dimensional collagen matrix, Curr Protoc Cell Biol. Chapter 10 (2010) Unit 10.18.1–20. doi:10.1002/0471143030.cb1018s48.

[17] C.A. Schneider, W.S. Rasband, K.W. Eliceiri, NIH Image to ImageJ: 25 years of image analysis, Nat. Methods. 9 (2012) 671–675.

[18] M. Barbier, S. Jaensch, F. Cornelissen, S. Vidic, K. Gjerde, R. de Hoogt, et al., Ellipsoid Segmentation Model for Analyzing Light-Attenuated 3D Confocal Image Stacks of Fluorescent Multi-Cellular Spheroids, PLoS ONE. 11 (2016) e0156942. doi:10.1371/journal.pone.0156942.

[19] M.P. Pinto, B.M. Jacobsen, K.B. Horwitz, An immunohistochemical method to study breast cancer cell subpopulations and their growth regulation by hormones in three-dimensional cultures, Front Endocrinol (Lausanne). 2 (2011) 15. doi:10.3389/fendo.2011.00015.

[20] A. Amann, M. Zwierzina, G. Gamerith, M. Bitsche, J.M. Huber, G.F. Vogel, et al., Development of an innovative 3D cell culture system to study tumour--stroma interactions in non-small cell lung cancer cells, PLoS ONE. 9 (2014) e92511. doi:10.1371/journal.pone.0092511.

[21] P.P. Provenzano, D.R. Inman, K.W. Eliceiri, J.G. Knittel, L. Yan, C.T. Rueden, et al., Collagen density promotes mammary tumor initiation and progression, BMC Med. 6 (2008) 11. doi:10.1186/1741-7015-6-11.

[22] A.K. Sasser, N.J. Sullivan, A.W. Studebaker, L.F. Hendey, A.E. Axel, B.M. Hall, Interleukin-6 is a potent growth factor for ER-alpha-positive human breast cancer, Faseb J. 21 (2007) 3763–3770. doi:10.1096/fj.07-8832com.

[23] G. Su, K.E. Sung, D.J. Beebe, A. Friedl, Functional screen of paracrine signals in breast carcinoma fibroblasts, PLoS ONE. 7 (2012) e46685. doi:10.1371/journal.pone.0046685.

[24] S. Krause, M.V. Maffini, A.M. Soto, C. Sonnenschein, The microenvironment determines the breast cancer cells' phenotype: organization of MCF7 cells in 3D cultures, BMC Cancer. 10 (2010) 263. doi:10.1186/1471-2407-10-263.

[25] S. Vukicevic, H.K. Kleinman, F.P. Luyten, A.B. Roberts, N.S. Roche, A.H. Reddi, Identification of multiple active growth factors in basement membrane Matrigel suggests caution in interpretation of cellular activity related to extracellular matrix components, Exp. Cell Res. 202 (1992) 1–8.

[26] A.E. Wakeling, M. Dukes, J. Bowler, A potent specific pure antiestrogen with clinical potential, Cancer Res. 51 (1991) 3867–3873.

[27] A. Montero, F. Fossella, G. Hortobagyi, V. Valero, Docetaxel for treatment of solid tumours: a systematic review of clinical data, Lancet Oncol. 6 (2005) 229–239. doi:10.1016/S1470-2045(05)70094-2.

[28] U.E. Martinez-Outschoorn, A. Goldberg, Z. Lin, Y.-H. Ko, N. Flomenberg, C. Wang, et al., Anti-estrogen resistance in breast cancer is induced by the tumor microenvironment and can be overcome by inhibiting mitochondrial function in epithelial cancer cells, Cancer Biol. Ther. 12 (2011) 924–938. doi:10.4161/cbt.12.10.17780.

[29] V. Härmä, J. Virtanen, R. Mäkelä, A. Happonen, J.-P. Mpindi, M. Knuuttila, et al., A comprehensive panel of three-dimensional models for studies of prostate cancer growth, invasion and drug responses, PLoS ONE. 5 (2010) e10431. doi:10.1371/journal.pone.0010431.

[30] J. Folkman, M. Hochberg, Self-regulation of growth in three dimensions, J. Exp. Med. 138 (1973) 745–753.

[31] G. Mehta, A.Y. Hsiao, M. Ingram, G.D. Luker, S. Takayama, Opportunities and challenges for use of tumor spheroids as models to test drug delivery and efficacy, J Control Release. 164 (2012) 192–204. doi:10.1016/j.jconrel.2012.04.045.

[32] D.R. Grimes, C. Kelly, K. Bloch, M. Partridge, A method for estimating the oxygen consumption rate in multicellular tumour spheroids, J R Soc Interface. 11 (2014) 20131124–20131124. doi:10.1098/rsif.2013.1124.

[33] R.G. Boyle, S. Travers, Hypoxia: targeting the tumour, Anticancer Agents Med Chem. 6 (2006) 281–286.

[34] D.J. Kerr, T.E. Wheldon, A.M. Kerr, R.I. Freshney, S.B. Kaye, The effect of adriamycin and 4'-deoxydoxorubicin on cell survival of human lung tumour cells grown in monolayer and as spheroids, British Journal of Cancer. 54 (1986) 423–429.

[35] H. Kobayashi, S. Man, C.H. Graham, S.J. Kapitain, B.A. Teicher, R.S. Kerbel, Acquired multicellular-mediated resistance to alkylating agents in cancer, Proc. Natl. Acad. Sci. U.S.a. 90 (1993) 3294–3298.

[36] A. Frankel, R. Buckman, R.S. Kerbel, Abrogation of taxol-induced G2-M arrest and apoptosis in human ovarian cancer cells grown as multicellular tumor spheroids, Cancer Res. 57 (1997) 2388–2393.

[37] J.P. Celli, I. Rizvi, A.R. Blanden, I. Massodi, M.D. Glidden, B.W. Pogue, et al., An imaging-based platform for high-content, quantitative evaluation of therapeutic response in 3D tumour models, Sci Rep. 4 (2014) 3751. doi:10.1038/srep03751.

[38] A.H. Kyle, L.A. Huxham, D.M. Yeoman, A.I. Minchinton, Limited tissue penetration of taxanes: a mechanism for resistance in solid tumors, Clin. Cancer Res. 13 (2007) 2804–2810. doi:10.1158/1078-0432.CCR-06-1941.

[39] E.R. Boghaert, X. Lu, P.E. Hessler, T.P. McGonigal, A. Oleksijew, M.J. Mitten, et al., The Volume of Three-Dimensional Cultures of Cancer Cells InVitro Influences Transcriptional Profile Differences and Similarities with Monolayer Cultures and Xenografted Tumors, Neoplasia. 19 (2017) 695–706. doi:10.1016/j.neo.2017.06.004.

[40] J. Barretina, G. Caponigro, N. Stransky, K. Venkatesan, A.A. Margolin, S. Kim, et al., The Cancer Cell Line Encyclopedia enables predictive modelling of anticancer drug sensitivity, Nature. 483 (2012) 603–607. doi:10.1038/nature11003.

[41] C. Wenzel, B. Riefke, S. Gründemann, A. Krebs, S. Christian, F. Prinz, et al., 3D high-content screening for the identification of compounds that target cells in dormant tumor spheroid regions, Exp. Cell Res. 323 (2014) 131–143. doi:10.1016/j.yexcr.2014.01.017.

[42] D. Loessner, K.S. Stok, M.P. Lutolf, D.W. Hutmacher, J.A. Clements, S.C. Rizzi, Bioengineered 3D platform to explore cell-ECM interactions and drug resistance of epithelial ovarian cancer cells, Biomaterials. 31 (2010) 8494–8506. doi:10.1016/j.biomaterials.2010.07.064.

[43] G.D. Prestwich, Evaluating drug efficacy and toxicology in three dimensions: using synthetic extracellular matrices in drug discovery, Acc. Chem. Res. 41 (2008) 139–148. doi:10.1021/ar7000827.

[44] T. Rampias, R. Favicchio, J. Stebbing, G. Giamas, Targeting tumor-stroma crosstalk: the example of the NT157 inhibitor, Oncogene. 35 (2016) 2562–2564. doi:10.1038/onc.2015.392.

[45] D. Blum, S. LaBarge, Reproducibility Project: Cancer Biology, Registered report: Tumour micro-environment elicits innate resistance to RAF inhibitors through HGF secretion, Elife. 3 (2014) R82. doi:10.7554/eLife.04034.

[46] N. Linde, C.M. Gutschalk, C. Hoffmann, D. Yilmaz, M.M. Mueller, Integrating macrophages into organotypic co-cultures: a 3D in vitro model to study tumor-associated macrophages, PLoS ONE. 7 (2012) e40058. doi:10.1371/journal.pone.0040058.

[47] J.S. Miller, K.R. Stevens, M.T. Yang, B.M. Baker, D.-H.T. Nguyen, D.M. Cohen, et al., Rapid casting of patterned vascular networks for perfusable engineered three-dimensional tissues, Nat Mater. 11 (2012) 768–774. doi:10.1038/nmat3357.

[48] C.M. Ghajar, H. Peinado, H. Mori, I.R. Matei, K.J. Evason, H. Brazier, et al., The perivascular niche regulates breast tumour dormancy, Nat. Cell Biol. 15 (2013) 807–817. doi:10.1038/ncb2767.

Chapter V

ex vivo model to study hormone response in human breast cancer

Marta F Estrada, Ana Luísa Cartaxo, Giacomo Domenici, Catarina Pinto, Ruben Roque, Dusica Rados, Rui Portela, Miguel Fuzeta, Paula M Alves, Saudade André and Catarina Brito. *ex vivo model to study hormone response in human breast cancer.* In preparation

Table of contents

Abstract 157
1 Introduction 158
2 Materials and Methods 159
2.1 Ethics statement 159
2.2 Processing of patient material 160
2.3 Culture of patient-derived material 160
2.4 Cell viability assessment 161
2.5 Immunohistochemistry 161
2.6 Fulvestrant treatment 162
2.7 Exomatabolome analysis by 1H-NMR 162
2.8 Statistical analysis 163
2.8.1 Standardization 163
2.8.2 Box Plots 164
2.8.3 Hypothesis tests 164
2.8.4 Principal Component Analysis 164
2.8.5 K-means clustering 165
2.8.6 Extension of the PCA and Scatter Plot 166
3 Results 166
3.1 Alginate encapsulation and orbital shacked culture is an efficient strategy for long-term maintenance of ER^+ BC explants 166
3.2 Explant viability and diversity within alginate capsules 169
3.3 Maintenance of the epithelial phenotype and ER expression in encapsulated explants with 1 month of culture 171
3.4 Fulvestrant, an ER antagonist, treatment promotes a metabolic shift in ER^+ breast cancer explants 174
4 Discussion 175
5 Acknowledgments 180
6 References 180
7 Supplementary Figure 183

Abstract

The interactions between tumour cells and their microenvironment modulate cancer progression and acquired drug resistance. The development of *ex vivo* cultures from ER^+ human breast cancer explants aims to retain the original tissue architecture, the epithelial and stromal phenotype and the expression of the Oestrogen. However, loss of cellularity and ER expression after a short-term culture period is a well-known culture-related phenomenon. To overcome these limitations, we have combined alginate encapsulation and agitation-based culture systems, to culture explants obtained from ER^+ breast cancer patients. After one month in culture, the morphological and molecular features of the encapsulated explants were consistent with the original tumour, showing maintenance of the epithelial and stromal components, expression of ER and detection of proliferating cells. In addition, exometabolome profiling revealed that samples could be grouped according with the level of cellularity. Preliminary data suggested that fulvestrant treatment leads to a mild increase in glutamate concentration in the extracellular space. The proposed model system constitutes a new tool with potential application in dissecting the long-term effects of anti-ER treatments, in an environment that more closely resembles the original tumor microenvironment *in vivo* situation. Moreover, the proposed model has potential for accessing therapeutic response in co-clinical assays with ER^+ breast cancer patients.

1 Introduction

Breast cancer (BC) is still the leading cause of cancer deaths in woman worldwide (WHO). Two-thirds of all breast cancers are Oestrogen Receptor $(ER)^+$ [1] and present a good prognosis, due to initial response to endocrine therapy [2]. However, the disease often relapses due to disease progression towards drug resistance and metastasis [2,3]. The tumour microenvironment plays a major role in modulating disease progression. It is composed by a network of fibroblasts, immune cells, adipocytes and endothelial cells, all embedded in an extracellular matrix (ECM) that allows migration and accumulation/release of soluble and insoluble factors [4]. Altogether, these components interact with epithelial cells and directly influence tumour behaviour towards more aggressive stages of the disease [5,6].

In an attempt to better represent the interactions between epithelial tumour cells and their microenvironment, *ex vivo* models have been developed throughout the past decades. A major challenge when performing primary breast cell cultures, is not only the maintenance of cell viability and architecture but also the luminal epithelial phenotype and the ER expression. Many have tried to culture these cells *ex vivo*, but in most reports, luminal cells lose ER expression [7]. Nonetheless, recent reports have shown that it is possible to maintain ex vivo cell-to-cell communication, as well as the hormone receptor expression and the interactions with the surrounding microenvironment [8]. Specifically, cultivation of tissue slices from patient- and cell line-derived mouse xenografts (PDX and CDX, respectively) allows the interrogation of specific signalling pathways and interactions between different cell types involved on cell survival and drug sensitivity [9]. In this study, however, the authors observed oxygen diffusion limitations due to the culture set-up that led to opposite zonation of ER and HIF1α expression, i.e., in the hypoxic region where HIF1α was expressed, ER expression was ablated and vice-versa. Alternatively, [10] developed a model in which tissue microstructures derived from healthy breast human tissue, are cultured up to 7 days, maintaining the original tissue architecture, heterotypic cell cross-talk and hormone receptor

expression (ER). Despite these improvements, both models allow only for short-term cultures since after one week, tissue architecture, cellularity and hormone receptor expression are lost. Only recently, [11] managed to maintain ER expression in long-term 2-dimentional cultures, by treating normal human breast epithelial cells with TGFβ inhibitors. In another recent study, the authors provided evidence for maintenance of ER^+ breast cancer tissue in collagen sandwiches under constant medium perfusion [12]. Nonetheless, the cellularity and the original tissue architecture were lost after 2 weeks in culture.

As most luminal A ($ER^+PR^+Her2^-$) breast cancers (BCs) are known to be low proliferative and low mutagenic [13,14], cancer progression typically occurs at a slow rate. Hence, there is a need to extend the life span of the tissue explants to obtain long-term cultures that can be studied for at least 30 days.

Here we employed the strategy previously developed by our team [15], alginate encapsulation, combined with orbital shaking culture system strategy for the *ex vivo* culture of ER^+ BC, using freshly isolated patient material. We received material from 21 patients, 70% of which were successfully maintained in culture up to 30 days. Samples presented a very high degree of intra- and inter-patient heterogeneity, reflected in the different phenotypes observed along the culture time. We demonstrated that after 1 month in culture, cell viability was maintained and the architecture of the encapsulated explants was similar to the initial tumour. To our knowledge this is the first report of maintenance of ER expression in culture for 30 days.

The model developed might be a useful tool for the scientific community, clinic and pharma industry to deepen the knowledge on heterotypic cell interactions and their impact on ER dependency.

2 Materials and Methods

2.1 Ethics statement

Breast tumours were collected at the Lisbon Oncology Hospital (Instituto Português de Oncologia de Lisboa Francisco Gentil – IPOLFG). The use of patient material has been approved by the IPOFLG ethics committee, and all

patients have signed an informed consent form to agree to donate the material for research purposes. All tissues were anonymized before transfer into the laboratory.

2.2 Processing of patient material

All collected tumours from ER^+ breast cancer patients, that were not subjected to any type of anti-cancer therapy, were included in this study. Tumour samples were collected in sterile conditions during surgery and immediately submerged in Dulbecco's Modified Eagle Medium: Nutrient Mixture F-12 (DMEM/F12; Life Technologies), supplemented with 1% (v/v) penicillin-streptomycin (P/S, Life Technologies) and 10% (v/v) fetal bovine serum (FBS, Life Technologies). Samples were kept at 4ºC and transported to the lab (1-3h post-surgery).

Tissue samples were mechanically dissociated with two surgical scalpels. Tissue digestion was performed with 0.09 U/mL of Collagenase A (Roche) and 30 U/mL of Benzonase (Merck Millipore), in a nutating mixer (GyroMini™), placed in an incubator, at 37ºC, with humidified atmosphere containing 5% CO_2 in air. Following enzymatic digestion (12-15h), the obtained tumour fragments (mean size: 1-2 mm^2) were pelleted by centrifugation at 100x g for 5 min at 4ºC and washed with Phosphate-Buffered Saline (PBS; Life Technologies), without Ca^{2+}/Mg^{2+}.

2.3 Culture of patient-derived material

Tumour fragments were encapsulated as described in [15]. Briefly, explants were dispersed in 1 mL of 2% (w/v) of Ultrapure Ca^{2+} MVG alginate (UP MVG NovaMatrix, Pronova Biomedical, Oslo, Norway) dissolved in NaCl 0.9% (w/v) solution. Encapsulation was performed using an electrostatic bead generator (Nisco VarV1, Zurich, Switzerland), with an air flow rate of 10 mL/h, at 5.3 V with air pressure of 1 bar. The alginate droplets were cross-linked in a 100 mM $CaCl_2$/10 mM HEPES (pH 7.4) solution for 10 min, further washed three times in a 0.9% (w/v) NaCl solution and finally equilibrated in culture

medium. Encapsulated explants were then transferred into 6-well plates and placed in an orbital shaker (100 rpm) in a humidified incubator, with 5% CO_2 in air, for 30 days with 50% medium exchange every 3 to 4 days. Cultures were maintained in Human Mammary Epithelial Cell Culture medium (HMEC; DMEM/F12 with 1% P/S (both from Life Technologies), 0.5 mg/mL Epidermal Growth Factor, 2 mg/mL Insulin, 1 mg/mL Hydrocortisone, 1 mg/mL Transferrin, 5E-3 mol/L Isoprotenol, 0.1M Ethanolamine, 0.1 M O-Phosphoethanolamine, 14 mg/mL Bovine Pituitary Extract (all from Sigma-Aldrich) and 100 µg/mL Primocin (InvivoGen Europe).

2.4 Cell viability assessment

Cell viability was assessed using fluorescein diacetate (FDA; Sigma Aldrich) at 10 µg/mL to label live cells, and Propidium iodide (PI, LifeTechnologies) at 10 µg/mL, for dead cells. Encapsulated explants were incubated for 5 min at room temperature (RT) and then analysed using a fluorescence microscope (DMI6000, Leica Microsystems GmbH, Wetzlar, Germany).

2.5 Immunohistochemistry

Encapsulated explants were collected after 30 days and alginate capsules were dissolved with a solution of 50 mM EDTA in mQ water, for 5 min at RT. Samples were centrifuged at 300x g, 5 min at 4ºC, washed with PBS and fixed with formol ON at RT, and pelleted by centrifugation at 1300x g for 5 min at RT. Pellets were pre-stained with 20 uL hematoxylin, centrifuged at 1300x g for 5 min at RT, and embedded into 30 uL of pre-warmed histogel (ThermoScientific; warmed in a water bath placed in a microwave for 45 sec, at 750 watt). Embedded samples were centrifuged at 2000x g for 1 min at RT and placed at -20ºC for 5 min. Histogel cones were removed from the tubes, sliced in half and placed in a cassette in formol, until further processing. For paraffin embedding, samples were dehydrated in graded alcohols and then embedded in paraffin wax. Paraffin blocks were sectioned (3 µm) for Hematoxylin & Eosin (H&E) and

immunohistochemical staining. Immunohistochemistry (IHC) was carried out using standard protocols from the IPOFLG hospital. Briefly, antigen retrieval was carried out with Cell Conditioning 1 (CC1, Ventana), optiview or ultraview were used for detection and all antibodies used are indicated in table 5.1. Staining was performed using a Ventana BenchMark Ultra (all from Ventana Medical Systems, Inc).

Table 5.1: Conditions used for immunohistochemistry analysis

Primary antibody (Clone)	Supplier	Dilution	Antigen Retrieval	Detection system
E-cadherin (NCH 38)	Dako	1:80	40 min with CC1*	Optiview#
Oestrogen Receptor (SP1)	Ventana	Pre-diluted	64 min with CC1*	Ultraview#
Progesterone Receptor (IE2)	Ventana	Pre-diluted	64 min with CC1*	Ultraview#
HER-2 (4B5)	Ventana	Pre-diluted	52 min with CC1*	Ultraview#
KI67 (30-9)	Ventana	Pre-diluted	32 min with CC1*	Optiview#
CD45 (2B11-PD7/26)	Dako	1:1000	86 min with CC1*	Optiview#
Vimentin (3B4)	Dako	1:150	24 min with CC1*	Optiview#
p63 (BC4A4)	Biocare Medical	1:80	No	Optiview#

* Cell Conditioning 1 (CC1), from Ventana

\# Both from Ventana

2.6 Fulvestrant treatment

Encapsulated explants were treated for 3 days with 0.4 nM or 100 nM of ICI 182,780 (Fulvestrant, Tocris), after 27 days of culture. Encapsulated explants were collected and the alginate capsules dissolved as described above. Samples were then centrifuged at 300x g, 5 min at 4ºC, washed with PBS, snap frozen in liquid nitrogen and stored at -80ºC until further processing. Culture supernatants were collected after centrifugation, and centrifuged again at 1000x g, 5 min at 4ºC, to remove cell debris. Clarified supernatants were snap frozen in liquid nitrogen and stored at -80ºC until further processing.

2.7 Exomatabolome analysis by 1H-NMR

For exometabolome analysis, stored supernatants were thawed on ice. Approximately 800 µL were filtered using 0.2 µm filter to remove any remaining cell debris. Then 450 µL of sample were mixed with 175 µL distilled water (D_2O)

and 50 µL 0.8 M phosphate buffer prepared in D_2O (pH 7.4). This mixture was filtered by using centrifugal filter units with a 3 kDa membrane cut off (Millipore), for 40 min at 10000x g at RT to remove proteins. Finally, 475 µL of the filtrate was mixed with 25 µL D_2O with Trimethylsilylpropanoic acid (TSP), 2 µL of NaN_3, and transferred into an NMR tube.

All spectra were acquired in Avance 500 (Bruker Biospin) using standard pulse sequences. For identification and quantification purpose, noesy1prde was used. Identification and quantification were assisted by Chenomx Suite 8.12. Additional 2D spectra such as jres, 1H-TOCSY and HSQC were ran to confirm identity of metabolites.

2.8 Statistical analysis

The following methods were used to: (A) identify the metabolic signatures from the BC encapsulated explants; and to (B) determine the impact of Fulvestrant treatment on the metabolism of ER^+ breast cancer encapsulated explants

2.8.1 Standardization

Z-score normalization [16] was used for standardization of A) and B). The values for the concentration of each metabolite, from each culture, were transformed according to equation 1. The concentration of the metabolite *m*, from patient *p*, was subtracted by the average concentration of metabolite *m* and this difference was divided by the standard deviation of the concentration of metabolite *m*.

$$Z_{m,p} = \frac{C_{m,p} - \overline{C_m}}{S_m} \quad (1)$$

2.8.2 Box Plots

For B), an exploratory data analysis based on box plots was made. For each quantified metabolite, a box plot was obtained, comparing the concentrations of this metabolite in 2 conditions (treated and untreated explants). These plots were obtained using the "boxplot" function in R. Box plots using Z-score normalization were obtained with the R script "Box Plot Treatment Z-score.R", which uses the excel file "Breast cancer exomet 23Aug17 DRanalysis Treatment Z-score.csv" as input.

2.8.3 Hypothesis tests

For B), in order to determine if the average concentration of certain metabolites was different between treated and untreated BC encapsulated explants, a panel of 4 hypothesis tests was applied. A two sample t-test, a Welch's t-test and a paired t-test were computed using different settings of the "t.test" function in R. A Mann- Whitney-Wilcoxon test was computed using the "wilcox.test" function in R. The P-values for these 4 tests, applied to each metabolite, were calculated in R, using the script "Statistic Tests Treatment Absolute.R", which uses the excel file "Breast cancer exomet 23Aug17 DR-analysis Treatment Absolute.csv" as input. All the t-tests are parametric tests, assuming that the data follow a normal distribution. The simple two sample t-test assumes identical variances. The Welch's t-test relaxes this assumption. The paired t-test determines the significance in the difference of paired data (in this case sample by sample), instead of just comparing two groups of data. The Mann-Whitney-Wilcoxon test is a non-parametric ranked test, which does not assume any normal distribution of the data.

2.8.4 Principal Component Analysis

A principal component analysis (PCA) was used in both A) and B), in order to reduce the data set into a smaller number of principal components (PCs). This transformation was performed in R, applying the "prcomp" function to the data set containing the metabolite concentrations for each explant. The

standard deviations and the proportion of variance for each PC was examined by applying the “summary” function to the result of the previous operation. The proportion of variances were also plotted. Two and three-dimensional plots of the PCA were obtained using the R package “pca3d”. Two-dimensional plots of the first 2 PCs were obtained using the “pca2d” function from this package and three-dimensional plots of the first 3 PCs were obtained using the “pca3d” function from this package. For A), a PCA was performed for the concentration of all the metabolites that were quantified at the end of the culture period (31 metabolites), for encapsulated explants of 10 patients. This was executed in R, using part of the script “PCA of Alginate 2% Control.R”, which uses the excel file “Controls.csv” as input. For B), a PCA was performed with the concentration of all the metabolites that were quantified at the end of the culture period (32 metabolites). PCA was applied for encapsulated explants of 5 patients. This was executed in R, using part of the script “PCA of Treatment Z-score.R”, which uses the excel file “Breast cancer exomet 23Aug17 DR- analysis Treatment Zscore. csv” as input. In this case the 2D plot of the PCA was executed with the “ggbiplot” function, from the package with the same name. The PCA could only be applied to metabolites that were quantified for all the encapsulated explants. Since certain metabolites could not be detected for all the encapsulated explants, the number of metabolites used for the analysis was reduced from 35 to either 31 metabolites for A) or 32 metabolites for B), depending on the encapsulated explants that were used for each analysis.

2.8.5 K-means clustering

For A), a k-means clustering was applied to the PCA. This was executed in R, applying the “kmeans” function to the first 3 PCs of the PCA, in order to observe the clusterings that could be formed from the previous 3D projection of the PCA. The clustering was observed using the “pca3d” function, with a grouping parameter set for the results of the k-means clustering. Three different clusterings were performed, using different values for k (2, 3 and 4). This was

executed in R, using part of the script “PCA of Alginate 2% Control.R”, which uses the excel file “Controls.csv” as input.

2.8.6 Extension of the PCA and Scatter Plot

For A), the weights of each metabolite on PC1 were obtained, by accessing the first column of the “rotation” field from the “prcomp” function in R. The 2 metabolites with the highest and the lowest PC1 weights were identified. A scatter plot with the concentrations of these 2 metabolites for the 10 patients was plotted in R, using the “plot” function. These operations were executed in R, using part of the script “PCA of Alginate 2% Control.R”, which uses the excel file “Controls.csv” as input.

3 Results

3.1 Alginate encapsulation and orbital shacked culture is an efficient strategy for long-term maintenance of ER^+ BC explants

Breast tumour samples from 21 women diagnosed with ER^+ breast cancer, with ages between 48 – 83 years, were donated for this study. As indicated in Table 5.2, 90% of the tumours were invasive ductal carcinomas (IDC). Tumour grade varied between grade 1 and grade 2, but most cases were grade 2. As illustrated in Figure 5.2, samples were very heterogeneous between and within patients. The proliferative index varied between 15% and 70%, as assessed by immunostaining for the mitosis marker KI67. ER expression was less variable since all patients presented 90 - 100% positive cells for ER. Nonetheless, ER expression levels varied between high, medium and low intensity immunostaining, reflecting also some degree of heterogeneity between and within samples, which was not considered at diagnosis. Tissue architecture varied in epithelial vs stromal content, cell organization and on the presence/absence of immune leucocytes ($CD45^+$ cells) (Figure 5.2). A complete mixture between epithelial and stromal cells was rarely observed

(Figure 5.2). Instead, there were islets/regions of epithelial cells surrounded by masses of stromal cells.

Table 5.2: Clinico-pathological parameters of the human breast cancer samples received

Clinico-pathological parameters	(n)	Percentage (%)
Samples	21	100
Histological subtype		
Invasive ductal	19	90.5
Invasive lobular	1	4.8
Benign fibroadenoma	1	4.8
Tumour grade		
1	1	4.8
2	10	47.6
3	5	23.8
Tumour size		
pT1	10	47.6
pT2	7	33.3
Lymph node status		
pN0	12	57.1
pN1	3	14.3
pN2	1	4.8
pnmi	1	4.8
Mean age at diagnosis	62	(48 - 83)

We hypothesized that by performing a partial tissue digestion followed by alginate encapsulation, the original tissue structure and cell populations would be maintained along the culture time, allowing for cell-to-cell communication, paracrine signalling and maintenance of tumour homeostasis. To establish ER^+ breast cancer *ex vivo cultures*, a dual step strategy was applied (Figure 5.1): firstly, freshly isolated tumour samples were mechanically and enzymatically

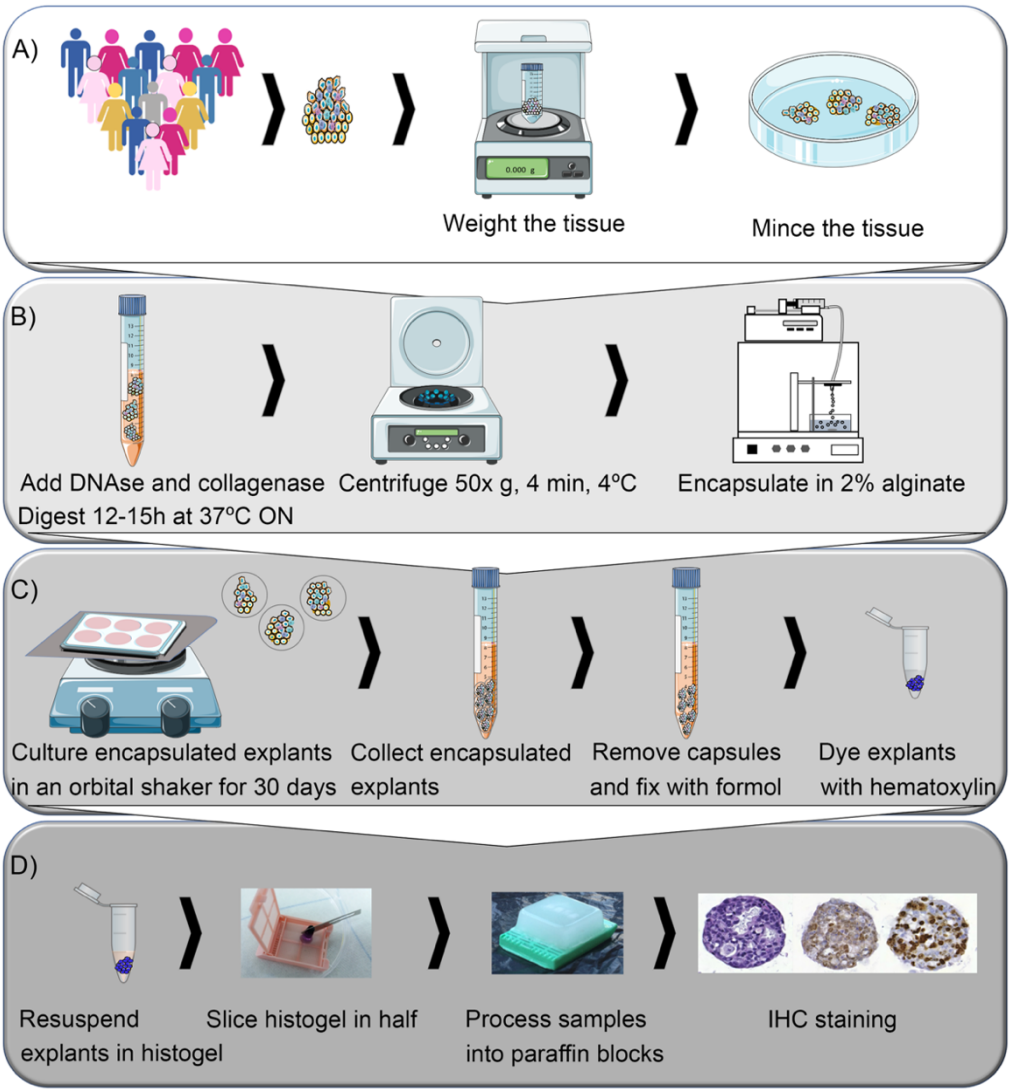

Figure 5.1: Schematic illustration of the experimental approach. (A) Tumour samples from ER^+ BC patients were collected, weighted and minced with two surgical scalpels. (B) Samples were digested ON, centrifuged and encapsulated in 2% alginate hydrogel. (C) Encapsulated explants were cultured on an orbital shaker for 30 days and then collected; alginate capsules were removed, encapsulated explants were fixed with formol and then dyed with hematoxylin. (D) Explants were resuspended in histogel, embedded into paraffin blocks, sectioned and stained for further phenotypic characterization.

dissociated into tumour fragments. To ensure that the tissue architecture and the epithelial and stromal compartments were retained, the dissociation process was optimized to obtain structures of sizes around 2 mm^2. We reasoned that, by providing the tissue fragments a physical support [15] and ensuring the maintenance of paracrine signalling, tissue fragment integrity would be extended beyond the typical 7 days of culture [10]. Therefore, the fragments were encapsulated into alginate capsules and cultured under stirring conditions in HMEC medium – encapsulated explants culture.

3.2 Explant viability and diversity within alginate capsules

Encapsulated explants obtained from ER^+ breast cancer patient samples were cultured for 30 days. Despite the high level of variability and heterogeneity between and within patient samples, viability of the encapsulated explants was generally maintained for 30 days. Live/dead assays showed that encapsulated explants maintained cell viability along the culture time. Once a week media exchange led to an outer ring of cell death which was avoided by increasing media exchange frequency to every 3 to 4 days (data not shown). These structures presented a heterogeneous morphology within the alginate capsules. For instance, some structures were circular and presented defined edges (Figure 5.3, B8 day 1), whilst others showed protruding cell masses (Figure 5.3, B19). Moreover, some encapsulated explants presented the ability to deform or leak out of the alginate capsules (Figure 5.3, B8 and B19, day 30); to develop phenotypic features such as appearance of large vacuoles, that are usually associated with entosis [17] (Figure 5.3, B8, day 30). Features of the original tumour microenvironment were also maintained, such as, the presence of adipocytes (Figure 5.3, B19 Day1) which are a major component of the breast microenvironment and are known to stimulate tumour progression [18]; or the mucous, which is highly produced by mucinous carcinomas [19] (Figure 5.3, B7, Day 1).

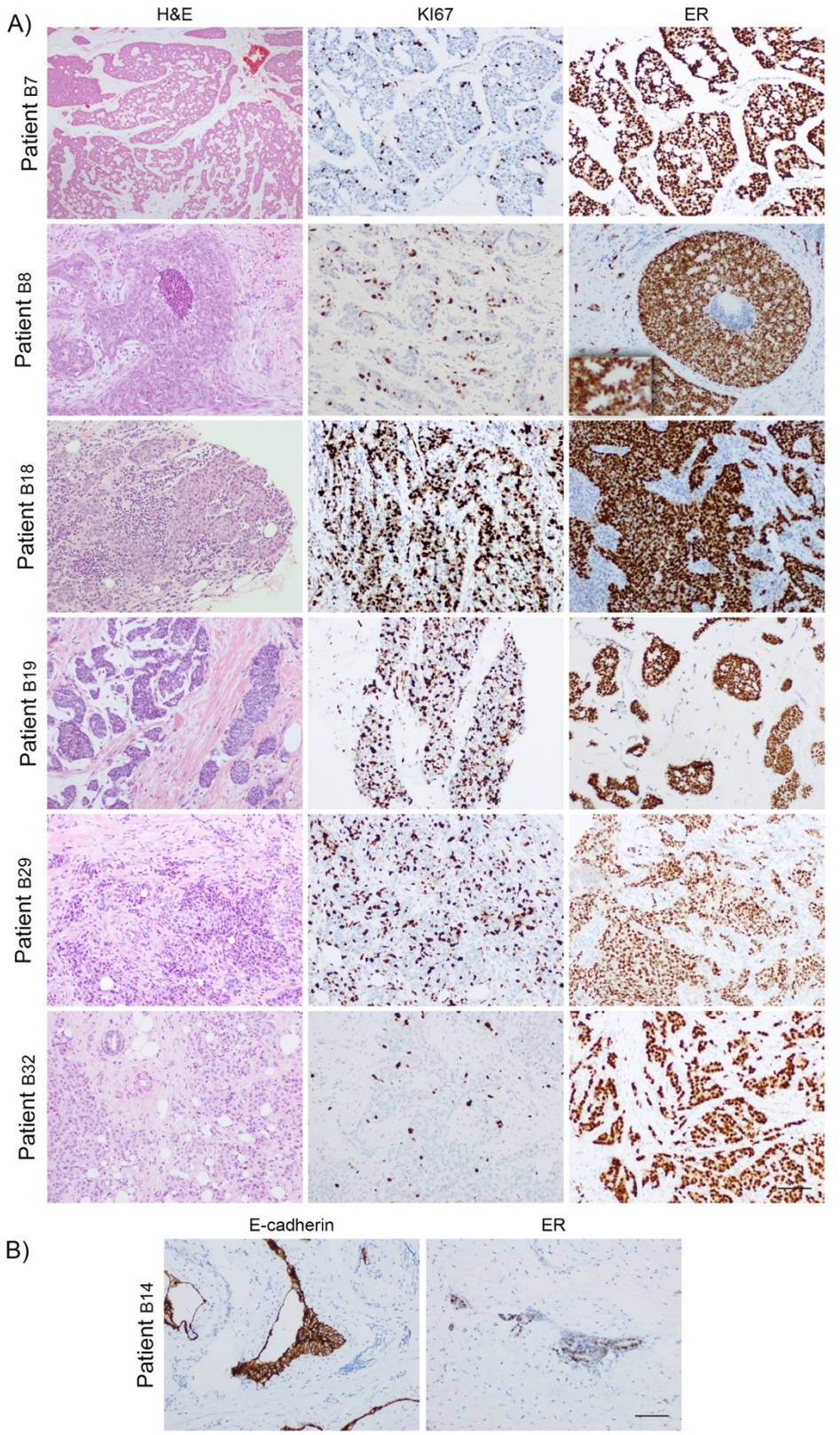
A)
H&E
KI67
ER
Patient B7
Patient B8
Patient B18
Patient B19
Patient B29
Patient B32
B)
E-cadherin
ER
Patient B14

Figure 5.2: Characterization of the collected tumour samples. IHC characterization of tumour samples used for patient diagnosis, in 3 µm thick sections. (A) From the left panel: Hematoxylin & Eosin staining (H&E), KI67, Oestrogen Receptor (ER). (B) From the left panel: E-cadherin and ER, from a Fibroadenoma. Scale bar 500 µm.

3.3 Maintenance of the epithelial phenotype and ER expression in encapsulated explants with 1 month of culture

Amongst the 15 samples analysed, 67% of the encapsulated explant cultures were considered successful based on the parameters as: high cellularity over the 30 days of culture (detected by H&E) and phenotypic characteristics similar to the initial tumour, which included, maintenance of epithelial and stromal compartments, proliferative capacity (Figures 5.2 and 5.4). Due to the heterogeneity of the tumours, cell organization differed between cultures of different samples: whilst some structures were exclusively composed of epithelial cells (Figure 5.4, B7) or stromal cells (Figure 5.4, B18); others were a disorganized mixture of both cell types (Figure 5.4, B18, B29). Epithelial and stromal identity were confirmed by E-cadherin and vimentin staining (Figure 5.4A). Furthermore, the presence of membranous E-cadherin staining indicated that epithelial cells maintained cell-cell adhesions and a differentiated epithelial phenotype [20]. Proliferative cells were detected in most encapsulated explants and were distributed throughout the structures, suggesting that oxygen or nutrient limitation did not occur. $CD45^+$ cells were also detected in cultures of 4 cases, indicating that the immune infiltrate was maintained. A reduced number of cells were positive for the basal/myoepithelial marker p63, as observed in the initial tumour. Importantly, ER positive cells were detected in 70% of the successfully cultured encapsulated explants. Nonetheless, ER nuclear staining seemed to decrease in most cultures, with moderate to low intensity (Figure 5.2 and 5.4).

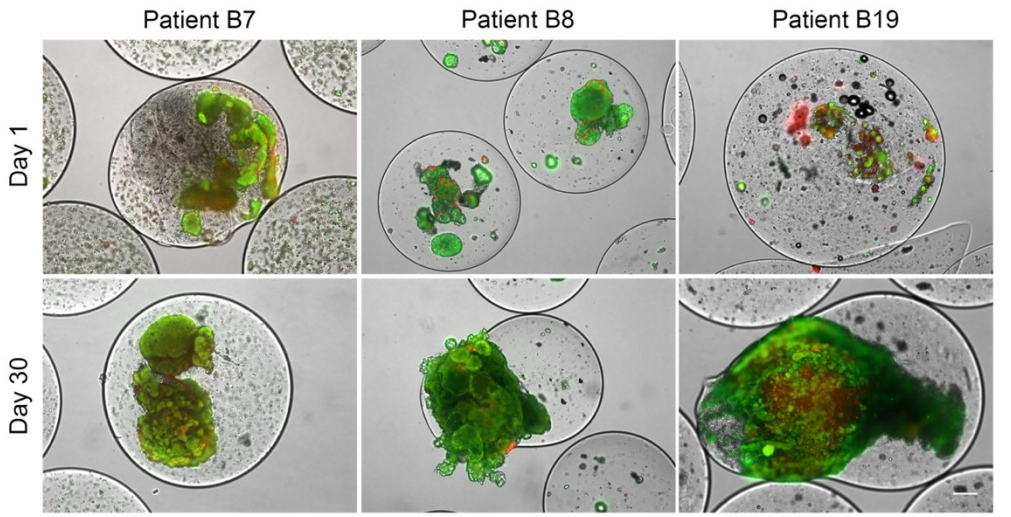

Figure 5.3: Evaluation of encapsulated explants viability and phenotype after 30 days in culture. Live/dead assay (FDA - green; PI - red, respectively) of encapsulated explants, at days 1 and 30. Scale bar 200 µm.

The exometabolome of the encapsulated explants was profiled by 1H-NMR. Culture supernatants were analysed after 30 days of culture and Principal Component Analysis (PCA) was performed using NMR metabolite concentrations. We analysed the dominant intrinsic variation in the data set and obtained an overview of variation amongst patients. Two separate groups of samples were mainly defined on PC1. IHC revealed that samples from group 1 presented low cellularity and complete ablation of ER expression, in contrast with group 2, where samples had high cellularity and ER^+ cells. Interestingly,

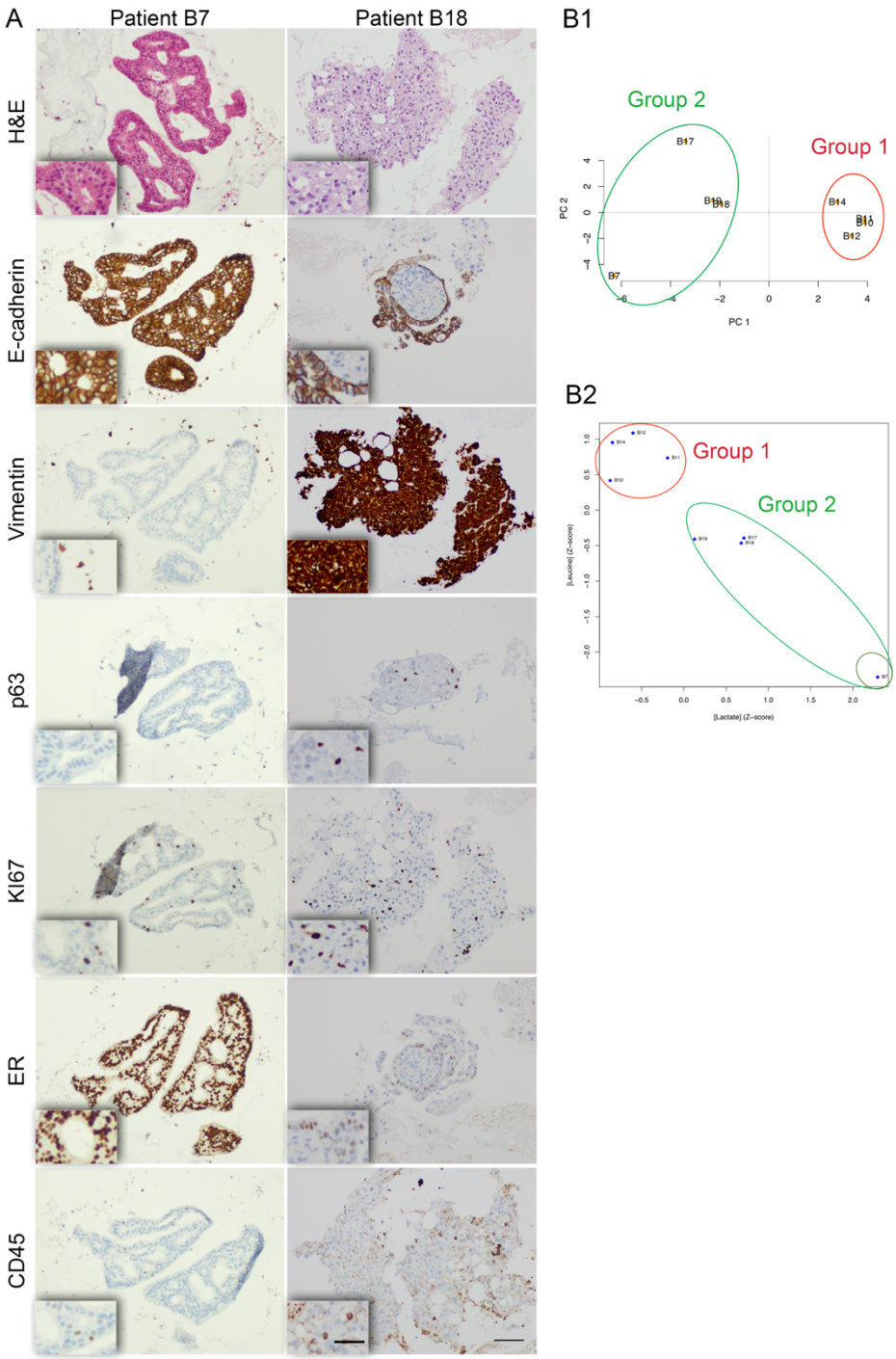

Figure 5.4: Characterization of encapsulated explants after 30 days in culture. (A) IHC characterization of encapsulated explants, in 3 µm thick sections after 30 days in culture. From the upper panel: Hematoxylin & Eosin staining (H&E), E-

cadherin, Vimentin, p63, KI67, Oestrogen Receptor (ER), CD45. High magnification on the left side of each image. Scale bars: 100 µm, and 50 µm for high-magnification inset. (B1) Principal Component Analysis (PCA) of the 31 metabolites identified by exometabolome profiling of encapsulated explants from 10 patients after 30 days of culture. 2D plot of the first 2 principal components shows 2 groups, corresponding to the maintenance or loss (group 2 and group 1, respectively) of cellularity and ER expression. (B2) Scatter plot of lactate and isoleucine concentrations (with a Z-score normalization), for each of the encapsulated explants from 10 patients, maintenance or loss (group 2 and group 1, respectively) of cellularity and ER expression.

the fibroadenoma, typically characterized by high fibroblast content and reduced number of epithelial cells (Figure 5.2), fell into group 1. Group 2 presented

the higher sample variability which may be correlated with higher metabolic activity. Again, patient variability was also reflected in this analysis, especially in the distance observed between B7, B17 and the other samples. Although 32 metabolites were identified by NMR, each group up could be defined by the high impact of 2 specific metabolites: group 2 was defined by high lactate concentration in the supernatant; whilst isoleucine was higher in all the samples from group 1 (Figure 5.4).

3.4 Fulvestrant, an ER antagonist, treatment promotes a metabolic shift in ER$^+$ breast cancer explants

We next asked whether these cells would respond to a 72h Fulvestrant treatment (0.4nM), an ER antagonist [1,21]. Exometabolome analysis, of Fulvestrant treated cells, led to a partial separation between treated and untreated samples. The separation corresponded to a shrinkage of the distance between treated samples, i.e., the treated samples presented decreased heterogeneity in what concerns metabolite concentration, when compared to the untreated group. Although this data are still preliminary, we could observe a tendency to increased glutamate concentration in the extracellular space of treated samples.

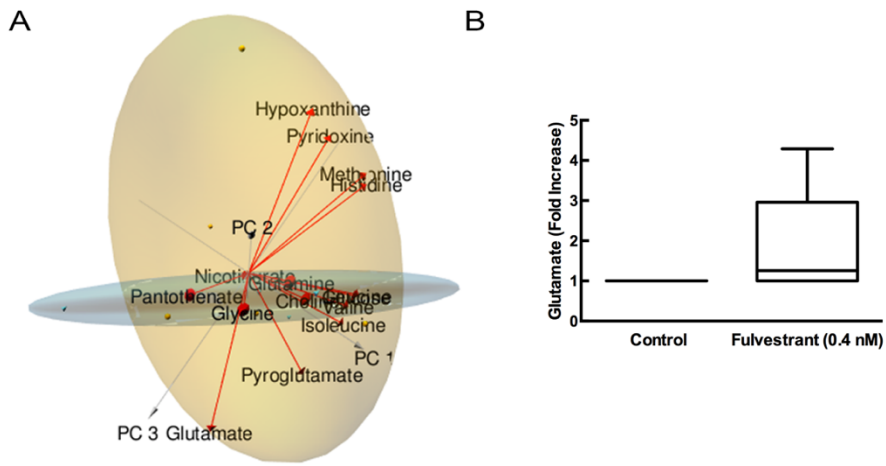

Figure 5.5: Characterization of encapsulated explants after Fulvestrant treatment. Encapsulated explants were treated for 72h with Fulvestrant and supernatants were collected at day 30 of culture. (A) 3D plot of the first 3 PCs from the PCA of all 32 metabolites obtained by exometabolome profiling of treated vs untreated encapsulated explants (n=5) with 0.4 nM of Fulvestrant. Untreated encapsulated explants are delimited by orange ellipsoids, while treated are delimited by blue ellipsoids. (B) Box plot of glutamate concentration, obtained by exometabolome profiling of treated vs untreated encapsulated explants with 0.4 nM of Fulvestrant.

4 Discussion

Many efforts have been made towards the development of long-term *ex vivo* cultures of ER^+ human breast cancer explants. These studies aimed to retain the original tissue architecture, the luminal epithelial phenotype and the expression of the nuclear hormone receptor – ER [9,12,20]. However, after a short-term culture period, cellularity and ER expression are lost, hampering the interrogation on the long-term effects of tumour-stromal interactions and on drug response mechanisms to ER antagonists.

In this work we have developed a new strategy for long-term maintenance of ER^+ BC explants, *ex vivo*, by combining alginate encapsulation and orbital shaking. This system enables the accumulation of secreted factors, provides

physical support to cells and promotes nutrient and oxygen diffusion [15]. Our results demonstrate that by using this strategy, encapsulated breast cancer explants could be successfully cultured for 30 days with high cellularity, maintenance of epithelial and stromal compartments, ER expression, proliferating cells and, detection of $CD45^+$ cells. After demonstration of ER functionality (on going studies), this system should allow the interrogation of the long-term effects of anti-ER treatments, in an environment that more closely resembles the *in vivo* situation.

In a previous work [10], the processing and culture of breast microstructures (tissue fragments with up to 2 mm in size), obtained from reduction mammoplasties, were optimized to preserve cell-matrix and cell-cell contacts. However, these could only be cultured for up to 7 days before tissue disintegration and loss of cell viability [10]. The use of an inert scaffold, alginate, allowed the extension of the culture period for at least 1 month. Preliminary studies, performed in collaboration with the same group, demonstrated that alginate encapsulation of normal mammary gland microstructures and orbital shaking conditions extended the culture period for at least 30 days (Figure S5.1).

Similarly, our results demonstrate that, encapsulated tumour explants maintained cell viability, high cellularity and both the epithelial and the stromal compartments, after 1 month in culture. In all successful cases, cells retained the epithelial phenotype and proliferative indexes were kept low, as typically observed for luminal A tumours [22]. The homogeneous distribution of proliferative cells and the absence of necrotic or apoptotic cores, demonstrates that, despite the explant sizes of approximately 2 mm, no oxygen nor nutrient limitations occurred. The use of a dynamic culture system improves mass transfer, reducing the formation of gradients typically observed for explants with this size range [23].

The maintenance of ER^+ cells in culture is a major accomplishment. For many years, scientists have tried to optimize a culture method that avoided ER ablation *ex vivo* [7]. The maintenance of ER is key to mimic luminal A breast

carcinomas, as cell proliferation is ER-dependent and targeted therapies typically rely on prolonged treatment with ER antagonists [24]. After 1 month in culture we were able to detect ER positive cells in approximately 70% of the successfully cultured encapsulated explants. Although the number of ER+ cells and the staining intensity seemed to decrease, further studies are required to evaluate ER expression along the time. Nonetheless, we speculate that the maintenance of the culture architecture and the native ECM, allowed heterotypic crosstalk that contributed to the maintenance of ER expression. One hypothesis could be that the oestradiol and the Epidermal Growth Factor (EGF) produced by breast fibroblasts [25-28], together with the EGF and insulin already present in the culture medium, would stimulate the proliferation of ER^+ cells [29].

To evaluate ER functionality breast explants were either stimulated with 10 nM of oestrogen or treated with Fulvestrant, an ER antagonist, for 24 or 72h. Evaluation of ER downstream effectors, like PR or PC2 is still ongoing. Nonetheless, exometabolome profiling of samples treated for 72h with 0.4 nM of Fulvestrant revealed a restriction of metabolic states, as the metabolic heterogeneity observed in controls was reduced after treatment. Although preliminary, the obtained results show a mild increase of extracellular glutamate concentration upon Fulvestrant treatment. This result is in line with previous reports showing that the blood glutamate levels are inversely correlated with the levels of oestrogen and progesterone, in pre-menopausal woman [30]. Glutamate is not only a metabolite but also a signalling molecule with paracrine and autocrine activity [31,32]. It has been shown that more aggressive breast cancers present increased expression of the metabotropic glutamate receptor 1 (mGLUR1) [33] and increased dependency on glutamate for cell proliferation [34]. Moreover, these aggressive BC also secrete higher amounts of glutamate which have been correlated with the disruption of bone homeostasis and consequent increase in bone metastasis [31]. Although a direct correlation between glutamate and ER has not yet been shown for breast cancer, several authors have already demonstrated this link for astrocytes. For instance, it has

been shown that *in vitro* treatment of astrocytes with Fulvestrant led to increased glutamate accumulation in the culture supernatant [35]. Moreover, immunoprecipitation studies have proven that membranous ER and glutamate receptors associate in the membrane of astrocytes [36]. Similarly to what is observed for membranous ER activation, mGLUR1 activation leads to interactions with G-proteins and consequent phosphorylation and activation of signalling pathways, such as, Akt and MAPK [37,38]. Until now, no direct association between ER and GLUR1 was demonstrated, except for the stimulation of MCF7 cells with estradiol that resulted in increased mGLUR1 expression [37]. Since, in our study, glutamate levels were in the NMR detection limit, further analysis need to be pursued by using complementary methods, such as HPLC or colorimetric assays, to confirm our result.

The maintenance of the tumour heterogeneity is critical to more closely mimic the *in vivo* situation. Amongst the samples received, there was a high degree of heterogeneity between and within patients. For example, encapsulated explants from B7, a pure mucinous carcinoma, were mainly composed of epithelial cell clusters, that retained cell-cell adhesions, presumably through E-cadherin, with small lumina, and very low stromal and myoepithelial content, as illustrated by the vimentin and p63 immunostainings, respectively (Figure 5.4). Importantly, after 30 days of culture, we observed that tissue organization was very similar to the initial tumour (Figure 5.2), which corresponds to what is described for mucinous carcinomas. In fact, pure mucinous carcinomas are composed of epithelial cell clusters that can still form secondary lumina, floating in mucous, and present sparse fibrous stroma [19]. Case B18 was completely distinct - a less differentiated tumour where cells have lost the epithelial organization and have invaded the stroma, as typically observed for invasive ductal carcinomas [13]. Nonetheless, epithelial and stromal cells were still compartmentalized in the initial tumour (Figure 5.2), which resulted, after digestion, in encapsulated explants either uniquely formed by epithelial or stromal cells or mixed. Since alginate capsules allow paracrine signalling, through secretion of soluble factors [15], we speculated that the

occasional separation of epithelial and stromal cells in different capsules would still contribute to the heterotypic crosstalk, allowing the maintenance of the original tumour identity. Immune infiltrate ($CD45^+$ cells) were detected in 4 cases and were always in very low amounts. This is in accordance with the ER^+ tumours that typically present low immune infiltrates, due to their low proliferative and low mutagenic characteristics [14]. Nonetheless, the detection of immune cells after 30 days of culture is a major achievement and it might allow future studies on tumour-immune interactions.

PCA analysis of the 32 metabolites identified by exometabolome profiling led to sample separation into 2 clusters, mainly defined on PC1 (Figure 5.4C1). Samples from group 1 presented higher isoleucine concentration and were correlated with low cellularity, no proliferating cells and complete ablation of ER expression, in contrast to group 2 where lactate concentration was higher, samples presented high cellularity, proliferating cells and ER expression was detected. Isoleucine is a branched chain amino acid, important for protein synthesis [39]. Higher isoleucine concentrations might be correlated with decreased biosynthesis, which would be expected for samples with low cellularity and no proliferation. In contrast, higher lactate concentrations are expected for tumour samples metabolically more active, as samples in group 2. Lactate, is an end product of the increased glycolysis typically described for tumour cells as the Warburg effect [33]. It has been described as an onco-metabolite whose increased accumulation results in the acidification of the extracellular space, promoting tumour progression [40,41]. Overall the increased accumulation of lactate and consumption of isoleucine are a good indicative that after 30 days in culture, these micro-tumours still present metabolic and biosynthetic activity.

In conclusion, we have developed an *ex vivo* culture system for long-term maintenance of ER^+ human breast cancer explants. By providing a physical support to cells and orbital shaking conditions we were able to extend the life span of the tissue explants for at least 30 days. This system allowed the maintenance of epithelial and stromal compartments, ER expression, cell

proliferation and detection of $CD45^+$ cells. The partial tissue digestion allowed the maintenance of the original tissue architecture and cell behaviour consistent to what was expected for each histologic subtype. Fulvestrant treatment led to a mild increase in glutamate concentrations in the extracellular space and further assays are being pursued to confirm ER functionality. This system should allow the interrogation of the long-term effects of anti-ER. These can be applied for research purposes and for co-clinical assays. Although in an artificial environment, the long-term cultures of human-derived ER^+ BC explants might help predicting resistance to ongoing treatments whose early detection would not be possible in patients.

5 Acknowledgments

We gratefully acknowledge Dr Cathrin Brisken and Dr Georgios A. Sflomos for their mentoring, fruitful discussions and for all the time invested in teaching how to handle human breast tissue. We also thank Dr Elizabeth Anderson and Dr Joana Paredes for critical advice and to Joao Sá for his help with the NMR analysis and result interpretation.

6 References

[1] K. Boér, Fulvestrant in advanced breast cancer: evidence to date and place in therapy, Ther Adv Med Oncol. 9 (2017) 465–479. doi:10.1177/1758834017711097.

[2] N. Yoshida, Y. Omoto, A. Inoue, H. Eguchi, Y. Kobayashi, M. Kurosumi, et al., Prediction of prognosis of estrogen receptor-positive breast cancer with combination of selected estrogen-regulated genes, Cancer Sci. 95 (2004) 496–502.

[3] M.P.V. Shekhar, S. Santner, K.A. Carolin, L. Tait, Direct involvement of breast tumor fibroblasts in the modulation of tamoxifen sensitivity, Am. J. Pathol. 170 (2007) 1546–1560. doi:10.2353/ajpath.2007.061004.

[4] M.J. Bissell, W.C. Hines, Why don't we get more cancer? A proposed role of the microenvironment in restraining cancer progression, Nat. Med. 17 (2011) 320–329. doi:10.1038/nm.2328.

[5] K.-V. Nguyen-Ngoc, K.J. Cheung, A. Brenot, E.R. Shamir, R.S. Gray, W.C. Hines, et al., ECM microenvironment regulates collective migration and local dissemination in normal and malignant mammary epithelium, Proc. Natl. Acad. Sci. U.S.a. 109 (2012) E2595–604. doi:10.1073/pnas.1212834109.

[6] Z.I. Khamis, Z.J. Sahab, Q.-X.A. Sang, Active roles of tumor stroma in breast cancer metastasis, Int J Breast Cancer. 2012 (2012) 574025–10. doi:10.1155/2012/574025.

[7] K.S. Kang, I. Morita, A. Cruz, Y.J. Jeon, J.E. Trosko, C.C. Chang, Expression of estrogen receptors in a normal human breast epithelial cell type with luminal and stem cell characteristics and its neoplastically transformed cell lines, Carcinogenesis. 18 (1997) 251–257.

[8] H. van der Kuip, T.E. Mürdter, M. Sonnenberg, M. McClellan, S. Gutzeit, A. Gerteis, et al., Short term culture of breast cancer tissues to study the activity of the anticancer drug taxol in an intact tumor environment, BMC Cancer. 6 (2006) 86. doi:10.1186/1471-2407-6-86.

[9] E.J. Davies, M. Dong, M. Gutekunst, K. Närhi, H.J.A.A. van Zoggel, S. Blom, et al., Capturing complex tumour biology in vitro: histological and molecular characterisation of precision cut slices, Sci Rep. 5 (2015) 17187. doi:10.1038/srep17187.

[10] T. Tanos, G. Sflomos, P.C. Echeverria, A. Ayyanan, M. Gutierrez, J.-F. Delaloye, et al., Progesterone/RANKL is a major regulatory axis in the human breast, Sci Transl Med. 5 (2013) 182ra55–182ra55. doi:10.1126/scitranslmed.3005654.

[11] A.J. Fridriksdottir, J. Kim, R. Villadsen, M.C. Klitgaard, B.M. Hopkinson, O.W. Petersen, et al., Propagation of oestrogen receptor-positive and oestrogen-responsive normal human breast cells in culture, Nat Commun. 6 (2015) 8786. doi:10.1038/ncomms9786.

[12] M.G. Muraro, S. Muenst, V. Mele, L. Quagliata, G. Iezzi, A. Tzankov, et al., Ex-vivo assessment of drug response on breast cancer primary tissue with preserved microenvironments, Oncoimmunology. 6 (2017) e1331798. doi:10.1080/2162402X.2017.1331798.

[13] J. Makki, Diversity of Breast Carcinoma: Histological Subtypes and Clinical Relevance, Clin Med Insights Pathol. 8 (2015) 23–31. doi:10.4137/CPath.S31563.

[14] S.E. Stanton, M.L. Disis, Clinical significance of tumor-infiltrating lymphocytes in breast cancer, J Immunother Cancer. 4 (2016) 59. doi:10.1186/s40425-016-0165-6.

[15] M.F. Estrada, S.P. Rebelo, E.J. Davies, M.T. Pinto, H. Pereira, V.E. Santo, et al., Modelling the tumour microenvironment in long-term microencapsulated 3D co-cultures recapitulates phenotypic features of disease progression, Biomaterials. (2015). doi:10.1016/j.biomaterials.2015.11.030.

[16] G.D. Hill, PLANT ANTINUTRITIONAL FACTORS | Characteristics, Encyclopedia of Food Sciences and Nutrition. (2003) 4578–4587. doi:10.1016/B0-12-227055-X/01318-3.

[17] M. Overholtzer, A.A. Mailleux, G. Mouneimne, G. Normand, S.J. Schnitt, R.W. King, et al., A nonapoptotic cell death process, entosis, that occurs by cell-in-cell invasion, Cell. 131 (2007) 966–979. doi:10.1016/j.cell.2007.10.040.

[18] L. Lapeire, A. Hendrix, K. Lambein, M. Van Bockstal, G. Braems, R. Van Den Broecke, et al., Cancer-associated adipose tissue promotes breast cancer progression by paracrine oncostatin M and Jak/STAT3 signaling, Cancer Res. 74 (2014) 6806–6819. doi:10.1158/0008-5472.CAN-14-0160.

[19] A. Dumitru, A. Procop, A. Iliesiu, M. Tampa, L. Mitrache, M. Costache, et al., Mucinous Breast Cancer: a Review Study of 5 Year Experience from a Hospital-Based Series of Cases, Maedica (Buchar). 10 (2015) 14–18.

[20] A.J. Ewald, A. Brenot, M. Duong, B.S. Chan, Z. Werb, Collective epithelial migration and cell rearrangements drive mammary branching morphogenesis, Dev. Cell. 14 (2008) 570–581. doi:10.1016/j.devcel.2008.03.003.

[21] C.K. Osborne, A. Wakeling, R.I. Nicholson, Fulvestrant: an oestrogen receptor antagonist with a novel mechanism of action, British Journal of Cancer. 90 (2004) S2–S6. doi:10.1038/sj.bjc.6601629.

[22] G. Sflomos, V. Dormoy, T. Metsalu, R. Jeitziner, L. Battista, V. Scabia, et al., A Preclinical Model for ERα-Positive Breast Cancer Points to the Epithelial Microenvironment as Determinant of Luminal Phenotype and Hormone Response, Cancer Cell. 29 (2016) 407–422. doi:10.1016/j.ccell.2016.02.002.

[23] G. Mehta, A.Y. Hsiao, M. Ingram, G.D. Luker, S. Takayama, Opportunities and challenges for use of tumor spheroids as models to test drug delivery and efficacy, J Control Release. 164 (2012) 192–204. doi:10.1016/j.jconrel.2012.04.045.

[24] M. Jia, K. Dahlman-Wright, J.-Å. Gustafsson, Estrogen receptor alpha and beta in health and disease, Best Practice & Research Clinical Endocrinology & Metabolism. 29 (2015) 557–568. doi:10.1016/j.beem.2015.04.008.

[25] R.J. Buchsbaum, S.Y. Oh, Breast Cancer-Associated Fibroblasts: Where We Are and Where We Need to Go, Cancers (Basel). 8 (2016) 19. doi:10.3390/cancers8020019.

[26] S.E. Bulun, D. Chen, I. Moy, D.C. Brooks, H. Zhao, Aromatase, breast cancer and obesity: a complex interaction, Trends Endocrinol. Metab. 23 (2012) 83–89. doi:10.1016/j.tem.2011.10.003.

[27] M. Kurobe, S. Furukawa, K. Hayashi, Synthesis and secretion of an epidermal growth factor (EGF) by human fibroblast cells in culture, Biochem. Biophys. Res. Commun. 131 (1985) 1080–1085.

[28] M. Majety, L.P. Pradel, M. Gies, C.H. Ries, Fibroblasts Influence Survival and Therapeutic Response in a 3D Co-Culture Model, PLoS ONE. 10 (2015) e0127948. doi:10.1371/journal.pone.0127948.

[29] S. Kato, H. Endoh, Y. Masuhiro, T. Kitamoto, S. Uchiyama, H. Sasaki, et al., Activation of the estrogen receptor through phosphorylation by mitogen-activated protein kinase, Science. 270 (1995) 1491–1494.

[30] A. Zlotnik, B.F. Gruenbaum, B. Mohar, R. Kuts, S.E. Gruenbaum, S. Ohayon, et al., The effects of estrogen and progesterone on blood glutamate levels: evidence from changes of blood glutamate levels during the menstrual cycle in women, Biol. Reprod. 84 (2011) 581–586. doi:10.1095/biolreprod.110.088120.

[31] J. Fazzari, H. Lin, C. Murphy, R. Ungard, G. Singh, Inhibitors of glutamate release from breast cancer cells; new targets for cancer-induced bone-pain, Sci Rep. 5 (2015) 8380. doi:10.1038/srep08380.

[32] A. Stepulak, R. Rola, K. Polberg, C. Ikonomidou, Glutamate and its receptors in cancer, J Neural Transm (Vienna). 121 (2014) 933–944. doi:10.1007/s00702-014-1182-6.

[33] J.-P. Long, X.-N. Li, F. Zhang, Targeting metabolism in breast cancer: How far we can go? World J Clin Oncol. 7 (2016) 122–130. doi:10.5306/wjco.v7.i1.122.

[34] L.J. Yu, B.A. Wall, J. Wangari-Talbot, S. Chen, Metabotropic glutamate receptors in cancer, Neuropharmacology. 115 (2017) 193–202. doi:10.1016/j.neuropharm.2016.02.011.

[35] J. Pawlak, V. Brito, E. Küppers, C. Beyer, Regulation of glutamate transporter GLAST and GLT-1 expression in astrocytes by estrogen, Brain Res. Mol. Brain Res. 138 (2005) 1–7. doi:10.1016/j.molbrainres.2004.10.043.

[36] P. Micevych, J. Kuo, A. Christensen, Physiology of membrane oestrogen receptor signalling in reproduction, J. Neuroendocrinol. 21 (2009) 249–256. doi:10.1111/j.1365-2826.2009.01833.x.

[37] M.S. Mehta, S.C. Dolfi, R. Bronfenbrener, E. Bilal, C. Chen, D. Moore, et al., Metabotropic glutamate receptor 1 expression and its polymorphic variants associate with breast cancer phenotypes, PLoS ONE. 8 (2013) e69851. doi:10.1371/journal.pone.0069851.

[38] J.-M. Renoir, V. Marsaud, G. Lazennec, Estrogen receptor signaling as a target for novel breast cancer therapeutics, Biochem. Pharmacol. 85 (2013) 449–465. doi:10.1016/j.bcp.2012.10.018.

[39] E. Ananieva, Targeting amino acid metabolism in cancer growth and anti-tumor immune response, World J Biol Chem. 6 (2015) 281–289. doi:10.4331/wjbc.v6.i4.281.

[40] J. Penkert, T. Ripperger, M. Schieck, B. Schlegelberger, D. Steinemann, T. Illig, On metabolic reprogramming and tumor biology: A comprehensive survey of metabolism in breast cancer, Oncotarget. 7 (2016) 67626–67649. doi:10.18632/oncotarget.11759.

[41] P. Mishra, S. Ambs, Metabolic Signatures of Human Breast Cancer, Mol Cell Oncol. 2 (2015) e992217. doi:10.4161/23723556.2014.992217.

7 Supplementary Figure

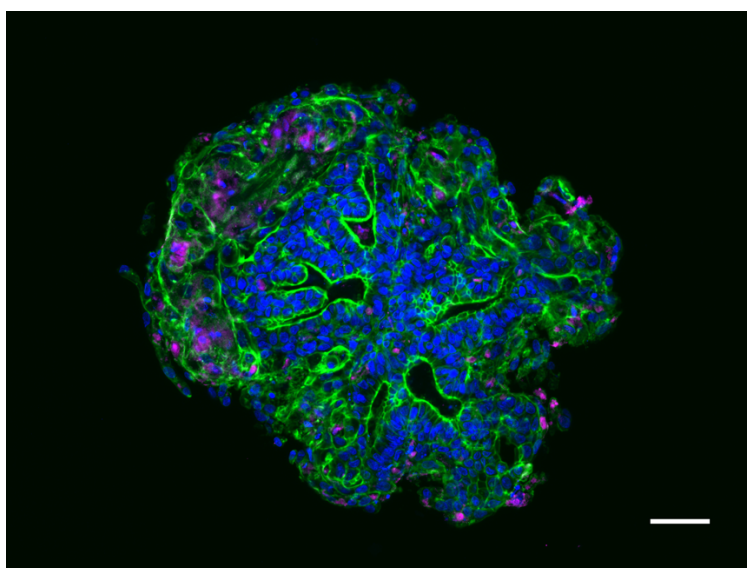

Figure S5.1: Phenotypic characterization of alginate encapsulated human breast explant cultures. Immunofluorescence microscopy of alginate capsules in 10 µm thick cryosections , at day 30, show human breast explant cultures: f-actin (phalloidin; green), Oestrogen receptor (ER, pink) and DAPI (blue). Scale bar: 50 µm,

Chapter VI

Improving MS identification of low molecular weight proteins in complex samples

Marta F Estrada, Sara Rosa, Ricardo Gomes, Cristina Peixoto, Paula M Alves, Patrícia Gomes-Alves, Catarina Brito. *Improving MS identification of low molecular weight proteins in complex samples*. Under submission.

Table of contents

Abstract 187
1 Introduction 188
2 Materials and Methods 190
2.1 Cell culture 190
2.2 Supernatant Harvest 191
2.3 Bovine Serum Albumin removal 191
2.4 Ammonium Sulphate precipitation 192
2.5 Protein quantification 192
2.6 BSA quantification 192
2.7 SDS-PAGE 193
2.8 In-gel digestion 193
2.9 In-solution digestion 193
2.10 Triple-TOF MS 194
2.11 Protein annotation 195
3 Results 195
3.1 Comparison of albumin depletion kits and fractionation methods 195
3.2 SDS-PAGE and Salting Out are complementary fractionation methodologies for the identification of LMW proteins 198
4 Discussion 200
5 References 202
6 Supplementary Figures 206

Abstract

Paracrine signalling occurs mainly through secretion of low molecular weight (LMW) proteins, such as cytokines, chemokines, growth factors and peptide hormones. Untargeted identification of signalling molecules has been hampered by the high dynamic range of protein concentrations, in cell culture supernatants supplemented with serum. In an attempt to improve the identification of low abundant low molecular weight (LMW) proteins, many strategies have been employed. Despite these efforts, none led to the substantial increase in the number of LMW proteins identified in cell culture supernatants. In this work we have combined two standard fractionation methods for sample decomplexation: SDS-PAGE and protein precipitation with ammonium sulphate. By using these methods, we improved 57 times the number of LMW proteins identified by MS-based techniques. Moreover, comparison of the proteins identified by each method revealed that these are complementary. Analysis of the protein lists with the Ingenuity Pathway Analysis software led to the prediction of 11 canonical pathways. This work demonstrates that simple in-house methods can be used for sample decomplexation improving significantly the identification of low abundant-LMW proteins. The methodology described is a feasible tool for untargeted analysis of the cell secretome. The identification of cytokines, growth factors or hormones can be useful to unravel cell signalling mechanisms and potentially contribute to uncover new targets/biomarkers of disease.

1 Introduction

Cellular crosstalk and inter-organ communication are major regulators of tissue homeostasis, inflammation and pathological states [1]. Neurodegenerative diseases [2,3], cancer [4] and type 2 diabetes mellitus [1,5] are examples of diseases in which modulation by heterotypic cell crosstalk has been described. The molecular mechanisms proposed are mostly related to remodelling of the extra-cellular matrix (ECM) and paracrine signalling through release of soluble factors, such as cytokines and growth factors [4,6]. Most of these secreted soluble factors are low molecular weight proteins (LMW; under 300 kDa), which also include peptide hormones, and peptides or proteins that originate from tissue leakage due to cell death [7]. However, the identification of LMW proteins has proven highly challenging due their low abundance [7] and high dynamic concentration range, when compared to highly abundant proteins (HAP), such as albumin [8,9]. In culture supernatants and in patient serum, HAP are a billion-fold more concentrated than low abundant LMW proteins [7]. Most studies based on cell models are performed using culture medium supplemented with serum, where albumin and other HAP, such as transferrin, immunoglobulins, fibrinogen, amongst others, mask the detection of low abundant LMW proteins [7,10]. As a strategy to reduce the high dynamic concentration range between HAP and LMW proteins, cells are typically subjected to serum starvation for 24-48h prior to medium collection [11-16]. However, this method is sub-optimal, since serum starvation causes cell stress leading to secretome alterations [17].

To overcome this challenge, several approaches for the identification of LMW proteins have been proposed in the past decades. These include untargeted mass spectrometry (MS)-based techniques and targeted antibody-based techniques [18]. The latter include enzyme-linked immunosorbent assays (ELISA) or antibody arrays, such as membrane bound antibodies for cytokine arrays and bead-based arrays [18-20]. MS-based techniques may require sample fractionation by size exclusion methods (gel-based or chromatography-based), organic solvent or inorganic salt precipitation, and

amino acid labelling with SILAC, ICAT or iTRAQ, prior to MS analysis [7,18]. Alternatively, affinity-based techniques, such as the commercially available albumin depletion kits, typically rely on antibody or ligand-based affinity depletion systems [21]. Nonetheless, albumin is a known carrier protein of many LMW proteins [22], resulting in the co-removal of bound proteins when using the albumin affinity-based methods [9,23,24]. Physiologically, LMW protein binding to albumin increases the solubility of the former in the serum, improving transport to specific tissues [25,26]. It also prevents the fast clearance of LMW proteins from the blood stream through glomerular filtration [7]. Albumin-LMW protein binding occurs through non-covalent interactions [7] that can either be electrostatic [22,25] or hydrophobic [27,28].

Sample fractionation methods are appealing alternatives as these are less expensive. Additionally, protein-protein interactions are typically destabilized during these procedures. A common approach is Sodium dodecyl sulphate polyacrylamide gel electrophoresis (SDS-PAGE). SDS-PAGE is a classical approach for sample preparation for MS-based proteome analysis [29] developed by Rosenfeld et al [30]. With this method, proteins are separated based on their molecular weight. Since it is performed in denaturing conditions, most hydrophobic and electrostatic protein interactions are broken [31]. Alternatively, protein precipitation with ammonium sulphate (AS) is a classical procedure for sample fractionation. This method relies on the salting-out effect of the protein when in the presence of a salt [32]. The dissolved salt competes with proteins for water molecules, which leads to exposure of the hydrophobic regions which ultimately causes hydrophobic collapse resulting in protein aggregation and precipitation. The salt saturation concentration necessary for protein precipitation is dependent on the physicochemical properties and concentration of the protein, as well as pH and temperature of the solution [33].

In this study, we have compared two affinity-based albumin removal kits with two fractionation methods: size exclusion by SDS-PAGE and protein precipitation by salting-out with AS. The methodologies were employed to process conditioned medium from 3D cultures of human fibroblasts [34]. The

culture medium was supplemented with 10% of fetal bovine serum (FBS) prior to cell culture and no serum starvation was performed before analysis. We report that the two fractionation approaches led to a substantial increase in the total number of proteins identified, including secreted LMW proteins, when compared to affinity-based methods. Moreover, SDS-PAGE and salting-out were complementary in terms of protein identification; the combination of the two methods led to a 57-fold increase in the number of LMW proteins identified, higher than the increase obtained by each of the individual methods employed.

These methods can be applied to the identification of LMW proteins in complex samples, such as complete cell culture medium or human/animal serum. Untargeted approaches for characterization of the cell secretome can potentially uncover novel cell signalling mechanisms modulating disease and drug response, with important implications in new target and biomarker discovery.

2 Materials and Methods

2.1 Cell culture

Human Dermal Fibroblasts (HDF), from Innoprot, were passaged once weekly for up to 12 passages at a seeding density of 0.5 X 10^4 cell/cm^2, in Iscove's Modified Dulbecco's Medium (IMDM) supplemented with 1% (v/v) penicillin-streptomycin and 10% (v/v) Fetal Bovine Serum (FBS; all from Life Technologies). HDFs were cultured in static culture systems, in an incubator at 37 ºC with humidified atmosphere containing 5% CO2 in air. For sub-culture, HDFs were trypsinized using 0.05% trypsin ethylenediaminetetraacetic acid (trypsin-EDTA, from Life Technologies), for 3-5 minutes. Viable cell concentration was determined by the trypan blue exclusion method, as described in [35].

HDFs were microencapsulated in alginate hydrogel, as described in [34]. Briefly, 25 X 10^6 cells were dispersed, as single cells, in 3 mL of 1.1% (w/v) of Ultrapure Ca_2^+ MVG alginate (UP MVG NovaMatrix, Pronova Biomedical, Oslo, Norway) dissolved in NaCl 0.9% (w/v) solution. Microencapsulation was

performed using an electrostatic bead generator (Nisco VarV1, Zurich, Switzerland), to produce beads of approximately 500 µm in diameter. The alginate droplets were cross-linked in a 100 mM $CaCl_2$/10 mM HEPES (pH 7.4) solution for 10 min, further washed three times in a 0.9% (w/v) NaCl solution and finally equilibrated in culture medium before being transferred to 125 mL stirred-tank vessels. The microencapsulated cultures were kept at 80 rpm, in a humidified incubator, with 5% CO2 in air, for 15 days with 50% medium exchange every 3-4 days.

2.2 Supernatant Harvest

Conditioned medium from HDFs was collected at day 15 of culture and clarified by centrifugation at 4ºC, first at 300× g and then at 1000x g for clearing live cells and cell debris, respectively. Clarified conditioned media was snap-frozen and stored at -80ºC until further use.

2.3 Bovine Serum Albumin removal

ProteoExtract Albumin Removal Kit (Millipore) and Pierce™ Albumin Depletion Kit (Thermo Fisher Scientific) were used to remove Bovine Serum Albumin (BSA) from the cell culture supernatants, according with the manufacturer's instructions.

To improve albumin removal, in the ProteoExtract Albumin Removal Kit, the number of medium passages per column and the number columns used varied as follows: 1 passage in 1 column; 2 passages in 1 column, 2 passages in 2 columns, 2 passages in 3 columns. For Pierce™ Albumin Depletion Kit, different buffer pH and salt concentrations were tested: 25 mM Tris, 75 mM NaCl, pH 7.5; 25 mM Tris, 25 mM NaCl, pH 7.5; 25 mM Tris, 25 mM NaCl, pH 6; 25 mM Tris, pH 7.5; 25 mM Tris, pH 6. Assay performance was analysed by SDS-PAGE.

2.4 Ammonium Sulphate precipitation

Conditioned media stored at -20ºC was thawed on ice and centrifuged at 15000× g for 15 minutes, at 4ºC. Ammonium sulphate (Millipore) was added to the supernatants to 20% of saturation. The samples were kept under continuous stirring, for 1 hour, at 4ºC. The precipitates were collected by centrifugation at 2000× g for 15 minutes at 4ºC. The pellets were dried at RT for 2 hours. To the remaining supernatants, the ammonium sulphate saturation was increased by 10%, to a saturation of 30%. The previous steps were repeated until the supernatant samples reached 70% ammonium sulphate saturation. The protein precipitates obtained in each step were dissolved in 0.1M of *Rapi*gest (Waters) surfactant, in 50 mM ammonium bicarbonate and boiled at 100ºC for 5 minutes.

2.5 Protein quantification

Pierce™ BCA Protein Assay Kit (Thermo Fisher Scientific) and Pierce™ Coomassie (Bradford) Protein Assay Kit (Thermo Fisher Scientific) were used to quantify total protein. Both assays were performed according to the manufacturer's instructions. Absorbance was measured using the Infinite 200 Pro plate reader (Tecan). Standard curves were prepared with BSA, in concentrations ranging from 0 - 2000 µg/mL.

2.6 BSA quantification

BSA concentration was assessed by BSA ELISA kit (Cygnus Technologies). The analysis was performed as described by the manufacturer's instructions. Absorbance was measured using an Infinite 200 Pro plate reader. Before analysis, the samples were diluted to a total protein concentration of 0.1 µg/mL with the BSA sample diluent supplied in the kit (Cygnus Technologies). BSA standard was used for the calibration curve, in concentrations raging from 0 to 32 ng/mL

2.7 SDS-PAGE

For SDS-PAGE, total protein from conditioned media was precipitated by the addition of ice cold EtOH to a final concentration of 80% (v/v). Samples were incubated overnight at -20ºC. Pellets were collected by centrifugation at 15 000 x g for 10 minutes at 4ºC. Pellets were then resuspendended in 10 µL of 8 M Urea and mixed with 10 µL of loading buffer (Invitrogen). The samples were loaded into 4–12% Bis–Tris NuPage® gels (Invitrogen), run under reducing conditions for 40 min (200 V, 400 mA) and stained with Simply Blue™ Safe Stain (Invitrogen). The gels were digitalized using Imagescanner III (GE Healthcare).

2.8 In-gel digestion

Protein in-gel digestion was performed in 4–12% Bis–Tris NuPage® gel (Invitrogen) loaded with 80 µg of sample, as above described. After staining, two lanes were excised into 12 gel fractions and independently digested with trypsin, as described in [36]. Briefly, gel fractions were destained using 50% (v/v) acetonitrile, reduced with 10 mM DTT, alkylated with iodoacetamide 55 mM, and digested at 37º C with 6.7 g\mL trypsin. Extraction of the digested peptides was performed using a water bath sonifier with alternate 100% acetonitrile and 5% formic acid incubations.

2.9 In-solution digestion

Protein pellets dissolved in 0.1M of *Rapi*gest (Waters), 50 mM ammonium bicarbonate were reduced with 10 mM of DTT for 40 minutes at 56ºC. Then, samples were alkylated with 20 mM iodoacetamide (IAA, 30 min at 20º C in the dark) and digested with trypsin overnight at 37ºC, using a trypsin:sample ratio of 1:50 [37]. Before MS analysis formic acid was added to a final concentration of 5%, samples were incubated for 30 minutes at 37ºC, centrifuged 10 minutes at 13 000x g and supernatants were dried until further analysis. Fractionated

samples were analysed both with and without desalting using home-made C18 microcolumns (3M Empore™ SPE).

2.10 Triple-TOF MS

Nano-liquid chromatography-tandem mass spectrometry (nanoLC-MS/MS) analysis was performed on an ekspert™ NanoLC 425 cHiPLC® system coupled with a TripleTOF® 6600 with a NanoSpray® III source (Sciex). Peptides were resuspended in 0.1% formic acid in water (Fisher Chemicals, Geel, Belgium) and separated through reversed-phase chromatography (RP-LC) in a trap-and-elute mode. Trapping was performed at 2 µl/min with 100% A (0.1% formic acid in water, Fisher Chemicals, Geel, Belgium), for 10 min, on a Nano cHiPLC Trap column (Sciex 200 µm x 0.5 mm, ChromXP C18-CL, 3 µm, 120 Å).

Separation was performed at 300 nl/min (90 min gradient), on a Nano cHiPLC column (Sciex 75 µm x 15 cm, ChromXP C18-CL, 3 µm, 120 Å).

Peptides were sprayed into the MS through an uncoated fused-silica PicoTip™ emitter (360 µm O.D., 20 µm I.D., 10 ± 1.0 µm tip I.D., New Objective, Oullins, France). The source parameters were set as follows: 12 GS1, 0 GS2, 30 CUR, 2.3 keV ISVF and 80 ºC IHT. An information dependent acquisition (IDA) method was set with a TOF-MS survey scan of 400-2000 m/z. The 40/50 most intense precursors were selected for subsequent fragmentation and the MS/MS were acquired in high sensitivity mode. The spectra obtained were processed and analysed using ProteinPilot™ software, with the Paragon search engine (version 5.0, Sciex). The search was performed against the Swissprot protein database (version 2015_05) with taxonomic restriction to *Homo sapiens*. Trypsin was selected as digestion type, Iodoacetamide was selected as source of Cys alkylation, gel-based ID was selected as a special factor (only when analysing the gel bands) and the TripleTOF 6600 as the Instrument. The ID focus was on biological modifications and Amino acid substitutions. The search effort was set as thorough. Only the proteins with Unused Protein Score above 1.3 and 95% confidence were considered.

2.11 Protein annotation

Analysis of the identified proteins was performed using Ingenuity Pathway Analysis (IPA), version 01-7, and the online tools DAVID Bioinformatics Resources 6.8 (https://david.ncifcrf.gov) and UniProt (http://www.uniprot.org).

3 Results

3.1 Comparison of albumin depletion kits and fractionation methods

To assess the best method for the identification of LMW proteins in culture medium, we used 10% FBS-containing medium, conditioned by human dermal fibroblasts in 3D cultures. Conditioned media was processed by several methodologies: commercially available affinity-based albumin depletion kits (the ProteoExtract Albumin Removal Kit or the Pierce™ Albumin Depletion Kit) followed by in-solution digestion; fractionation either by SDS-PAGE followed by in-gel digestion or by protein precipitation by salting out with AS followed by in-solution digestion.

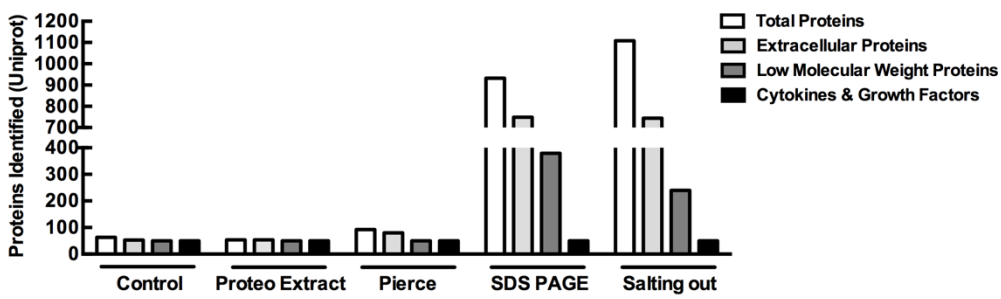

	Control	Proteo Extract	Pierce	SDS PAGE	Salting Out
Total Proteins	63	54	92	932	1108
Extracellular Proteins	53 (84.1%)	54 (100%)	80 (87%)	749 (80.4%)	744 (67.1%)
Low Molecular Weight (LMW) Proteins	8 (13%)	10 (19%)	26 (29%)	379 (41%)	240 (22%)
Cytokines & Growth factors	1 (1.6%)	0	1 (1.1%)	14 (1.5%)	17 (1.5%)

SDS PAGE & Salting out
1592
1097 (69%)
457 (29%)
17 (1.3%)

Figure 6.1: Secretome analysis of 10% FBS-containing culture medium conditioned by human dermal fibroblast. Proteins identified by MS-based techniques in fibroblast conditioned medium, after processing by four different methods: ProteoExtract Albumin Removal Kit (ProteoExtract), Pierce Albumin Depletion Kit (Pierce), SDS-PAGE and protein precipitation with AS (Salting out).

Protein annotation was performed with Ingenuity Pathway Analysis (IPA) and DAVID Bioinformatics Resources. Protein size was evaluated with UniProt.

As both albumin depletion kits employed were developed for human albumin removal, we performed several optimization steps following the manufacturer's suggestions to maximize the efficiency of BSA removal. Concerning the ProteoExtract kit, we manipulated the number of passages per column and the number of columns used for each sample. Employing 3 columns sequentially, with 2 passages per column, maximized albumin removal, although there was a decrease in the LMW proteins detected in the gel when compared to unprocessed samples (condition no. 5 Figure S6.1A), For the Pierce kit, the optimization steps were mostly focused on improving the antibody binding efficiency by manipulation of the pH and of the salt concentration of the binding buffer.

Condition no.2 (25 mM Tris, 75 mM NaCl, pH 7.5) was the most effective in removing BSA, as observed by SDS-PAGE (Figure S6.1B). Alternatively, conditioned medium was fractionated by SDS-PAGE and 11 fractions were collected from each lane (Figure S6.1C), or precipitated with AS. As the optimal salt concentration for precipitation of LMW proteins was not known, we started by adding AS to conditioned medium to attain a 20% salt saturation (0.8 M). Supernatants were then collected and salt concentration was increased by 10%, to reach 30% of salt saturation. Step-wise increments of 10% were performed until 70% of salt saturation (approximately 3 M) was achieved; a total of 6 fractions were obtained (Figure S6.1D). Mass Spectrometry (MS)-based protein identification was performed on samples processed under the conditions optimized for each of the albumin removal kits and by the two fractionation methods.

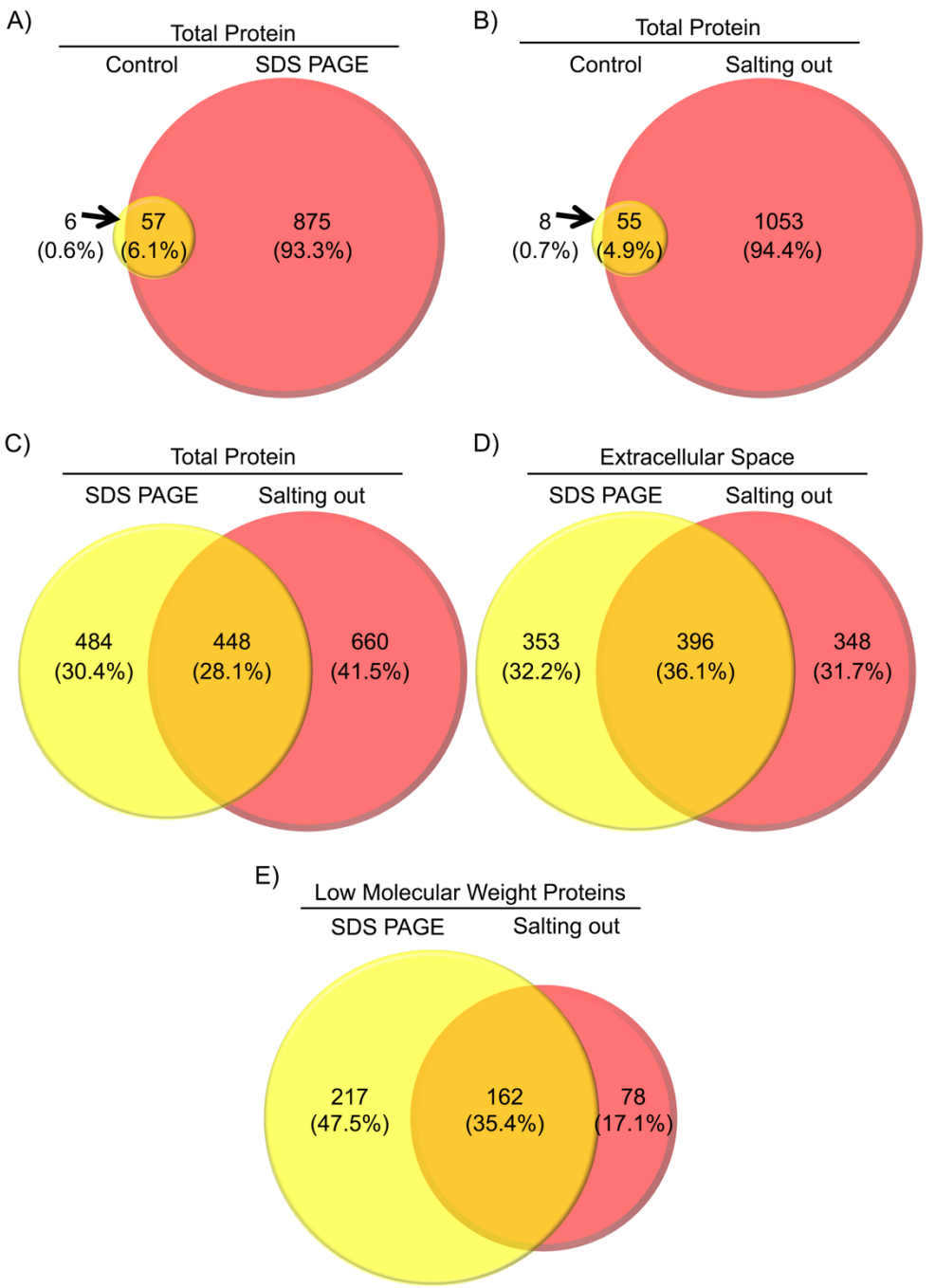

Figure 6.2: Proteins identified in fibroblast conditioned medium after sample decomplexation by fractionation methods. The Venn diagrams illustrate the number of proteins identified in: the 11 gel fractions obtained by SDS-PAGE vs unprocessed

sample (A); the 6 fractions obtained by protein precipitation with AS (salting out) vs unprocessed sample (B); total (C), extracellular (D) and low molecular weight (E) proteins identified after fractionation by SDS-PAGE vs protein precipitation with AS (salting out).

The number of proteins identified by each method was distinct (Figure 6.1). With the ProteoExtract and Pierce kits, the number of total proteins identified was of 54 and 92, respectively. These were within the same range of the number of proteins identified in the unprocessed sample (control, 63 proteins). The number of LMW proteins identified was of 10 and 26, for ProteoExtract and Pierce, respectively, also within the range of the number of LMW proteins identified in the control condition (8 proteins). Nonetheless, in both methods there was a reduction in the number of albumin peptides identified (Figure S6.2). In contrast, both fractionation methods led to the identification of a total number of proteins approximately 17 times higher than in the control, a notable increase. For both SDS-PAGE and salting out, approximately 750 extracellular proteins (ECP) were identified, compared to 53 in the control. The number of LMW proteins identified was 30-fold higher in the fractionated conditions than the control sample and the number of cytokines and growth factors was also higher (14 and 17 proteins, for SDS-PAGE and salting out, respectively vs 1 in control).

3.2 SDS-PAGE and Salting Out are complementary fractionation methodologies for the identification of LMW proteins

Although the number of proteins identified by each of the fractionation methods was similar, protein identity differed (Figure 6.2). Combining the proteins identified by both methods raised the total number of proteins to 1592, of which 1097 were ECP and 457 were LMW proteins (Figure 6.1B). SDS-PAGE was the most efficient method concerning the enrichment in LMW proteins: 47.5% were identified after SDS-PAGE fractionation, compared to the 17.1% obtained after salting out (Figure 6.2E). Nonetheless, the percentage of

total proteins and ECP identified was similar in both methods (approximately 30%; Figure 6.2C and D). Despite these improvements, albumin peptides were still detected in all fractions (Figure S6.2).

Most of the LMW proteins secreted by cells are cytokines, chemokines, growth factors and peptide hormones, which are typically involved in the activation of specific signalling pathways. Canonical pathway analysis of the LMW protein dataset was carried out using IPA software (Figure 6.3). The analysis rendered the identification of 11 canonical pathways (-log (p-values) above 1.3, Figure 6.3), potentially activated in human dermal fibroblast 3D cultures. The pathways with higher -log (p-values) (≥2.5) were the Insulin Growth Factor-1 signalling pathway, the superoxide radical degradation and the antigen presentation pathways. In contrast, the unprocessed sample led to the prediction of only one pathway with a -log (p-value) above 1.3 (growth hormone signalling; data not shown).

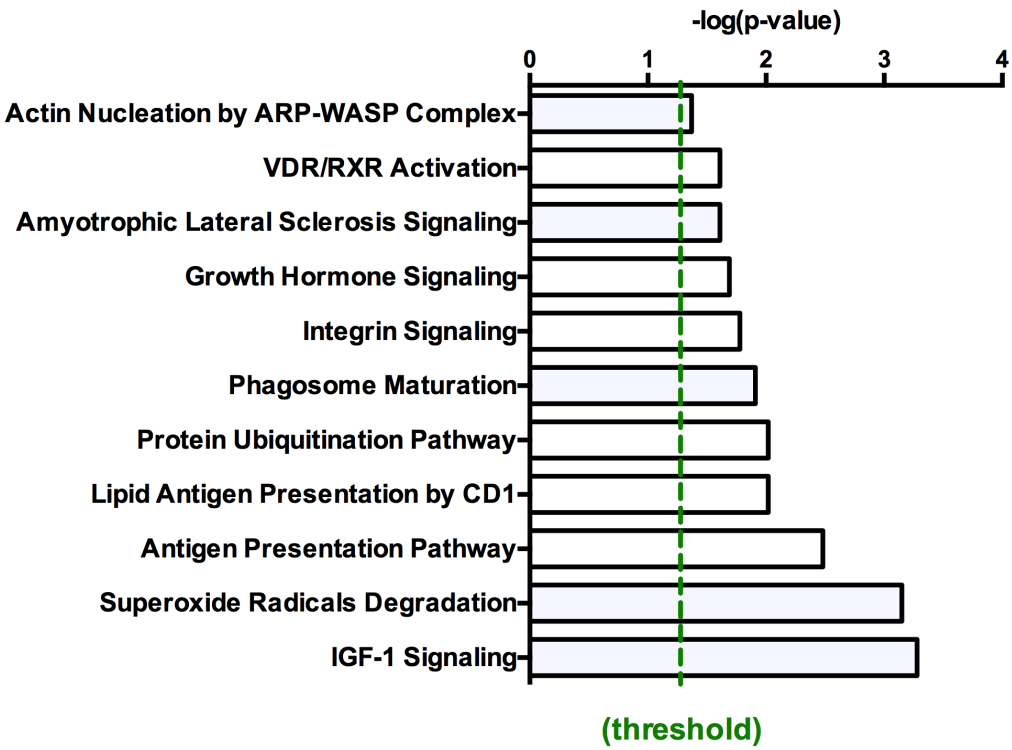

Figure 6.3: IPA analysis of the low molecular weight proteins identified. Bar chart displays the canonical pathways predicted by the Ingenuity Pathway Analysis

software, with the combination of the LMW proteins identified after sample processing with the 2 fractionation methods.

4 Discussion

Proteome profiling of the cell secretome is highly compromised by the high dynamic range of protein concentrations which accounts for at least billion-fold of difference between HAP like albumin, and LMW proteins - such as cytokines, chemokines, growth factors and peptide hormones [7,9]. As a result, HAP hamper the identification of LMW proteins [7]. To tackle this issue, many attempts have been made towards decomplexation of cell culture supernatants and of human serum samples [7,10]. However, most of the available methods rely on affinity-based techniques or filtration techniques that potentially lead to the co-removal of LMW proteins bound to the HAP [22-24].

In this work we have combined two distinct fractionation strategies - SDS-PAGE followed by in-gel digestion and protein precipitation by salting out with AS followed by in-solution digestion to improve the identification of LMW proteins of the cell secretome. The samples tested consisted in culture medium supplemented with 10% FBS, conditioned by human fibroblasts cultured in 3D for 15 days. The combination of the two fractionation strategies increased by 57 times the number of LMW proteins identified (457 vs 8 in the unprocessed conditioned medium).

Our results show that affinity-based albumin removal kits led to a reduction on the number of BSA peptides (Figure S6.2), despite being optimized for removal of human albumin. However, these approaches did not improve the identification of LMW proteins nor increased the total number of identified proteins (Figure 6.1). This may be explained by the fact that albumin is a carrier of many LMW proteins, such as cytokines and growth factors [22]. Amongst others, these interactions avoid fast cytokine clearance from the blood stream through glomerular filtering [7,25]. Efficient sample decomplexation would require a first step of destabilization of protein-protein interactions. Most albumin-LMW protein interactions are non-covalent [7], either electrostatic

[22,25] or hydrophobic [27,28]. Due to the strength and different nature of these interactions, effective destabilization would probably interfere with albumin conformation and consequently binding to the affinity resins of the albumin removal columns. In addition, other HAP, such as immunoglobulins and fibrinogen also contribute to mask the detection of LMW proteins [7,10].

In order to reduce the high dynamic range of concentrations between high and low abundant proteins we chose two low-cost methods, available in-house, that do not require maintenance of protein conformation: SDS-PAGE and protein precipitation by salting out with saturating concentrations of AS. These methods led to a substantial increase in the total number of identified proteins to 1592 (Figures 6.1 and 6.2). Of these, 1097 were extracellular; intracellular proteins were also identified (31%), probably released due to cell death [9]. Aiming at characterizing human dermal fibroblast secretome, we pursued the analysis of ECP. Although the number of ECP proteins identified was similar, protein identity revealed that these methods were in fact complementary (Figure 6.2). Approximately one third of the identified ECP were exclusive to each of the methods and only one third was common to both (Figure 6.2D). This complementarity was also observed for the LMW proteins: 47.5% were exclusive to fractionation by SDS-PAGE whilst AS precipitation rendered 17.1% of the identified LMW proteins (Figure 6.2E). It is possible that LMW proteins co-precipitated in the same fraction of their carriers since AS only allows a 2 to 5 times purification from the previous fraction [38]. Another hypothesis is the co-precipitation due to incomplete dissociation of LMW proteins from their carrier proteins, although less likely. The principle for AS salting out is the destabilization of electrostatic interactions causing exposure of the hydrophobic regions leading to hydrophobic collapse [39]. Although a full characterization of the thermodynamics of their association would be required, typically, disruption of protein-protein interactions requires less energy than the interactions needed to maintain protein structure [40]. Nevertheless, the combined use of these methodologies increased the number of LMW proteins identified by 57 times, when compared with the identification of unprocessed condition and the affinity-

based albumin removal techniques. This result shows that the low-cost methods can be used for decomplexation of cell culture supernatants, overcoming the need for serum starvation that will change the cell physiological status and can therefore lead to changes in cell secretome.

Canonical Pathway Analysis by IPA of the proteins identified with both fractionation methods predicted 11 canonical pathways, in contrast with the untreated control where only 1 canonical pathway was predicted, with -log (p-values) above 1.3. Amongst the 11 predicted canonical pathways, the Insulin Growth Factor -1 (IGF-1) signalling was the one presenting the higher p-value. IGF-1 is produced by many cell types, namely, by dermal fibroblasts [41]. In the dermis it plays a protective role in keratinocytes and is activated in response to UV exposure [41]. In addition, in the mammary epithelium, it is known to be a potent mitogenic and to be associated with breast cancer development, progression and metastasis [42]. In this case, IPA prediction is merely indicative since MS analysis was not quantitative. Nonetheless, it poses a proof-of-concept that these methods can be used for identification of novel molecular players paving the way to unravel new mechanisms of cellular crosstalk and potential identification of biomarkers.

5 References

[1] J. Eckel, The Cellular Secretome and Organ Crosstalk, Academic Press, 2018.

[2] F.G. Teixeira, M.M. Carvalho, K.M. Panchalingam, A.J. Rodrigues, B. Mendes-Pinheiro, S. Anjo, et al., Impact of the Secretome of Human Mesenchymal Stem Cells on Brain Structure and Animal Behavior in a Rat Model of Parkinson's Disease, Stem Cells Transl Med. 6 (2017) 634–646. doi:10.5966/sctm.2016-0071.

[3] N.J. Abbott, L. Rönnbäck, E. Hansson, Astrocyte-endothelial interactions at the blood-brain barrier, Nat. Rev. Neurosci. 7 (2006) 41–53. doi:10.1038/nrn1824.

[4] M.J. Bissell, W.C. Hines, Why don't we get more cancer? A proposed role of the microenvironment in restraining cancer progression, Nat. Med. 17 (2011) 320–329. doi:10.1038/nm.2328.

[5] E.D. Rosen, B.M. Spiegelman, Adipocytes as regulators of energy balance and glucose homeostasis, Nature. 444 (2006) 847–853. doi:10.1038/nature05483.

[6] S.Y. Kim, B.E. Porter, A. Friedman, D. Kaufer, A potential role for glia-derived extracellular matrix remodeling in postinjury epilepsy, J. Neurosci. Res. 94 (2016) 794–803. doi:10.1002/jnr.23758.

[7] T. Cai, F. Yang, Strategies for Characterization of Low-Abundant Intact or Truncated Low-Molecular-Weight Proteins From Human Plasma, Enzymes. 42 (2017) 105–123. doi:10.1016/bs.enz.2017.08.004.

[8] C.E. Parker, C.H. Borchers, Mass spectrometry based biomarker discovery, verification, and validation--quality assurance and control of protein biomarker assays, Mol Oncol. 8 (2014) 840–858. doi:10.1016/j.molonc.2014.03.006.

[9] R.S. Tirumalai, K.C. Chan, D.A. Prieto, H.J. Issaq, T.P. Conrads, T.D. Veenstra, Characterization of the low molecular weight human serum proteome, Mol. Cell Proteomics. 2 (2003) 1096–1103. doi:10.1074/mcp.M300031-MCP200.

[10] R. Millioni, S. Tolin, L. Puricelli, S. Sbrignadello, G.P. Fadini, P. Tessari, et al., High abundance proteins depletion vs low abundance proteins enrichment: comparison of methods to reduce the plasma proteome complexity, PLoS ONE. 6 (2011) e19603. doi:10.1371/journal.pone.0019603.

[11] L. Yao, Y. Zhang, K. Chen, X. Hu, L.X. Xu, Discovery of IL-18 as a novel secreted protein contributing to doxorubicin resistance by comparative secretome analysis of MCF-7 and MCF-7/Dox, PLoS ONE. 6 (2011) e24684–. doi:10.1371/journal.pone.0024684.

[12] C.-C. Wu, C.-W. Hsu, C.-D. Chen, C.-J. Yu, K.-P. Chang, D.-I. Tai, et al., Candidate serological biomarkers for cancer identified from the secretomes of 23 cancer cell lines and the human protein atlas, Mol. Cell Proteomics. 9 (2010) 1100–1117. doi:10.1074/mcp.M900398-MCP200.

[13] M.A. Blanco, G. LeRoy, Z. Khan, M. Alečković, B.M. Zee, B.A. Garcia, et al., Global secretome analysis identifies novel mediators of bone metastasis, Cell Research. 22 (2012) 1339–1355. doi:10.1038/cr.2012.89.

[14] T.B.M. Schaaij-Visser, M. de Wit, S.W. Lam, C.R. Jiménez, The cancer secretome, current status and opportunities in the lung, breast and colorectal cancer context, Biochim. Biophys. Acta. 1834 (2013) 2242–2258. doi:10.1016/j.bbapap.2013.01.029.

[15] K. Lawrenson, P. Mhawech-Fauceglia, J. Worthington, T.J. Spindler, D. O'Brien, J.M. Lee, et al., Identification of novel candidate biomarkers of epithelial ovarian cancer by profiling the secretomes of three-dimensional genetic models of ovarian carcinogenesis, Int. J. Cancer. 137 (2015) 1806–1817. doi:10.1002/ijc.29197.

[16] X. Liang, J. Huuskonen, M. Hajivandi, R. Manzanedo, P. Predki, J.R. Amshey, et al., Identification and quantification of proteins differentially secreted by a pair of normal and malignant breast-cancer cell lines, Proteomics. 9 (2009) 182–193. doi:10.1002/pmic.200700957.

[17] S. Pirkmajer, A.V. Chibalin, Serum starvation: caveat emptor, Am. J. Physiol., Cell Physiol. 301 (2011) C272–9. doi:10.1152/ajpcell.00091.2011.

[18] Á. Marrugal, L. Ojeda, L. Paz-Ares, S. Molina-Pinelo, I. Ferrer, Corrigendum to "Proteomic-Based Approaches for the Study of Cytokines in Lung Cancer", Dis. Markers. 2018 (2018) 1404780–1. doi:10.1155/2018/1404780.

[19] A. Khan, Detection and quantitation of forty eight cytokines, chemokines, growth factors and nine acute phase proteins in healthy human plasma, saliva and urine, J Proteomics. 75 (2012) 4802–4819. doi:10.1016/j.jprot.2012.05.018.

[20] L. Zhong, J. Roybal, R. Chaerkady, W. Zhang, K. Choi, C.A. Alvarez, et al., Identification of secreted proteins that mediate cell-cell interactions in an in vitro model of the lung cancer microenvironment, Cancer Res. 68 (2008) 7237–7245. doi:10.1158/0008-5472.CAN-08-1529.

[21] M. Stastna, J.E. Van Eyk, Investigating the secretome: lessons about the cells that comprise the heart, Circ Cardiovasc Genet. 5 (2012) o8–o18. doi:10.1161/CIRCGENETICS.111.960187.

[22] J.L. Richens, E.A.M. Lunt, D. Sanger, G. McKenzie, P. O'Shea, Avoiding nonspecific interactions in studies of the plasma proteome: practical solutions to prevention of nonspecific interactions for label-free detection of low-abundance plasma proteins, J. Proteome Res. 8 (2009) 5103–5110. doi:10.1021/pr900487y.

[23] J. Granger, J. Siddiqui, S. Copeland, D. Remick, Albumin depletion of human plasma also removes low abundance proteins including the cytokines, Proteomics. 5 (2005) 4713–4718. doi:10.1002/pmic.200401331.

[24] S.-B. Ahn, A. Khan, Detection and quantitation of twenty-seven cytokines, chemokines and growth factors pre- and post-high abundance protein depletion in human plasma, EuPA Open Proteomics. 3 (2014) 78–84. doi:10.1016/j.euprot.2014.02.012.

[25] V. Arroyo, R. García-Martinez, X. Salvatella, Human serum albumin, systemic inflammation, and cirrhosis, J. Hepatol. 61 (2014) 396–407. doi:10.1016/j.jhep.2014.04.012.

[26] T.-A. Chen, Y.-C. Tsao, A. Chen, G.-H. Lo, C.-K. Lin, H.-C. Yu, et al., Effect of intravenous albumin on endotoxin removal, cytokines, and nitric oxide production in patients with cirrhosis and spontaneous bacterial peritonitis, Scand. J. Gastroenterol. 44 (2009) 619–625. doi:10.1080/00365520902719273.

[27] A.I. Denesyuk, M.S. Johnson, V.P. Zav'yalov, T. Korpela, Structure of cytokine hydrophobic cores, J. Theor. Biol. 180 (1996) 297–307. doi:10.1006/jtbi.1996.0104.

[28] A. Hawe, W. Friess, Stabilization of a hydrophobic recombinant cytokine by human serum albumin, J Pharm Sci. 96 (2007) 2987–2999. doi:10.1002/jps.20909.

[29] J.R. Wiśniewski, A. Zougman, N. Nagaraj, M. Mann, Universal sample preparation method for proteome analysis, Nat. Methods. 6 (2009) 359–362. doi:10.1038/nmeth.1322.

[30] J. Rosenfeld, J. Capdevielle, J.C. Guillemot, P. Ferrara, In-gel digestion of proteins for internal sequence analysis after one- or two-dimensional gel electrophoresis, Anal. Biochem. 203 (1992) 173–179.

[31] A. Shevchenko, H. Tomas, J. Havlis, J.V. Olsen, M. Mann, In-gel digestion for mass spectrometric characterization of proteins and proteomes, Nat Protoc. 1 (2006) 2856–2860. doi:10.1038/nprot.2006.468.

[32] K.C. Duong-Ly, S.B. Gabelli, Salting out of proteins using ammonium sulfate precipitation, Meth. Enzymol. 541 (2014) 85–94. doi:10.1016/B978-0-12-420119-4.00007-0.

[33] Y.U. Moon, R.A. Curtis, C.O. Anderson, H.W. Blanch, J.M. Prausnitz, Protein—Protein Interactions in Aqueous Ammonium Sulfate Solutions. Lysozyme and Bovine Serum Albumin (BSA), Journal of Solution Chemistry. 29 (2000) 699–718.

[34] M.F. Estrada, S.P. Rebelo, E.J. Davies, M.T. Pinto, H. Pereira, V.E. Santo, et al., Modelling the tumour microenvironment in long-term microencapsulated 3D co-cultures recapitulates phenotypic features of disease progression, Biomaterials. (2015). doi:10.1016/j.biomaterials.2015.11.030.

[35] V.E. Santo, M.F. Estrada, S.P. Rebelo, S. Abreu, I. Silva, C. Pinto, et al., Adaptable stirred-tank culture strategies for large scale production of multicellular spheroid-based tumor cell models, Journal of Biotechnology. 221 (2016) 118–129.

[36] H.R. Soares, R. Castro, H.A. Tomás, A.F. Rodrigues, P. Gomes-Alves, B. Bellier, et al., Tetraspanins displayed in retrovirus-derived virus-like particles and their immunogenicity, Vaccine. 34 (2016) 1634–1641. doi:10.1016/j.vaccine.2015.12.015.

[37] B. Cunha, T. Aguiar, S.B. Carvalho, M.M. Silva, R.A. Gomes, M.J.T. Carrondo, et al., Bioprocess integration for human mesenchymal stem cells: From up to downstream processing scale-up to cell proteome characterization, Journal of Biotechnology. 248 (2017) 87–98. doi:10.1016/j.jbiotec.2017.01.014.

[38] S. Englard, S. Seifter, Precipitation techniques, Meth. Enzymol. 182 (1990) 285–300.

[39] R.R. Burgess, Protein precipitation techniques, Meth. Enzymol. 463 (2009) 331–342. doi:10.1016/S0076-6879(09)63020-2.

[40] Y.V. Sergeev, M.B. Dolinska, P.T. Wingfield, The thermodynamic analysis of weak protein interactions using sedimentation equilibrium, Curr Protoc Protein Sci. 77 (2014) 20.13.1–20.13.15.

[41] D.A. Lewis, J.B. Travers, A.-K. Somani, D.F. Spandau, The IGF-1/IGF-1R signaling axis in the skin: a new role for the dermis in aging-associated skin cancer, Oncogene. 29 (2010) 1475–1485. doi:10.1038/onc.2009.440.

[42] P.F. Christopoulos, P. Msaouel, M. Koutsilieris, The role of the insulin-like growth factor-1 system in breast cancer, Mol. Cancer. 14 (2015) 43. doi:10.1186/s12943-015-0291-7.

6 Supplementary Figures

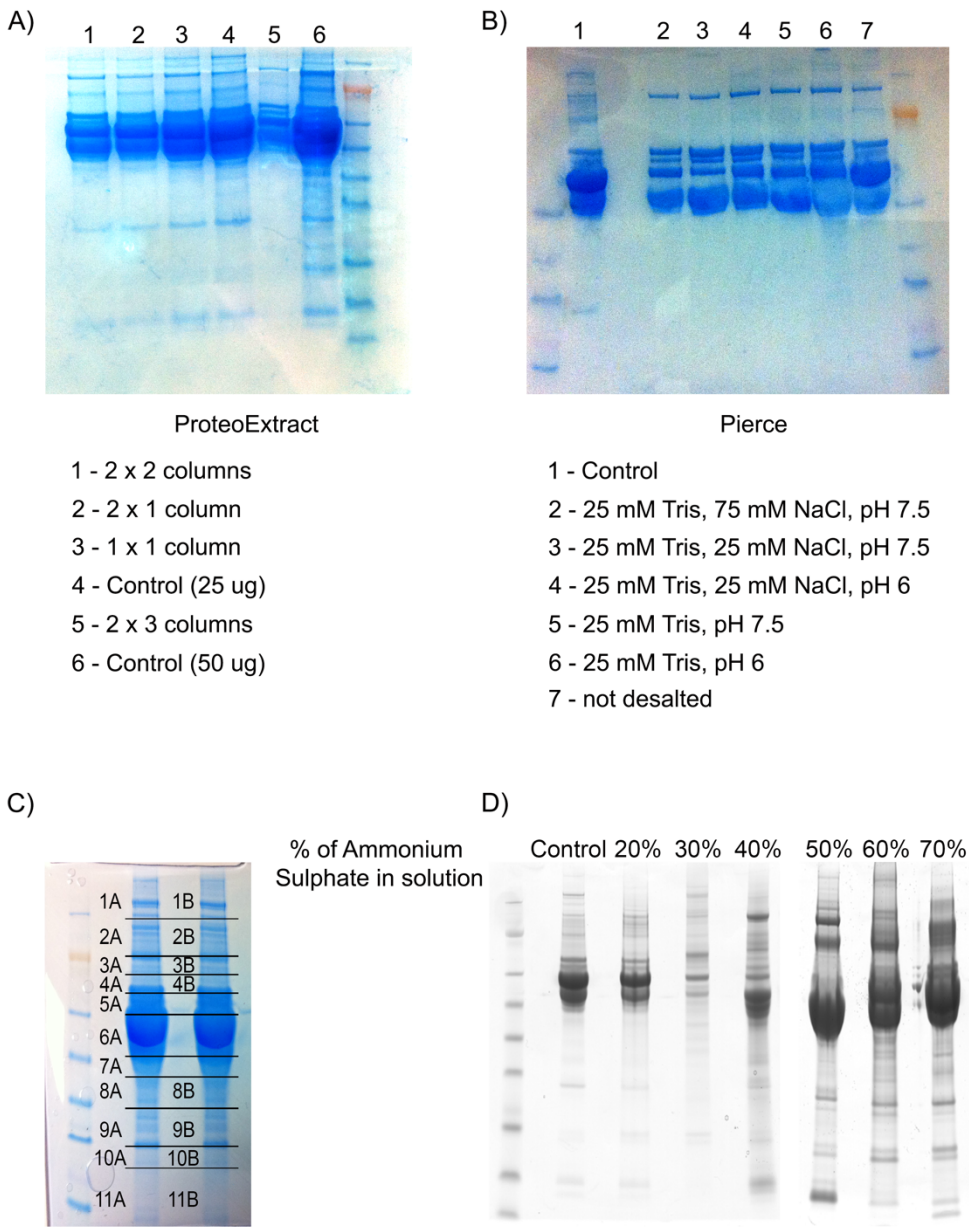

Figure S6.1: **SDS-PAGE of the conditions tested for optimization of bovine serum albumin (BSA) removal** with (A) ProteoExtract Albumin Removal Kit; (B) Pierce Albumin Depletion Kit; (C) SDS PAGE fractionation and (D) protein precipitation with ammonium sulphate.

	Albumin peptides	SDS Page		Salting out	
		Lane nº	Albumin peptides	Fraction	Albumin peptides
Control	160	1	80	20%	140
ProteoExtract	112	2	40	30%	65
Pierce	57	3	84	40%	34
		4	130	50%	16
		5	106	60%	15
		6	224	70%	1
		7	425		
		8	138		
		9	143		
		10	39		
		11	55		

Figure S6.2: Albumin peptides identified by MS-based techniques, after sample decomplexation by 4 different strategies. ProteoExtract Albumin Removal Kit, Pierce Albumin Depletion Kit, SDS-PAGE-in-gel digestion and protein precipitation with ammonium sulphate.

Chapter VII

Discussion and Perspectives

Table of Contents

1 Discussion 211
1.1 Modulation of the tumour microenvironment in long-term microencapsulated 3D cultures recapitulates features of disease progression 213
1.2 Influence of the culture system on tumour and stromal cell behaviour 217
1.3 Development of human breast cancer models: complementarity between *in vitro* and *ex vivo* models 219
2 Conclusions and perspectives 222
3 References 224

1 Discussion

Oestrogen Receptor positive (ER^+) breast cancers represent more than 70% of all breast cancers and have a favourable prognosis due to good response to endocrine therapy. However, the disease often relapses 5-10 years after diagnosis, due to drug resistance and metastatic behaviour [1]. Although many progresses have been made in the past decades, there is still a lack of understanding on the mechanisms behind disease progression and drug resistance. The tumour microenvironment plays a pivotal role in these mechanisms, through the secretion of matrix components, enzymes and soluble factors that, together, modulate tumour cell behaviour [2,3]. Thus, the development of long-term culture systems capable of recapitulating features of the tumour microenvironment, and amenable for interrogation of disease progression and drug response mechanisms, are a major challenge in the cancer research field.

The work described in this thesis aimed at developing new pre-clinical and co-clinical models that would better mimic the tumour microenvironment and recapitulate tumour progression. With this purpose, long-term culture model systems were developed by combining cell microencapsulation in alginate, an inert scaffold, and stirred culture systems. This strategy was developed and implemented for *in vitro* co-cultures of cell-line derived spheroids and primary human fibroblasts (**Chapter 2** and **Chapter 3**), and later extended to *ex vivo* cultures of human-derived ER^+ breast cancer explants (**Chapter 5**). A cross comparison of the developed cell-line based model with alternative *in vitro* model systems was also performed (**Chapter 4**). Moreover, a wide range of characterization methods were implemented and/or improved, such as imaging, metabolomics, proteomics and development of data mining approaches. The major contributions were the development of new strategies for evaluation of the cell secretome, under physiological conditions (**Chapter 6**) and the collaboration on the development of a novel high-throughput light-sheet microscopy tool, for fast evaluation of the phenotypic alterations occurring in the long-term heterotypic cultures. Altogether, these models are expected to

contribute to improve the clinical translational success rates and help predict the acquisition of resistance mechanisms to specific drug treatments.

	Aim	Strategy	Achievements
Chapter 2	Optimize stirred-tank culture strategies for large scale production of multicellular tumour spheroids	Manipulation of the cell inoculum, stirring rate and aggregation time, for breast, lung and colon cancer cell lines	**1.** Efficient cell aggregation; **2.** Maintenance of cell-line dependent spheroid phenotype: - spheroid size distribution, - epithelial cell compactness and organization, - stromal cell distribution, - oxygen gradients
Chapter 3	Develop a strategy for reconstruction of the TME and recapitulation of disease progression features	Combination of stirred-tank culture systems and alginate microencapsulation of tumour spheroids and human fibroblasts	**1.** Epithelial cell organization in tissue-like structures **2.** Creation of distinct epithelial and stromal compartments **3.** Reconstruction of features of the TME **4.** Recapitulation of key aspects of tumour progression
Chapter 4	Evaluate the influence of the culture system on tumour and stromal cell behaviour	Cross-comparison of 2D and 3D heterotypic culture systems	**1.** Successfull harmonization of cell culture conditions and analytical methods **2.** Acquisition of distinct phenotypes depending on the culture system **3.** Protective effect of fibroblasts against SOC treatments
Chapter 5	Optimize a culture strategy for *ex vivo* culture of patient-derived ER+ BC explants	Combination of agitation-based system with alginate encapsulation of patient-derived explants	**1.** Long-term maintenance of tumour architecture and phenotype **2.** Maintenance of ER expression and functionality maintained *ex vivo*
Chapter 6	Improve identification of low abundant-low molecular weight proteins from cell culture conditioned media, by MS-based methods	Sample pre-fractionation by 1D SDS PAGE in-gel digestion and protein precipitation with Amonium Sulphate	**1.** Improvement of the number of low abundant-low molecular weight proteins identified by MS-based techniques improved 57 times

1.1 Modulation of the tumour microenvironment in long-term microencapsulated 3D cultures recapitulates features of disease progression

As referred in the introductory section, numerous 3D *in vitro* tumour models have been developed in the past decade, aiming at recapitulating the tumour microenvironment. However, these models are generated in short-term culture systems, with no control of the physicochemical parameters and allow only for end-point analysis [4-6]. Additionally, most of these models make use of bioactive scaffolds, that alone modulate tumour and stromal cell phenotype, namely through the presence of cytokines, growth factors, and extracellular matrix (ECM) content and cross-linking [7-9]. In contrast, inert biocompatible scaffolds provide physical support to cells, allow cell-to-cell communication, accumulation of secreted factors and cell migration [10]. Nonetheless, the stiffness of the matrix also influences cell behaviour through tensional forces that promote activation of specific signalling pathways [11]. One example is the activation of fibroblasts into myofibroblasts upon culture in a PEG hydrogel with higher stiffness [12]. Additionally, [13] it was also shown that intestinal stem cells (ISC) required higher matrix stiffness (1.3 kPa) for survival and proliferation whilst matrix softening (300 Pa) led to ISC differentiation and organoid formation.

When modelling the tissue architecture, it is important to consider not only the epithelial compartment, but also the surrounding microenvironment, since it confers physical support to tumour cells and provides signals to specific epithelial pathways, both in tissue homeostasis and in cancer [14]. The breast tumour microenvironment is composed by a network of fibroblasts, immune cells and adipocytes embedded in an ECM that allows cell migration and accumulation/release of soluble and insoluble factors [14].

These components interact with epithelial cells and directly modulate tumour behaviour towards more or less aggressive stages of the disease [2]. To study the establishment and consequence of these interactions (cell-cell and cell-matrix) we developed an *in vitro* model that combines alginate

microencapsulation of tumour cell spheroids with primary human fibroblasts (co-cultures), cultured in stirred-tank culture systems, up to 20 days.

Tumour cell aggregation, in stirring conditions, was optimized in **chapter 2**, through manipulation of cell inoculum, stirring rate and aggregation time. A panel of nine cell lines from three different pathologies (breast, lung and colon cancer) were successfully aggregated, demonstrating the robustness of the strategy proposed. Spheroid phenotype varied between cell lines, in terms of spheroid size distribution, compactness, cellular organization and oxygen gradients. HT29 cells, a colon cancer cell line, generated large spheroids leading to oxygen zonation and formation of apoptotic cores. In contrast, H1650 cells, a Non-Small-Cell Lung Cancer cell line, formed smaller spheroids and no hypoxia gradients were detected. This is in line with the characteristics of the native tumour environment, where the heterogeneous distribution of vascularization in primary tumours contributes to poor diffusion of oxygen and nutrients, thus leading to the formation of gradients even under agitation [15].

When fibroblasts were simultaneously inoculated with tumour cells, during the aggregation phase, their distribution pattern varied greatly between cell lines. Whilst in H1650 spheroids, fibroblasts were homogeneously distributed through the spheroids, with MCF-7 cells, an ER^+ breast cancer cell line, fibroblasts accumulated in the centre of the spheroid. The same was observed by our collaborators with static co-cultures of MCF-7 and fibroblasts (**chapter 4**). Although the reason for the heterogeneous fibroblast distribution could not be explained by us, it corroborates published literature on MCF-7 co-cultures, both in static and stirred culture systems [16,17]. The complete or partial mixture of epithelial and stromal compartments resembles invasive carcinomas [18], not allowing the investigation of tumour progression from earlier stages of the disease. In early stage breast carcinomas, luminal epithelial cells are typically surrounded by a stromal compartment, separated by a basement membrane (BM) [3,14]. Through rupture of the BM, tumour cells invade the stromal space and both compartments become indistinguishable [14]. In order to mimic the tissue architecture at these initial stages, tumour spheroids of

MCF-7 cells were microencapsulated in alginate, either alone or in combination with human fibroblasts as single cells, and then cultured for 15 days (**chapter 3**). By using this strategy, fibroblasts arranged themselves around tumour spheroids creating distinct epithelial and stromal compartments, as observed for early stage breast carcinomas.

After 5 days in culture, microencapsulated MCF-7 cells self-organized into tissue-like structures by establishing cell-cell contacts through E-cadherin and by partial polarization at the surface of multiple small lumen, in both mono and co-cultures (**chapter 3**). These features, together with the relatively limited proliferative capacity of MCF-7 cells, are reminiscent of well differentiated human breast tumours of the luminal subtype [19,20]. The ability for MCF-7 cells to polarise has been demonstrated by other groups, but only when cultured in BM gels [21] or for very long culture periods in scaffold free conditions (155 days) [22]. In the second case, long culture periods were required as laminin needed to be *de novo* secreted, in contrast to the BM gels where laminin is the main component [23]. However, laminin was not detected in the stirred cultures (**chapter 2** and **3**). Nonetheless, cell polarization is not only dependent on integrin-laminin binding, but also on the physical forces exerted in the plasma membrane [24]. These forces can be exerted by the neighbouring cells and by the surrounding environment [25]. This might explain why partial cell polarization was detected in the microencapsulated cultures (**chapter 3**), although laminin was not detected. In this case, alginate provides the physical support to cells and allows cell movement, which is required for lumen formation and cell polarization [19], by day 5 of culture.

We hypothesized that alginate would not only provide physical support and cell confinement, but also prevent the washout of *de novo* secreted molecules, in the stirred system. The presence of fibroblasts resulted in the secretion of pro-inflammatory cytokines, such as IL8, IL6 and CXCL1, and deposition of *de novo* synthesized collagen within the microcapsule. The use of an inert scaffold indeed prevented the washout of *de novo* secreted molecules, resulting in the accumulation of collagen and specific cytokines, such as sICAM, a cytokine

associated with tumour cell growth and angiogenesis [26]. The retention of these molecules, in the alginate microcapsules, contributed to the reconstruction of features of the tumour microenvironment [14,27].

The ability to sample from the spinner vessel in a non-destructive manner, allowed continuous monitoring of the culture progression, by collecting samples throughout the culture period. By day 15, tumour spheroids in co-culture presented an irregular shape and loss of circularity which was accompanied by spheroid migration out of the alginate capsules. The directionality of spheroid migration together with the stabilization of tumour cell concentration, is suggestive of an event of collective cell migration rather than the cell movement associated with expansive cell growth [28]. Ductal elongation, is described as a directional collective migration process [19], which might explain the observed directionality in spheroid migration out of the microcapsules. The accumulation of collagen in the stromal compartment of co-cultures might be enough to stimulate collective tumour cell migration, that typically occurs in breast carcinomas [29]. In addition, co-cultures presented a reduced nuclear ER expression which could be observed by day 5 of co-culture. Nuclear ER expression also declined in the mono-cultures but at a much slower rate, and was only apparent after 15 days of culture. This difference between mono and co-culture suggests that fibroblasts are accelerating ER depletion, as previously demonstrated by others [30]. A reduction in membranous E-cadherin was also observed although with a very high percentage of spheroid heterogeneity in co-cultures compared to mono-cultures. Loss of hormone dependency accompanied by altered sub-cellular localization of E-cadherin and altered cell polarity have been described as common features of more aggressive and invasive breast cancers [31-33]. In addition, co-cultures also presented a higher capacity to induce angiogenesis, when compared to those from mono-cultures. This increase might be related to the increased expression of pro-angiogenic cytokines in co-cultures, such as CXCL1 and IL8 [34-36]. Interestingly, infiltrated fibroblasts, in the tumour spheroids, were detected only after 20 (**Chapter 4**) and 30 days (*data not shown*), but never after 15 days of

culture. Although we could not reason why 15 days of culture were not enough to allow fibroblast infiltration, we hypothesized the increasing concentrations of ECM components within the alginate capsules were needed to allow fibroblast migration.

Altogether these results demonstrate that alginate microencapsulation combined with stirred culture systems are a good approach to mimic key aspects of disease progression caused by heterotypic cell crosstalk.

1.2 Influence of the culture system on tumour and stromal cell behaviour

In **chapter 4**, we compared the alginate microencapsulation model with commonly used 2D and 3D cell models. Evaluations were done within the IMI-funded project PREDECT (www.predect.eu), where several partners performed parallel studies for validation and comparison of cell behaviour using different cell culture models. All partners used the same MCF-7 cell clone, and harmonized culture conditions and analytical methods. In this study, the alginate microencapsulation model system was compared with 2D and with several static 3D cell culture set-up. These included scaffold-free cultures in ultra-low adhesion plates (floaters) or embedded in bioactive scaffolds, such as BM gels (matrigel), collagen or a mix of matrigel-collagen.

The results demonstrate that fibroblasts stimulated tumour cell growth in all cultures, except for matrigel-containing cultures, where tumour cell growth was equal in both mono and co-cultures. Quantification of the proliferative indexes showed similar results. In alginate microencapsulated cultures, the growth stimulatory effect of fibroblasts was statistically significant only after 20 days of culture, which corroborates the results described in **chapter 3**. In contrast, the growth stimulatory effect of fibroblasts in collagen-embedded cultures was observed at an early time point and was similar to the tumour cell growth observed in matrigel-containing cultures. Although growth factor depleted, matrigel still contains significant amounts of undefined growth factors and cytokines that may mask the effect of stromal cells and stimulate tumour

cell growth [37,38]. In contrast, collagen gels are routinely used for the evaluation of the effect of fibroblasts on tumour cell growth and invasiveness [39,40]. This was demonstrated when mammary carcinomas were cultured either in collagen or matrigel, and tumour cell dissemination occurred in collagen gels only [2]. Another example was the co-culture of colon carcinoma spheroids with fibroblasts in collagen gels [41]. In this co-culture system, stromal cells migrated towards the tumour spheroids and, through the concerted action of paracrine signalling and direct cell-cell interactions, modulated tumour progression. Although collagen gels are less rich in growth factors, collagen stiffness and fibre alignment also modulate tumour cell migration speed, invasion distance and cellular protrusion dynamics [9].

Tumour cells, from all models evaluated, were treated with standard of care drugs (docetaxel, a chemotherapeutic; and Fulvestrant, an ER antagonist). In most of culture set-up, except for 2D and scaffold-free 3D cultures, fibroblasts provided partial protection against one of the treatments. In alginate microencapsulated co-cultures, tumour cells were refractory to Fulvestrant treatment. This was demonstrated by analysis of tumour cell growth and through H&E staining, which showed that treated co-cultures were indistinguishable from controls. However, proliferative indexes showed that tumour cells presented a reduced number of proliferating cells, in both mono and co-cultures, when compared to untreated controls. Still, the number of proliferating cells was higher in co-cultures than in mono-cultures. The mechanisms by which fibroblasts protected tumour cells from Fulvestrant treatments were not explored in this thesis. However, we can speculate that the oestradiol secreted by fibroblasts [42,43], might compete with Fulvestrant and decrease the binding affinity of Fulvestrant to ER [44,45], reducing the treatment efficacy. Moreover, the Epidermal Growth Factor (EGF) [46,47] and Insulin Growth Factor (IGF) [48] secreted by fibroblasts might also activate ER, through phosphorylation of the serine residue 118, in the AF-1 domain of the receptor [49], thus contributing to ER stimulation in co-cultures. Although further studies need to be performed, identification of the fibroblast secretome by MS-

based tools led to the prediction of IGF-1 signalling pathway with higher -log(p-value) (**chapter 6**). Although this analysis was not quantitative, it is a good indicative that identification of the tumour-stromal secretome should be performed, in order to understand the protective effect of fibroblasts in anti-oestrogens therapy.

1.3 Development of human breast cancer models: complementarity between *in vitro* and *ex vivo* models

Ex vivo cultures of freshly isolated tumour samples aim to preserve the original tissue architecture - inter and intra-patient heterogeneity - and the surrounding microenvironment [50-52]. Although many efforts have been made towards the development of methods to maintain explants from ER^+ breast cancer patients for long periods of culture, most have failed due to loss of cell viability, tissue structure and ER expression [50]. Recently, [51] reported the development of a new culture strategy for maintenance of breast cancer explants in culture for long periods. Explants were cultured in collagen sandwiches under constant medium perfusion. However, after 15 days in culture, tissue architecture and cellularity were lost and ER expression was significantly decreased. Since most luminal A BCs are slow proliferative and low mutagenic [53,54], it is of most importance to perform long-term studies to observe heterotypic cell interactions, and their effects on drug treatment and on ER dependency. Therefore, in **chapter 5**, we have applied the culture methodology developed in **chapter 3** for culturing human patient-derived ER^+ BC explants. We already demonstrated, that alginate microencapsulation not only provides structural support to cells but also allows the accumulation of secreted factors and cell migration (**chapter 3**). The use of a dynamic culture system should improve mass transfer through the explants and thus prevent or reduce oxygen and nutrient zonation, which were a major limitation observed in previous studies [50]. The results presented in **chapter 5** demonstrate that by employing this strategy, explants cellularity and architecture was maintained for at least 30 days of culture. Molecular evaluation showed a high degree of

heterogeneity between and within patient samples, although all tumours belonged to the luminal A subtype ($ER^+PR^+Her2^-$). Epithelial and stromal compartments were retained, and proliferative indexes were kept low, as typically observed for luminal A BCs [53]. The homogeneous distribution of proliferative cells and the absence of apoptotic or necrotic centres showed that, despite the explant sizes of approximately 2 mm, oxygen and nutrient diffusion were not a limiting factor.

A major achievement was the long-term maintenance of ER expression *ex vivo*. Many authors have tried to maintain ER in human-derived breast cancer primary cultures but this was never accomplished [51,55]. Although we cannot conclude on the reason behind ER maintenance in our culture system, we hypothesized that by providing a physical support to cells, and promoting an efficient mass-transfer, whilst preventing the washout of secreted molecules, allowed the maintenance of the native tumour architecture and environment. In contrast, the use of collagen sandwiches in the model developed by [51] led to tumour cell spreading into the gel, after 15 days in culture [2,11]. As a result, the native tumour architecture and microenvironment were lost. This might explain the reduced cellularity and ER expression in [51] model. Additionally, the oestradiol and EGF, which are secreted by the fibroblasts [42,43,46,47] also stimulates the proliferation of ER^+ cells [56]. Altogether, we speculate that by promoting oxygen and nutrient diffusion whilst maintaining the native tumour architecture, ECM and tumour-stromal communication, it is possible to maintain ER expression.

Exometabolome analysis of the *ex vivo* cultures revealed a lower metabolic activity after Fulvestrant treatment (0.4 nM). Interestingly, glutamate concentration was slightly increased in treated conditions. It has been described that **i**n addition to controlling gene expression, ER is a known key player in regulating cell metabolism, namely through mTOR activation [57]. Although a direct correlation between glutamate and ER has not yet been shown for breast cancer, it has been reported that aggressive BC secrete higher amounts of glutamate. Moreover, this has been correlated with

disruption of bone homeostasis and consequent increase in bone metastasis [58]. At this point, we can only speculate that glutamate increased concentrations could be a side effect of Fulvestrant treatments, which might play a role in modulating bone metastasis [59].

The work developed in **chapter 5** shows that the combination of alginate encapsulation with a dynamic culture system is a good strategy for long term maintenance of ER^+ BC explants, *ex vivo*, and for the interrogation of the drug treatment effects on a culture setting more similar with the *in vivo* situation.

The use of a common strategy for both cell models developed in **chapters 3** and **5**, proves that this method is robust and can be applied to multiple culture systems. Although each model presents its limitations, the combined usage of *in vitro* and *ex vivo* models, with a panel of analytical tools, might significantly contribute to obtain robust and reproducible results in cancer research. The high degree of heterogeneity observed in *ex vivo* models is both advantageous and disadvantageous, i.e., whilst it mimics the heterogeneity observed in human tumours, it increases the complexity on result interpretation. One way to overcome this limitation is to increase the number of replicates and do develop more robust analytical and statistical methodologies. In contrast, *in vitro* models are already robust and reproducible, allow a step-wise increase in complexity, and also present some degree of heterogeneity. In **chapter 3**, quantification of membranous E-cadherin revealed a very high percentage of spheroid heterogeneity in co-cultures compared to mono-cultures. A similar result was observed for loss of spheroid circularity in co-cultures, where only 40% of the spheroids leaked out of the alginate microcapsules. Still, additional variables need to be taken into account when treating patients that, although belong to the same BC subtype, present many differences on the tissue architecture, tumour - stromal ratio, degree of epithelial differentiation and polarity, heterogeneity in ER and KI67 expression, immune infiltrates, amongst many others.

2 Conclusions and perspectives

This thesis describes the development of new pre-clinical and co-clinical *in vitro* and *ex vivo* model systems to better mimic the tumour architecture and microenvironment, and to recapitulate tumour progression. These models were developed by combining cell microencapsulation in an inert scaffold (alginate) and dynamic culture systems. The use of a dynamic culture system promoted cell aggregation in the *in vitro* model and contributed to oxygen and nutrient homogeneity, in both culture systems. In the *in vitro* model, alginate microcapsules allowed epithelial and stromal cell self-organization into tissue-like structures, and *de novo* synthesis and accumulation of soluble factors and ECM. Together, these allowed the reconstruction of features of the breast tumour microenvironment. Long-term co-culture periods led to phenotypic alterations on tumour cells, typical of more aggressive stages of the disease. To mimic the heterogeneity observed in human tumours, a long-term *ex vivo* culture system was developed, for human-derived ER^+ breast cancer explants, by making use of the same strategy. Explant cultures from approximately 20 patients were kept in culture for 30 days, with good cell viability and maintenance of epithelial and stromal components, and detection of immune infiltrates. Expression of the ER was also maintained. With this thesis we propose that *in vitro* and *ex vivo* models should be used as complementary tools for a correct evaluation of tumour progression and drug response mechanisms. Additionally, the developed *ex vivo* model can be applied to translational medicine, especially for co-clinical assays on drug treatments and to help identifying resistant cell clones that might be responsible for future disease relapses.

This PhD thesis contributed for the improvement of the state-of-the-art breast tumour models and can be used in the fields of breast cancer research and translational research, and be incorporated in drug discovery cascades. The developed models can be further improved by a step-wise increase on the model complexity, by adding extra cell types (endothelial cells or immune cells), or by manipulation of physicochemical parameters (oxygen, glucose or pH).

One example would be to mimic the intermittent hypoxia environment typically observed during tumour growth. It has been widely discussed that the hypoxic environment *per se* does not induce tumour aggressiveness, but instead, the free oxygen radicals generated during the re-oxygenation process, are responsible for promoting mutations that lead to tumour progression. The recapitulation of these events may enable a more closely recapitulation of key pathological events described to occur *in vivo*.

In combination with *in vitro* models, the use of *ex vivo* models might help to uncover variables inherent to tumour heterogeneity and to validate conclusions taken from less complex *in vitro* models. The concerted action between the multiple cell types, growth factors and ECM present in the native tumour environment, might modulate tumour cell behaviour in a different manner to what was identified in the *in vitro* model. However, due to the complexity of result interpretation in explant cultures, the analytical tools used should also be improved. Routine histopathological analysis of patient samples, used for comparison with the results obtained from explant cultures, is performed by IHC staining against specific molecular markers, such as, ER, PR, Her2 and KI67 [60]. This technique allows the visual evaluation of the sample and a semi-quantification of the number and intensity of the stained cells. However, inter-observer variation is very high and the number of sections analysed is low. To tackle this issue, slide scanners coupled with image analysis software's are being developed to speed up the analysis process and to generate quantitative data. This will allow clinicians to increase the number of analysed slides and to improve robustness of the conclusions taken. Machine learning tools for automatic image analysis and accurate quantification of stained sections, still need to be improved to enable softwares to distinguish between different cell types and the intracellular location of each stained protein.

Altogether, these models should help predict disease progression and drug response mechanisms and contribute to a deeper understanding on the effects of stromal cells on tumour cell behaviour. Routine analysis should be performed

by using a set of analytic tools for result validation, instead of focusing on one type of assay only, which is typically done in research labs, hospitals and pharma industry. The era of translational medicine has promoted collaborations between researchers and physicians, which is contributing to a deeper understanding of the disease and to the implementation of new analytical tools in hospitals. Although proof-of-concept is still ongoing, there is great expectation on the use of these and other models for co-clinical trials both for evaluation of first line treatments (short-time assays), and for prediction of disease relapse mechanisms (long-term assays). Finally, pharma industry is already implementing some of these models as pre-clinical tools, instead of using the simplistic mono-cultures performed in 2D. In fact, the *in vitro* model developed in this thesis (**Chapter 3**) is already being used by 2 pharmaceutical companies. This reflects the awareness of pharma in including additional variables in the drug discovery cascades which should improve the success rates of drug development.

In conclusion, this thesis showed that it is possible to mimic disease progression mechanisms through modulation of the tumour microenvironment, and that the combined usage of *in vitro* and *ex vivo* model systems are key for robust interpretation of tumour progression events, drug-response and tumour-stromal interactions.

3 References

[1] N. Yoshida, Y. Omoto, A. Inoue, H. Eguchi, Y. Kobayashi, M. Kurosumi, et al., Prediction of prognosis of estrogen receptor-positive breast cancer with combination of selected estrogen-regulated genes, Cancer Sci. 95 (2004) 496–502.

[2] K.-V. Nguyen-Ngoc, K.J. Cheung, A. Brenot, E.R. Shamir, R.S. Gray, W.C. Hines, et al., ECM microenvironment regulates collective migration and local dissemination in normal and malignant mammary epithelium, Proc. Natl. Acad. Sci. U.S.a. 109 (2012) E2595–604. doi:10.1073/pnas.1212834109.

[3] Z.I. Khamis, Z.J. Sahab, Q.-X.A. Sang, Active roles of tumor stroma in breast cancer metastasis, Int J Breast Cancer. 2012 (2012) 574025–10. doi:10.1155/2012/574025.

[4] L.C. Kimlin, G. Casagrande, V.M. Virador, In vitro three-dimensional (3D) models in cancer research: an update, Mol. Carcinog. 52 (2013) 167–182. doi:10.1002/mc.21844.

[5] J.W. Haycock, 3D cell culture: a review of current approaches and techniques, Methods Mol. Biol. 695 (2011) 1–15. doi:10.1007/978-1-60761-984-0_1.

[6] B. Weigelt, C.M. Ghajar, M.J. Bissell, The need for complex 3D culture models to unravel novel pathways and identify accurate biomarkers in breast cancer, Adv. Drug Deliv. Rev. 69-70 (2014) 42–51. doi:10.1016/j.addr.2014.01.001.

[7] P. Mafi, S. Hindocha, R. Mafi, W.S. Khan, Evaluation of biological protein-based collagen scaffolds in cartilage and musculoskeletal tissue engineering--a systematic review of the literature, Curr Stem Cell Res Ther. 7 (2012) 302–309.

[8] K.E. Sung, D.J. Beebe, Microfluidic 3D models of cancer, Adv. Drug Deliv. Rev. 79-80 (2014) 68–78. doi:10.1016/j.addr.2014.07.002.

[9] D.O. Velez, B. Tsui, T. Goshia, C.L. Chute, A. Han, H. Carter, et al., 3D collagen architecture induces a conserved migratory and transcriptional response linked to vasculogenic mimicry, Nat Commun. 8 (2017) 1651. doi:10.1038/s41467-017-01556-7.

[10] T. Andersen, P. Auk-Emblem, M. Dornish, 3D Cell Culture in Alginate Hydrogels, Microarrays 2015, Vol. 4, Pages 133-161. 4 (2015) 133–161. doi:10.3390/microarrays4020133.

[11] O. Chaudhuri, S.T. Koshy, C. Branco da Cunha, J.-W. Shin, C.S. Verbeke, K.H. Allison, et al., Extracellular matrix stiffness and composition jointly regulate the induction of malignant phenotypes in mammary epithelium, Nat Mater. 13 (2014) 970–978. doi:10.1038/nmat4009.

[12] M.E. Smithmyer, L.A. Sawicki, A.M. Kloxin, Hydrogel scaffolds as in vitro models to study fibroblast activation in wound healing and disease, Biomater Sci. 2 (2014) 634–650. doi:10.1039/C3BM60319A.

[13] N. Gjorevski, N. Sachs, A. Manfrin, S. Giger, M.E. Bragina, P. Ordóñez-Morán, et al., Designer matrices for intestinal stem cell and organoid culture, Nature. 539 (2016) 560–564. doi:10.1038/nature20168.

[14] M.J. Bissell, W.C. Hines, Why don't we get more cancer? A proposed role of the microenvironment in restraining cancer progression, Nat. Med. 17 (2011) 320–329. doi:10.1038/nm.2328.

[15] G.M. Thurber, M.M. Schmidt, K.D. Wittrup, Antibody tumor penetration: transport opposed by systemic and antigen-mediated clearance, Adv. Drug Deliv. Rev. 60 (2008) 1421–1434. doi:10.1016/j.addr.2008.04.012.

[16] P. Kaur, B. Ward, B. Saha, L. Young, S. Groshen, G. Techy, et al., Human breast cancer histoid: an in vitro 3-dimensional co-culture model that mimics breast cancer tissue, J. Histochem. Cytochem. 59 (2011) 1087–1100. doi:10.1369/0022155411423680.

[17] C. Angelucci, G. Maulucci, G. Lama, G. Proietti, A. Colabianchi, M. Papi, et al., Epithelial-stromal interactions in human breast cancer: effects on adhesion, plasma membrane fluidity and migration speed and directness, PLoS ONE. 7 (2012) e50804. doi:10.1371/journal.pone.0050804.

[18] G.K. Malhotra, X. Zhao, H. Band, V. Band, Histological, molecular and functional subtypes of breast cancers, Cancer Biol. Ther. 10 (2010) 955–960. doi:10.4161/cbt.10.10.13879.

[19] A.J. Ewald, A. Brenot, M. Duong, B.S. Chan, Z. Werb, Collective epithelial migration and cell rearrangements drive mammary branching morphogenesis, Dev. Cell. 14 (2008) 570–581. doi:10.1016/j.devcel.2008.03.003.

[20] M.J. Piccart-Gebhart, New developments in hormone receptor-positive disease, Oncologist. 16 Suppl 1 (2011) 40–50. doi:10.1634/theoncologist.2011-S1-40.

[21] C.E. Smart, B.J. Morrison, J.M. Saunus, A.C. Vargas, P. Keith, L. Reid, et al., In vitro analysis of breast cancer cell line tumourspheres and primary human breast epithelia mammospheres demonstrates inter- and intrasphere heterogeneity, PLoS ONE. 8 (2013) e64388. doi:10.1371/journal.pone.0064388.

[22] J.B. do Amaral, M.S. Urabayashi, G.M. Machado-Santelli, Cell death and lumen formation in spheroids of MCF-7 cells, Cell Biol. Int. 34 (2010) 267–274. doi:10.1042/CBI20090024.

[23] N. Akhtar, C.H. Streuli, An integrin-ILK-microtubule network orients cell polarity and lumen formation in glandular epithelium, Nat. Cell Biol. 15 (2013) 17–27. doi:10.1038/ncb2646.

[24] A. Diz-Muñoz, D.A. Fletcher, O.D. Weiner, Use the force: membrane tension as an organizer of cell shape and motility, Trends Cell Biol. 23 (2013) 47–53. doi:10.1016/j.tcb.2012.09.006.

[25] Y. Mao, B. Baum, Tug of war--the influence of opposing physical forces on epithelial cell morphology, Dev. Biol. 401 (2015) 92–102. doi:10.1016/j.ydbio.2014.12.030.

[26] C. Chen, C.A. Duckworth, B. Fu, D.M. Pritchard, J.M. Rhodes, L.-G. Yu, Circulating galectins -2, -4 and -8 in cancer patients make important contributions to the increased circulation of several cytokines and chemokines that promote angiogenesis and metastasis, British Journal of Cancer. 110 (2014) 741–752. doi:10.1038/bjc.2013.793.

[27] A. Qiao, F. Gu, X. Guo, X. Zhang, L. Fu, Breast cancer-associated fibroblasts: their roles in tumor initiation, progression and clinical applications, Front Med. 10 (2016) 33–40. doi:10.1007/s11684-016-0431-5.

[28] P. Friedl, S. Alexander, Cancer invasion and the microenvironment: plasticity and reciprocity, Cell. 147 (2011) 992–1009. doi:10.1016/j.cell.2011.11.016.

[29] K.J. Cheung, E. Gabrielson, Z. Werb, A.J. Ewald, Collective invasion in breast cancer requires a conserved basal epithelial program, Cell. 155 (2013) 1639–1651. doi:10.1016/j.cell.2013.11.029.

[30] S.E. Holton, A. Bergamaschi, B.S. Katzenellenbogen, R. Bhargava, Integration of molecular profiling and chemical imaging to elucidate fibroblast-microenvironment impact on cancer cell phenotype and endocrine resistance in breast cancer, PLoS ONE. 9 (2014) e96878. doi:10.1371/journal.pone.0096878.

[31] J.L.L. Robinson, K.A. Holmes, J.S. Carroll, FOXA1 mutations in hormone-dependent cancers, Front Oncol. 3 (2013) 20. doi:10.3389/fonc.2013.00020.

[32] A.M. Scherbakov, O.E. Andreeva, V.A. Shatskaya, M.A. Krasil'nikov, The relationships between snail1 and estrogen receptor signaling in breast cancer cells, J. Cell. Biochem. 113 (2012) 2147–2155. doi:10.1002/jcb.24087.

[33] Y.J. Suh, J.H. Chang, C.S. Chun, Restoration of Hormone Dependency in Estrogen Receptor-Lipofected MDA-MB-231 Human Breast Cancer Cells, Journal of the Korean Cancer Association. (1999).

[34] J.K. Singh, B.M. Simões, S.J. Howell, G. Farnie, R.B. Clarke, Recent advances reveal IL-8 signaling as a potential key to targeting breast cancer stem cells, Breast Cancer Res. 15 (2013) 210. doi:10.1186/bcr3436.

[35] P. DelNero, M. Lane, S.S. Verbridge, B. Kwee, P. Kermani, B. Hempstead, et al., 3D culture broadly regulates tumor cell hypoxia response and angiogenesis via pro-inflammatory pathways, Biomaterials. 55 (2015) 110–118. doi:10.1016/j.biomaterials.2015.03.035.

[36] S. Acharyya, T. Oskarsson, S. Vanharanta, S. Malladi, J. Kim, P.G. Morris, et al., A CXCL1 paracrine network links cancer chemoresistance and metastasis, Cell. 150 (2012) 165–178. doi:10.1016/j.cell.2012.04.042.

[37] S. Vukicevic, H.K. Kleinman, F.P. Luyten, A.B. Roberts, N.S. Roche, A.H. Reddi, Identification of multiple active growth factors in basement membrane Matrigel suggests caution in interpretation of cellular activity related to extracellular matrix components, Exp. Cell Res. 202 (1992) 1–8.

[38] G. Benton, I. Arnaoutova, J. George, H.K. Kleinman, J. Koblinski, Matrigel: from discovery and ECM mimicry to assays and models for cancer research, Adv. Drug Deliv. Rev. 79-80 (2014) 3–18. doi:10.1016/j.addr.2014.06.005.

[39] A. Rudisch, M.R. Dewhurst, L.G. Horga, N. Kramer, N. Harrer, M. Dong, et al., High EMT Signature Score of Invasive Non-Small Cell Lung Cancer (NSCLC) Cells Correlates with NFκB Driven Colony-Stimulating Factor 2 (CSF2/GM-CSF) Secretion by Neighboring Stromal Fibroblasts, PLoS ONE. 10 (2015) e0124283. doi:10.1371/journal.pone.0124283.

[40] C. Unger, N. Kramer, A. Walzl, M. Scherzer, M. Hengstschläger, H. Dolznig, Modeling human carcinomas: physiologically relevant 3D models to improve anti-cancer drug development, Adv. Drug Deliv. Rev. 79-80 (2014) 50–67. doi:10.1016/j.addr.2014.10.015.

[41] H. Dolznig, C. Rupp, C. Puri, C. Haslinger, N. Schweifer, E. Wieser, et al., Modeling colon adenocarcinomas in vitro a 3D co-culture system induces cancer-relevant pathways upon tumor cell and stromal fibroblast interaction, Am. J. Pathol. 179 (2011) 487–501. doi:10.1016/j.ajpath.2011.03.015.

[42] R.J. Buchsbaum, S.Y. Oh, Breast Cancer-Associated Fibroblasts: Where We Are and Where We Need to Go, Cancers (Basel). 8 (2016) 19. doi:10.3390/cancers8020019.

[43] S.E. Bulun, D. Chen, I. Moy, D.C. Brooks, H. Zhao, Aromatase, breast cancer and obesity: a complex interaction, Trends Endocrinol. Metab. 23 (2012) 83–89. doi:10.1016/j.tem.2011.10.003.

[44] C.K. Osborne, A. Wakeling, R.I. Nicholson, Fulvestrant: an oestrogen receptor antagonist with a novel mechanism of action, British Journal of Cancer. 90 (2004) S2–S6. doi:10.1038/sj.bjc.6601629.

[45] A.E. Wakeling, J. Bowler, Steroidal pure antioestrogens, J. Endocrinol. 112 (1987) R7–10.

[46] M. Kurobe, S. Furukawa, K. Hayashi, Synthesis and secretion of an epidermal growth factor (EGF) by human fibroblast cells in culture, Biochem. Biophys. Res. Commun. 131 (1985) 1080–1085.

[47] M. Majety, L.P. Pradel, M. Gies, C.H. Ries, Fibroblasts Influence Survival and Therapeutic Response in a 3D Co-Culture Model, PLoS ONE. 10 (2015) e0127948. doi:10.1371/journal.pone.0127948.

[48] D.A. Lewis, J.B. Travers, A.-K. Somani, D.F. Spandau, The IGF-1/IGF-1R signaling axis in the skin: a new role for the dermis in aging-associated skin cancer, Oncogene. 29 (2010) 1475–1485. doi:10.1038/onc.2009.440.

[49] R. de Leeuw, J. Neefjes, R. Michalides, A role for estrogen receptor phosphorylation in the resistance to tamoxifen, Int J Breast Cancer. 2011 (2011) 232435–10. doi:10.4061/2011/232435.

[50] E.J. Davies, M. Dong, M. Gutekunst, K. Närhi, H.J.A.A. van Zoggel, S. Blom, et al., Capturing complex tumour biology in vitro: histological and molecular characterisation of precision cut slices, Sci Rep. 5 (2015) 17187. doi:10.1038/srep17187.

[51] M.G. Muraro, S. Muenst, V. Mele, L. Quagliata, G. Iezzi, A. Tzankov, et al., Ex-vivo assessment of drug response on breast cancer primary tissue with preserved microenvironments, Oncoimmunology. 6 (2017) e1331798. doi:10.1080/2162402X.2017.1331798.

[52] K.A.T. Naipal, N.S. Verkaik, H. Sánchez, C.H.M. van Deurzen, M.A. den Bakker, J.H.J. Hoeijmakers, et al., Tumor slice culture system to assess drug response of primary breast cancer, BMC Cancer. 16 (2016) 78. doi:10.1186/s12885-016-2119-2.

[53] J. Makki, Diversity of Breast Carcinoma: Histological Subtypes and Clinical Relevance, Clin Med Insights Pathol. 8 (2015) 23–31. doi:10.4137/CPath.S31563.

[54] S.E. Stanton, M.L. Disis, Clinical significance of tumor-infiltrating lymphocytes in breast cancer, J Immunother Cancer. 4 (2016) 59. doi:10.1186/s40425-016-0165-6.

[55] A.J. Fridriksdottir, J. Kim, R. Villadsen, M.C. Klitgaard, B.M. Hopkinson, O.W. Petersen, et al., Propagation of oestrogen receptor-positive and oestrogen-responsive normal human breast cells in culture, Nat Commun. 6 (2015) 8786. doi:10.1038/ncomms9786.

[56] S. Kato, H. Endoh, Y. Masuhiro, T. Kitamoto, S. Uchiyama, H. Sasaki, et al., Activation of the estrogen receptor through phosphorylation by mitogen-activated protein kinase, Science. 270 (1995) 1491–1494.

[57] E.M. Ciruelos Gil, Targeting the PI3K/AKT/mTOR pathway in estrogen receptor-positive breast cancer, Cancer Treat. Rev. 40 (2014) 862–871. doi:10.1016/j.ctrv.2014.03.004.

[58] J. Fazzari, H. Lin, C. Murphy, R. Ungard, G. Singh, Inhibitors of glutamate release from breast cancer cells; new targets for cancer-induced bone-pain, Sci Rep. 5 (2015) 8380. doi:10.1038/srep08380.

[59] I. Bado, Z. Gugala, S.A.W. Fuqua, X.H.-F. Zhang, Estrogen receptors in breast and bone: from virtue of remodeling to vileness of metastasis, Oncogene. 36 (2017) 4527–4537. doi:10.1038/onc.2017.94.

[60] H.G. Russnes, O.C. Lingjærde, A.-L. Børresen-Dale, C. Caldas, Breast Cancer Molecular Stratification: From Intrinsic Subtypes to Integrative Clusters, Am. J. Pathol. 187 (2017) 2152–2162. doi:10.1016/j.ajpath.2017.04.022.